



SAPIENZA
UNIVERSITÀ DI ROMA

PhD School of Pharmaceutical Sciences XXVI cycle

“Sapienza” University of Rome

PAOLO MELLINI

Design and Synthesis of Novel Sirtuin Inhibitors as Useful
Tools in Understanding Their Potential Activity Against
Cancer

Doctoral Dissertation

Department of Chemistry and Drug Technologies
Faculty of Medicine and Pharmacy
“Sapienza” University of Rome

Rome 2014

In Memory of My Beloved Aunt Franca

Supervisors:

Professor Antonello Mai Ph.D. (tutor and main supervisor)

Department of Drug Chemistry and Technology “Sapienza” University of Rome P.le Aldo Moro, 5 – 00185 - Rome (Italy).

Adjunct Professor Maija Lahtela-Kakkonen Ph.D. (foreign supervisor) School of Pharmacy University of Eastern Finland P. O. Box 1627, 70211 Kuopio (Finland).

Doctor Barbara Di Rienzo (supervisor) Department of Drug Chemistry and Technology “Sapienza” University of Rome P.le Aldo Moro, 5 – 00185 - Rome (Italy).

ACKNOWLEDGEMENTS

“The research made with passion and in respect of the people that are working with you, make you a better person”

Barbara Di Rienzo

I would like to express all my gratitude to my family for their love, support and encouragement through my entire life. My special thanks to my lovely sisters Monica and MariaPaola for your constant presence in my life.

I am deeply indebted to Dr. Barbara Di Rienzo my first supervisor that initiated me to this beautiful work. Your encouragements, support and suggestions, made me grow in the research field in complete intellectual freedom. Thank you for each advise, word and smile that you gave to me, and made me proud to be your student.

My sincere and deep gratitude to my supervisor Prof. Antonello Mai for guiding my research, helping me to develop my scientific background and for your huge patience. You have accepted me in your research group like a son, opening to me each possibilities, thank you epigenetic Prof.

I would like to thank my senior scientist Dr. Sergio Valente (amicably called Big Sergio) it is a real pleasure work with you. Your passion for the science mixed with your enthusiasm, is something that burn and that you are able to transmit to each of your collaborators.

I want to thank my lovely colleagues M.Sc. Alessia Lenoci, Biagina Marrocco and Donatella Labella (close to be doctor), work together with you, is more than a pleasure. Whatever we will do in the future, we will be forever the epigenetics brothers and sisters.

I would like to express my gratitude to Dr. Daniela De Vita, Melissa D'Ascenzio, Simone Carradori and M.Sc. Flavio Della Sala for each thing shared together, from a coffee to science. All this things let me understand that we are not only colleagues but friends.

I am very grateful to my foreign supervisor Prof. Maija Lahtela-Kakkonen, you not only allowed me to conduct my research in your group for half of my PhD program, but you made me feel at home. Thank you Maija for introducing me to the molecular modelling world, for your guidance, advices, meeting, availability and for the

delightful person that you are. I would like to express my sincere gratitude to Dr. Elina Jarho for your guidance and help in my synthetic work and for each priceless advice. Your way to conduct research for me has been and is nowadays an example to follow. My special thanks to M.Sc. Heikki Salo and Piia Kokkonen, I cannot forget your help and advices in the molecular modelling lab. and our talks around the sirtuin world, in particular about the topic “how design potent inhibitors”. Our background exchange has not been only very formative for me but a real pleasure. I would like to thank Prof. Jukka Leppänen, without your precious advices and patience when I was working in the HPLC lab. I would never been able to purify my pretty probes. Many thanks to Dr. Tarja Kokkola and Tiina Suuronen, I greatly appreciated your availability. All my gratitude to MSc Jayendra Patel for your sincere friendship, for your smiles and positive encouraging words, it has been a pleasure work with you and share each talks during our coffee time. I want to thank Mrs. Miia Reponen and Tiina Koivunen for your precious technical assistance. I also owe my special thanks to B.Sc. Laura Tolvanen, Olli Pekka Nyrhilä and M.Sc. Rosella Palmieri my master students I really have enjoyed working with you. My deep thanks are for my best friends Sara Pierantoni, Corinne Cappelletti and my little cousin Elisabetta Lisi, for your support during these years and to have been friends of mine not only in good times but also in bad times. Finally, my cordial thanks to the ASV Allumiere because if it’s true that “mens sana in corpore sano” in that gym I grew up healthy. For this I want to express my gratitude to my volleyball best friends Enzo Brutti (Taz), Fabio Mazzarani (the exhausted) and Dario Lisi (blond).

Allumiere, January 2014

A handwritten signature in black ink, appearing to read "Rob Keller". The signature is written in a cursive, flowing style.

ABBREVIATIONS

A549, lung cancer cell line; **AceCS1/2**, acetyl-CoA synthetase 1/2; **ADP**, adenosine diphosphate; **ARPE-19**, Human retinal pigment epithelial cells; **BCL-6**, B-cell lymphoma 6; **Boc**, tert-butoxycarbonyl; **Cbz**, carbonyloxybenzyl; **COMU**, ((1-Cyano-2-ethoxy-2-oxoethylideneaminoxy)dimethylamino-morpholino-carbenium hexafluoro-phosphate); **CPS1**, carbamoyl phosphatase 1; **DMA**, N,N-dimethylacetamide; **CRC**, colorectal carcinoma; **CSCs**, cancer stem cells; **DIPEA**, N,N-diisopropylethylamine; **DMF**, N,N-dimethylformamide; **DMEM**, Dulbecco's modified Eagle medium; **DMSO**, dimethyl sulfoxide; **ERKs**, extracellular-signal-regulated kinases; **FBS**, fetal bovine serum; **FOXO**, forkhead box class O; **GDH**, glutamate dehydrogenase; **GBM**, glioblastoma multiforme; **GST**, glutathione-S-transferase; **HCC**, hepatocellular carcinoma; **HeLa**, Henrietta Lacks; **HepG2**, hepatocellular carcinoma G2; **HDAC**, histone deacetylase; **HIC1**, hypermethylated in cancer; **HSC**, hematopoietic stem cell; **LCAD**, long chain acyl-CoA dehydrogenase; **LDH**, lactate dehydrogenase; **LXR**, liver X receptor; **m/z**, mass-to-charge ratio; **MAPK**, mitogen-activated protein kinase; **MCD**, malonyl CoA decarboxylase; **MCF-7** breast cancer cell line; **MEF2**, myocyte enhancer factor-2; **MOE**, molecular operating environment; **MOLT4**, Human acute lymphoblastic leukemia cell line; **NAD**, nicotinamide adenine dinucleotide; **NF- κ B**, Nuclear Factor-KappaB; **NSAID**, nonsteroidal antiinflammatory drug; **PKD1**, polycystic kidney disease; **PGC-1 α** , peroxisome proliferator-activated receptor γ coactivator; **SH-SY5Y**, human derived neuroblastoma cell line; **SIRT**, silent information regulator; **TBTU**, O-(benzotriazol-1-yl)-N,N,N',N'-tetramethyluronium tetrafluoroborate; **TMS**, tetramethylsilane; **U937**, Human leukemic monocytic lymphoma cell line.

PUBLICATIONS

1. Kokkonen, P.; **Mellini, P.**; Nyrhilä, O.; Rahnasto-Rilla, M.; Poso, A.; Lahtela-Kakkonen, M.; and Jarho, E.M. QSAR Modeling in the Design of Pseudopeptidic SIRT1 Inhibitors. *Eur J Pharm Sci* (manuscript in preparation)
2. **Mellini, P.**; Kokkola, T.; Suuronen, T.; Salo, H.; Tolvanen, L.; Mai, A.; Lahtela-Kakkonen, M.; Jarho, E.M. Screen of Pseudopeptidic Inhibitors of Human Sirtuins 1-3: Two Lead Compounds with Antiproliferative Effects in Cancer Cells. *J Med Chem* **2013**, 56: 6681-6695.
3. **Mellini, P.**; De Vita, D.; Di Rienzo, B.; La Rosa, S.; Padova, A.; Scipione, L.; Tortorella, S.; Friggeri, L. Efficient Synthesis of 3,5-Dicarbamoyl-1,4-dihydropyridines from Pyridinium Salts: Key Molecules in Understanding NAD(P)⁺/NAD(P)H Pathways. *J Het Chem* **2013** (just accepted DOI: 10.1002/jhet.2031).
4. Rotili, D.; Tarantino, D.; Nebbioso, A.; Paolini, C.; Huidobro, C.; Lara, E.; **Mellini, P.**; Lenoci, A.; Pezzi, R.; Botta, G.; Lahtela-Kakkonen, M.; Poso, A.; Steinkühler, C.; Gallinari, P.; De Maria, R.; Fraga, M.; Esteller, M.; Altucci, L.; Mai A. Discovery of Salermide-Related Sirtuin Inhibitors: Binding Mode Studies and Antiproliferative Effects in Cancer Cells Including Cancer Stem Cells. *J Med Chem* **2012**, 55: 10937-10947.
5. **Mellini, P.**; Carafa, V.; Di Rienzo, B.; Rotili, D.; De Vita, D.; Cirilli, R.; Gallinella, B.; Provisiero, D.P.; Di Maro, S.; Novellino, E.; Altucci, L.; Mai A. Carprofen Analogues as Sirtuin Inhibitors: Enzyme and Cellular Studies. *Chem Med Chem* **2012**, 7: 1905-1908.
6. De Vita, D.; Scipione, L.; Tortorella, S.; **Mellini, P.**; Di Rienzo, B.; Simonetti, G.; D'Auria, F.D.; Panella, S.; Cirilli, R.; Di Santo, R.; Palamara, A.T. Synthesis and antifungal activity of a new series of 2-(1H-imidazol-1-yl)-1-phenylethanol derivatives. *Eur J Med Chem* **2012**, 49: 334-342.
7. Piccaro, G.; Filippini, P.; Giannoni, F.; Scipione, L.; Tortorella, S.; De Vita D.; **Mellini, P.**; Fattorini, L. Activity of Drugs Against Dormant Mycobacterium tuberculosis. *Journal of Chemotherapy* **2011**, 23: 175-178.

8. Di Rienzo, B.; **Mellini, P.**; Tortorella, S.; De Vita, D.; Scipione, L. Facile and Efficient Synthesis of 4-Alkyl Derivatives of 3-Carbamoyl- and 3,5-Dicarbamoylpyridines as Nicotinamide Mimetics. *Synthesis* **2010**, 22: 3835-3838.

The present doctoral dissertation is based on the following original publications and early stage research projects listed below:

LIST OF ORIGINAL PUBLICATIONS

- I** **Mellini, P.**; Carafa, V.; Di Rienzo, B.; Rotili, D.; De Vita, D.; Cirilli, R.; Gallinella, B.; Provvvisiero, D.P.; Di Maro, S.; Novellino, E.; Altucci, L.; Mai A. Carprofen Analogues as Sirtuin Inhibitors: Enzyme and Cellular Studies. *Chem Med Chem* **2012**, 7: 1905-1908.
- II** Rotili, D.; Tarantino, D.; Nebbioso, A.; Paolini, C.; Huidobro, C.; Lara, E.; **Mellini, P.**; Lenoci, A.; Pezzi, R.; Botta, G.; Lahtela-Kakkonen, M.; Poso, A.; Steinkühler, C.; Gallinari, P.; De Maria, R.; Fraga, M.; Esteller, M.; Altucci, L.; Mai A. Discovery of Salermide-Related Sirtuin Inhibitors: Binding Mode Studies and Antiproliferative Effects in Cancer Cells Including Cancer Stem Cells. *J Med Chem* **2012**, 55: 10937-10947.
- III** **Mellini, P.**; Kokkola, T.; Suuronen, T.; Salo, H.; Tolvanen, L.; Mai, A.; Lahtela-Kakkonen, M.; Jarho, E.M. Screen of Pseudopeptidic Inhibitors of Human Sirtuins 1-3: Two Lead Compounds with Antiproliferative Effects in Cancer Cells. *J Med Chem* **2013**, 56: 6681-6695.
- IV** Kokkonen, P.; **Mellini, P.**; Nyrhilä, O.; Rahnasto-Rilla, M.; Poso, A.; Lahtela-Kakkonen, M.; and Jarho, E.M. QSAR Modeling in the Design of Pseudopeptidic SIRT1 Inhibitors. *Eur J Pharm Sci* (manuscript in preparation)

In publication **I**, the present PhD student Paolo Mellini has cured the design and synthesis of the carprofen analogues, moreover the design of each experiment. Enzymatic and cellular assays showed in the thesis have been carried out mainly by Dr. Vincenzo Carafa and other co-authors.

In publication **II**, the present PhD student Paolo Mellini has cured homology modelling and docking simulations. Synthetic work, enzymatic and biological assays are an exclusive contribution of the other co-authors and are only partially included in the thesis.

In publication **III**, the present PhD student Paolo Mellini has cured the design, synthesis, homology modelling and molecular docking, moreover the design of each experiment. Enzymatic and cellular assays showed in the thesis have been carried out by the other co-authors.

In publication **IV**, the present PhD student Paolo Mellini has cured the main part of synthetic work. Molecular modelling, QSAR and part of the synthesis of compounds are an exclusive contribution of Piia Kokkonen and are not included in the thesis.

EARLY STAGE RESEARCH PROJECTS

I Mellini, P.; Kokkola, T.; Suuronen, T.; Nyrhilä, O.; Leppänen, J.; Mai, A.; Lahtela-Kakkonen, M. and Jarho, E.M. Design and Synthesis of Pseudopeptidic and Peptidic Activity-Based Probes as SIRT1-3 Inhibitors. Useful Tools in Understanding their Subcellular Localization and Specificity.

II Mellini, P.; Carafa, V.; Altucci, L.; Mai A. Design and Synthesis of Pyridinium Salts as Inhibitors of Human Sirtuins.

CONTENTS

1 GENERAL INTRODUCTION.....	1
2 SIRTUINS	3
2.1 Discovery and identification.....	3
2.2 Mechanism of Sirtuin deacetylation	4
2.3 Sirtuins catalytic core domain.....	7
2.4 NAD ⁺ binding site	7
2.5 Substrate binding site.....	9
3 THE SEVEN HUMAN ISOFORMS SIRT1-7 AND THEIR BIOLOGICAL RELEVANCE IN DISEASE.....	11
3.1 Sirtuins and metabolic functions.....	17
3.2 Sirtuins and cancer.....	20
3.2.1 SIRT1 and breast cancer	22
3.2.2 SIRT1 and prostate cancer	23
3.2.3 SIRT1 and lung cancer	23
3.2.4 SIRT1 and liver cancer	24
3.2.5 SIRT1 in lymphoma and leukemia	25
3.2.6 SIRT1 and neuroblastoma	25
3.2.7 SIRT1 and pancreatic cancer	26
3.2.8 SIRT1 and colorectal cancer.....	26
3.2.9 SIRT1 and gastric cancer	27
3.3 SIRT1 and polycystic kidney disease	28
3.4 Sirtuins and neurodegenerative disease	28
3.4.1 SIRT1 and Alzheimer's disease.....	28
3.4.2 SIRT1, SIRT2 and Huntington's disease.....	29

3.4.3 SIRT2 and Parkinson's disease.....	30
3.4.4 SIRT2 and Wallerian degeneration.....	30
4 SIRTUIN INHIBITORS	31
4.1 Adenosine mimetics.....	31
4.2 AGK2.....	32
4.3 Anilinobenzamides	32
4.4 Cambinol and its derivatives.....	33
4.5 Chroman-4-one derivatives.....	34
4.6 EX-527.....	35
4.7 NAD ⁺ analogues	36
4.8 Peptides and Pseudopeptides	37
4.9 Sirtinol/Salermide derivatives.....	45
4.10 Splitomicin and its derivatives.....	47
4.11 Suramin.....	48
4.12 Tenovin and its derivatives	49
4.13 Thienopyrimidine.....	50
4.14 Thiobarbiturates	51
4.15 Miscellaneous Inhibitors.....	52
5 SIRTUIN ACTIVATORS	55
6 AIMS OF THE STUDY	62
7 CARPROFEN ANALOGUES AS SIRTUIN INHIBITORS: ENZYME AND CELLULAR STUDIES	63
6.1 Introduction.....	64
6.2 Chemistry.....	64
6.3 Results and discussion	65
6.4 Conclusions.....	69

6.5 Experimental Section.....	70
7 DISCOVERY OF SALERMIDE-RELATED SIRTUIN INHIBITORS: BINDING MODE STUDIES AND ANTIPROLIFERATIVE EFFECTS IN CANCER CELLS INCLUDING CANCER STEM CELLS	79
7.1 Introduction.....	80
7.2 Results and discussion	80
7.3 Conclusions.....	87
7.4 Experimental Section.....	88
8 SCREEN OF PSEUDOPEPTIDIC INHIBITORS OF HUMAN SIRTUINS 1-3: TWO LEAD COMPOUNDS WITH ANTIPROLIFERATIVE EFFECTS IN CANCER CELLS	96
QSAR MODELING IN THE DESIGN OF PSEUDOPEPTIDIC SIRT1 INHIBITORS.....	96
8.1 Introduction.....	97
8.2 Chemistry.....	99
8.3 Results and discussion	100
8.4 Conclusions.....	121
8.5 Experimental Section.....	123
9 DESIGN AND SYNTHESIS OF PSEUDOPEPTIDIC AND PEPTIDIC ACTIVITY-BASED PROBES AS SIRT1-3 INHIBITORS. USEFUL TOOLS IN UNDERSTANDING THEIR SUBCELLULAR LOCALIZATION AND SPECIFICITY.....	152
9.1 Introduction.....	153
9.2 Chemistry.....	153
9.3 Results and discussion	159
9.4 Conclusion	162
9.5 Experimental Section.....	163

10 DESIGN AND SYNTHESIS OF PYRIDINIUM SALTS AS INHIBITORS OF HUMAN SIRTUINS	172
10.1 Introduction.....	173
10.2 Chemistry.....	174
10.3 Results and discussion	174
10.4 Conclusions.....	177
10.5 Experimental Section.....	178
11 REFERENCES	182

1 GENERAL INTRODUCTION

Proteins that bind DNA to form eukaryotic chromosome are divided in two general classes : histones and non-histone proteins. The structural complex created between these two classes and nuclear DNA is known as chromatin, that is a dynamic entity that change its shape in each phase of cellular cycle.

Half of chromatin weight is constituted by proteins that in mayor part are histones. There are five main classes of histones: H1, H2a, H2b, H3, H4 containing residues positively charged (Arg, Lys) that allow to interact with DNA phosphoric groups negatively charged.¹ The aminoacid sequences of histones H2a, 2b, 3, and 4 are highly conserved and this evolutionary stability let understand that these proteins have a well-adapted structure that is become intolerant to each variation. The histones are subjected to post-translational modifications and most of them are reversible and tend to decrease the histones positive charge that result in an alteration to their ability to bind DNA. The histones are responsible of the first level in the chromosome organization, the nucleosome. The structural organization has been determined by Roger Kornberg in 1974, by suggesting that nucleosome, were formed by histone octamer $(H2a)_2(H2b)_2(H3)_2(H4)_2$ associated with DNA in which H1 played a not well defined role¹ (Figure 1).

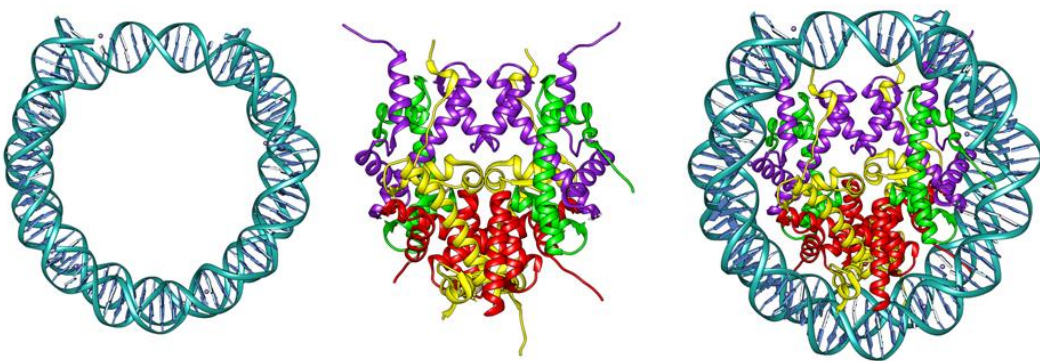


Figure 1. Crystal structure of nucleosome PDB: 3AFA.² UCSF Chimera 1.7

The histone covalent modifications such as acetylation, methylation, phosphorylation and ubiquitination are responsible for the compartmentalization of the genome as transcriptionally silent heterochromatin or active euchromatin. These modifications allow the regulation of nuclear processes such as replication, transcription and

chromosome condensation.³ Alterations and dysfunctions of the normal operations of these processes can be at the basis of different pathologies.^{4,5}

The most studied epigenetic marks are histone acetylation⁶ and methylation that are coupled to various cellular functions such as DNA recognitions by proteins, DNA-protein interactions, protein stability etc.^{7,8} The DNA transcriptional silencing is associated to histone hypoacetylation mediated by HDAC, while genomic transcriptional activation involves histone acetylation HAT catalysed.

In eukaryotes the deacetylases are grouped in four classes I-IV according to their homology to yeast prototypes. The sirtuin family constitutes class III (SIRT1-7) and have no similarity to other HDACs; Class I members are Rpd3-like, include HDAC1-3 and 8. HDAC4, 5, 7, 9 being to class IIa while HDAC6 and 10 to IIb; finally the class IV is made by HDAC11.⁹

2 SIRTUINS

2.1 Discovery and identification

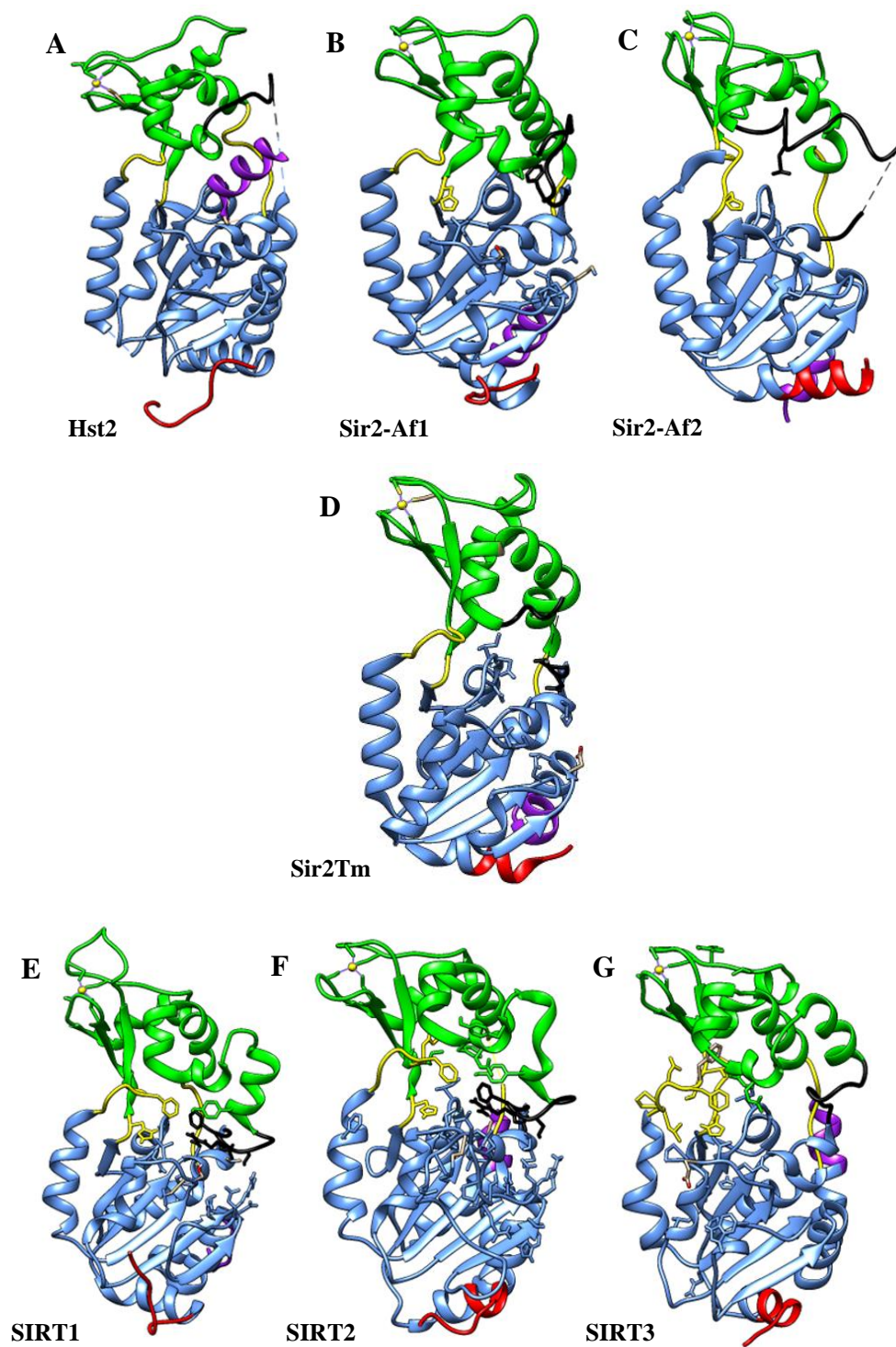
In 1979 the first sirtuin Sir2 from *S. cerevisiae* originally known as MARI (mating-type regulator 1) has been discovered by Klar and co-workers.¹⁰ Ten years later Gottlieb and Esposito¹¹ proved that SIR2's (silent information regulator) function is not restricted to controlling mating type expression but also may function in excluding the rDNA region from the general recombination system.¹¹ In 1991 Gottschling and co-workers¹² showed that SIR genes are involved in a general mechanism for silencing chromosomal domains in *S. cerevisiae* by providing a complete silencing at HML (Hidden MAT Left) and HMR (Hidden MAT Right) preventing switching from the silent to the active transcriptional state. After two years in 1993 Braunstein¹³ demonstrate that the silencing of silent mating-type cassettes and telomeres is strictly associated with acetylation of the epsilon-amino groups of lysine in the amino-terminal domains of three of the four core histones. The SIR2 overexpression induced a substantial histone deacetylation, an additional characteristic that distinguished SIR2 from other SIR genes. In 1995 Brachman¹⁴ and Derbyshire¹⁵ discovered four *Saccharomyces cerevisiae* homologs of the SIR2 silencing gene (HSTs), as well as conservation of this gene family from bacteria to mammals. They found that HST1 was closely related to SIR2, showing 71% sequence identity over 84% of its length. Polymerase chain reaction with degenerate primers on *S. cerevisiae* DNA, identified three additional SIR2-related genes designated HST2, HST3 and HST4. In addition, HST3 and HST4 together were able to influence cell cycle progression and genomic stability, establishing new connections between silencing and these fundamental cellular processes. In 1999 and 2000 Frye^{16,17} discovered seven human sirtuins (SIRT1-7) of which SIRT1 showed the closest homology to the *S. cerevisiae* Sir2p. Furthermore Frye¹⁷ carried out a molecular phylogenetic analysis of 60 sirtuin conserved core domain sequences from a diverse array of organisms (including Achaeans, bacteria, yeasts, plants, protozoans, and metazoans) that allowed their classification into four main branches classes I-IV. Prokaryotic sirtuins are included in classes II and III. Gram positive bacteria and *Thermotoga maritime* sirtuins being to class V. *Saccharomyces*

cerevisae has class I sirtuins. *Caenorhabditis elegans* and *Drosophila melanogaster* have sirtuin genes from classes I, II, and IV. Finally the seven human sirtuin genes include all four classes: SIRT1, SIRT2, and SIRT3 are class I, SIRT4 is class II, SIRT5 is class III, and SIRT6 and SIRT7 are class IV. Close to the end of 2000 Landry¹⁸ and Smith¹⁹ described the importance of NAD⁺ in the deacetylation reaction catalyzed by the SIR2 family of enzymes.²⁰ They showed that the products of the reaction detected by HPLC analysis were ADP-ribose, nicotinamide, and a deacetylated peptide substrate, indicating that deacetylation involves the hydrolysis of one NAD⁺ to ADP-ribose and nicotinamide for each acetyl group removed. Subsequent crystallographic (will be discussed in details in a separate paragraph) studies have allowed to precisely define the catalytic core domain. After 34 years more than three thousand publications that touch the sirtuins from pharmacology, biology, biochemistry to medicinal chemistry have been written, but still a lot have to be discovered.

2.2 Mechanism of Sirtuin deacetylation

Sirtuins as introduced previously being to the III class of histone deacetylases and are NAD⁺ dependent enzymes. From yeast to humans they contain an highly conserved catalytic core domain formed by 275 amino acid (Figure 2) and N, C-terminal extension, that are variable in length and sequence that can affect the binding with interacting partners, mediate interactions with other sirtuin forms, and direct cellular localization. In mammals there are seven sirtuin isoforms (SIRT1-7) that are able to catalyze substrate specific deacetylation.^{18,21} SIRT4²² and SIRT6 possess mainly NAD⁺-dependent mono-ADP-ribosyltransferase activity. Recently has been reported that SIRT5 has potent demalonylase/ desuccinylase activity²³ and deacylation reaction can be catalyzed by SIRT6.^{24,25} The poor deacetylases activity showed by SIRT6 in vitro seems depends on specific conditions, in which SIRT6 activity is nucleosome dependent and its binding to the nucleosome might convert it into an active structure.²⁴ The accepted deacetylation mechanism (Figure 3) begins with Michaelis complex formation (when both NAD⁺ and substrate are bound) and start with a nucleophilic attack of C1' nicotinamide ribose moiety by the carbonyl oxygen

of the lysine substrate through S_N2 mechanism that led the nicotinamide cleavage and the 1'-*O*-alkylamidate intermediate formation.



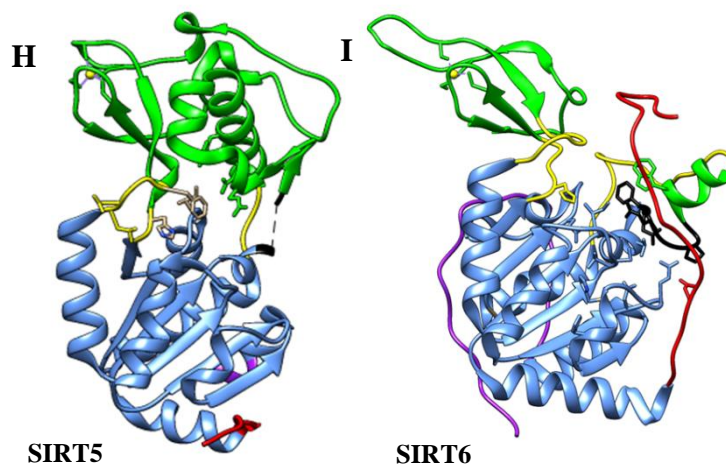


Figure 2. Crystal structure of sirtuins. The small domain is colored in green, the Rossmann-fold domain in cornflower blue, the connection loops in yellow, the cofactor binding loop in black, the N-terminal in red and the C-terminal in magenta. (A) *S.cerevisiae* Hst2 (PDB: 1Q14). (B) *A. fulgidus* Sir2-Af1 (PDB: 1ICI). (C) *A. fulgidus* Sir2-Af2 (PDB: 1MA3). (D) *T.maritima* Sir2Tm (PDB: 2H4J). (E) *H. sapiens* SIRT1 (PDB: 4IF6). (F) *H. sapiens* SIRT2 (PDB: 3ZGV). (G) *H. sapiens* SIRT3 (PDB: 3GLR). (H) *H. sapiens* SIRT5 (PDB: 4F4U). (I) *H. sapiens* SIRT6 (PDB: 3ZG6). UCSF Chimera 1.7.

Once the nicotinamide has been released it can rebinds in the C-pocket and react with the intermediate to reform NAD^+ . In this step Phe33 (Sir2Tm numbering) appears to play a role as gatekeeper in the nicotinamide exchange reaction in which it helps to shield the *O*-alkylamidate intermediate from free nicotinamide. After the formation of 1'-*O*-alkylamidate intermediate, the 2'-hydroxyl group of the ribose is activated by a conserved His116 (Sir2Tm numbering) to afford 1', 2'-cyclic intermediate (Figure 3). Then a protonated histidine can act as acid, protonates the amino-acetal and led the deacetylated substrate release. Finally an activated water molecule attacks the cyclic intermediate to furnish 2'-*O*-acetyl-ADP ribose (might be in equilibrium with its corresponding 3' isomer).^{26,27}

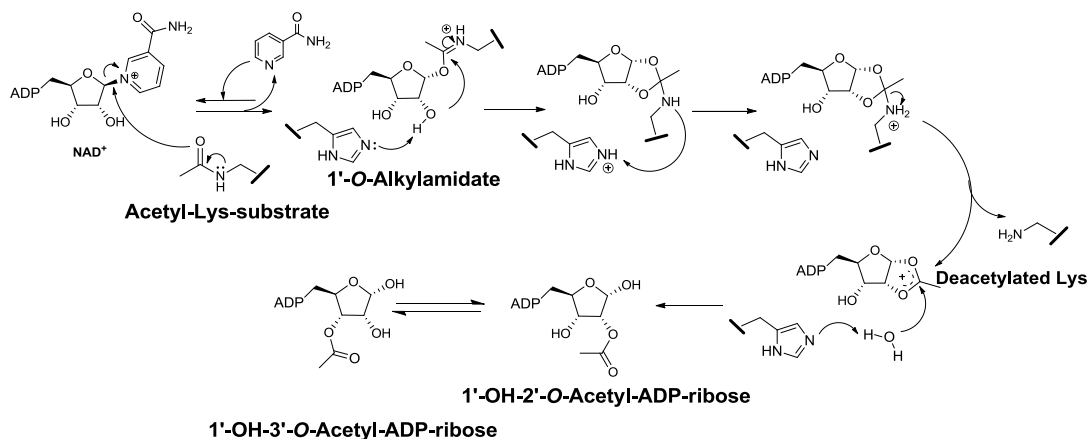


Figure 3. Mechanism of sirtuin deacetylation.

2.3 Sirtuins catalytic core domain

The sirtuins catalytic region (Figure 2) consists of a Rossmann-fold (light blue) a zinc-binding domain (green) and connecting loops (yellow). The loops between the two domains form a cleft where NAD⁺ and Ac-Lys substrate can bind the enzyme. For instance the human SIRT1 catalytic core domain is composed of a central six-stranded β -parallel sheet (β 1- β 3 and β 7- β 9) and height α helices (α A, α B, α B, α H and α J- α M), the Zn²⁺ binding domain (also called small domain) is composed of three β strands (β 4- β 6) and five α helices (α C- α F and α I) in which the Zn²⁺ ion is tetrahedrally coordinated by four cysteine residues Cys371, Cys374, Cys395 and Cys398.²⁸ The Zn ion is located far from the active site, it does not participate directly to the catalytic mechanism like for class I/II but its presence is essential for deacetylase activity in fact seems to be required in order to holding together the β strand in the small domain. The small domains of the eukaryotic enzymes show variability among three-dimensional topology. Differently to SIRT2 and SIRT3, SIRT5 has an insertion loop that blocks a groove between the zinc binding motif and the helical bundle region. One explanation is probably that the small domains play a role in the needs to discriminate the substrates or in the protein-protein interactions.

2.4 NAD⁺ binding site

The connection loops together with large and small domain form a cleft in which substrate and the cofactor (NAD⁺) can bind. This region is highly conserved and has the highest homology sequence among the protein sequence; indeed mutations of its

residues can drastically reduce the enzymatic activity. The NAD^+ binds in a cleft adjacent to the acetyl lysine side chain that is formed by three pockets: A, B, C (Figure 4). The adenine-ribose binding site (pocket A) is an exposed surface area in which adenine has, van der Waals interaction with Leu215, Val232, Gly23 (Sirt2Tm numbering PDB code: 2H4F), H bonds with backbone amides Leu215, Val232 and side chains Asp231 and Thr26. The ribose moiety has H bond with Gly216 and van der Waals contact with Ser189.²⁶ The phosphate groups binds between A and B pockets and show several H bonds with Ala22, Phe33, Arg34, Ser189, Ser190 and with a conserved water molecule.²⁶ Conserved residues His116 and Phe33 located in the B pocket makes H bonds and van der Waals interactions with the nicotinamide ribose ring. Finally the nicotinamide moiety is positioned in hydrophobic cavity the so called C pocket and forms H bonds interactions with Ile100, Asp101 and a conserved water molecule.²⁶ The NAD^+ binding conformation object of crystallographic studies has been found be influenced by the occupancy of the lysine binding tunnel. The substrate binding, promotes the burial of the nicotinamide ring in the C pocket that seems destabilize the glycosidic bond between nicotinamide and ribose with a potential disruption of the electronic resonance and promotes NAD^+ to adopt a strained conformation required for deacetylation activity. One of the connection loops is called cofactor binding loop (in black) that form part of NAD^+ binding site, may play also a role during the catalytic reaction steps. It shows an interesting dynamism and its conformation depends on what is bound in the substrate/cofactor binding site. The cofactor binding loop is disordered when NAD^+ is not bound and becomes ordered when both substrate and cofactor are bound. Recently Steegborn and co-workers²⁹ have reported a well defined SIRT2 crystal structures in which the cofactor binding loop is perfectly defined in both the apo- and the ligand-bound state, confirming that the binding of NAD^+ and the substrate induce its structural rearrangements.

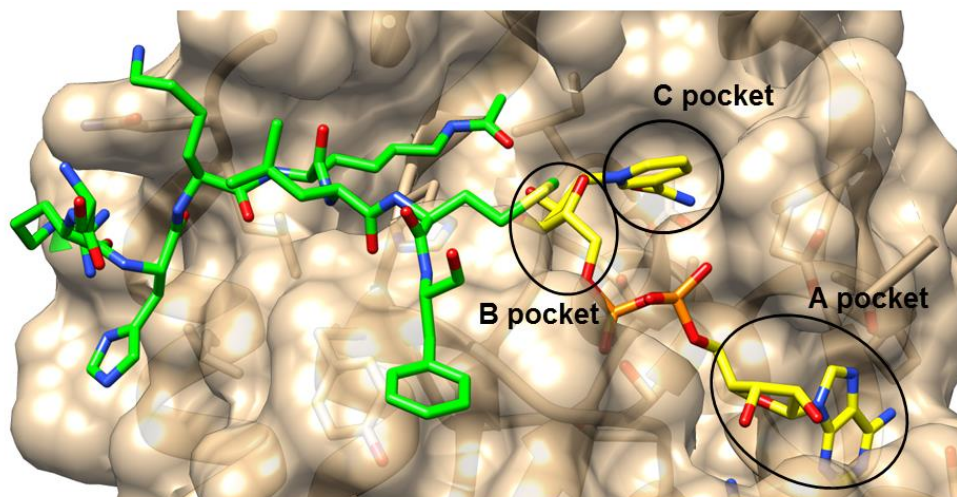


Figure 4. NAD⁺ binding site overview (PDB: 2H4F). The peptidic substrate is colored in green and NAD⁺ is colored in yellow. UCSF Chimera 1.7.

2.5 Substrate binding site

The peptide substrate binds to the cleft between the small and the large domains with the acetyl-lysine placed into a hydrophobic tunnel located within the cleft. Main chain atoms of the peptide substrate for instance AceCS2 peptide in SIRT3 (Figure 5) make several hydrogen bonds with main chain atoms of one connection loop (Val292, Gly295, Glu296) and another loop from the large domain (Glu323, Glu325) of the protein (SIRT3 numbering PDB code : 3GLR).³⁰

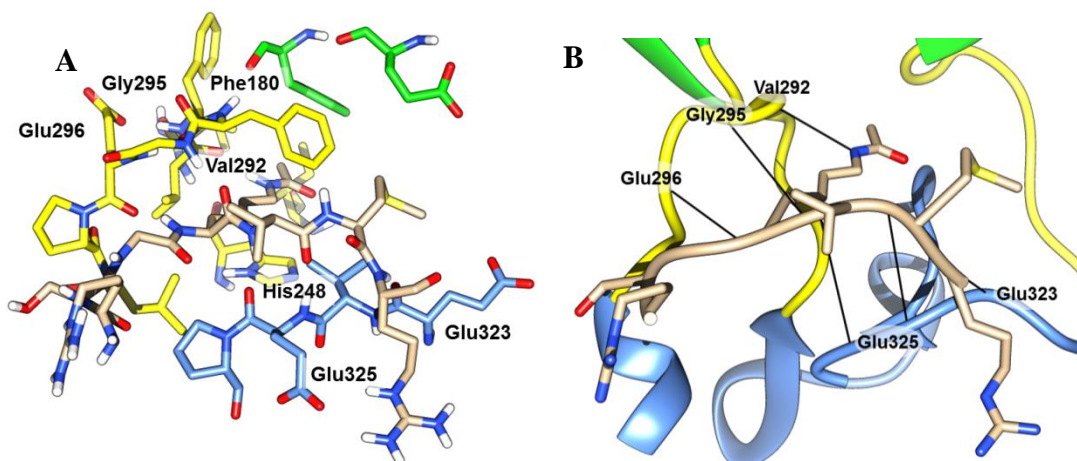


Figure 5. AceCS2-K_{ac} peptide in complex with SIRT3 (PDB: 3GLR). Residues belonging to small domain are colored in green, connection loops in yellow, large

domain in cornflower blue and acetylated substrate in default color. (A) Substrate binding site around the acetylated lysine. (B) Substrate binding site represented in ribbon, and main H-bonds are represented by black lines. UCSF Chimera 1.7.

The lysine acetyl group is sandwiched between His248 and Phe180 (SIRT3 numbering). His248 has been found to be critical for the deacetylation activity of sirtuins and is conserved in all the SIRT isoforms SIRT1-7. A comparison of sirtuin crystal structures has suggested that both peptide and NAD^+ binding induce a significant shift in the position of the cofactor loop but also of the small domain, indeed not significant shift can be seen for the large domain (Figure 6). A direct overlay between SIRT3 crystal structure in apo-form and bound with a trapped intermediate, confirm that the protein bioactive conformation is characterized by a close conformation, in which the two domains result more closer to each other and this led the residue organization in the binding site for the deacetylation reaction (Figure 6).

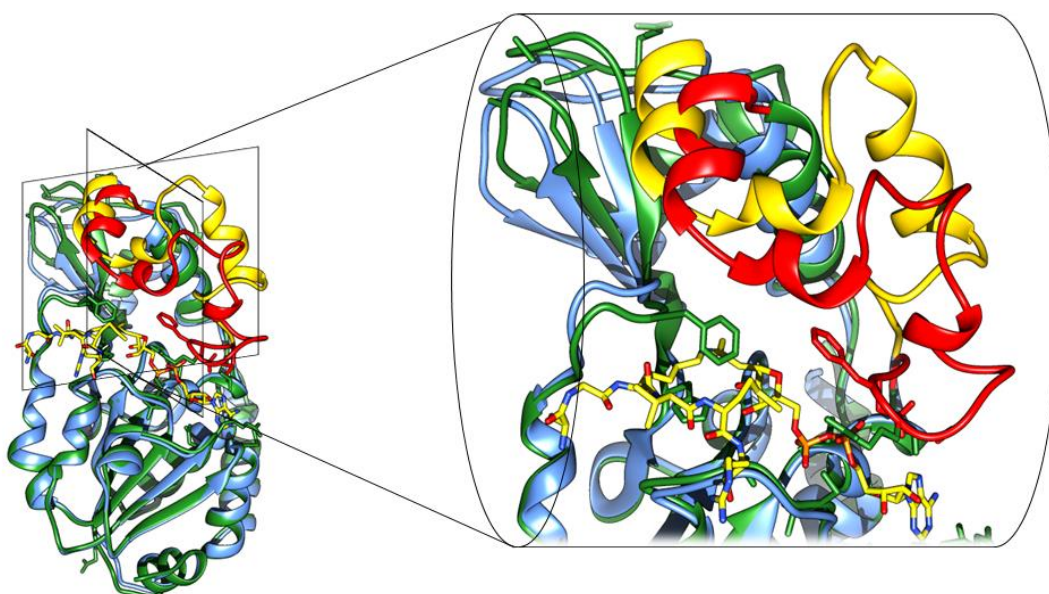


Figure 6. A superimposition between SIRT3 apoform (cornflower blue PDB: 3GLS) and SIRT3 bound with trapped AceCS2- K_{SAC} -ADPR (green PDB: 3GLT) are represented in ribbon (left). Superimposition that evidence the shift of cofactor binding loop from SIRT3 apoform (yellow) to SIRT3 bound with trapped AceCS2- K_{SAC} -ADPR (red) are represented on the right window. UCSF Chimera 1.7.

3 THE SEVEN HUMAN ISOFORMS SIRT1-7 AND THEIR BIOLOGICAL RELEVANCE IN DISEASE

The seven isoforms SIRT1-7 are differently located within the cellular compartments (Table 1) and it depends upon cell type, stress conditions and interaction with other proteins.³¹ SIRT1, SIRT6 and SIRT7 being nuclear.³¹ SIRT1 can be also found in cytoplasm in which SIRT2³² is predominantly located. SIRT3,³³ 4,²² 5³¹ are localized to the mitochondria but SIRT3 localization is still debated because of its potential translocation to the nucleus under cellular stress conditions. As reviewed by Chen³⁴ sirtuins show histone and several non-histone substrates and it can explain the wide range of biological processes in which this enzymes are involved (Table 2-5).

Table 1. Cellular localization and activity of Sirtuins

Sirtuin	Molecular mass	Cellular localization	Activity
SIRT1	82 kDa	Nucleus and Cytoplasm	Deacetylase
SIRT2	43 kDa	Cytoplasm and Nucleus	Deacetylase
SIRT3	45 kDa (nuclear encoded with N terminal mitochondrial targeting sequence) 28 kDa (after mitochondrial cleavage)	Mitochondria and Nucleus ?	Deacerylase
SIRT4	35 kDa	Mitochondria	ADP-ribosyl- transferase Weak Deacetylase
SIRT5	34 kDa	Mitochondria	Deacetylase Demalonylase Desuccinylase
SIRT6	39 kDa	Nucleus	Deacetylase Deacylase ADP-ribosyl- transferase

SIRT7	45 kDa	Nucleolus and Cytoplasm	Deacetylase
	47.5 kDa (Cytoplasmic SIRT7)		

Table 2. SIRT1 substrates an overview

SIRT1 substrates	SIRT1 functions
AceCS1 (K661) (acetyl-CoA synthetase1)	Promotes AceCS1 activity and metabolism
Akt, PDK1 (protein kinase B, phosphoinositide-dependent protein kinase 1)	Enhances their binding with PIP3 and membrane localization during tumorigenesis and cardiac hypertrophy
Androgen receptor	Represses dihydrotestosterone-induced androgen receptor signaling
APE1 (apuric/aprimidinic endonuclease-1)	Promotes base excision repair activity
ATG (autophagy genes Atg5, 7 and Atg8)	Promotes autophagy
β-catenin	Suppress its ability to activate transcription and to drive cell proliferation
BMAL1 (heterodimeric basic helix-loop-helix transcription factor)	Modulates CLOCK-mediated chromatin remodeling and circadian control
CIITA (class two transactivator of histocompatibility complex II (MHC II))	Augments MHC II transcription by protecting CIITA from proteasomal degradation and promoting nuclear accumulation
c-MYC (transcription factor that activates expression of many genes through binding on consensus sequences)	Stabilizes or destabilizes C-MYC oncoprotein
Cortactin (monomeric protein located in the cytoplasm when activated promote polymerization and rearrangement of the actin cytoskeleton)	Promotes cell migration
CRTC1 (CREB-regulated transcription coactivator 1)	Activates TORC1 by promoting its dephosphorylation and its interaction with CREB for neuroprotection
CRTC2	Attenuates CRTC2 activity and glucose output during fasting

DNMT1 (DNA methyltransferase 1)	Deacetylation of lysines on DNMT1
EVI1 (ecotropic viral integration site 1)	Triggers EVI1 degradation
eNOS (endothelial nitric oxide synthetase)	Stimulates eNOS activity, increases endothelial nitric oxide, promotes endothelium-dependent vascular relaxation
ERα (estrogen receptor alpha) ?	Represses its DNA binding and transcriptional activity
FOXO1 (forkhead box protein O1)	Potentiates FOXO1-mediated transcription through its deacetylase activity
FOXO3a (forkhead box protein O3)	Increases FOXO3's ability to induce cell cycle arrest and resistance to oxidative stress but inhibits FOXO3's ability to induce cell death
FOXO4 (forkhead box protein O4)	Cell survival upon oxidative stress
FOXp3 (forkhead box P3)	Promotes its degradation
FXR (nuclear bile acid receptor)	Decreases its stability but enhances transactivation activity in lipid and glucose metabolism regulation
HIF1α (hypoxia inducible factor 1-alpha)	Inactivates HIF-1 alpha under hypoxia
HIF2α (hypoxia inducible factor 2-alpha)	Promotes HIF-2 signaling during hypoxia
Histone H1 (K26), H3 (K9, K56), H4 (K16)	Transcription regulation and chromatin function
HSF1 (heat shock protein 1)	Prolongs HSF1 binding to the heat shock promoter Hsp70
Ku70 (protein that together with Ku80 make up the Ku heterodimer, which binds to DNA)	Promotes DNA repair activity
LXR (K432) (Liver X receptor)	Positively regulates its function for cholesterol and lipid homeostasis
MeCP2 (Methyl-CpG binding protein 2)	Promotes MeCP2-mediated BDNF expression
MMP2 (matrix metalloproteinase 2)	Enhances MMP2 protein stability
MyoD (protein that regulates muscle differentiation. MyoD belongs to myogenic regulatory factors (MRFs))	Inhibits myogenesis
NBS1 (nijmegen breakage syndrome protein)	Maintains NBS1 in a hypoacetylated state,

1)	which is required for ionizing radiation-induced NBS1 Ser343 phosphorylation
NF-κB p65 (nuclear factor kappa-light chain enhancer of activated B cells)	Reduces NF-κB transcriptional activity, augments apoptosis in response to TNFα
NHLH2 (nescient helix loop helix 2)	Activates MAO-A to mediate anxiety
N-MYC (proto-oncogene protein)	Promotes protein stability
NICD (notch 1 intracellular domain)	Acts as a negative modulator of Notch signaling in endothelial cells
NoRC (nitric oxide reductase)	Leads to enhanced promoter-associated RNA binding and an increase in heterochromatic histone marks
p300 (K1020/K2014) (play an essential role in regulating cell growth and division)	Represses its transactivation activity
p53 (K382) (tumor suppressor)	Promotes cell survival under stress
p73	Suppression of transcriptional activity and apoptosis p73 mediated
PARP1 (poly(adenosine diphosphate ribose) polymerase 1)	Promotes cell survival under stress
PER2	Promotes PER2 degradation to regulate circadian clock gene expression
PGC1α (peroxisome proliferator-activated receptor gamma coactivator 1-alpha)	Positively and negatively controls gene expression for glucose homeostasis
PIP5 Kγ (phosphatidylinositol 4-phosphate 5-kinase)	Regulates thyroid-stimulating hormone release by enhancing PIP5 Kgamma activity
PTEN (phosphatase and tensin homolog)	Modulates PTEN interaction with PDZ domain-containing proteins
RARβ (retinoic acid receptor beta)	Activates alpha-secretase gene ADAM10, suppresses beta-amyloid production
Rb (retinoblastoma tumor suppressor protein)	Inactivates retinoblastoma tumor suppressor protein
Smad7 (mothers against decapentaplegic homolog 7)	Inhibits transforming growth factor beta-induced apoptosis in glomerular mesangial cells

SREBP-1C (sterol regulatory element-binding protein)	Inhibits SREBP-1C activity in regulation of hepatic lipid metabolism
STAT3 (signal transducer and activator of transcription 3)	Suppresses the inhibitory effect of STAT3 on gluconeogenesis
Survivin (inhibitor of apoptosis)	Suppresses survivin thus inhibits cell survival
SUV39H1 (Histone-lysine N-methyltransferase)	Increases SUV39H1 activity during heterochromatin formation
Tat (trans-activating proteins)	Facilitates the recycling of Tat Inhibits their acetyltransferase activity and promotes their degradation in DNA damage response
Tip60, hMOF (histone acetyl transferase)	Increases its helicase and exonuclease activities, promotes its translocation from nucleoplasm to nucleoli after DNA damage
WRN (Werner syndrome)	Inhibits its transcriptional activity
XBPIs (X-box binding protein)	Promotes nucleotide excision repair activity
Xpa, Xpc (xeroderma pigmentosum group A, B)	

Table 3. SIRT2 substrates an overview

SIRT2 substrates	SIRT2 functions
α-tubulin	Abrogates resistance to axonal degeneration
CDH1, CDC20 (cadherin protein , cell-division cycle protein 20)	Promotes their degradation and cell cycle exit
FOXO1	Inhibits adipocyte differentiation
FOXO3a	Mediated its degradation
Histone H3K56	Inhibits its assembly into chromatin in response to DNA damage
Histone H4K16	Promotes cell cycle G2/M transition
Keratin 8 (K207) (cytoskeletal keratin protein)	Increases its solubility
NF-kB p65 (K310)	Suppresses NF-kB dependent gene expression
p53 (K382)	Increase its instability
p300	Promotes its transcription
PAR-3 (protease activated receptor 3)	Regulates myelin formation

PEPCK1 (phosphoenolpyruvate carboxykinase 1)	Stabilizes PEPCK1 for gluconeogenesis
PR-Set7 (histone-lysine N-methyltransferase)	Increases its chromatin localization
RIP1 (receptor interaction protein 1)	Required for programmed necrosis

Table 4. SIRT3-5 substrates

Sirtuins	Substrate	Sirtuin function
SIRT3	AceCS2 (K642)	Promotes AceCS2 activity
	Cyclophilin D	Induces dissociation of hexokinase II from the mitochondria and suppress age related cardiac hypertrophy
	FOXO3a	Promotes its nuclear localization and mitochondrial biogenesis
	GDH (glutamate dehydrogenase)	Increases its activity
	Histone H4K16	Gene transcription
	IDH2 (K413) (isocitrate dehydrogenase 2)	Activates its activity and protects the cells from oxidative stress, prevents age-related hearing loss under caloric restriction
	Ku70	Protects cells from stress mediated cell death
	LCAD (K318/K322) (long chain Acyl CoA dehydrogenase)	Increases its enzymatic activity
	LKB1 (liver kinase B1)	Activates LKB1 and increase the activity of the LKB1-AMPK pathway
	HMGCS2 (mitochondrial 3-hydroxy-3-methylglutaril coenzyme A synthase 2)	Enhances its enzymatic activity
	MnSOD (manganese superoxide dismutase)	Enhances its enzymatic activity
	MRPL10 (mitochondrial ribosomal protein)	Suppress translational activity of mitochondrial ribosomes
	NDUFA9 (NADH dehydrogenase (ubiquinone))	Augments complex I activity of the electron transport chain
	OTC (ornithine transcarbamoylase)	Stimulates its activity

	SDH (succinate dehydrogenase)	Promotes its enzyme activity
SIRT4	GDH (glutamate dehydrogenase)	Mono-ADP-ribosylates it, reduces GDH activity
	MCD (K741) (malonyl coenzyme A decarboxylase)	Deacetylase and inhibits the activity of MCD
SIRT5	CPS1 (carbamoyl phosphate synthetase 1)	Deacetylase and upregulates its activity to regulate the urea cycle
	Pyruvate and Succinate dehydrogenase	Desuccinylates and represses their biochemical activity and thus cellular respiration

Table 5. SIRT6 and SIRT7 substrates

Sirtuins	Substrate	Sirtuins function
SIRT6	CtIP (C-terminal binding protein interaction protein)	Deacetylates it promote DNA end resection
	DNA-PK (DNA dependent protein kinase)	Deacetylates and stabilizes it at chromatin for DNA double-strand break repair
	GCN5 (histone acetyltransferase)	Enhances GCN5vactivity to acetylate PGC1 α and suppresses hepatic glucose production
	Histone H3K56	Deacetylates to promote genomic stability
	Histone H3K9	Deacetylates to maintain telomeric chromatin
	PARP1	Mono-ADP-ribosylates it and stimulates its poly-ADP-ribosylase activity
	TNF-α	Remove the fatty Acyl modifications on K19 and K20 to promote TNF- α secretion
SIRT7	Histone H3K18	Maintains the transformation phenotype of cancer cells

3.1 Sirtuins and metabolic functions

SIRT1 exert profound effects on metabolic pathways such as lipogenesis, stimulation of fatty acid β -oxidation and gluconeogenesis. Overexpression of SIRT1 by knock-in generates phenotypes in mice similar to calorie restriction conditions, on contrary SIRT1^{-/-} mice die shortly after birth. SIRT1 is involved in the regulation of the food

intake and has been shown to affect lipogenesis through the regulation of acetyl CoA synthetase and PPAR γ . An interesting study by Xu et al.³⁵ carried out by using 129 SIRT1^{+/-} mice, shows that a reduction of SIRT1 activity increased a risk of fatty liver by increase in lipogenesis, reduction in fat export and inflammation of epididymal adipose tissue. SIRT1 deficiency increased PPAR γ and NF-kB activity in the liver in response to dietary fat. SIRT1 inhibits lipid accumulation and promotes lipid mobilization in adipocytes through inhibition of PPAR γ activity. Another mechanism that connects SIRT1 with fatty acid oxidation involves the deacetylation of PGC1 α that increases the expression of PPAR α gene targets promoting catabolism of fatty acids. On the contrary, an opposite role seems to be played by GCN5 that acetylates PGC1 α with a resulting inhibitory effect on this system. A balance between SIRT1 and GCN5 activity might be fundamental for induction of PPAR α gene targets.³⁶ In pancreatic β cells, SIRT1 is implicated in control of metabolic glucose by repression of UCP2 (uncoupling protein 2) that has a role in regulating insulin secretion and glucose tolerance, moreover, it has been proposed that SIRT1 protects β cells against oxidative stress with a mechanism involving FOXO proteins.³⁷ SIRT1 plays a role in cholesterol homeostasis by a positive regulation of LXR (nuclear receptor that functions as cholesterol sensors) through deacetylation at lysine 432 in a loop adjacent to the ligand-dependent activation domain with a resulting up-regulation and promotion of cholesterol efflux from cells.³⁸

All major mitochondrial processes, such as Krebs cycle, fatty acid metabolism, antioxidant response, amino acid catabolism etc. are regulated by the balance of N^ε-lysine acetylation/deacetylation. SIRT3, the most well characterized mitochondrial sirtuin, shows a robust deacetylase activity.³⁹ SIRT3 exists as a nuclear full-length form FLSIRT3 that is processed as a result of cellular stress to the short mitochondrial form. Nuclear FLSIRT3⁴⁰ exhibits deacetylase activity coherently with the fact that SIRT3 regulates the expression and activity of nuclear genes such as PGC1 α and MnSOD and modulates FOXO3a by direct deacetylation. SIRT3 may regulate cellular energy status both at transcriptional level in the nucleus and by posttranscriptional mechanism in mitochondria. SIRT3 expression is highest in metabolically active tissues including the brain, liver, heart, brown adipose tissue and skeletal muscle.⁴¹ The levels of SIRT3 are responsive to the nutrient availability of

the cell including fasting and calorie restriction and in response to low intake SIRT3 activates a large array of proteins associated with metabolism.⁴² SIRT3 knock out mice show a reduced capacity of fatty acid oxidation in different tissues such as heart, muscle, liver and brown adipose tissue.⁴³ This may be due to LCAD (long chain acyl-CoA dehydrogenase) hyperacetylation a key fatty acid oxidation enzyme target of SIRT3. LCAD deacetylation of lysine K318 and K322 by SIRT3 has been found positively modulate its enzymatic activity by coordination of FAD (LCAD cofactor) in the active site.⁴⁴ SIRT3 has antioxidant effects mediated by deacetylation of MnSOD and isocitrate dehydrogenase 2. MnSOD the primary mitochondrial antioxidant enzyme, converts $O_2^{\cdot -}$ to H_2O_2 that is further converted in H_2O by catalase. IDH2 is an enzyme of the tricarboxylic acid cycle associated with the Krebs cycle which produces NADPH a molecule implicate in the regeneration of antioxidant. IDH2 deacetylation mediated by SIRT3 increase its activity. SIRT3 deacetylates OTC an enzyme involved in the urea cycle that might improve aminoacid catabolism during fasting. SIRT3 is involved also in energy production by deacetylation/activation of AceCS2 that catalyse the ligation of acetate with CoA to produce Acetyl-CoA, an essential molecule utilized in various metabolic pathways including fatty acid and cholesterol synthesis and the tricarboxylic acid cycle.²²

SIRT4 is located in the mitochondrial matrix and its first 28 amino acids are removed after import into mitochondria. SIRT4 exhibit prevalently ADP-ribosylase and a weak deacetylase activity. Little is known about the physiological relevance of SIRT4 and its role in metabolism. SIRT4 in pancreatic beta cells is involved in GDH regulation by ADP-ribosylation that cause the decrease of GHD activity and repression of amino acid-stimulated insulin secretion. Recently Haigis and co-workers⁴⁵ showed that SIRT4 promoted lipid synthesis and inhibition of fatty acid oxidation by deacetylation of MCD (malonyl CoA decarboxylase) an enzyme that produces acetyl CoA from malonyl CoA.

The enzymatic role of SIRT5 in metabolism is still unclear. SIRT5 has weak deacetylase activity, one of the substrate reported to be deacetylated is carbamoyl phosphatase 1 (CPS1) a key enzyme of the urea cycle. Deacetylation of CPS1 by SIRT5 was found improve the ammonia detoxification. Recently by Lin and co-workers²³ showed that SIRT5 has potent demalonylation and desuccinylation

enzymatic activity and that CPS1, IDH2, GHD and HMGCS2 are subjected to this post-translational modification. The involvement of SIRT5 in metabolic pathways need to further investigation.

The first indication of the connection between SIRT6 and metabolism was provided by Mostoslavsky et al.⁴⁶ (2006) who showed that SIRT6 deficient mice had loss of subcutaneous fat, lymphopenia and acute hypoglycaemia. SIRT6 regulates glucose homeostasis via inhibition of glycolytic genes such as Glut1 a glucose transporter.⁴⁶ SIRT6 corepresses HIF-1 α by deacetylating H3K9 at the promoters of several glycolytic genes, it has been linked with the potential tumor suppression activity of SIRT6.⁴⁷

3.2 Sirtuins and cancer

Of the sirtuin family, the involvement of SIRT1 function in cancer is the most studied and is decisively controversial and contradictory. SIRT1 is overexpressed in different kind of tumors such as prostate, breast, lung, hepatocellular, ovarian, epithelial, colorectal and melanoma, instead is reduced in bladder, colon carcinoma, glioblastoma, ovary an prostate cancer. This divergence has been explained by considering that SIRT1 normally protects cells from oncogenic transformation, but after, its enzymatic activity can promote cancer growth by deacetylation /inactivation of proapoptotic factors.^{48,49}

During tumorigenesis, SIRT2 can function as both tumor promoter and suppressor, this behaviour seems depend on the cellular context. The expression of SIRT2 has been found downregulated in several cancers such as gliomas,⁵⁰ breast cancer,⁵¹ head and neck squamous cell carcinoma⁵² and esophageal adenocarcinoma⁵³. Also SIRT2 seems have tumor promoter properties, indeed its expression is elevated in different cancers such as neuroblastoma,⁵⁴ pancreatic cancer and acute myeloid leukemia⁵⁵.

Several studies highlight a prosurvival role for SIRT3 in both normal and cancer cells in which seems control proliferative and survival pathways. Recently Alhazzazi et al.⁵⁶ reviewed that SIRT3 is overexpressed in head and neck squamous cell carcinoma in which reduce ROS levels and maintain a proliferative and aggressive phenotype by preventing apoptosis. Guo and co-workers⁵⁷ reported that

overexpression of SIRT3 in esophageal cancer tissue was associated with a poor outcome. A proapoptotic role has also been proposed but this dualism tumor promote/suppressor showed by SIRT3 needs to further investigations.

Growing evidences show that SIRT6 is a tumor suppressor.⁵⁸ SIRT6 involvements in cancer progression regards mainly its ability to regulates metabolic functions. Tumor cells needs to readjust their energy metabolism to fuel cell growth and division, and glucose metabolism is the best known example of metabolic reprogramming in cancer cells. SIRT6 regulates aerobic glycolysis in cancer cells and its inhibition in SIRT6 deficient cells rescue their tumorigenic potential.⁴⁶ Furthermore SIRT6 regulates cell proliferation by co-repressing c-MYC.⁴⁷ Decreased SIRT6 expression and the consequent deregulation of related genes was found posses oncogenic effect in hepatocarcinogenesis.⁵⁹

The nucleolar sirtuin SIRT7 recently found exist also as cytoplasmic form, has been supported play a crucial role in oxidative and genotoxic stress response.⁶⁰ Homozygous knockout of SIRT7 in mice causes diminished lifespan and leads to hearth hypertrophy and inflammatory cardiopathy. SIRT7 is more abundant in highly proliferative tissues than in lowly proliferative and a role for SIRT7 as a activator of proliferation has been proposed. Barber et al.²¹ in 2012 reported that SIRT7 was responsible in the maintenance of cancer phenotype and transformation. They found that SIRT7 directly deacetylates histone H3K18 as a single histone mark. SIRT7 is reported to be upregulated in breast and thyroid cancers and the consequent H3K18 hypoacetylation was considered a marker of malignancy. SIRT7 is responsible for maintaining some features of human cancers such as anchorage independent growth, growth in low serum and loss of contact inhibition. Depletion of SIRT7 inhibited growth of human cancer cells and in tumor xenografts in mice.^{61,62} Kim et al.⁶³ in 2013 noted that SIRT7 expression was increased from precancer to overt cancer and it was upregulated in a subset of human HCCs. SIRT7 inactivation induced p21^{WAF1/Cip1} expression and suppressed cyclin D1 in HCC cells. The cyclin D1 expression SIRT7 mediated can be a potent mitotic stimulation that causing uncontrolled cell growth during HCC progression.

3.2.1 SIRT1 and breast cancer

The expression of SIRT1 was seen in most human breast cancer specimens, and its expression was associated with metastasis and poor prognosis. SIRT1 upregulation in breast cancer is associated with inactivation of tumor suppressor hypermethylated in cancer 1 (HIC1) by DNA hypermethylation. HIC1 binds to the SIRT1 promoter, represses its transcription and promotes p53 expression.⁶⁴ When HIC1 is silenced in breast cancer, this results in SIRT1 upregulation and tumorigenesis promotion. Another well established pathway involves the association of estrogen receptor ER α and SIRT1 in development and progression of breast cancer, in which SIRT1 is essential for oncogenic signaling. SIRT1 is the binding partner of ER α and this complex functions as transcriptional activator of SOD and Gpx (antioxidant activity and decrease of ROS production) and a repressor of p53 and cyclin G2 with inhibition of senescence, apoptosis and increase of cell survival both in normal and tumor cells. ER α binds to p53 promoter and suppress its expression with a process SIRT1 dependent.⁶⁴ Thus ER α -SIRT1 complex function as suppressor of p53 in breast cancer. SIRT1 inactivation suppresses ER α induced cell growth and tumor development, and induced apoptosis.⁶⁴ SIRT1 positively regulates the expression of aromatase that is responsible for the biosynthesis of estrogen in breast cancer. Furthermore SIRT1 can promote cell migration by deacetylation cortactin.⁶⁴ More controversial is the case of connection between DBC1-SIRT1 in breast cancer.⁶⁵ Initially DBC1 has been proposed to function as negative regulator of SIRT1 with pro-apoptotic effects, then was found overexpressed in several breast cancer tissues and high levels of DBC1 were associated with short survival. DBC1 stabilizes ER α by SIRT1 inhibition and the consequent ER α acetylation enhance its DNA binding and transcriptional activity. On the other hand ER α signalling is oncogenic to the breast and DBC1 upregulation could enhance ER α function that can lead to development and progression of breast cancer.⁶⁶ The data reported suggest that DBC1 and SIRT1 levels are critical for determining the fate of cancer, moreover this indicate that both these proteins have potential tumor promoter or tumor suppression functions.

3.2.2 SIRT1 and prostate cancer

SIRT1 is overexpressed in human prostate cancer (PCa) cell lines compared with normal prostate epithelial cells. SIRT1 has been found also highly expressed in advanced prostate cancer tissues in which it can promote metastasis and cell invasion through metalloproteinase-2 and cortactin. In transgenic mouse model, SIRT1 expression promotes prostate carcinogenesis. Ahmad and co-workers⁶⁷ in 2009 showed that mRNA level of SIRT1 and SIRT1 were high in a panel of prostate cancer cells. LNCaP and 22Rv1 that possess mutant but functional androgen receptor and wild type p53, DU145 cells (androgen receptor negative and mutant p53), and PC3 cells (androgen receptor and p53 null when compared to normal prostate epithelial cell PrEC). They found that SIRT1 was localized to the nucleus and also showed cytoplasmic localization. When the PCa cell lines were treated with nicotinamide the physiological SIRT1 inhibitor there was a reduction in growth and viability of the cancer lines without any effect on the normal prostate cells. Furthermore Ahmad and co-workers evaluated the effect of SIRT1 knockdown on PCa cells, found that there was a marked decrease on the growth and viability of PCa cells when compared with nonsense shRNA control.⁶⁷ In 2012 Ito and co-workers⁶⁸ showed the effect of cortactin in invasion and migration of prostate cancer. Cytoplasmic SIRT1 interact and deacetylates cortactin improving its ability to promote cancer cell migration. On the contrary knockdown of cortactin and SIRT1 were found reduce and inhibit migration ability of DU145 cell line. The acetylation level of cortactin were found higher in SIRT1 knockdown cells than control, and SIRT1 knockdown inhibited cell migration and invasion more effectively than cortactin knockdown. They found that SIRT1 promote DU145 proliferation and migration by cortactin deacetylation but also it might depend on interaction with other molecular pathways.⁶⁸

3.2.3 SIRT1 and lung cancer

SIRT1 and cortactin were found significantly overexpressed in 144 patients with invasive non-small cell lung cancers (NSCLC), their expression was observed in 67% and 58% of patients with invasive NSCLC.⁶⁹ SIRT1 and cortactin expression

was significantly associated with unfavorable clinicopathological factors, including high pathological T stage, lymphonode metastasis, and advanced tumor invasion. Furthermore cytoplasmic SIRT1 was associated with high pathological T stage and large tumor size compared to nuclear SIRT1. SIRT1 expression was correlated with a deregulation of HIC1-SIRT1-p53 loop in 118 lung cancer patients resulting in a low expression of HIC1 and reduced p53 acetylation.⁷⁰ High expression of SIRT1 and low of DBC1 induced a p53 deacetylation and low HIC1 expression that may be correlated with the pathogenesis of lung SCC (squamous cell carcinoma). High expression of SIRT1 was found also in A549 lung AD (adenocarcinoma) cells but differently to SCC, an epigenetic alteration by hypermethylation of HIC1 promoter region associated with DNMT (DNA methyltransferase) overexpression attenuated its transcription. Acetylated p53 resulted from DBC1 positive expression in A549 cells, but it cannot bind to the epigenetically inactivated HIC1 at the promoter region to restore HIC1 expression. Another interesting pathway in which SIRT1 results involved is the modulation of DLL4/Notch signalling, essential for vascular development in lung cancer.⁷¹ SIRT1, was associated with the downregulation of DLL4/Notch signalling through Notch 1 deacetylation, and the inhibition of endothelial cell growth by DLL4/Notch that was enhanced in SIRT1-silenced lung cancer-derived cells ECs (vascular endothelial cells lung cancer-derived).

3.2.4 SIRT1 and liver cancer

HCC (hepatocellular carcinoma) is the third most common cause of cancer related death worldwide and nowadays only the early stage of HCC is curable. In the work reported by Portmann et al.⁷² SIRT1 expression was examined in a panel of 20 human HCC tumors and non tumor tissue. A strong overexpression of SIRT1 was observed and its inhibition by knockdown or with cambinol reduced the tumor cell growth by removing its promoting growth signals. Furthermore they found that of the sirtuin family only SIRT1 mRNA and SIRT1 protein levels were consistently expressed. SIRT1 silencing was associated with FOXO1 acetylation and cellular senescence in SK-Hep1 and HepG2 (transduced HCC p53 wild type) that showed an enhanced p53 acetylation and induction of p21.⁷³

3.2.5 SIRT1 in lymphoma and leukemia

In 104 diffuse large B-cell lymphoma patients, the expression of SIRT1 was seen in 74% of cases and associated with short overall survival.⁷⁴ Furthermore a recent study proposed a direct correlation between SIRT1 and DBC1 in DLBCL (diffuse large B cell lymphoma) in which DBC1 activates AR (androgen receptor) by inhibiting SIRT1 that may be involved in the progression of DLBCL.⁷⁵ SIRT1 is also overexpressed in chronic myelogenous leukemia (CML) in which plays a crucial role in development and chemoresistance.⁷⁶ CML results from a malignant transformation of a hematopoietic stem cell (HSC) by the BCR-ABL oncogene targets of imatinib a tyrosine kinase inhibitor. CML has a chronic phase (CP) that progress to an accelerated phase (AP) and a terminal blast crisis (BC); unfortunately the disease recurrence happen because of cessation of drug treatment even in patients with undetectable BCR-ABL expression.⁷⁶ Bhatia and co-workers⁷⁶ in 2012 have found that both SIRT1 mRNA and SIRT1 protein levels were elevated in CO and BC CML CD34⁺ cells compared to CD34⁺ cells from cord blood and normal peripheral blood stem cell. SIRT1 knockdown inhibited CML progenitor, CB CD34⁺ and CML CD34⁺ proliferation. Furthermore the combination of imatinib and SIRT1 inhibition enhanced apoptosis of quiescent CML progenitors via p53 activation. SIRT1 inhibition in combination with BCR-ABL tyrosine kinase inhibitors can be explored as a novel approach to eradicate leukemic stem cells and residual disease in chronic phase CML.⁷⁷ SIRT1 is highly expressed in adult T-cell leukemia lymphoma (ATL) an aggressive peripheral T-cell neoplasm characterized by poor prognosis with overall survival at 3 years only 24%. SIRT1 inhibition by Sirtinol has an apoptotic effect on primary ATL cells and HTLV-1 infected T cells.⁷⁸

3.2.6 SIRT1 and neuroblastoma

Neuroblastoma is a tumour derived from primitive cells of the sympathetic nervous system and is the most common solid tumour in childhood in which N-Myc and c-Myc are seen in a quarter of tumour and found correlated with poor prognosis. Myc oncoproteins induce malignant transformation by modulating gene transcription with a consequent cell proliferation. Their stabilization is controlled by phosphorylation

at S62 regulated by ERK (protein kinase) signalling, while T58 phosphorylation induces ubiquitylation and degradation.^{79,80} The neuroblastoma cell proliferation is induced by a positive feedback loop in which N-Myc oncoprotein upregulates SIRT1 transcription by binding to its gene promoter and SIRT1 binds N-Myc to form a transcriptional repressor complex that block MKP3 (mitogen protein kinase phosphatase 3) transcription. The repression of MPK3 that normally dephosphorylate and inactivates ERK led the N-Myc stabilization. The suppression of SIRT1 catalytic activity by Cambinol and Tenovin-6 reactivated MPK3 gene expression and induced neuroblastoma cell growth arrest.⁸¹

3.2.7 SIRT1 and pancreatic cancer

Pancreatic carcinoma is characterized by poor prognosis and fast progression and nowadays, gemcitabine is still the standard chemotherapeutic and first line drug for patients suffering from pancreatic cancer. SIRT1 overexpression was observed in pancreatic ductal adenocarcinoma (PDAC) and has been associated with increased cell viability and poorly differentiated tumor.⁸² Recently Gong et al.⁸³ have found that the combination treatment of gemcitabine and sirtinol inhibits growth of pancreatic cancer in vitro in cell cultures as well as in vivo in xenogeneic athymic nude mice improving efficacy and survival time compared to treatment with single agent. Inhibition of SIRT1 is effective in suppression of ADM (acinar ductal metaplasia) and in reducing cell viability in established PDAC tumors in which the regulator of acinar differentiation such as transcription factor-1a and β -catenin can be deacetylated by SIRT1.⁸⁴

3.2.8 SIRT1 and colorectal cancer

Colorectal cancer (CRC) is the third most common cancer in the world and is the second commonest cause of cancer deaths in the United States and United Kingdom.⁸⁵ Malignant transformation is associated with the activation of Wnt/beta-catenin signaling pathway which leads to the transcriptional induction of the c-MYC oncogene. Most lesions with high grade intraepithelial neoplasia and invasive carcinomas were characterized by high c-MYC and SIRT1 expression.⁸⁶ Recently

Takano and co-workers⁸⁷ measured the expression levels of SIRT1 and DBC1 by Western blot analysis of proteins extracted from fresh normal and cancerous tissues of 96 colorectal cancer patients. While expressions of SIRT1 and its inhibitor DBC1 are concomitantly increased in cancers, high SIRT1 expression appears to be related to poor patients prognosis while high DBC1 expression was correlated only with poor differentiation. Another interesting pathway in the connection between SIRT1 and colorectal cancer involve the downregulation of miR-34a a known post-transcriptional inhibitor of SIRT1. A positive feedback loop was proposed in which p53 induced expression of miR-34a which suppresses SIRT1, increasing p53 activity.⁸⁸ Overexpression of miR-34a decreased SIRT1 expression, leading to an increase in acetylated p53 levels and also an increase in p53 targets such as p21 and PUMA. MiR-34a was found induce apoptosis in HCT116 cells (HCT116 WT), but not HCT116 cells which do not have p53 (HCT116 p53 KO).

3.2.9 SIRT1 and gastric cancer

Gastric cancer is the second cause of death from malignant disease worldwide, with especially high mortality rates in East, South, and Central Asia; Central and Eastern Europe; and South America. In 2008, there were approximately 989 000 new cases of gastric cancer and 738 000 deaths worldwide. The prognosis of advanced gastric cancer remains poor, and curative surgery is regarded as the only option for cure.⁸⁹ Jang and co-workers⁹⁰ in order to understand the impact of SIRT1 and DBC1 on gastric carcinoma reported a study conducted on six hundred forty-three cases of patients. The expression of DBC1 and SIRT1 was found associated with unfavorable clinicopathologic variables and a significantly shorter survival in gastric carcinoma patients. It is known that DBC1 binds SIRT1 and inhibits its deacetylation activity promoting p53 mediated apoptosis. Therefore considering SIRT1 as potential oncogene DBC1 should play an antioncogenic role, but DBC1 and SIRT1 expression was found high and correlated with advanced clinicopathologic factors. The role of DBC1 in cancer is still controversial in which it can acts as tumor suppressor or tumor promoter. May be that DBC1 expression, results increased to

compensate SIRT1 activity but another explanation could be that DBC1 is tumor promoter.⁹⁰

3.3 SIRT1 and polycystic kidney disease

Polycystic kidney disease an autosomal dominant pathology is one of the most common genetic disorders in humans caused by mutations of PKD1 and PKD2. The disease is characterized by the development of multiple bilateral renal cysts with a consequent renal failure.⁹¹ The cyst formation and expansion involve hyperproliferation, dedifferentiation and liquid secretion. SIRT1 and c-MYC expression was found increased in PDK1 mutant renal epithelial cells and genetic deletion of SIRT1 by knockout mice or inhibition by nicotinamide delayed renal cyst formation in postnatal kidneys. The cystic cellular proliferation was found regulated by Rb in which its inactivation by SIRT1 deacetylation induced cellular proliferation. Knockdown of SIRT1 or its inhibition by nicotinamide increased Rb acetylation and decreases Rb phosphorylation. The treatment with nicotinamide induced apoptosis and p53 acetylation in cystic cells that also may depend on the involvement of other SIRT1 mediated pathways such as FOXO3 α and E2F1.⁹²

3.4 Sirtuins and neurodegenerative disease

3.4.1 SIRT1 and Alzheimer's disease

Alzheimer disease (AD) is one of the most common and devastating age related neurodegenerative disease. The typical neuropathological hallmarks are, extracellular lesions (protein aggregates formed by a peptide derived from enzymatic proteolysis of amyloid precursor protein the β -amyloid), loss of neurons (progressive neuronal death due to apoptosis) and reactive inflammation or gliosis (chronic inflammation that contributes to neuronal death). In mixed cortical cultures, microglia-dependent A β toxicity was associated with strong activation of NF-kB signaling in both microglia and astrocytes. In in vitro model the expression of SIRT1 protects microglia cells through inhibition of NF-kB signalling by deacetylation at Lys310 of RelA/p65.⁹³ The AD in mouse model APP^{swe}/PS1^{dE9} (A β plaque formation and

learning and memory deficits) was mitigated by SIRT1 overexpression and exacerbated in mice with SIRT1 knocked out in the brain. Overexpression of SIRT1 reduced A β plaque formation by α -secretase stimulation through activation of ADAM10. The mechanism of activation of ADAM10 by SIRT1 appears to be deacetylation of the RAR β , which is known to activate ADAM10 transcription resulting in a reduced production of A β .⁹⁴ In another mechanism SIRT1 expression/activity is involved in the regulation of the serine/threonine Rho kinase ROCK1, known in part for its role in the inhibition of the non-amyloidogenic- α -secretase. The expression of exogenous human (h) SIRT1 in the brain of hSIRT1 transgenics, resulted in decreased ROCK1 expression and elevated α -secretase activity in vivo.⁹⁵

3.4.2 SIRT1, SIRT2 and Huntington's disease

Huntington's disease (HD) is a neurodegenerative genetic polyglutamine (polyQ) disorder. Classical HD is characterized by personality changes, weight loss, cognitive disorders and motor impairment, including the hallmark feature of chorea. The disease is caused by an autosomal dominant mutation of two copies of a gene called Huntingtin, which gradually damages cells in the brain. Life expectancy in HD is generally around 20 years. The largest risk of death are pneumonia, heart disease, suicide, physical injury from falls, and malnutrition.^{96,97} In a *C. elegans* model for HD suggest the promotion of Sir2 activity was found protective against the early phases of polyQ cytotoxicity through activation of daf-16 (member of FOXO family).⁹⁸ These observations raised the possibility that caloric restriction and a Sir2 activator that promotes cell survival by inhibiting stress induced apoptotic cell death and functions in a FOXO3-dependent manner, may be protective to neurons expressing alleles associated with Huntington disease. Krainc and co-workers⁹⁹ in 2012 found that SIRT1 knockout mouse model of Huntington's disease resulted in exacerbation of brain pathology, instead its expression improved survival. SIRT1 had neuroprotective effects through activation of TORC1 by promoting its dephosphorylation and its interaction with CREB with a resulting positive modulation of BDNF (brain-derived neurotrophic factor) activity. In contrast with

the findings above mentioned a potent SIRT1 inhibitor EX527 (Selisistat) is in phase II for HD (clinical trials.gov identifier: NCT01521585) and only the outcome from the clinical trials will reveals the beneficial effects of SIRT1 inhibition in Huntingotn's disease.

The major beneficial effects of SIRT2 on HD depends on its hypomodulation. Decreased level of SIRT2 increased the viability of photoreceptor neurons in fly model of Huntington's disease¹⁰⁰ and as showed by Luthi-Carther et al SIRT2 inhibition reduced the sterols levels via SREBP-2 cytoplasmic retention with a consequent downregulation of cholesterol biosynthetic genes.¹⁰¹

3.4.3 SIRT2 and Parkinson's disease

After Alzheimer's disease Parkinson (PD) is the most common neurodegenerative disease. The pathology is due to degeneration and lost of nigrostriatal dopaminergic neurons characterized by the presence of evident symptoms such as bradykinesia, rigidity and tremor. The pathology of the disease is characterized by the accumulation of a protein alpha-synuclein into inclusions Lewy bodies.¹⁰² Inhibition of SIRT2 by small molecule such as AGK2 or by knockout models result in the rescue of α -synuclein mediated toxicity and promoted fewer and larger Lewy body-like inclusions.¹⁰³ Recently has been proposed that SIRT2 increase nigrostriatal damage after treatment with MPTP (1-methyl-4-phenyl-1,2,3,6-tetrahydropyridine) via FOXO3a deacetylation and activation of proapoptotic factor Bim.¹⁰⁴

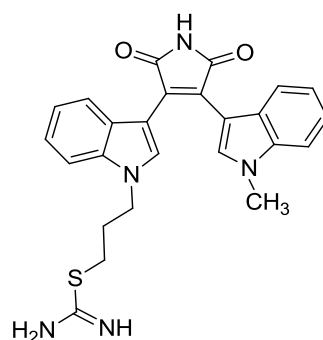
3.4.4 SIRT2 and Wallerian degeneration

Wallerian degeneration also named anterograde degeneration is a process that occur when a nerve fiber is damaged or cut and involves the separation between the axon and neuron's cell body. In 2007 Suzuki and Koike¹⁰⁵ found a connection between Wallerian degeneration and tubulin deacetylation SIRT2 mediated. They found that levels of SIRT2 in *Wld^S* mice (mouse model with delayed Wallerian degeneration) granule cells were reduced and that SIRT2 overexpression abrogated microtubule hyperacetylation and resistance to axonal degeneration. Conversely, SIRT2

knockdown by using a lentiviral vector expressing small interfering RNA, enhanced microtubule acetylation and resistance to axonal degeneration.

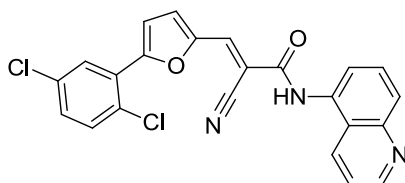
4 SIRTUIN INHIBITORS

4.1 Adenosine mimetics



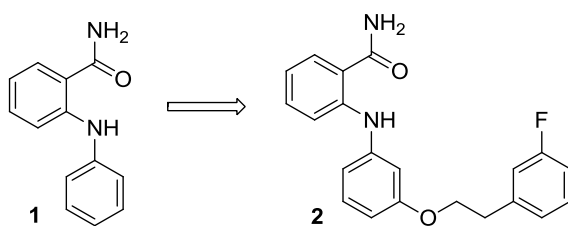
Adenosine mimetic compounds have been proposed as SIRT1, 2 inhibitors by Jung and co-workers¹⁰⁶ in 2006 starting from the consideration that a class of kinase inhibitors (CDK) also inhibit NAD⁺ dependent mitochondrial malate dehydrogenase (mMDH). A library of commercial available kinase and phosphatase inhibitors formed by 84 compounds were tested toward SIRT2 and only selected compounds tested against SIRT1. In order to avoid false positive, the most active compound (showed above) was assayed using two different SIRT1/2 protocols. Fluorescent deacetylase assay in which show IC₅₀ value of 3.5 μM and 0.8 μM on SIRT1 and SIRT2 respectively (ZMAL substrate 10.5 μM, NAD⁺ 500 μM),¹⁰⁷ and a scintillation assay in which the same magnitude of inhibition was observed (radioactive deacetylase assay has been performed as described by North et al.¹⁰⁸ with acetylated H4 histone N-terminal peptide, residues 1-25). Competitions studies indicate that the scaffold proposed was competitive with respect to NAD⁺ and not competition with substrate was observed. Furthermore SIRT2 was confirmed one of the cellular target by Western blot analysis.

4.2 AGK2



During a screening carried out on 200 structural analogues of B2 a nitroquinoline compound, AGK2 a selective SIRT2 inhibitor was discovered. The fluorimetric *in vitro* screening performed using the commercially available BIOMOL assay reveals that AGK2 is a SIRT2 selective inhibitor with IC_{50} of 3.5 μM on SIRT2 with a poor SIRT1, 3 inhibition profile. AGK2 was found able to inhibit the deacetylation of α tubulin via immunoblot and on overexpressed SIRT2 immunoprecipitated from HeLa cells. The compound has only minimal toxicity at 50 μM on after 72 h incubation in HeLa cells, and in Parkinson disease model AGK2 rescued dopamine neurons from α -synuclein toxicity.¹⁰³ Furthermore AGK2 can exacerbate the H_2O_2 -induced decrease in the level of intracellular ATP in PC12 cells (pheochromocytoma of the rat adrenal medulla cells).¹⁰⁹

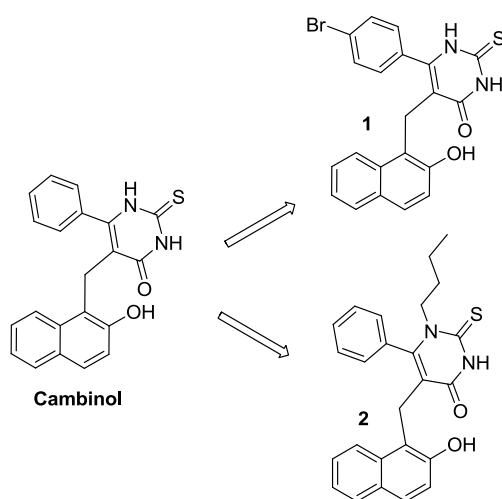
4.3 Anilinobenzamides



2-Anilinobenzamides were identified in 2006 by Suzuki et al.¹¹⁰ as potential nicotinamide mimetic compounds. The most potent compound of the serie **1** showed an IC_{50} value of 17 μM on SIRT1, 74 μM and 235 μM on SIRT2 and SIRT3 respectively (BIOMOL drug discovery kit AK555-557 with 25 μM of both substrate and NAD^+). The enzyme kinetic study (Lineweaver-Burk plot) proved that **1** was not competitive with NAD^+ but with the acetylated lysine substrate. The ability of compound **1** to induce p53 acetylation was confirmed by Western blot analysis on

HCT116 cell lines after etoposide induced DNA damage. In 2012 Suzuki et al.¹¹¹ improved the knowledge around this scaffold by designing and synthesizing several derivatives of compound **1** that led them to identify a series of potent, SIRT2 selective and cell permeable inhibitors. Compound **2** represents the lead with an IC₅₀ value of 0.57 μM on SIRT2 and up to 300 μM on SIRT1, 3 respectively. Compound **2** was found able to induce α-tubulin hyperacetylation in HCY116 cell lines greater than AGK2 a known SIRT2 inhibitor.

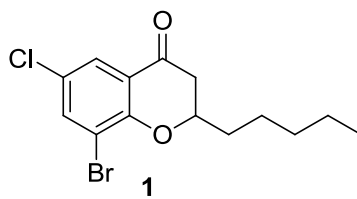
4.4 Cambinol and its derivatives



Bedalov and co-workers¹¹² in order to improve the stability of splitomicin a weak SIRT1 inhibitor discovered Cambinol a SIRT1, 2 inhibitor with moderate potency with IC₅₀ of 56 μM and 59 μM on SIRT1 and SIRT2 respectively (assayed with scintillation assay by using [³H]acetyl-H4 peptide). Cambinol was found to be competitive with histone H4 peptide substrate and hyperacetylation of p53, α-tubulin, FOXO3a and Ku70 were observed after Cambinol treatment of NCI H460 lung cancer and HeLa cells, moreover it shows to impair the growth of Burkitt lymphoma xenografts. A SAR investigation around Cambinol¹¹³ led to the identification of compound **1** with an appreciable SIRT1 selectivity (SIRT1 IC₅₀ of 12.7 μM and > 90 μM on SIRT2) and a series of SIRT2 selective compounds when the N-1 position was substituted, among which the most potent one was the N-tertbutyl derivative **2** with IC₅₀ = 1 μM (BIOMOL drug discovery kit AK555, 556 with 15 μM of substrate, 1 mM of NAD⁺ and 15 μL, 0.07 U/μL for SIRT1 and 0.03 U/μL for SIRT2). Western

blot analysis show that the treatment of H1299 cells with compound **2** increased the amount of acetylated α -tubulin. Cambinol inhibited the expression of cytokines (TNF, IL-1 β , IL-6, IL-12p40, and IFN- γ), NO and CD40 by macrophages, dendritic cells, splenocytes and whole blood stimulated with a broad range of microbial and inflammasome stimuli.¹¹⁴ Cambinol lead to a G1 arrest in p53wt-HepG2 cells (hepatocellular carcinoma cells) without impair the regenerative capacity of normal liver. Furthermore tumor growth was reduced in animals treated with cambinol without change the normal physiological growth response in non-malignant liver cells.⁷² Preventative treatment with Cambinol reduced tumorigenesis in TH-MYCN transgenic mice.⁸¹

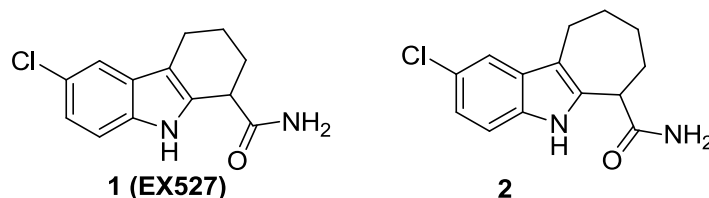
4.5 Chroman-4-one derivatives



Chroman-4-one constitute one of the most recent scaffold with SIRT2 selective properties. The structural investigation proposed by Luthman and co-workers¹¹⁵ allowed the identification of an hit series of potent and highly selective SIRT2 inhibitors, of which compound **1** with n-butyl alkyl chain in position 2 and the intact carbonyl function in position 4 was found the most active. The reported SIRT2 IC₅₀ is 4.3 μ M and no relevant inhibition against SIRT1 and SIRT3 at concentration of 200 μ M was observed. In order to confirm that the activity of **1** was not only an artefact caused by the fluorophore, a SIRT2 assay based on the release of ¹⁴C-nicotinamide, and western blot analysis of the SIRT2 mediated deacetylation of acetylated α -tubulin were carried out. Compound **1** is clearly a SIRT2 selective inhibitor of which S enantiomer was a more potent inhibitor with IC₅₀ value of 1.5 μ M. The enzymatic assay has been performed using a BIOMOL like protocol, with homemade GST-SIRT1/2 enzyme, recombinant His-SIRT3 and substrates commercially available. Km values were experimentally found be 58 μ M for SIRT1, 198 μ M for SIRT2 and 32 μ M for SIRT3 (reported by BIOMOL). The assay was

carried out using 0.7 Km of substrate concentration and 0.9 Km of NAD^+ concentration.

4.6 EX-527

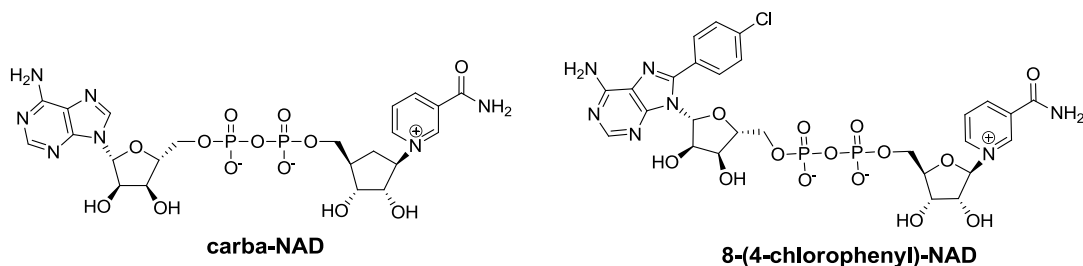


EX-527 and its derivatives have been discovered in 2005 by Napper et al.¹¹⁶ through an high-throughput screening of 280.000 compounds using the commercially available fluorimetric assay (BIOMOL). Selected compounds were also assayed by radiochemical assay that monitors the enzymatic release of nicotinamide from NAD^+ . Among the hit series EX-527 is the most potent and selective compound with a SIRT1 IC_{50} of 0.098 μM as racemic mixture (in the manuscript the reported IC_{50} values of the separated enantiomers are e1 IC_{50} 0.123 μM and e2 IC_{50} >100 μM) SIRT2 of 19.6 μM and SIRT3 48.7 μM . SAR studies reveal the importance of the primary amide as functional group, and the reduction of tetrahydrocarbazole to hexahydro drastically reduced the inhibition activity. Enzyme kinetic analysis and nicotinamide exchange assay have revealed that EX-527 is a mixed-type inhibitor with the ability to inhibit the nicotinamide exchange reaction, suggesting that the compound could occupy the nicotinamide binding site. Recently Steegborn and co-workers¹¹⁷ described the molecular basis of sirtuin inhibition by EX-527. A kinetic analysis using a continuous assay, confirmed the previously reported NAD^+ dependent non-competitive inhibition mechanism. Furthermore the SIRT3 crystal structure with bound 2'-O-acetyl-ADP ribose and EX-243 (the EX527 active enantiomer) show that the cofactor binding loop is trapped in a closed conformation instead of being open for product release. Zhao et al.¹¹⁸ in 2013 solved the crystal structure of the SIRT1 catalytic domain with bounded NAD^+ and an analogue of EX-527 (2). Interestingly the racemic mixture of 2 was added to the protein crystallization but only the (S)- enantiomer that is also the most active in vitro can be seen in the crystal structure. Thus confirming the stereoisomeric binding

discrimination. Crystal structures of EX-527 on SIRT3 (PDB code : 4BV3) and its analogue (2) on SIRT1 (PDB code : 4I5I) endorse the inhibition mechanism proposed by Napper et al. in which both the inhibitors are able to bind in the C pocket with a resulting displacement of NAD⁺ nicotinamide moiety that induces the cofactor to adopt a non-productive binding mode that might preclude on SIRT1 the substrate binding by steric interference.

EX-527 is able to induce p53 acetylation in different cell lines such as NCI-H460, U-2 OS, MCF7 and HMEC cells, without affect cell survival or cell proliferation.¹¹⁹ The effectiveness of EX-527 as SIRT1 binders has also been confirmed by Sinclair and co-workers that reported the ability of this scaffold to inhibit the complex formation between DBC1 (a known SIRT1 inhibitor) -SIRT1, suggesting the idea to develop potential SIRT1 activators with the capacity to block DBC1 binding without affect the SIRT1 catalytic activity.¹²⁰ EX-527 (also called Selisistat) is in phase II for HD (clinical trials.gov identifier: NCT01521585) and only the outcome from the clinical trials will reveals the beneficial effects of SIRT1 inhibition in Huntington's disease.

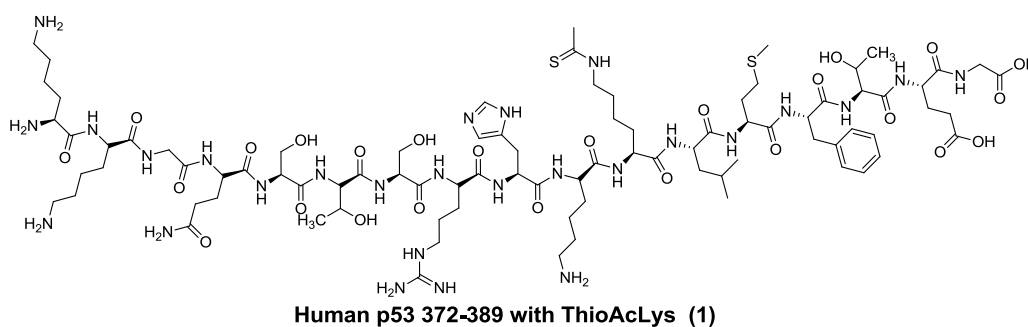
4.7 NAD⁺ analogues



Non hydrolysable NAD⁺ analogue carba-NAD have represented one of the most important starting point in understanding the sirtuin catalysed deacetylation.¹²¹ Its chemical stability is due to the substitution of an oxygen atom with a carbon, that stabilizes the bond between nicotinamide and C1 of the cyclopentyl ring. Carba-NAD has been a useful tool in studying Sirtuin bioactive conformation because, crystallization of sirtuins ternary complex SIRTs-NAD⁺-substrate was challenging due to the short lived nature of the ternary complex. On the contrary carba-NAD

does not react with acetylated substrate and it has allowed the crystallization of its ternary complex on HST2, SIRT3 and SIRT5.^{122,123} Carba-NAD derivatives can serve also as sirtuin inhibitors thank to their ability to compete with NAD⁺, but the lack of cellular permeability due to their physiochemical properties, make them a non-suitable scaffold for further investigations. In 2011 Wagner and co-workers¹²⁴ developed a small series of NAD⁺ analogues of which 8-(4-chlorophenyl) derivative was a moderate SIRT2 inhibitor with an IC₅₀ of 35 μM. The compounds were assayed using a BIOMOL like assay with GST-SIRT1 and His-SIRT2, 10.5 μM of ZMAL substrate and 500 μM of NAD⁺.

4.8 Peptides and Pseudopeptides



Fatkins et al.¹²⁵ in 2006 discovered the first thioacetylated peptidic inhibitor (1) of SIRT1 simply starting from the consideration that residues 372-389 of human p53 N^ε-acetylated at Lys382 were an in vitro substrate of SIRT1. N^ε-Thioacetyl group was incorporated into Lys382 as acetyl mimetic and was found increase the rate of nicotinamide formation, and potently inhibit SIRT1 with an IC₅₀ of 2 μM (HPLC assay using 0.5 mM NAD⁺, 0.3 mM 372-389 of human p53 as substrate and 14 μM GST-SIRT1) with a retardation of 400 fold the de(thio)-acetylation SIRT1 mediated. In 2007 Smith and Denu¹²⁶ determined the chemical mechanism of thioacetyl-lysine peptide inhibition through mass spectrometry, pre-steady state, steady state kinetics and mutagenesis. Starting from 11-mer peptide based on the human histone H3 a small array of N^ε substituent at Lys-14 were explored (Figure 7). Thioacetyl derivative was found the best inhibitor with IC₅₀ value of 2.0 μM, 5.6 μM, 2.3 μM

and 1.0 μM for SIRT1, SIRT2, SIRT3 and Hst2 respectively (scintillation assay with 50 μM NAD^+ , 20 μM [^3H]acetyl-lysine peptide, 0.1-0.2 μM enzyme).

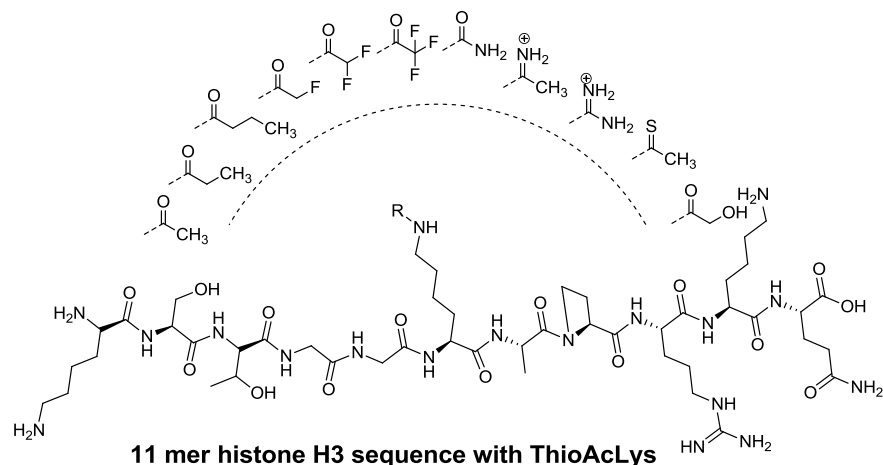


Figure 7. N^ϵ modifications at Lys-14 of human histone H3 peptidic sequence.

Differently to monofluoroacetyl-, difluoroacetyl-, and trifluoroacetyl peptides that would be inhibitor through competition with AcH3, Thioacetyl derivative inhibited by stalling a reaction step after Michaelis complex formation (Figure 8).

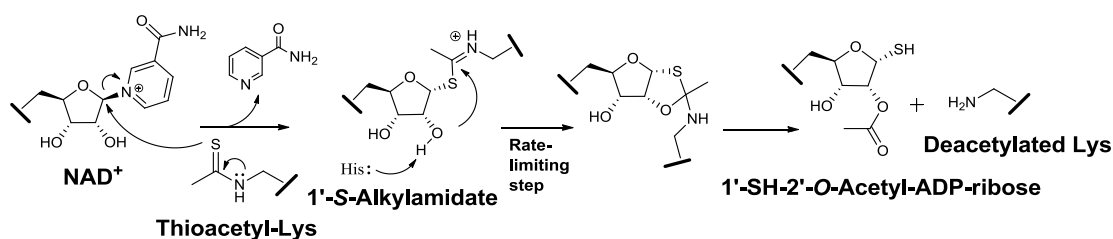


Figure 8. Mechanism of sirtuin inhibition of thioacetylated peptides.

After a fast nicotinamide cleavage, the thioacetyl inhibitor is readily converted to a stalled intermediate 1'-S-alkylamidate with a consequent retardation of the overall turnover rate.¹²⁷ In 2008 Fatkins et al.¹²⁸ starting from the results previously obtained with thioacetylated SIRT1 substrate **1** (p53 372-389), synthesized also α -tubulin sequence 36-44 (a known SIRT2 substrate) and Acetyl-coenzyme A synthetase 2

sequence 633-652 (as substrate of SIRT3), with the aim to obtain not only potent inhibitors, but informations in term of selectivity. From the results reported by the authors (Table 6) peptide **1** was found a potent SIRT1 and SIRT2 inhibitor, instead **2** and differently to compound **3** that was a pan inhibitor, is the only one that showed a considerable selectivity.

Table 6. IC₅₀ Values for compounds **1-3**¹²⁸

Peptide	IC ₅₀ μM		
	SIRT1	SIRT2	SIRT3
² HN-KKGQSTSRHKK(ThAc)LMFKTEG-COOH (1)	1.7	1.8	67.3
² HN-MPSDK(ThAc)TIGG-COOH (2)	116.8	11.4	449.4
² HN-KRLPKTRSGK(ThAc)VMRLLLRKH-COOH (3)	0.9	4.3	4.5

These results opened the street to further structural investigations in which the most relevant SAR has been proposed by Kiviranta et al.¹²⁹ in 2009. Penta and tripeptides (Figure 9) were found good SIRT1 and SIRT2 inhibitors demonstrating that, additional C and N-terminal residues were not necessary for a tight binding.

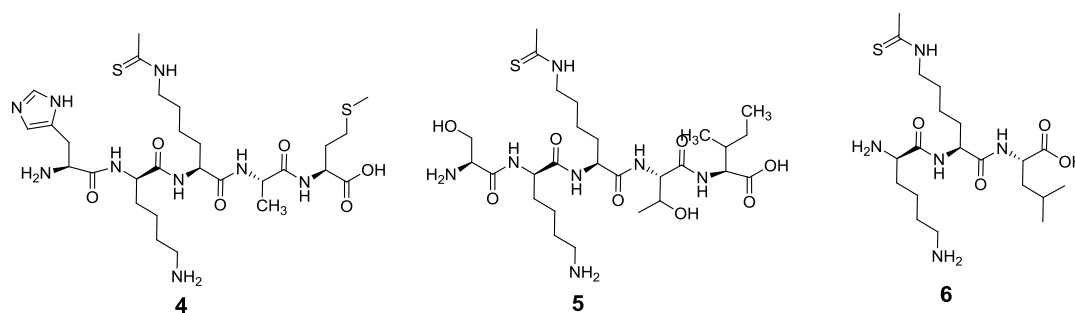


Figure 9. The most representative penta and tripeptides SIRT1/2 inhibitors.

Compounds were designed considering p53 and α -tubulin based sequences and potent SIRT1, SIRT2 inhibitors were found (Table 7). The tripeptide **6** was the compound with the highest SIRT1 selectivity, opening the perspective that the correct selection of sidechains was important for obtain a good inhibitory activity and selectivity. Following this direction Kokkonen et al.¹³⁰ in 2012 proved that a

specific selection of a peptidic/pseudopeptidic compounds from an homemade library could be applied also for design inhibitors of SIRT6 deacetylase activity.

Table 7. IC₅₀ Values for compounds **4-6**¹²⁹

Peptide	IC ₅₀ μM	
	SIRT1	SIRT2
4	0.18	3.8
5	0.18	6.9
6	0.57	151

In this scenario in which peptidic inhibitors gave potent inhibition but negligible druglike properties, Suzuki et al.^{131,132} reported new substrate mimetic pseudopeptidic inhibitors with the aim to improve cell permeability (Figure 10).

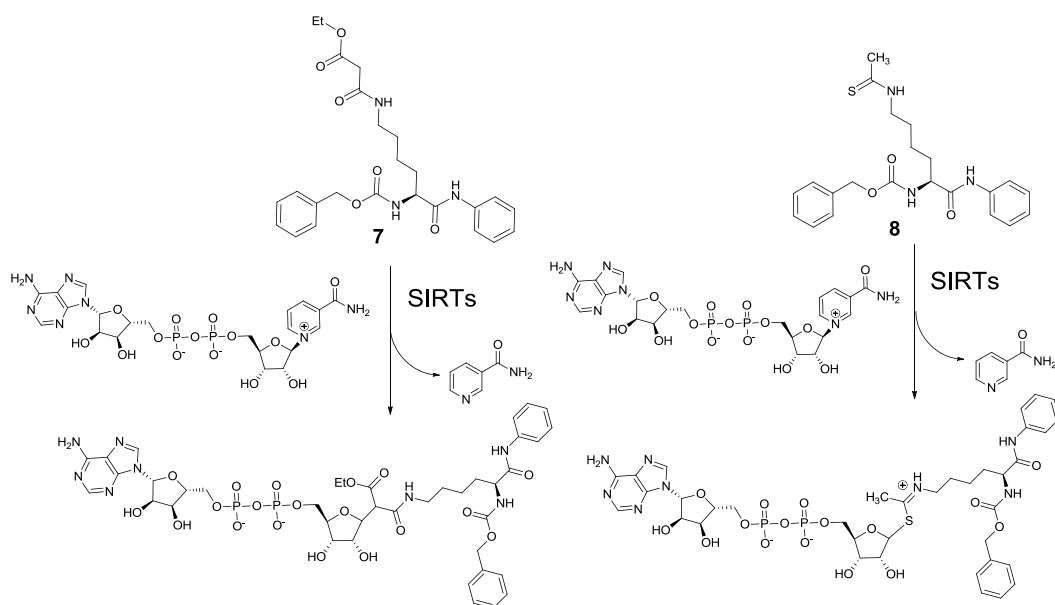
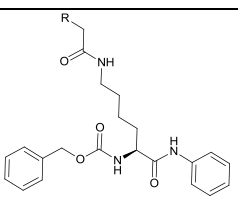


Figure 10. NAD⁺ conjugates generated by compounds **7**, **8**.

Compound **7** was the best result (Figure 10, Table 8) of a SAR investigation to the N^ε-Lys position, carried out with the aim to find a new functional groups able to keep a tight binding with the enzyme by reacting with NAD⁺. Instead compound **8** (Figure 10) represents the first structural optimization of thioacetyl Lys substrate

based inhibitors, demonstrating that peptidic scaffold could be replaced with a pseudopeptidic backbone retaining a good SIRT1 inhibition profile. The mechanism of SIRT1 inhibition by compounds **7** and **8** was investigated by mass spectroscopic analysis, in which a stable adduct formation as result of SIRT1-catalyzed reaction was observed (Figure 10).

Table 8. IC₅₀ Values for N^ε- Lys modified compounds¹³¹



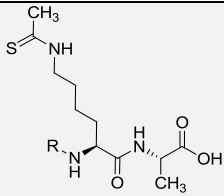
R	IC ₅₀ μM
SIRT1	
-CN	300
-CF ₃	>300
-SCH ₃	>300
-SOCH ₃	>300
-SO ₂ CH ₃	N.D.
2-CF ₃ Ph	>300
4-CF ₃ Ph	>300
2-NO ₂ Ph	>300
4-NO ₂ Ph	N.D.
-COOCH ₃	35
-COOEt (7)	3.9
-COOn-Pr	62
-COOi-Pr	47
-COOn-Bu	73
-COOt-Bu	>300
-COOCH ₂ -c-Pr	14
-COOCH ₂ CF ₃	15
-COOCH ₂ Ph	96
-CONH ₂	>300
-CONHCH ₃	>300
-CON(CH ₃) ₂	>300

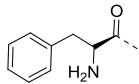
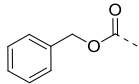
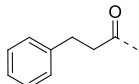
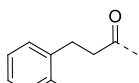
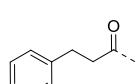
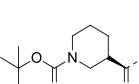
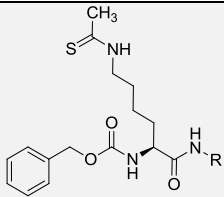
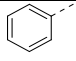
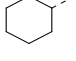
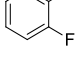
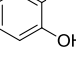
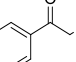
-COCH ₃	>300
-COEt	88
-CO _n -Pr	56
-COCF ₃	>300
-COPh	>300

IC₅₀ values were experimentally calculated using SIRT fluorimetric BIOMOL assay AK555, AK556 and AK557 (25 μM NAD⁺ and 25 μM of substrate) showed that both compounds **7** and **8** were good SIRT1 inhibitors with IC₅₀ of 3.9 μM and 2.7 μM respectively and weak SIRT2 inhibitors (IC₅₀ > 65 μM and 23 μM respectively) without show activity against SIRT3. Unlike peptidic inhibitors, **7** and **8** were found cell permeable with the ability to induce p53 hyperacetylation after DNA damage in HCT116 cells.

In 2010 Huhtiniemi et al.¹³³ proposed, one of the last SAR investigation to the N^ε-Lys position of a peptidic scaffold. Thioacetyl moiety was confirmed the most promising N^ε- substituent of the series. In 2011 Lahtela-Kakkonen and co-workers¹³⁴ created the first binding hypothesis in designing new pseudopeptidic inhibitor of SIRT1 and SIRT2. The authors designed a small array of pseudopeptidic inhibitors (Table 9) of SIRT1/2 considering the potential interactions in the substrate binding area by docking simulations. The enzymatic assay performed using a BIOMOL like protocol (homemade GST-SIRT1/2 enzymes 40 μM of SIRT1 substrate, 138 μM for SIRT2 and NAD⁺ 500 μM) shows that most of the compounds were potent SIRT1 inhibitors with a considerable inhibition profile also on SIRT2.

Table 9. IC₅₀ Values for pseudopeptidic inhibitors¹³⁴

R	IC ₅₀ μM	
	SIRT1	SIRT2
	0.77	6.5

	18	ND
	13	17
	0.99	56
	1.3	27
	1.0	53
	0.97	13
		
	9.9	15
	23	ND
	7.4	16
	5.1	7.4
	1.6	4.3

Furthermore selected compounds were found able to induce p53 hyperacetylation after etoposide induced DNA damage in different cellular lines such as NHA, SH-SY5Y and ARPE cell lines. Zheng and co-workers¹³⁵ in 2010 investigated on the possibility to make structural changes on the substrate acetyl lysine moiety. Starting from sequence 380-384 of p53 a known SIRT1 substrate in vitro, a series of peptides containing acetyl lysine analogues were synthesized (Figure 11). Each compound of the series doesn't show substrate property and neither significant inhibitory activity even when L-Acetyl lysine was replaced with non-natural D isomer.

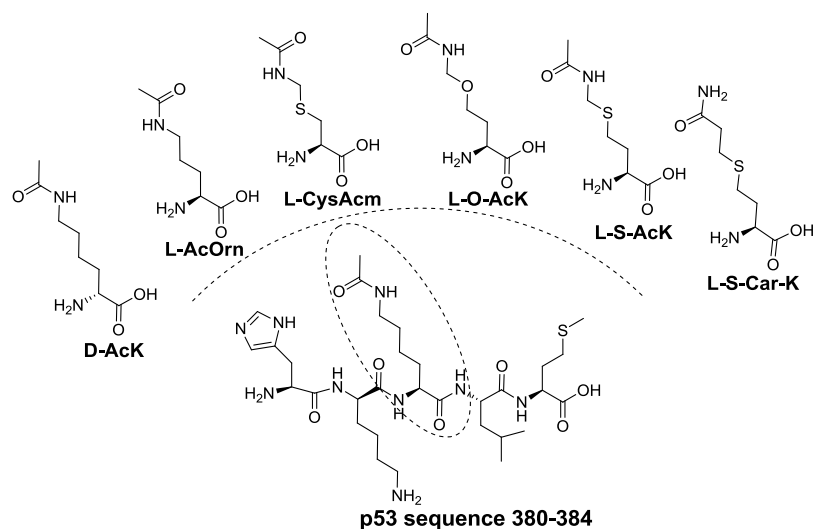


Figure 11. Modification proposed at acetyl lysine moiety.

The structural investigation proposed reveals that substrate binding site has stringent requirements and poor plasticity in which the distance between lysine α -carbon and its acetoamido group is critical for the correct substrate placements. This let understand the difficulty in designing acetyl lysine mimetic compounds as potential sirtuin inhibitors. Furthermore the full inactivity showed by p53 380-384 containing D-isomer of AcLys evidences also the stereospecificity of deacetylation SIRT1 catalyzed. The versatility of peptidic scaffold has been applied by Lin and co-workers after the discovery of demalonylase and desuccinylase activity of SIRT5.²³ The specificity of this enzymatic reaction was evidenced designing histone H3 lysine 9 (H3K9) thiosuccinyl peptide (H3K9TSu) (Figure 12) and the corresponding H3K9 thioacetyl derivative as control.¹³⁶ H3K9TSu differently to H3K9 thioacetyl derivative, (active in low micromolar concentration on SIRT1-3 but not on SIRT5) was found a selective and a competitive inhibitor of SIRT5 with an IC_{50} of 5 μ M (by HPLC assay, 1 μ M of Sirtuin 0.3 mM acetyl/succinyl peptide H3K9, K_m 41 μ M and 0.5 mM NAD^+) without show any significant activity on the other sirtuin isoforms.

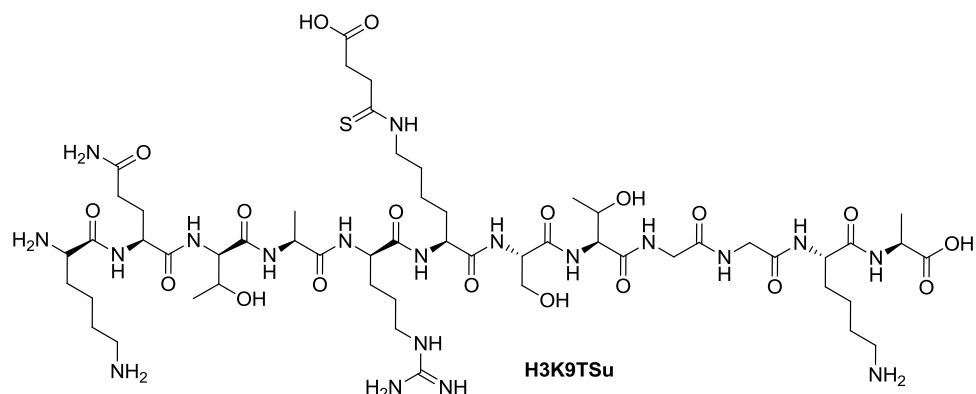
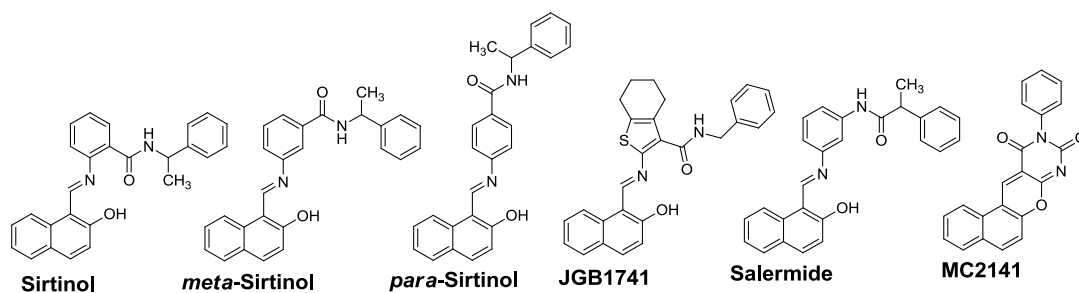


Figure 12. Histone H3 lysine 9 thiosuccinyl peptide (H3K9TSu)

4.9 Sirtinol/Salermide derivatives

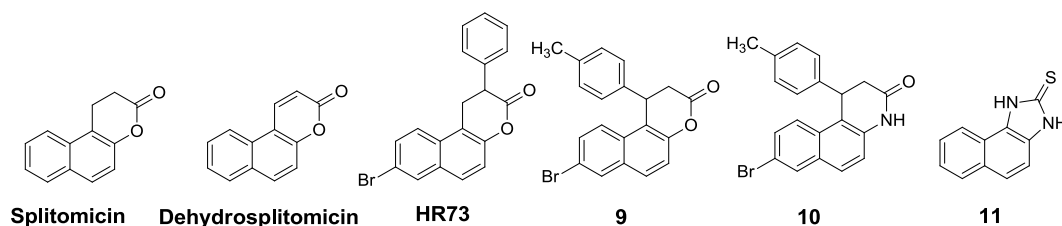


Sirtinol was discovered in 2001 by high throughput cell-based screening of 1600 compounds¹³⁷ in which cell-based URA3 reporter-based screen was used to identify the potential inhibitors. Sirtinol was able to inhibit yeast Sir2p and SIRT2 enzymatic activity with an IC_{50} of 68 μM and 38 μM respectively (scintillation assay). In 2005 Mai et al.¹³⁸ proposed a small SAR investigation in which the hydroxyl function of naphthyl group was found essential for the activity, moreover R and S sirtinol, *meta*-sirtinol and *para*-sirtinol were prepared and assayed on human SIRT1 and SIRT2. The IC_{50} values experimentally calculated with fluorescent BIOMOL assay (1 μg of SIRT1 or SIRT2, 250 μM of substrate and 200 μM of NAD^+) show that the switch from *meta* to *para* sirtinol improved the inhibition profile in which this latter had IC_{50} of 13 μM and 26 μM on SIRT1 and SIRT2 respectively. Sirtinol has different biological activities; it reduces inflammation in human dermal microvascular endothelial cells by reduction of monocyte adhesion,¹³⁹ induces apoptotic and autophagic cell death in MCF7 breast cancer cells,^{140,141} prostate cancer cells (PCa)⁶⁷

and a significant growth inhibition and apoptosis in adult T-cell leukemia-lymphoma (ATL)⁷⁸.

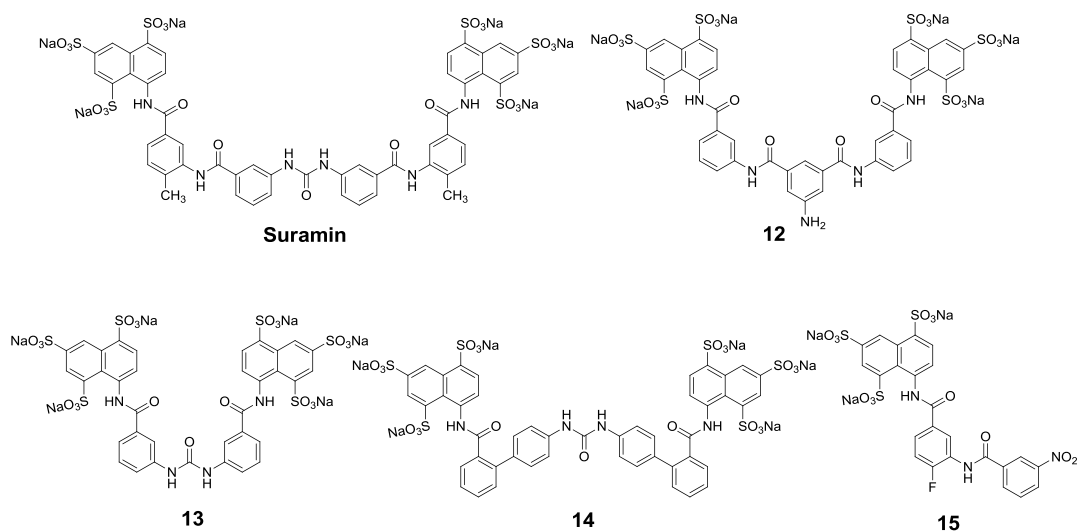
In 2009 Fraga¹⁴² and few years later Mai¹⁴³ and co-workers focused their effort to rationally modify the sirtinol structure in order to create stronger sirtuin inhibitors. The founder of this series so called Salermide with a medium SIRT1/2 inhibition profile (IC₅₀ 43 μM and 25 μM on SIRT1 and SIRT2 respectively) shows specific proapoptotic effect in several cancer cell lines such as leukemia (MOLT4, KG1A, K532, U937), lymphoma (Raji), colon (SW481, RKO), breast (MDA-MB-231, MCF7) and cancer stem cells (CSCs) colorectal carcinoma (CRC), glioblastoma multiforme (GBM), without affect the viability of non-tumorigenic MRC5 cells. The effect of Salermide was dependent on SIRT1 by reactivation of proapoptotic genes (CASP8, TNF, TNFRSF10B and PUMA) through SIRT1 mediated K16H4 deacetylation.^{142,143} JGB1741¹⁴⁴ instead was discovered by docking simulations of sirtinol analogues, in which JGB1741 resulted the best scored compound. JGB1741 was found a SIRT1 selective inhibitor with an IC₅₀ value of 15 μM on SIRT1 and >100 μM on SIRT2 and SIRT3 (using BIOMOL assay, other information are not reported). JGB1741 inhibits cell proliferation of K562 (myelogenous leukemia), HepG2 (hepatocellular carcinoma) and MDA-MB231 (breast cancer) cell lines without show any cytotoxicity on HEK293 (Human Embryonic Kidney 293 cells). Furthermore on MDA-MB231, JGB1741 was able to induce apoptosis by increasing cytochrome c release and H3K9, p53 K382 hyperacetylation. MC2141¹⁴⁵ is the founder compound of a series of benzodeazaflavins proposed by Mai and co-workers in 2010 as a result of cambinol's chemical manipulation. MC2141 is a selective SIRT1 inhibitor, with IC₅₀ values of 8.4 μM and 191.2 μM on SIRT1 and SIRT2 respectively (Fluor de Lys fluorescence based assay kit based on the method described in the BIOMOL product sheet AK-555, AK-556). MC2141 induces p53 acetylation at Lys382 on MCF7 cell line and apoptosis in different cancer cell lines such as Raji (lymphoblastoid cells derived from Burkitt's lymphoma), DLD1 (colon carcinoma), Hela (cervical carcinoma), U937 (leukemia), two colorectal carcinoma (CSC-CRO, CSC 1.1) and two glioblastoma multiforme (CSC 30P, CSC 30PT) cancer stem cells.^{146,147}

4.10 Splitomicin and its derivatives



In a cell based screening on 6000 compounds from the National Cancer Institute, Splitomicin was identified a specific inhibitor of yeast Sir2p with a minimum growth stimulating concentration (MCG) of 0.49 μM and with low and no inhibitory activity against Hst1p, Hst2p, Hst3p and Hst4p isoforms.¹⁴⁸ After the identification of critical residues responsible of its inhibitory discrimination a library of 100 analogues was synthesized and screened against Sir2p and Hst1p in which Dehydrosplitomicin was Hst1p specific inhibitor.^{149,150} This first approach on yeast isoforms gave the input to develop splitomicin derivatives active on human sirtuins. HR73 has been identified a potent SIRT1 inhibitor with $\text{IC}_{50} < 5 \mu\text{M}$.¹⁵¹ Compound **9** and its hydrolytically stable derivative **10** were found SIRT2 inhibitors in low micromolar concentration with IC_{50} of 1.5 μM and 6.4 μM respectively (homogeneous fluorescent assay 10.5 μM of ZMAL substrate, 500 μM of NAD^+).¹⁵² Compound **11** the result of Splitomicin structural optimization in order to achieve a more stable and less hydrolysable derivative, is an equipotent SIRT1/SIRT2 inhibitor with an IC_{50} value of 9.6 μM and 10 μM (homogeneous fluorescent assay 10.5 μM of ZMAL substrate, 500 μM of NAD^+) on SIRT1 and SIRT2 respectively.¹⁵³

4.11 Suramin



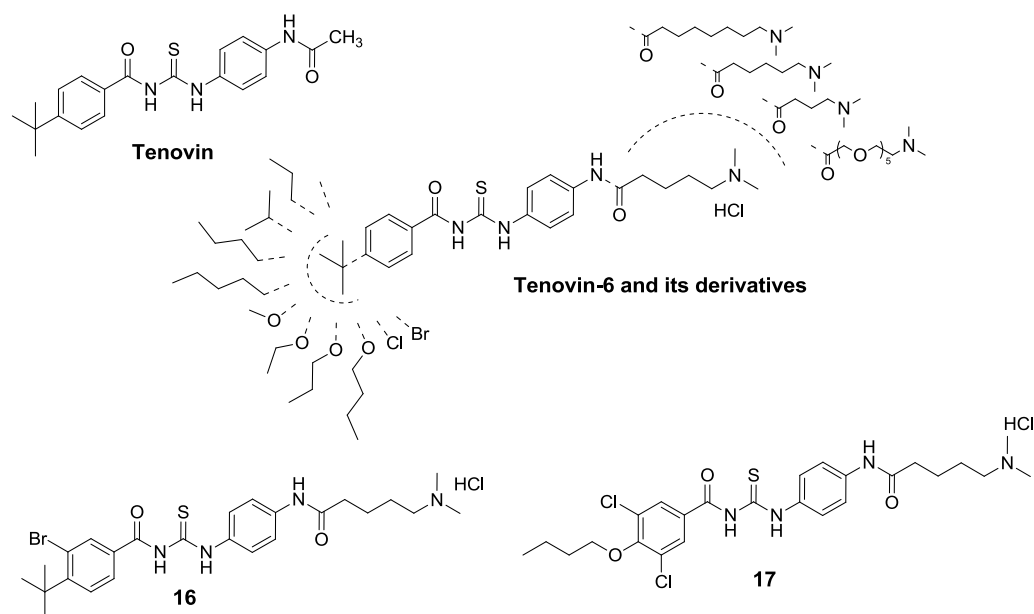
The inhibitory activity of Suramin against SIRT1 was discovered by Sinclair and co-workers during a screening of potential Sirtuin activators.¹⁵⁴ In 2007 Trapp et al.¹⁵⁵ performed a structure activity study of 30 Suramin analogues tested on SIRT1 and SIRT2. The replacement of the urea central moiety with isophthalic acid **12** led a potent SIRT1 inhibitor (Table 10).

Table 10. IC₅₀ Values for the most representative Suramin derivatives¹⁵⁵

Compound	IC ₅₀ μM	
	SIRT1	SIRT2
Suramin	0.29	1.1
12	0.093	2.3
13	0.23	7.9
14	0.58	60% at 20 μM
15	0.52	15.5

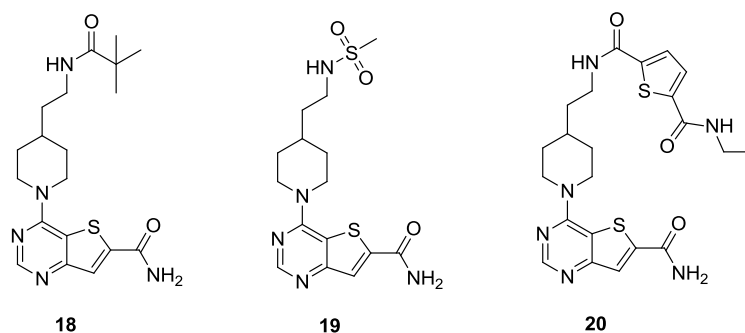
Downsizing of the central core with **13** and **15** and a pronounced structural rearrangement **14** gave compounds with marked but also drastically reduced SIRT1/SIRT2 inhibition profile (homogeneous fluorescent assay 10.5 μM of ZMAL substrate, 500 μM of NAD⁺) on SIRT1 and SIRT2 respectively.

4.12 Tenovin and its derivatives



An high-throughput cell-based screening of 30 000 drug-like small molecule, carried out to detect compounds that activate p53 led the identification of Tenovin.¹⁵⁶ Due to Tenovin poor water solubility Tenovin-6 was synthesized and found a SIRT1/2 inhibitor with an IC_{50} of 21 μ M and 10 μ M on SIRT1 and SIRT2 respectively (BIOMOL assay AK555-557, 7 μ M of substrate and 1mM of NAD^+). Structural investigations around Tenovin-6^{157,158} (a schematic example in figure above) let understand the difficulties in order to gain more potent derivatives in which compounds **16** and **17** represent the most optimized structures with IC_{50} of 18.3, 21.5 μ M and 4.6, 0.8 μ M on SIRT1 and SIRT2 respectively.^{157,158} Tenovin-6 rapidly increase the level of K382-Ac-p53 in MCF7 and H1299 cell lines and the treatment of aggressive melanoma cell line (ARN8) with Tenovin-6 decreases its growth. Tenovin-6 significantly increases apoptosis of CML (chronic myelogenous leukemia) $CD34^+CD38^-$ and $CD34^+CD38^+$ cells but not normal cells.⁷⁶

4.13 Thienopyrimidine



Thienopyrimidine are a new class of low nanomolar SIRT1-3 inhibitors discovered through an in vitro SIRT3 affinity selection through an encoded library technology (ELT).¹⁵⁹ The screened library was generated using 16 bis acids, 134 diamines and 570 heteroaryl building blocks that afford a library of 1.2 million compounds. An intensive SAR investigation was carried out, moreover the crystallization of compounds **18-20** with SIRT3 allowed to understand their binding mode. Compounds **18-20** were low nanomolar inhibitors with IC₅₀ values that range from 3.6-15 nM for SIRT1, 2.7-10 nM for SIRT2 and 4.0-33 nM for SIRT3. IC₅₀ were measured by a discontinuous OAADPr mass spectrometry assay with Ac-RHKK_{Ac}W-NH₂ as substrate (used at K_m value 2 μM SIRT1, 10 μM SIRT2 and 2.2 μM for SIRT3). Test compounds were preincubated with either SIRT1 (5 nM), SIRT2 (10 nM) and SIRT3 (5nM) then peptidic substrate was added along with NAD⁺ at K_m value (80 μM SIRT1, 50 μM SIRT2 and 2.2 μM for SIRT3). As can be seen by SIRT3 crystal structures (PDB: 4JSR, 4JT8, 4JT9) the three inhibitors have the same binding mode in with thienopyrimidine scaffold occupy the C-pocket in which the carboxamide makes four hydrogen bonds with Asp231, Ile230 and a conserved water molecule (Figure 13), the thienopyrimidine ring has stack interaction with Phe157 and the ethylpiperidine moiety is placed in the hydrophobic cleft of the acetyl-lysine substrate channel.

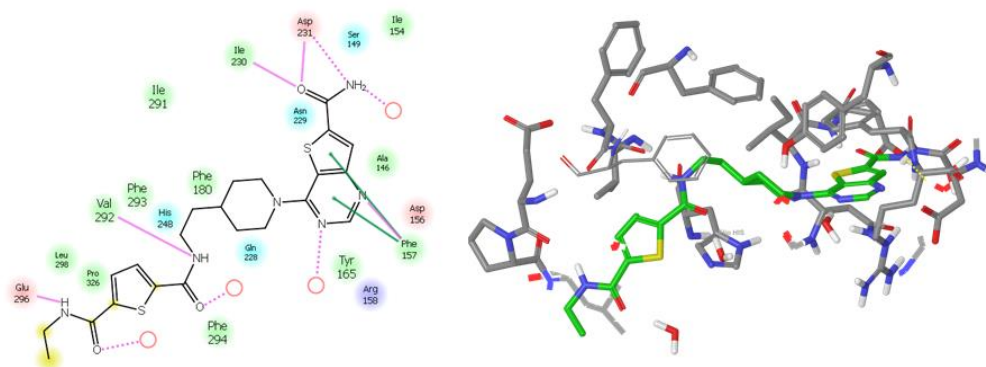
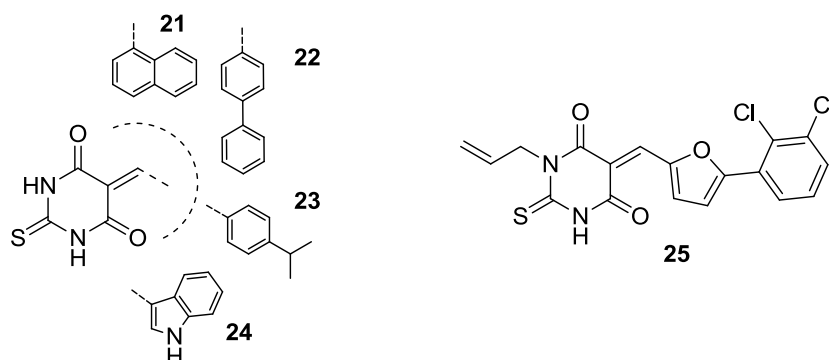


Figure 13. Binding mode of compound **20** (PDB: 4JSR). Maestro 9.2 Schrödinger, LLC, New York, NY, 2011.

4.14 Thiobarbiturates



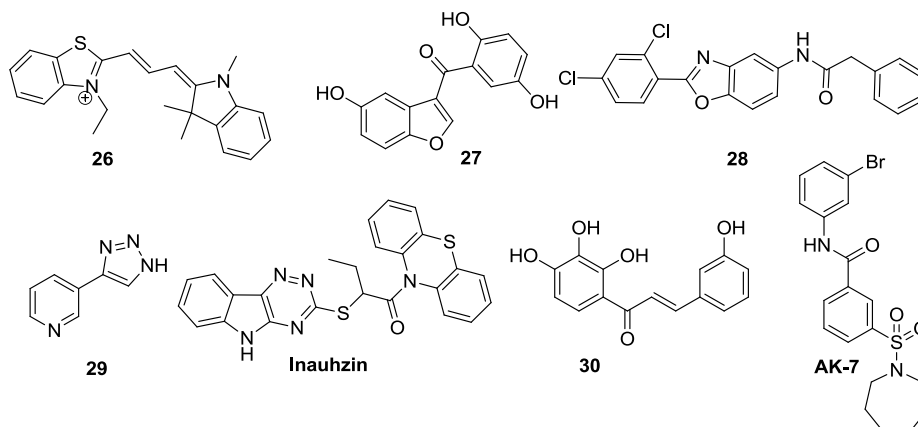
A virtual screening of 328 000 molecules followed by MM-PBSA approach allowed the identification of thiobarbiturate scaffold as Sirtuin inhibitor.¹⁶⁰ From Cambridge database containing 328 000 compounds, 390 that showed structural similarity to a Cambinol derivative were selected and docked into SIRT2, then 131 molecules were successfully docked into C-pocket and 5 barbiturate and thiobarbiturate were purchased and tested. After this preliminary screening in which compound **21** was the best SIRT2 inhibitor with IC_{50} of 9.1 μ M and 13.2 μ M (Table 11, fluorescent assay ZMAL substrate 10.5 μ M and NAD^+ 500 μ M) on SIRT2 and SIRT1 respectively, a small array of other derivatives were designed and synthesized. The most potent SIRT2 inhibitor was compound **22** with IC_{50} of 8.7 μ M (Table 11), on the contrary **24** showed the greatest SIRT1 inhibition with IC_{50} of 5.9 μ M (Table 11). The versatility of thiobarbiturate scaffold was applied also on SIRT5 when Jung

and co-workers¹⁶¹ in 2012 assayed a small library of thiobarbiturates against SIRT5 that were found inhibitors in micromolar range. Among them compound **25** was the best inhibitor (Table 11, Fluorescent assay, ZK(s)A substrate 200 μ M, Km 17.4 μ M, NAD⁺ 500 μ M).

Table 11. IC₅₀ Values for derivatives **21-25**^{160,161}

Compound	IC ₅₀ μ M			
	SIRT1	SIRT2	SIRT3	SIRT5
21	13.2	9.1	unavailable	unavailable
22	50.5	8.7	40.3	30.0
23	12.4	14.7	13% at 50 μ M	39.4
24	5.9	20.3	14% at 50 μ M	46.5
25	5.3	9.7	41% at 50 μ M	2.3

4.15 Miscellaneous Inhibitors



Compound **26** also named AC-93253¹⁶² reported as potent agonist of the retinoic acid receptor (RAR) was found SIRT2 inhibitor with an IC₅₀ of 6.0 μ M (fluorescent assay) with lower potency on SIRT1 and SIRT3 (IC₅₀ of 45.3 μ M and 24.6 μ M respectively). The treatment of HeLa cells with **26** induced hyperacetylation of p53 K382, H4 K16 and α -tubulin K40 showing also cytotoxic effect on DU-145 (PC3 human prostate cancer cell lines).

From a screening of an homemade library, very recently J.Wu et al.¹⁶³ reported a series of benzofuran SIRT1 inhibitors of which compound **27** was the most active with IC₅₀ of 2.8 μM on SIRT1 (NAD⁺ quantification assay with Ac-RHKK_{Ac}-NH₂ substrate)¹⁶⁴ showing the ability to induce p53 hyperacetylation on treated MCF7 cell line.

With the aim to move from pseudopeptides to small molecules Salo et al.¹⁶⁵ approached a virtual screening on 50 000 compounds from Cambridge database that were docked on SIRT3. Selected compounds that showed favourable interactions in the substrate binding area were purchased and assayed on SIRT1-3. Compound **28** that showed 71% and 72% inhibition on SIRT3 and SIRT1 respectively, is the most promising scaffold of the serie that can be used for further investigations.

Starting from nicotinamide the physiological SIRT1 inhibitor, a small array of nicotinamide derivatives were synthesized and screened on SIRT1-3.¹⁶⁶ From the series only compound **29** showed an interesting inhibition profile as SIRT3 selective inhibitor with IC₅₀ value of 23 μM (fluorescent assay BIOMOL drug discovery kit).

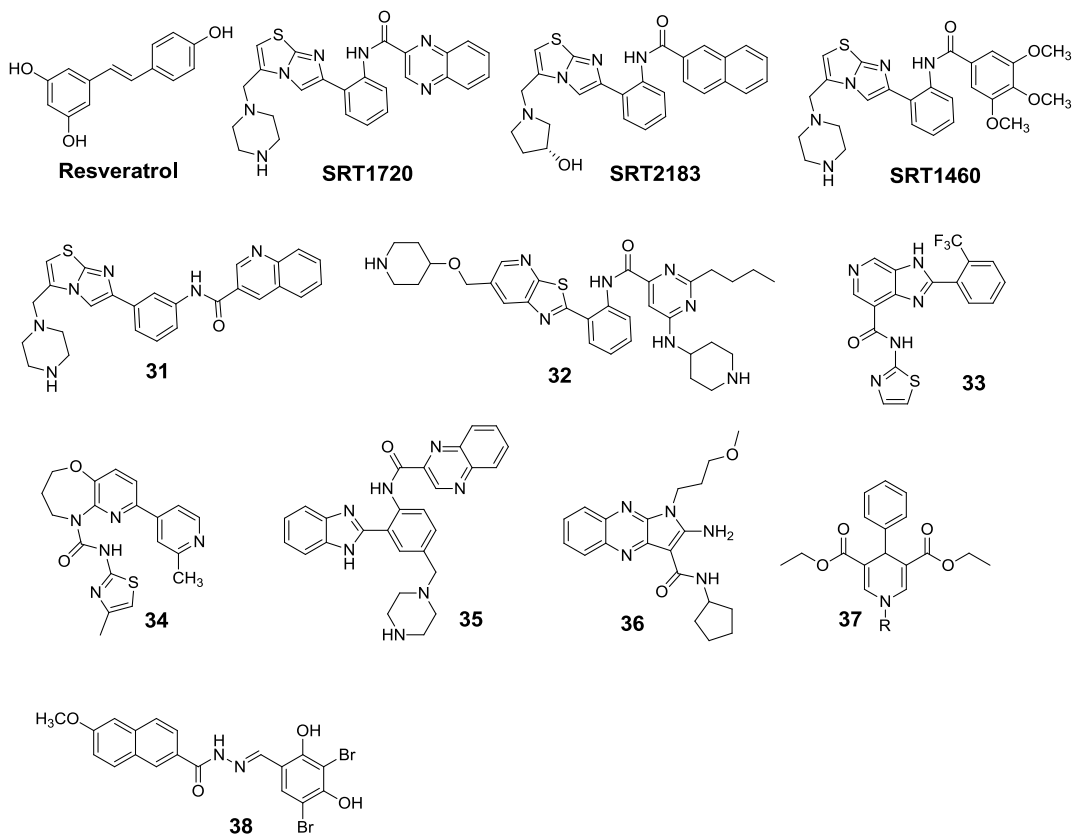
Inauhzin was discovered through a computational screening of 500 000 compounds in which 50 top candidates were purchased and tested in a cell based assay for their ability to increase p53 level in human lung carcinoma (H460).¹⁶⁷ Inauhzin was the most effective compound of the library showing the ability to reduce cancer cell growth by p53 dependent fashion with the ability to prevent p53 ubiquitylation from MDM2. Inauhzin induced p53 level and apoptosis in several cancer cell lines such as HCT116 (colon cancer), H460, A549 (lung cancer), A2780 (ovarian cancer), U87 (glioma), U2OS and SJSA (osteosarcoma) cells. Interestingly Inauhzin did not induce apoptosis in p53 deficient H1299 and HCT116 cells. An extensive study that ranged from cellular (SIRT1 knockdown, Western blot etc.) to enzymatic assays proven that Inauhzin was a non-competitive and selective SIRT1 inhibitor with an IC₅₀ in enzymatic assay of 0.7-2 μM (Fluor de Lys BML AK555, AK556, AK518). Administration of Inauhzin 30mg/Kg via intraperitoneal significantly reduced the tumour weight nearly 40% in xenograft tumor derived from H460 cells without change body weight, behaviour and appetite of treated animals. Interestingly in p53 null HCT116 xenografts no significant difference in apoptosis were observed between Inauhzin and vehicle treatments. All this findings let understand that

Inauhzin is a promising SIRT1 inhibitor and an optimal candidate for further structural investigations.¹⁶⁷

A series of chalcone, flavone, flavanone and stilbene derivatives were synthesized and screened on SIRT1 by Setou and co-workers¹⁶⁸ with the aim to find new SIRT1 activators.¹⁶⁸ Among the series in which none of proposed compounds showed activators properties, on the contrary compound **30** was found a SIRT1/3 inhibitor with IC₅₀ of 40.3 μM and 48.0 μM respectively.

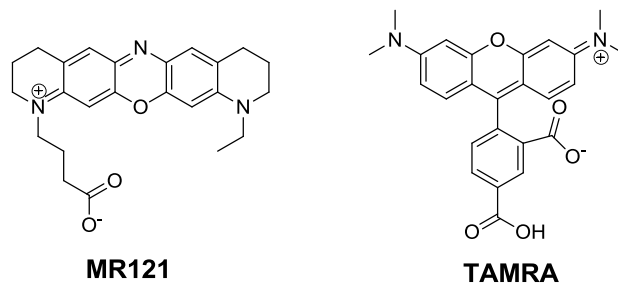
From a panel of compounds previously characterized as polyglutamine aggregate inhibitors, AK-7 was found SIRT2 specific inhibitor.^{169,170} Pharmacokinetic studies demonstrates that AK-7 has brain permeable properties but limited metabolic stability. Furthermore AK-7 stimulated the cytoplasmic retention of SREBP-2 (sterol regulatory element binding protein-2) with a resulting reduction of cholesterol in primary striatal neurons. In 2012 Kazantsev and co-workers¹⁷¹ reported also the neuroprotective effect of AK-7 in Huntington's disease mouse model in which improved motor function, extended survival and reduced brain a atrophy.

5 SIRTUIN ACTIVATORS



In 2003, resveratrol a polyphenol found in the red wine has been proposed by Sinclair and co-workers as the first SIRT1 activator, after a screening conducted using the BIOMOL fluorescent assay.¹⁵⁴ In 2004, Sinclair co-founded Sirtris Pharmaceuticals with Christoph Westphal which has been acquired in 2008 for \$720 million by GlaxoSmithKline. In 2005 Borra et al.¹⁷² investigated SIRT1 activation mediated by resveratrol using three different assays such as coumarin and rhodamine fluorescent assay, charcoal binding assay and HPLC based assay. They found that SIRT1 activation was independent of the peptide sequence but dependent on the presence of fluorophore. In 2006 Stükel and co-workers¹⁷³ in a HTS of 147 000 commercially available compounds using fluorescent BIOMOL assay identified a small hit of potential SIRT1 activators that showed at 10 μM a % activation > 216% of which compound **36** was the best one. Compound **36** in a cell based adipogenesis differentiation assay reduced the size of intracellular cytosolic and fat deposit, moreover in human leukemia cell line THP-1, differently to resveratrol compound **36** suppressed TNF- α release.

In search for more potent compounds in 2007 Westphal, Sinclair and co-workers¹⁷⁴ performed an HTS using a 20 aminoacid peptide substrate (Ac-Glu-Glu-Lys(biotin)-Gly-Gln-Ser-Thr-Ser-Ser-His-Ser-Lys(Ac)-Nle-Ser-Thr-Glu-Gly-Lys(MR121 or Tamra)-Glu-Glu-NH₂) "derived from p53" that was N-terminal linked with biotin and C-terminal to a fluorescent TAMRA or MR121.



In this screening three selective SIRT1 activators more potent than resveratrol ($EC_{1.5}$ 46.2 μ M) named SRT1720, 2183, 1460 were identified and showed $EC_{1.5}$ of 0.16 μ M (781% activation), 0.36 μ M (296 % activation), and 2.9 μ M (447% activation) respectively ($EC_{1.5}$ is the concentration required to increase enzyme activity of 50%).¹⁷⁴ The proposed mechanism of activation depended on decreasing of K_m of SIRT1 acetylated substrate (with fluorescent tag) by promoting a more productive conformation that enhance catalytic activity. Isothermal titration calorimetry studies of SRT1460 against SIRT1 showed that binding occurred only in presence of acetylated substrate (with fluorescent tag). Furthermore the authors claimed that resveratrol, SRT1720 and related activators in diet-induced obese (DIO) and genetically obese mice (*Lep^{ob/ob}*) improved insulin sensitivity, lowered plasma glucose and increased mitochondrial capacity, moreover in Zucker *fa/fa* rats (genetically obese rodents used for study insulin resistance) SRT1720 ameliorated gluconeogenic capacity and decreased gluconeogenesis.¹⁷⁴ In 2009 Perni¹⁷⁵ (Sirtris) and later Toyooka¹⁷⁶ and co-workers improved the medchem knowledge of "SIRT1 activators" by developing a SAR around SRT1720 such as compound **31**, moreover new oxazolo[4,5-b]pyridines series with related derivatives as **35**¹⁷⁷ were developed. In the same year Mai et al.¹⁷⁸ prepared a small library of 1,4-dihydropyridine (DHP), they found that DHPs derivatives that bearing a benzyl moiety at the N1 position were potent SIRT1-3 activators (Fluor de Lys BIOMOL assay). Furthermore N-benzyl-DHP compounds induced hypoacetylation on α -tubulin in U937 cells

(leukemia cell line), reduced the number of senescent cells in primary human mesenchymal stem cells (hMSC) up to 40%, and when tested in murine C2C12 myoblast showed a dose dependent increase of mitochondrial function by a mechanism involving PGC-1 α .

In these years the growing interest around sirtuins captured the interest of Pfizer Global Research and Development, that in 2010 published an independent work¹⁷⁹ in which the Sirtris's compounds SRT1720, SRT2183, SRT1460 and resveratrol failed to activate SIRT1. In details, by using an HPLC method which separated deacetylated TAMRA-p53 peptide product from the acetylated substrate, Sirtris compounds activated SIRT1. When the same experiment was repeated using a native p53 substrate that lacking fluorophore or when native full length SIRT1 substrates such as p53 and AceCS1 were used, no activation of SIRT1 was detected. In order to confirm that SIRT1 activation was dependent only by fluorophore tag, NMR chemical shift perturbation and isothermal calorimetry studies were carried out. NMR chemical shift perturbation detected a resonance shift of lysine acetyl (CH₃) group only when SRT1460 was incubated with TAMRA containing substrate, moreover isothermal calorimetry (ITC) demonstrated that SRT1460 bound to the SIRT1-TAMRA-peptide substrate complex but not to the SIRT1-native peptide substrate complex. In the same report Pacholec et al.¹⁷⁹ reported that SRT1720 neither lowers plasma glucose nor improved mitochondrial capacity in mice fed a high fat diet. Furthermore the concentration used in the Sirtris experiments of 100mg/Kg for SRT1720 was not tolerated and resulted in the death of three of the eight mice used in the study. After the demonstration that resveratrol and Sirtris series were not direct SIRT1 activators, an in vitro selectivity profile was carried out. The compounds were tested at 10 μ M against over 100 targets that included receptors, enzymes, kinases, ion channels and transporters. SRT1720, SRT2183 and SRT1460 did not activate SIRT1 and moreover were found highly promiscuous compounds able to exhibit > 50% inhibition of 38 (Table 12), 14 and 20 targets on 100, while resveratrol 7 on 100 targets.

Table 12. Inhibition profile of SRT1720¹⁷⁹

Target	SRT1720 % inhibition at 10 μ M
5-HT1B	88
5-HT1D	99
5-HT2A	77
5-HT2A (agonist site)	72
5-HT2B (agonist site)	55
5-HT6	54
A3	101
alpha 2A	60
alpha 2C	91
D2S (agonist site)	72
D3	56
delta 2 (DOP)	82
H2	69
H4	69
kappa (KOP)	51
M1	100
M2	88
M3	90
M4	91
M5	81
MC3	67
MCH1	85
Motilin	73
NK1	59
NK2	90
sst4	75
UT1(GPR14)	88
Carbonic anhydrase II	58
PDE11	66
PDE2	81
PDE3	59
PDE4	54
PDE6	51
Ca ²⁺ channel (N-type)	76
Na ⁺ channel (site 2)	63

Choline transporter (CHT1)	94
DA transporter	85
NE transporter	86

Later Huber et al.¹⁸⁰ (Elixir Pharmaceuticals, Inc.) reported that SRT1720 and SRT2183 when tested in different enzymatic assays did not activate SIRT1, and were effectively able to decrease the acetylation of p53 in cells but do so in cells that lack SIRT1, and this was attributed to inhibition of histone methyltransferase p300. The scientist of Sirtris in response to the Pacholec work published a paper that suggested a direct interaction of SRT compounds with SIRT1 and that the activation followed an allosteric mechanism.¹⁸¹ In order to clarify the molecular mechanism of Sirtuin activation by resveratrol Steegborn and co-workers¹⁸² solved SIRT3 and SIRT5 crystal structure in complex with fluorogenic substrate (FdL1) and piacetannol/resveratrol. In this study 0.2 mM of resveratrol and piacetannol could stimulate SIRT5 deacetylase activity when fluorophore modified peptide substrate was used, but on contrary inhibited SIRT3 dependent deacetylation. In the SIRT5 complex resveratrol (Figure 14 A) is positioned next to the substrate in direct contact to the coumarin fluorophore moiety. A similar binding mode was observed also by piacetannol (resveratrol metabolite) in complex with SIRT3 where the scaffold shows direct interaction with coumarin moiety (Figure 14 B).

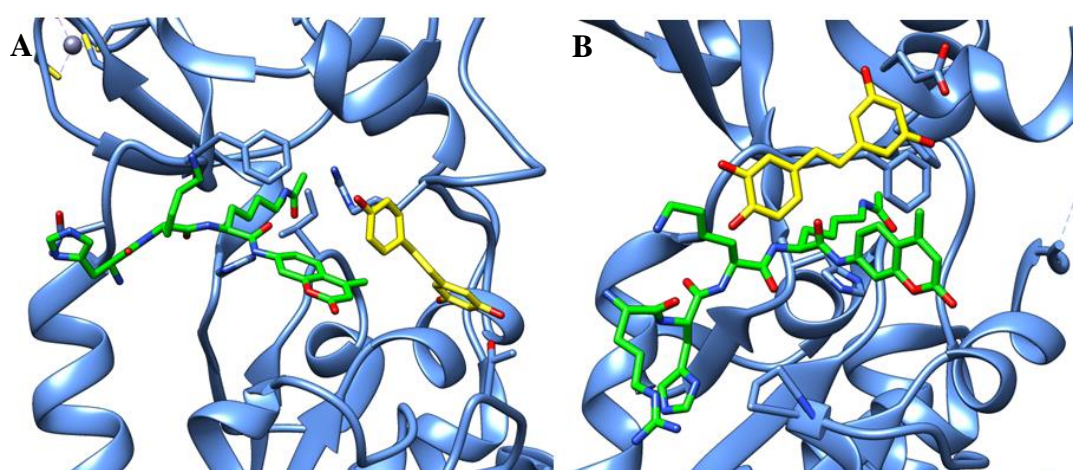


Figure 14. Binding mode of Resveratrol in SIRT5 (PDB: 4HDA) and Piacetannol in SIRT3 (PDB: 4HD8). Substrates are colored in green. UCSF Chimera 1.7.

In the two complexes both acetylated substrates are bound in the substrate binding site but differently to SIRT3 complex in which substrate seems not optimal positioned for a productive binding, in SIRT5 complex with resveratrol the acetyl lysine moiety is positioned deeper in the hydrophobic binding tunnel, resulting in a more productive binding conformation. The direct interaction between resveratrol and fluorescent substrate reveals the importance of this latter in the resveratrol SIRT1 mediated activation. Interestingly the authors found that resveratrol activates SIRT5 dependent deacetylation of FdL1-peptide, Prx1-Lys197 peptidic sequence (SKEYFSK(Ac)QK without fluorescent tag) and full length substrate and Cytochrome c full length but had no effect on deacetylation of p53-Lys382 (RHKK(Ac)LMFK. These interesting findings indicate the possibility develop sirtuin modulators targeting only specific substrates.¹⁸²

In 2013 Wu et al.¹⁸³ proposed a new library of SIRT1 activators bearing to hydrazone scaffold after a screening of an in-house library using fluorescent assay with coumarin-labeled substrate. Compound **38** was the most promising SIRT1 activator of the series with EC_{1.5} of 0.9 μ M and 624 % of activation but as well as SRT series when the compounds were assayed with fluorescent unlabeled substrate the deacetylation was not observed.

To address the controversy of Sirtris activators, Sinclair and co-workers¹⁸⁴ tested an alternative hypothesis in which the failure of STACs to deacetylate native substrates could be explained by the fact that fluorophore mimicking the characteristic of specific SIRT1 substrates containing bulky groups. SRT derivatives such as **SRT1460** and compound **32** that activated SIRT1 only with AMC-tagged substrate were able to activate SIRT1 when PGC-1 α K778 (PASTKSK(Ac)YDSLDF) and FOXO3a K290 (Ac-DSPSQLSK(Ac)WPGSPTS-NH₂) were used as substrates. Kinetic analysis revealed that activation was primarily through a lowering of peptide Km. PGC-1 α K778 and FOXO3a K290 in position +1 contain hydrophobic bulky residues tryptophan and tyrosine respectively and their substitution with alanine blocked the activation mediated by **SRT1460** and **32**. The finding that the ability of SIRT1 to be activated by resveratrol was attenuated in one mutant that substituted a lysine for a glutamate at position 230 whether an AMC-tagged substrate was used, led postulate an allosteric mechanism of SIRT1 activation. Furthermore the

substitution of Glu230 with a Lys or Ala attenuated the SIRT1 activation also by 117 structural diverse activators such as compounds **33** and **34** by using Ac-RHKK(Ac)W-NH₂ as substrate.¹⁸⁴ Beside the controversial SIRT1 activation mechanism resveratrol and STR1720 has been shown to mitigate negative effects of obesity and high-fat diets in both rats and mice as reviewed by Baur et al.¹⁸⁵

6 AIMS OF THE STUDY

1. To develop new SIRT1-3 inhibitors by designing diverse structural scaffolds.
2. To study the structure activity relationship from a simple medicinal chemistry functionalization to a fragment based approach.
3. To gain information of putative binding mode of the inhibitors by docking simulations.
4. To focus the attention on SIRT1/2 inhibition in understanding the proved connection with cancer, thanks to collaboration with biochemists and biologist.
5. To design specific molecular probes as useful tools to study the cellular localization of the SIRT1-3 inhibitors.

7 CARPROFEN ANALOGUES AS SIRTUIN INHIBITORS: ENZYME AND CELLULAR STUDIES

Abstract: SIRT1/2 inhibitors were developed by combining chemical features of selisistat (EX527) and carprofen (anti-inflammatory drug). The most potent compound increased acetyl-p53 and acetyl- α -tubulin levels, and induced slight apoptosis at 50 μ m in U937 cells, differently from selisistat and carprofen.

*Adapted with the permission from Mellini, P.; Carafa, V.; Di Rienzo, B.; Rotili, D.; De Vita, D.; Cirilli, R.; Gallinella, B.; Provisiero, D.P.; Di Maro, S.; Novellino, E.; Altucci, L.; Mai A. *Chem Med Chem* 2012, 7: 1905-1908. Copyright 2012 Wiley-VCH Verlag GmbH & Co. KGaA, Weinheim.

6.1 Introduction

The nonsteroidal anti-inflammatory drug (NSAID) carprofen (Figure 1) was shown to activate the p38 mitogen-activated protein kinase (MAPK) pathway leading to increased level of p75^{NTR} protein and induction of apoptosis in prostate (PC-3 and DU-145) and bladder (T24) cancer cells.¹⁸⁶ In this assay, carprofen was one order of magnitude more potent than a series of related profens. Due to the structure similarity between carprofen and EX-527, we prepared a small library of carprofen-related derivatives (compounds **1-11**) by retaining the carbazole core and replacing the carboxylic acid function with an ester, (substituted)amide, or (substituted)hydroxamate group (Figure 1). Compounds **1-11** were then tested against SIRT1 and SIRT2, and among them compound **2** was selected for evaluation of p53 and α -tubulin acetylation levels in the p53 wild-type breast cancer MCF-7 cells. Moreover, the effects of the 6-chloro-9*H*-carbazol-2-ylamides **2, 4, 6, 9, and 11** on cell cycle, apoptosis, and granulocytic differentiation in U937 cells have been explored.

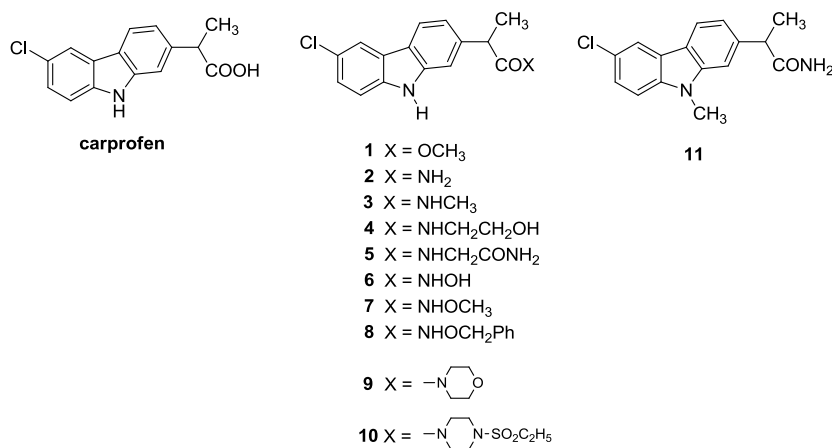


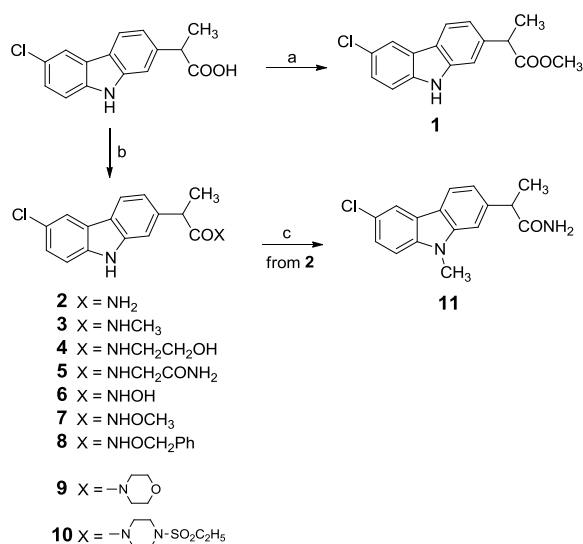
Figure 1. Carprofen analogues described in this study.

6.2 Chemistry

The synthetic pathway followed for preparation of **1-11** is depicted in Scheme 1. The methylester **1** was prepared by heating carprofen, methanol, and 96% sulphuric acid at reflux temperature for 5 h according to literature (US patent: 3,896, 1451 1975). Reaction of carprofen with thionyl chloride led to the formation of the corresponding acyl chloride, which was treated with the appropriate amines to afford the

carboxamides **2-10**. Finally, the use of iodomethane in the presence of potassium carbonate in dry *N,N*-dimethylformamide (DMF) converted **2** into the related *N*-methylcarbazole derivative **11**.

Scheme 1^a



^a(a) CH₃OH, H₂SO₄, reflux, 5 h; (b) 1) SOCl₂, reflux, 4 h, 2) amine or amine hydrochloride/triethylamine, CH₃CN (CH₃CN/CH₃OH for **6-8**), rt, 3 h to overnight; (c) CH₃I, K₂CO₃, DMF, rt, 24 h.

6.3 Results and discussion

Carprofen and its analogues **1-11** were tested in vitro against hSIRT1 and hSIRT2 at the concentration of 50 μM using a fluorescent biochemical assay. Since the carprofen-based compounds possess a chiral center, the enantiomers of 2-(6-chloro-9*H*-carbazol-2-yl)propanamide **2** and its *N*-methylpropanamide derivative **3** were isolated on a semipreparative scale by enantioselective HPLC (Figure 2) and submitted to individual biological investigations. As shown in Table 1, carprofen as well as its methyl ester **1** showed low SIRT1 inhibitory effects. Among the 6-chloro-9*H*-carbazol-2-ylamides **2-11**, the highest SIRT1 inhibition activities were observed with the primary propanamide **2** (with no differences between the two enantiomers) and its 9-methyl analogue **11**, with 78.3 and 59.5% of inhibition at the tested dose,

respectively. The IC_{50} (inhibitory concentration 50, compound dose required to inhibit the enzyme activity of 50%) values for **2** and **11** against SIRT1 were 7.1 ± 0.4 and $38.0 \pm 1.9 \mu\text{M}$, respectively. The hydroxamic acid derivative **6** is still active (50% of SIRT1 inhibition at $50 \mu\text{M}$), but lost its inhibitory action when it was substituted at the *O* atom (**7** and **8**, *O*-methyl and *O*-benzyl hydroxamates).

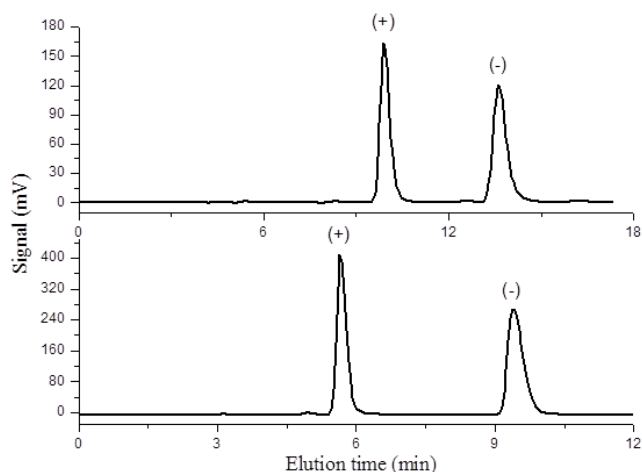


Figure 2. Typical analytical HPLC chromatogram illustrating the enantioseparation of **2** (top) and **3** (bottom). Column: Chiralpak AD (250 mm x 4.6 mm I.D.); eluent: *n*-hexane-ethanol 70/30 (v/v); flow rate: 1 mL/min; column temperature: 25 °C; detector: UV at 254 nm.

The introduction of other than hydrogen substituents at the primary amide function of **2** induced moderate to null SIRT1 inhibition (**4**, bearing a 2-hydroxyethyl group, displayed 36% of inhibition at $50 \mu\text{M}$, while the *N*-methylpropanamide **3** was totally inactive). The insertion of cyclic amines (morpholine (**9**), *N*-ethylsulfonylpiperazine (**10**) at the carprofen scaffold gave rise to appreciable (**9**, >50%) or low (**10**, 14%) SIRT1 inhibition. Against SIRT2, **2** displayed the highest inhibitory activity (59.6 % of inhibition at $50 \mu\text{M}$; $IC_{50} = 64.9 \pm 5.8 \mu\text{M}$; no stereoselectivity), followed by *O*-benzyl hydroxamate **8** (54.4 % inhibition). *O*-Methyl hydroxamate **7**, *N*-methyl derivatives **3** and **11** ($IC_{50} = 99.7 \pm 8.8 \mu\text{M}$), and *N*-glycinamide **5** all exhibited greater than 30% inhibition of SIRT2, while the remaining compounds displayed only very low SIRT2 inhibitory activities at $50 \mu\text{M}$. The SIRT1 and -2 inhibition by **2** was functionally confirmed by functional assays through Western blot analyses.

The acetylation levels of p53 (MCF7 cells) a well-known SIRT1 substrate, and α -tubulin (U937 cells) as a substrate of SIRT2 were determined after treatment of the cells with 50 μ M **2**.

Table 1. hrSIRT1 and hrSIRT2 inhibition assay performed on carprofen and **1-11**.^a

Compd	% inhibiting activity @ 50 μ M	
	SIRT1	SIRT2
1	37.2 \pm 1.5	NI ^b
2	78.3 \pm 3.9	59.6 \pm 2.4
(+)- 2	79.0 \pm 2.8	61.7 \pm 1.8
(-)- 2	77.5 \pm 3.9	59.1 \pm 1.5
3	NI ^b	34.2 \pm 1.7
(+)- 3	NI ^b	23.3 \pm 1.2
(-)- 3	NI ^b	34.7 \pm 1.7
4	36.0 \pm 1.8	9.8 \pm 0.4
5	21.5 \pm 0.9	30.5 \pm 1.5
6	50.0 \pm 2.6	21.0 \pm 0.8
7	19.2 \pm 1.0	39.3 \pm 2.0
8	NI	54.4 \pm 2.2
9	56.4 \pm 2.8	6.0 \pm 0.3
10	14.0 \pm 0.7	21.2 \pm 1.1
11	59.5 \pm 3.0	33.9 \pm 1.7
carprofen	20.2 \pm 1.0	13.8 \pm 0.4
EX-527	83.6 \pm 4.2	45.5 \pm 2.8

^aValues are means \pm SD of at least two experiments. ^bNI, no inhibition at the dose evaluated.

Selisistat (10 μ M), SAHA (5 μ M) and AGK-2 (50 μ M), a SIRT2 selective inhibitor were used as reference agents. In these assays, the level of Lys 373-382 acetylated p53 increased after the treatment with **2**, correlating with p53 activation (Figure 3A), and also the acetyl- α -tubulin level showed an increase after **2** treatment (Figure 3B). Selected SIRT inhibitors **2**, **4**, **6**, **9**, and **11** were tested at 50 μ M for 30 h in the human U937 leukemia cell line to detect their effects on cell cycle progression and apoptosis (Figure 4). Carprofen and EX-527 (both at 50 μ M) were added as reference drugs. After the treatment with EX-527 and **6**, an arrest at the G1 phase was observed, while with **4**, **9**, and **11** an increase of the S phase was obtained (Figure 4A).

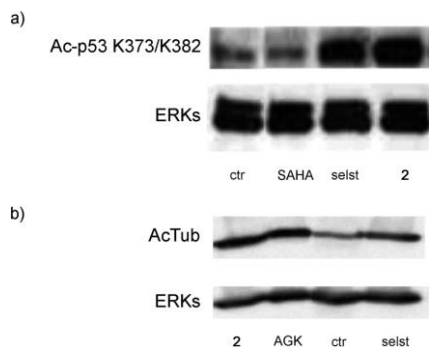


Figure 3. Western blot analyses performed with **2** (50 μ M) to detect p53 or α -tubulin acetylation in MCF-7 cells. EX-527 (10 μ M), SAHA (5 μ M) and AGK-2 (50 μ M) were used as reference.

With regards to apoptosis, compounds **2**, **4**, and **9** gave a little but significant increase of the DNA fragmentation (pre-G1 pick), whereas EX-527 and carprofen did not display any detectable effect at the tested conditions (Figure 4B).

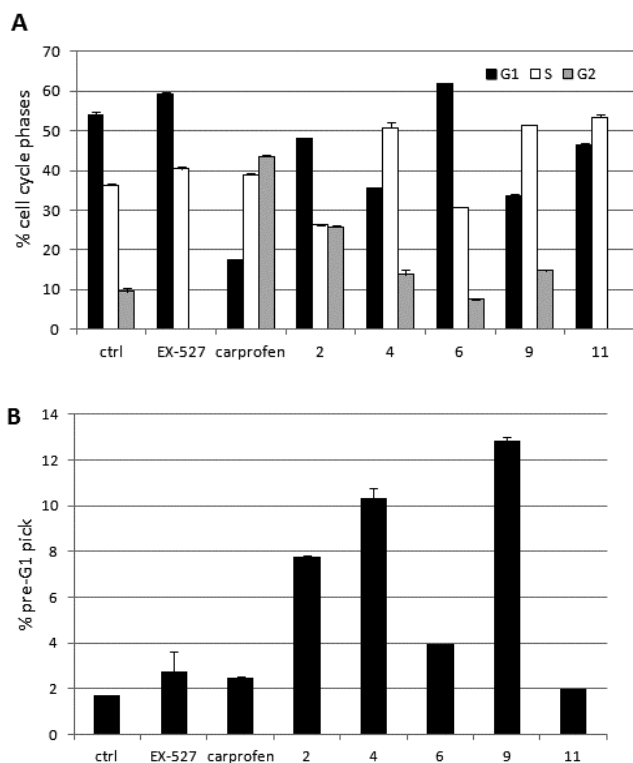


Figure 4. Cell cycle effect (A) and death induction (B) of **2**, **4**, **6**, **9**, and **11** (50 μ M, 30 h) in U937 cells.

In addition, granulocytic differentiation was evaluated for **2**, **4**, **6**, **9**, and **11** (50 μ M, 24 h) in U937 cells by the increase of % CD11c positive/propidium iodide (PI) negative cells (Figure 5). At the tested conditions, a significant induction of granulocytic differentiation was not detected.

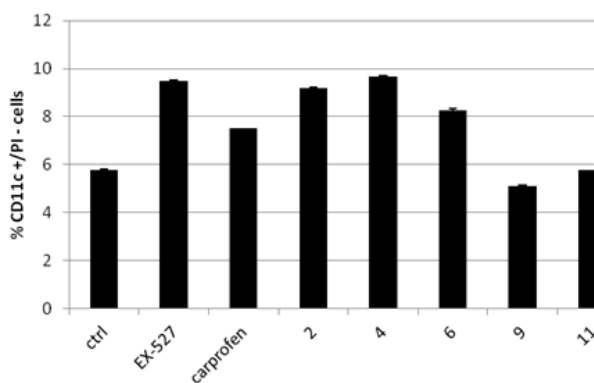


Figure 5. Granulocytic differentiation induced by **2**, **4**, **6**, **9**, and **11** in U937 cells at 50 μ M for 24 h. EX-527 and carprofen (both at 50 μ M) were added as reference drugs.

6.4 Conclusions

In conclusion, we highlighted the usefulness of the carprofen's carbazole scaffold for design and synthesis of novel SIRT1/2 inhibitors. Analogously to the related EX-527, the 2-(6-chloro-9*H*-carbazol-2-yl)propanamide **2** was the most efficient against both SIRT1 and SIRT2, since further substitutions at the carboxamide function or at the carbazolyl nitrogen atom yielded less potent or inactive compounds. Differently from EX-527 and carprofen, **2** and some analogues (**4** and **9**) induced to some extent cell death in human leukemia U937 cells when tested at 50 μ M for 30 h. Further studies have to be addressed to improve the potency and selectivity of the novel compounds against sirtuins, as well as their ability to induce anticancer effects.

6.5 Experimental Section

Chemistry. Chemical reagents including carprofen and solvent used in this study were purchased from Sigma-Aldrich Chemical Co. (Milano, Italy) and were of analytical grade. Melting points were determined on a Tottoli apparatus (Buchi) and are uncorrected. Infrared spectra were recorded on neat compounds on a Perkin-Elmer Spectrum-One spectrophotometer equipped with an ATR detector; band frequencies are reported in wave number (cm^{-1}). ^1H NMR spectra were acquired on a Bruker Avance 400 spectrometer operating at 400 MHz. Chemical shift values, unless otherwise stated, are reported as δ (ppm) relatively to TMS (tetramethylsilane) as internal reference; coupling constants are given in Hz. Yields of all reactions refer to the purified products. Mass spectra were recorded on: API-TOF Mariner by Perspective Biosystem (Stratford, Texas, USA), samples were injected by an Harvard pump using a flow rate of 5-10 $\mu\text{l}/\text{min}$, infused in the Electrospray system. Elemental analyses were obtained by a PE 2400 (Perkin-Elmer) analyser and have been used to determine purity of the described compounds, that is $>95\%$. Analytical results are within $\pm 0.40\%$ of the theoretical values. Analytical and semipreparative HPLC resolutions were performed using the commercially available 250 mm \times 4.6 mm I.D. and 250 mm \times 10 mm I.D. Chiralpak AD columns (Chiral Technologies Europe, Illkirch, France).

The analytical HPLC apparatus consisted on a Dionex P580 LPG pump, an ASI-100 T autosampler, a STH 585 column oven, a PDA-100 UV detector; data were acquired and processed by a Chromeleon Datasystem (Dionex Corporation, Sunnyvale, CA). For semipreparative separation a Perkin-Elmer (Norwalk, CT, USA) 200 LC pump equipped with a Rheodyne (Cotati, CA, USA) injector, a 1 mL sample loop, a Perkin-Elmer LC 101 oven and Waters 484 detector (Waters Corporation, Milford, MA, USA) were used. The signal was acquired and processed by Clarity software (DataApex, Prague, The Czech Republic). Specific rotations were measured at 589 nm by a Perkin-Elmer polarimeter model 241 equipped with a Na/Hg lamp. The volume of the cell was 1 mL and the optical path was 10 cm. The system was set at a temperature of 20 $^\circ\text{C}$.

Synthesis of 2-(6-Chloro-9H-carbazol-2-yl)propanamide (2). A mixture of carprofen (0.7 g, 2.5 mmol) and thionyl chloride (8.7 mL) was heated at 45 °C for 5 h. After this time, the obtained yellow solution was carefully evaporated under reduced pressure, then dry acetonitrile (20 mL) was added, and NH_{3(g)} was bubbled into the solution at room temperature for 3 h. Afterwards, the solvent was evaporated and the remaining solid was treated with aqueous saturated potassium carbonate (10 mL), filtered-off, and washed with water (3 × 4 mL). Finally, the solid was dried under reduce pressure and crystallized by acetonitrile to give pure **2** (0.6 g, 2.2 mmol, 88.0%). Mp: 204-206 °C (from acetonitrile). IR (neat): 3402 (NH_{carbazole} + NH_{amide}), 3176 (NH_{amide}) 2977-2899 (CH-CH₃), 1655 (C=O) cm⁻¹. ¹H NMR (CD₃CN): δ = 9.43 (s, 1H, NH), 8.06 (d, 1H, *J* = 2.2 Hz, H-5), 8.0 (d, 1H, *J* = 8.1 Hz, H-4), 7.51 (d, 1H, *J* = 1.47 Hz, H-1), 7.46 (d, 1H, *J* = 8.5 Hz, H-8), 7.35 (dd, 1H, *J* = 2.2, 8.5 Hz H-7) 7.18 (dd, 1H, *J* = 1.47, 8.1 Hz, H-3), 6.1 (s br, 1H, CONH), 5.6 (s br, 1H, CONH), 3.72-3.77 (q, 1H, *J* = 7.1 Hz, -CH-CH₃), 1.46 (d, 3H, *J* = 7.1 Hz -CH-CH₃). Anal. (C₁₅H₁₃ClN₂O) C, H, N. MS, *m/z* : 273 [M+H].

2-(6-Chloro-9H-carbazol-2-yl)-N-methylpropanamide (3). A mixture of carprofen (0.2 g, 0.73 mmol) and thionyl chloride (2.5 mL, strong excess) was heated at 45 °C for 5 h. Then the obtained yellow solution was carefully evaporated under reduced pressure, diluted in dry acetonitrile (10 mL) and treated with methylamine_(g) bubbled through the solution at room temperature for 3 h. Afterwards, the solvent was evaporated and the remaining thick oil was treated with aqueous saturated potassium carbonate (5 mL) and extracted with ethyl acetate (4 × 30 mL). The combined organic extracts were collected, dried (sodium sulphate), and evaporated under vacuum to give a yellow solid, that was purified on silica gel column chromatography by eluting with ethyl acetate/methanol 8/2 v/v to afford pure **3** (0.09 g, 0.32 mmol, 44 %). Mp 164-166 °C. IR (neat): 3262 (NH_{carbazole} + NH_{amide}), 2969-2934 (CH-CH₃), 1623 (C=O) cm⁻¹. ¹H NMR (DMSO-*d*₆): δ = 11.34 (s, 1H, NH), 8.15 (d, 1H, *J* = 2 Hz, H-5), 8.05 (d, 1H, *J* = 8.1 Hz, H-4), 7.9 (q, 1H, *J* = 4.6 Hz, CONH-CH₃), 7.47 (d, 1H, *J* = 8.6 Hz, H-8), 7.43 (s, 1H, H-1), 7.35 (dd, 1H, *J* = 2, 8.6 Hz, H-7), 7.13 (d, 1H, *J* = 8.1 Hz, H-3), 3.69-3.75 (q, 1H, *J* = 6.9 Hz, -CH-CH₃),

2.56 (d, 3H, $J = 4.6$ Hz, CONH-CH₃), 1.40 (d, 3H, $J = 6.9$ Hz, -CH-CH₃). Anal. (C₁₆H₁₅ClN₂O) C, H, N. MS, m/z : 287 [M + H]⁺.

Synthesis of 2-(6-Chloro-9H-carbazol-2-yl)-N-(2-hydroxyethyl)propanamide (4).

A solution of 2-(6-chloro-9H-carbazol-2-yl)propanoyl chloride in dry acetonitrile (5 mL) [prepared following the same procedure as described for **3** from carprofen (0.2 g, 0.73 mmol) and thionyl chloride (2.5 mL, strong excess)] was added to a stirred solution of 2-aminoethanol (0.27 mL, 4.4 mmol) in dry acetonitrile (5 mL). After stirring at room temperature for 3 h the solvent was evaporated and the remaining solid was treated with aqueous saturated potassium carbonate (5 mL). The obtained suspension was extracted with ethyl acetate (3 × 35 mL), and the combined organic extracts were dried (sodium sulphate) and evaporated under reduced pressure. The solid residue was recrystallized by acetonitrile to give pure **4** (0.1 g, 0.31 mmol, 42.5%). Mp 168-170 °C (from acetonitrile). IR (neat): 3402-3253 (NH_{carbazole}, NH_{amide}, OH), 2977-2877 (CH_{aliphatic}), 1627 (C=O) cm⁻¹. ¹H NMR (DMSO-*d*₆): δ = 11.32 (s, 1H, NH), 8.15 (d, 1H, $J = 1.7$ Hz, H-5), 8.05 (d, 1H, $J = 8.1$ Hz, H-4), 7.94 (t, 1H, $J = 5.4$ Hz, CONH), 7.47 (d, 1H, $J = 8.6$ Hz, H-8), 7.45 (s, 1H, H-1), 7.35 (dd, 1H, $J = 1.7, 8.6$ Hz, H-7), 7.15 (d, 1H, $J = 8.1$ Hz, H-3), 4.62 (s br, 1H, -OH), 3.75-3.81 (q, 1H, $J = 6.9$ Hz, CH-CH₃), 3.38 (pseudo s br, 2H, -CH₂-OH), 3.04-3.20 (m, 2H, -CH₂-NH), 1.41 (d, 3H, $J = 6.9$ Hz, -CH-CH₃). Anal. (C₁₇H₁₇ClN₂O₂) C, H, N. MS m/z : 317 [M + H]⁺.

N-(2-Amino-2-oxoethyl)-2-(6-chloro-9H-carbazol-2-yl)propanamide (5). A solution of 2-(6-chloro-9H-carbazol-2-yl)propanoyl chloride in dry acetonitrile (10 mL) [prepared from carprofen (0.2 g, 0.73 mmol) and thionyl chloride (2.5 mL, strong excess)] was added to a suspension of glycine hydrochloride (0.243g, 2.2 mmol) and triethylamine (1 mL, 7.3 mmol) in acetonitrile/methanol 8/2 v/v (25 mL), prepared 15 min before. The reaction was stirred at room temperature for 12 h, then the solvent was evaporated and the solid residue was treated with aqueous saturated potassium carbonate (5 mL). The obtained suspension was extracted with ethyl acetate (3 × 35 mL) and the combined organic extracts were dried (sodium sulphate) and evaporated under reduced pressure. The solid residue was recrystallized by

acetonitrile to give pure **5** (0.076 g, 0.23 mmol, 31.6 %). Mp 185-187°C (from acetonitrile). IR (neat): 3400-3193 (NH_{carbazole}, NH_{I amide}, NH_{II amide}), 2977-2892 (CH_{aliphatic}), 1652 (C=O), 1625 (C=O) cm⁻¹. ¹H NMR (DMSO-*d*₆): δ = 11.32 (s, 1H, NH), 8.14 (d, 1H, *J* = 1.71 Hz, H-5), 8.07 (t, 1H, *J* = 5.87 Hz, -CONHCH₂-) 8.05 (d, 1H, *J* = 8.1 Hz, H-4), 7.47 (d, 1H, *J* = 8.46 Hz, H-8), 7.45 (s, 1H, H-1), 7.34 (dd, 1H, *J* = 1.71, 8.46 Hz, H-7), 7.18 (s br, 1H, -CONH₂), 7.15 (d, 1H, *J* = 8.1 Hz, H-3), 6.97 (s br, 1H, -CONH₂), 3.88-3.83 (q, 1H, *J* = 7.34 Hz, -CHCH₃), 3.72-3.66 (dd, 1H, *J* = 5.87, 10.76 Hz, -CH₂CONH₂), 3.58-3.52 (dd, 1H, *J* = 5.87, 10.76 Hz, -CH₂CONH₂), 1.41 (d, 3H, *J* = 7.34 Hz, -CHCH₃). Anal. (C₁₇H₁₆ClN₃O₂) C, H, N. MS, *m/z* : 330 [M + H]⁺.

Synthesis of 2-(6-Chloro-9H-carbazol-2-yl)-N-hydroxypropanamide (6).

Triethylamine (1 mL, 7.3 mmol) was added to a suspension of hydroxylamine hydrochloride (0.15 g, 2.2 mmol) in a mixture acetonitrile/methanol 9.5/0.5 v/v (10 mL), and the resulting mixture was stirred for 20 min. Afterwards, the reaction was treated with a solution of 2-(6-chloro-9H-carbazol-2-yl)propanoyl chloride [from carprofen (0.2 g, 0.73 mmol) and thionyl chloride (2.5 mL, strong excess)] in dry acetonitrile (5 mL) and stirred at room temperature for 12 h. Then, the solvent was evaporated, the solid residue was treated with aqueous saturated potassium carbonate (5 mL), and the obtained suspension was extracted with ethyl acetate (3 × 35 mL). The combined organic extracts were dried (sodium sulphate) and evaporated under reduced pressure, and the solid residue was recrystallized by acetonitrile to give pure **6** (0.13 g, 0.44 mmol, 60.2%). Mp 174-177 °C (from acetonitrile). IR (neat): 3479 (NH_{carbazole}), 3334 (NH_{amide}), 3147 (OH), 2971-2877 (CH-CH₃), 1632 (C=O) cm⁻¹. ¹H NMR (DMSO-*d*₆): δ = 11.33 (s, 1H, NH), 10.64 (s, 1H, CONH-OH), 8.76 (s, 1H, CONH-OH), 8.14 (d, 1H, *J* = 2 Hz, H-5), 8.04 (d, 1H, *J* = 8.1 Hz, H-4), 7.46 (d, 1H, *J* = 8.8 Hz, H-8), 7.44 (s, 1H, H-1), 7.33 (dd, 1H, *J* = 2, 8.8 Hz, H-7), 7.12 (d, 1H, *J* = 8.1 Hz, H-3), 3.55-3.60 (q, 1H, *J* = 7.1 Hz, -CH-CH₃), 1.40 (d, 3H, *J* = 7.1 Hz, -CH-CH₃). Anal. (C₁₅H₁₃ClN₂O₂) C, H, N. MS, *m/z* : 289 [M + H]⁺.

2-(6-chloro-9H-carbazol-2-yl)-N-methoxypropanamide (7). The same procedure reported for the synthesis of **6** was employed using carprofen and *O*-

methylhydroxylamine hydrochloride. Yield, 38.5 %. Mp 219-220 °C (from acetonitrile). IR (neat): 3471 (NH_{carbazole}), 3329 (NH_{amide}), 2970-2879 (CH-CH₃), 1638 (C=O) cm⁻¹. ¹H NMR (DMSO-*d*₆): δ = 11.33 (s, 1H, NH), 11.22 (s, 1H, -NHOCH₃), 8.15 (d, 1H, *J* = 1.71 Hz, H-5), 8.06 (d, 1H, *J* = 8.07 Hz, H-4), 7.47 (d, 1H, *J* = 8.56 Hz, H-8), 7.43 (s, 1H, H-1), 7.35 (dd, 1H, *J* = 1.71, 8.56 Hz, H-7), 7.12 (d, 1H, *J* = 8.07 Hz, H-3) 3.55 (pseudo s, 4H, -CHCH₃ + -OCH₃), 1.41 (d, 3H, *J* = 7.09 Hz, -CHCH₃). Anal. (C₁₆H₁₅ClN₂O₂) C, H, N. MS, *m/z* : 303 [M + H]⁺.

***N*-Benzyloxy-2-(6-chloro-9*H*-carbazol-2-yl)propanamide (8).** The same procedure reported for the synthesis of **6** was employed using carprofen and *O*-benzylhydroxylamine hydrochloride. Yield, 42.5 %. Mp 234-235 °C (from acetonitrile). IR (neat): 3467 (NH_{carbazole}), 3324 (NH_{amide}), 2974-2883 (CH-CH₃), 1637 (C=O) cm⁻¹. ¹H NMR (DMSO-*d*₆): δ = 11.35 (s, 1H, NH), 11.24 (s, 1H, -NHOCH₂), 8.17 (d, 1H, *J* = 1.96 Hz, H-5), 8.06 (d, 1H, *J* = 8.07 Hz, H-4), 7.48 (d, 1H, *J* = 8.56 Hz, H-8), 7.44 (s, 1H, H-1), 7.36 (dd, 1H, *J* = 1.96, 8.56 Hz, H-7), 7.30 (pseudo s, 5H, -Ar), 7.11 (d, 1H, *J* = 8.07 Hz, H-3), 4.74 (s, 2H, -OCH₂), 3.61-3.55 (q, 1H, *J* = 7.09 Hz, -CHCH₃), 1.42 (d, 3H, *J* = 7.09 Hz, -CHCH₃). Anal. (C₂₂H₁₉ClN₂O₂) C, H, N. MS, *m/z* : 379 [M + H]⁺.

2-(6-Chloro-9*H*-carbazol-2-yl)-1-morpholinopropan-1-one (9). A solution of 2-(6-chloro-9*H*-carbazol-2-yl)propanoyl chloride [from carprofen (0.2 g, 0.73 mmol) and thionyl chloride (2.5 mL, strong excess)] and triethylamine (0.20 mL, 1.46 mmol) in dry acetonitrile (5 mL) was added to a stirred solution of morpholine (0.08 mL, 0.87 mmol) in dry acetonitrile (5 mL). After stirring at room temperature for 12 h the solvent was evaporated and the solid residue was treated with aqueous saturated potassium carbonate (5 mL). The obtained suspension was extracted with ethyl acetate (3 × 35 mL), dried (sodium sulphate), and evaporated under reduced pressure. The solid residue was purified on alumina column chromatography by eluting with dichloromethane/methanol 9/1 v/v and recrystallized by acetonitrile to give pure **9** (0.11 g, 0.32 mmol, 43.8%). Mp 217-220 °C (from acetonitrile). IR (neat): 3254 (NH), 2978-2842 (CH-CH₃), 1613 (C=O) cm⁻¹. ¹H NMR (MeOD/DMSO-*d*₆ 9.5/0.5 v/v): δ = 8.80 (d, 1H, *J* = 2 Hz, H-5), 8.77 (d, 1H, *J* = 8.1 Hz, H-4), 8.18 (d, 1H, *J* =

8.6 Hz, H-8), 8.10 (s, 1H, H-1), 8.08 (dd, 1H, $J = 2$, 8.6 Hz, H-7), 7.83 (d, 1H, $J = 8.1$ Hz, H-3), 4.92-4.97 (q, 1H, $J = 6.6$ Hz, -CH-CH₃), 4.06-4.39 (m, 7H, morpholine), 3.81 (m, 1H, morpholine), 2.17 (d, 3H, $J = 6.6$ Hz, -CH-CH₃). Anal. (C₁₉H₁₉ClN₂O₂) C, H, N. MS, m/z 343 [M + H]⁺.

2-(6-Chloro-9H-carbazol-2-yl)-1-[4-(ethylsulfonyl)piperazin-1-yl]propan-1-one

(10). A solution of 2-(6-chloro-9H-carbazol-2-yl)propanoyl chloride [from carprofen (0.2 g, 0.73 mmol) and thionyl chloride (2.5 mL, strong excess)] in dry acetonitrile (10 mL) was added to a stirred solution of 1-(ethylsulfonyl)piperazine (0.65 g, 9.65 mmol) in dry acetonitrile (10 mL). After stirring at room temperature for 12 h, the solvent was evaporated and the remaining solid was treated with aqueous saturated potassium carbonate (5 mL). The obtained suspension was extracted with ethyl acetate (3 × 30 mL), dried (sodium sulphate), and evaporated under reduced pressure. The obtained solid was washed with water (2 × 3 mL), dried and purified using PLC (Preparative Layer Plates) Silica gel 20 × 20 cm by eluting with ethyl acetate/cyclohexane/methanol 6/3/1 v/v/v to give pure **10** (0.135 g, 0.31 mmol, 42.5%). Mp 123-125 °C (from cyclohexane). IR (neat): 3461 (NH_{carbazole}), 3329 (NH_{amide}), 2979-2889 (CH_{aliphatic}), 1628 (C=O), 1338 (S=O) cm⁻¹. ¹H NMR (CD₃CN): δ = 9.42 (s br, 1H, NH), 8.05 (d, 1H, $J = 1.96$ Hz, H-5), 8.02 (d, 1H, $J = 8.07$ Hz, H-4), 7.47 (d, 1H, $J = 8.56$ Hz, H-8), 7.39 (s, 1H, H-1), 7.36 (dd, 1H, $J = 1.96, 8.56$ Hz, H-7), 7.12 (d, 1H, $J = 8.07$ Hz, H-3), 4.18-4.13 (q, 1H, $J = 6.85$ Hz, -CH-CH₃), 3.77-3.71 (m, 1H, piperazine), 3.57-3.50 (m, 2H, piperazine), 3.44-3.39 (m, 1H, piperazine), 3.25-3.17 (m, 1H, piperazine), 3.07-3.02 (m, 2H, piperazine), 2.88-2.73 (q, 2H, $J = 7.34$ Hz, -CH₂-CH₃), 2.55-2.49 (m, 1H, piperazine), 1.41 (d, 3H, $J = 6.85$ Hz, -CH-CH₃), 1.12 (t, 3H, $J = 7.34$ Hz -CH₂CH₃). Anal. (C₂₁H₂₄ClN₃O₃S) C, H, N. MS, m/z : 434 [M + H]⁺.

Synthesis of 2-(6-Chloro-9-methyl-9H-carbazol-2-yl)propanamide (11). Dry potassium carbonate (0.3 g, 2.1 mmol) was added to a solution of 2-(6-chloro-9H-carbazol-2-yl)propanamide **2** (0.15 g, 0.55 mmol) in *N,N*-dimethylformamide (3 mL) and the suspension was stirred at room temperature for 20 min. Afterwards, methyl iodide (0.13 mL, 2.1 mmol) was added dropwise and the reaction was stirred at room

temperature for 24 h. Then water (20 mL) was added to the reaction, and the obtained suspension was extracted with ethyl acetate (3 × 50 mL), dried (Na₂SO₄), and evaporated under reduced pressure. The thick oil was washed with petroleum ether (4 × 3 mL), and the obtained yellow solid was purified on silica gel column chromatography eluting with a mixture of dichloromethane/methanol 9/1 to afford pure **3** (0.05 g, 0.17 mmol, 32.0 %). Mp 176-179 °C. IR (neat): 3403, 3191 (-NH₂), 2977-2929 (CH-CH₃), 1651 (C=O) cm⁻¹. ¹H NMR (DMSO-*d*₆): δ = 8.20 (d, 1H, J= 1.7 Hz, H-5), 8.11 (d, 1H, J= 8.1 Hz, H-4), 7.62 (d, 1H, J= 8.6 Hz, H-8), 7.52 (s, 1H, H-1), 7.44 (dd, 1H, J= 1.7, 8.6 Hz, H-7), 7.37 (s br, 1H, CONH), 7.21 (d, 1H, J= 8.1 Hz, H-3), 6.82 (s br, 1H, CONH), 3.86 (s, 3H, CH₃), 3.75-3.80 (q, 1H, J= 6.8 Hz, -CH-CH₃), 1.44 (d, 3H, J= 6.8 Hz, -CH-CH₃). Anal. (C₁₆H₁₅ClN₂O) C, H, N. MS, m/z : 287 [M+H].

Enantioseparation of **2 and **3** pure enantiomers.** The direct HPLC enantioseparation of the compounds **2** and **3** was achieved on the polysaccharide-type Chiralpak AD chiral stationary phase (CSP) using the mixture *n*-hexane/ethanol 70/30 (v/v) as eluent. The enantiomeric forms were isolated on a semipreparative scale with high yields (> 90%) and enantiomeric purity (enantiomeric excess > 99%). The specific rotations of the enantiomers of **2** and **3** in ethanol solution were: (+)-**2**: + 11 (c = 0.1, EtOH), first eluted enantiomer; (-)-**2**: - 10 (c = 0.1, EtOH), second eluted enantiomer; (+)-**3**: + 28 (c = 0.1, EtOH) first eluted enantiomer; (-)-**3**: -27 (c = 0.1, EtOH), second eluted enantiomer.

Elemental analyses for compounds 2-10.

cpd	MW	calculated, %			found, %		
		C	H	N	C	H	N
2	272.73	66.06	4.80	10.27	66.12	4.86	9.96
3	286.76	67.02	5.27	9.77	66.91	5.19	9.92
4	316.78	64.46	5.41	8.84	64.77	5.52	8.68
5	329.78	61.91	4.89	12.74	62.09	4.97	12.56
6	288.73	62.40	4.54	9.70	62.63	4.49	9.46
7	302.76	63.47	4.99	9.25	63.61	5.09	9.11
8	378.85	69.75	5.05	7.39	69.94	5.17	7.13
9	342.82	66.57	5.59	8.17	66.78	5.62	7.91
10	433.95	58.12	5.57	9.68	57.96	5.49	9.84
11	286.76	67.02	5.27	9.77	67.21	5.36	9.52

SIRT1/2 Inhibition Assay. The SIRT activity assay was performed using human recombinant SIRT1 and SIRT2 produced in *E. coli*. Compounds were tested using a modified Fluor de Lys fluorescence-based assay kit (AK-555, AK-556 Biomol). The assay procedure has two steps: in the first part the SIRT1/2 substrate, an acetylated Lys side chain comprising amino acids 379-382 (Arg-His-Lys-Lys(Ac)) (for SIRT1 assay) or 317-320 (Gln-Pro-Lys-Lys(Ac)) (for SIRT2 assay) of human p53 conjugated with aminomethylcoumarin is deacetylated during incubation at 37 °C for 1 h by SIRT1 or SIRT2 in the presence of NAD⁺ and the tested compounds. The second stage is initiated by the addition of the Developer II, including nicotinamide (NAM), a sirtuin inhibitor that stops the SIRT1/2 activity, and the fluorescent signal is produced. The fluorescence was measured on a fluorometric reader (Inphinite 200 TECAN) with excitation set at 360 nm and emission detection set at 460 nm. Experiments on the SIRT1 and 2 inhibition have been performed in triplicate. IC₅₀ data were analyzed using GraphPad Prism Software.

Cell lines. Human leukemia cell lines (U937) was grown in RPMI 1640 medium (EuroClone) supplemented with 10% heat-inactivated FBS (Sigma Aldrich), 1% glutamine (EuroClone), 1% penicillin/streptomycin (EuroClone) and 0.1% gentamycin (EuroClone), and kept at 37°C in air and 5% CO₂. Conversely, adherent MCF7 (human breast cancer) cells were grown in D-MEM medium (EuroClone) supplemented with the same components described above and in the same incubation settings.

Western Blot analyses of p53 and α -tubulin acetylation. To detect acetylation of p53 (K373/382) and α -tubulin, 50 μ g and 20 μ g of total protein extracts (MCF7 cells), respectively, were separated on a 10% polyacrylamide gels and blotted for 2 h at 70V. Western blots were shown for acetylated p53 (K373/382) (Upstate, dilution 1:500) and α -tubulin (Sigma, dilution 1:1000). Total ERKs (Santa Cruz, dilution 1:1000) represent equal loading.

Cell Cycle and Cell death Analysis on U937 cells. Cells were collected and resuspended in 500 μL of hypotonic buffer (0.1% Triton X-100, 0.1% sodium citrate, 50 $\mu\text{g}/\text{mL}$ propidium iodide (PI)). Then the cells were incubated in the dark for 30 min. Samples were acquired on a FACS-Calibur flow cytometer using the Cell Quest software (Becton Dickinson). Analyses were performed with standard procedures using ModFit LT version3 software (Verity). All experiment were performed in triplicate.

Granulocytic differentiation on human leukemia U937 cells. Cells were resuspended in 10 μL phycoerythrine-conjugated CD11c (CD11c-PE). Control samples were incubated with 10 μL of PE conjugated mouse IgG1. The incubations were performed at 4 $^{\circ}\text{C}$ in dark for 30 min. After cells were collected, washed in phosphate buffered saline (PBS), and resuspended in 500 μL of PBS containing propidium iodide (PI) (0.25 $\mu\text{g}/\text{mL}$). Samples were analyzed by FACS with Cell Quest technology (Becton Dickinson). PI positive cells have been excluded from the analysis.

7 DISCOVERY OF SALERMIDE-RELATED SIRTUIN INHIBITORS: BINDING MODE STUDIES AND ANTIPROLIFERATIVE EFFECTS IN CANCER CELLS INCLUDING CANCER STEM CELLS

Abstract: Chemical manipulations performed on sirtinol (**1a**) led to a series of SIRT1/2 inhibitors (**2-6**) in some cases more potent than **1a** mainly against SIRT1. The higher inhibitory activity showed by **4b** with respect to **1a** has been rationalized through docking studies. Most of the **2-6** derivatives were assayed against different cancer cell lines such as U937, MOLT4, MDA-MB-231, RKO cancer cell lines and on colorectal carcinoma and glioblastoma multiforme cancer stem cells (CSCs) in which showed antiproliferative effects.

* Adapted with the permission from: Rotili, D.; Tarantino, D.; Nebbioso, A.; Paolini, C.; Huidobro, C.; Lara, E.; Mellini, P.; Lenoci, A.; Pezzi, R.; Botta, G.; Lahtela-Kakkonen, M.; Poso, A.; Steinkühler, C.; Gallinari, P.; De Maria, R.; Fraga, M.; Esteller, M.; Altucci, L.; Mai A. *J Med Chem* 2012, 55: 10937-10947. Copyright 2012 American Chemical Society.

7.1 Introduction

Among the SIRT1/2 inhibitors described so far, sirtinol (**1a**), cambinol, JGB1741 and MC2141 sharing the same 2-hydroxy-1-naphthyl pharmacophore moiety (Figure 1) were found active antiproliferative agents alone or in combination with other chemotherapeutics, in a variety of cancer cells.^{67, 72,78,112,140,141,144,147}

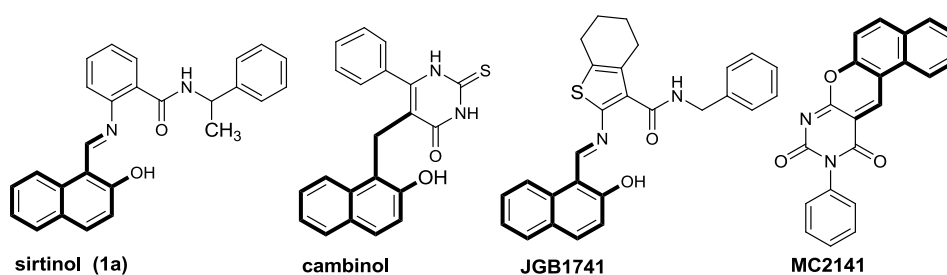


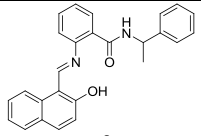
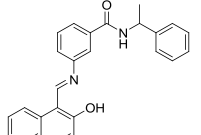
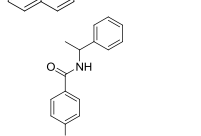
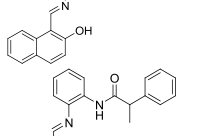
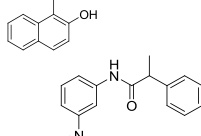
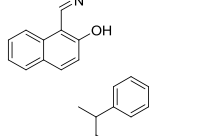
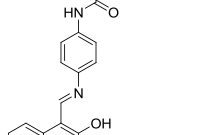
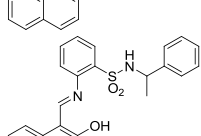
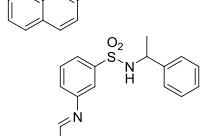
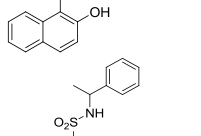
Figure 1. Known SIRT1/2 inhibitors sharing the 2-hydroxy-1-naphthyl pharmacophore moiety.

In 2005 we reported some sirtinol analogues and among them, only compounds bearing the N-(1-phenylethyl)amino side chain shifted from *-ortho* to *-meta* or *-para* position of the benzene ring showed improved activity against SIRT1 and SIRT2.¹³⁸ Pursuing our research on Sirtuin modulators we designed a small library of sirtinol derivatives by replacing the benzoyl amide linkage of the prototype with other bioisosteric groups such as retromide, sulphonamide, thiomethyl, sulfinylmethyl and sulfonylmethyl and bearing the 1-phenylethyl side chain with *-ortho*, *-meta* and *-para* regiochemistry. The compounds **2-6** were tested in vitro and their potential binding mode on SIRT1 and SIRT2 was studied (for detailed results concerning anticancer activity of **2-6** see Rotili et al. 2012).

7.2 Results and discussion

The (2-hydroxy-1-naphthylmethylene)amino-*N*-phenyl derivatives **2-6** were tested in vitro against hrSIRT1 and hrSIRT2 using a fluorogenic substrate and NAD⁺ (Table 1). IC₅₀ values of **1a**, **1b**, **1c** against hrSIRT1 and hrSIRT2 were added for comparison.

Table 1. IC₅₀ values of **1-6** against SIRT1 and SIRT2.

Compd	IC ₅₀ μM		
	SIRT1	SIRT2	
1a (Sirtinol)		123.3 ± 14.2	45.9 ± 6.4
1b		58.6 ± 8.1	34.5 ± 4.0
1c		48.1 ± 5.2	29.9 ± 4.1
2a		55.0 ± 5.3	75.5 ± 4.5
2b		42.8 ± 7.9	25.0 ± 3.8
2c		40.9 ± 6.1	37.3 ± 9.5
3a		90.8 ± 10.6	57.0 ± 0.4
3b		55.6 ± 8.1	61.6 ± 6.5
3c		44.1 ± 6.2	22.6 ± 4.2
4a		55.1 ± 5.0	48.0 ± 9.0

4b		40.3 ± 8.1	19.2 ± 4.5
4c		45.5 ± 7.0	28.2 ± 3.0
5a		44.9 ± 5.6	33.0 ± 6.0
5b		67.3 ± 8.2	43.0 ± 8.1
5c		56.3 ± 4.6	48.2 ± 9.5
6a		64.0 ± 8.8	24.2 ± 7.7
6b		65.8 ± 6.2	48.9 ± 6.9
6c		74.9 ± 7.2	57.5 ± 5.4

Against hrSIRT1, compounds **2-6** showed quite similar inhibiting activity with IC₅₀ values ranging from 40.3 to 67.3 μM, regardless to the nature or regiochemistry of the side chain. The only exceptions were **3a** and **6c**, which displayed lower potency, whereas the 4-phenylpropionamide derivative **2c** and the (2-phenylpropyl)thio derivative **4b** were the most efficient inhibitors, with IC₅₀ values of 40.9 and 40.3 μM, respectively. In comparison with the reference compounds, the majority of **2-6**

displayed higher inhibition than **1a** and similar as **1b** and **1c**. In general terms, in the SIRT2 assay the tested compounds **2-6** exhibited similar or higher inhibiting activities respect to those against SIRT1, with some exceptions (**2a** and **3b**). Among compounds substituted with 2-phenylpropionamide function, the meta analogue **2b** (salermide) displayed the highest activity ($IC_{50} = 25.0 \mu M$), while in the **3** series the 4-*N*-(1-phenylethyl)benzenesulphonamide **3c** was the most efficient ($IC_{50} = 22.6 \mu M$). In the (2-phenylpropyl)thio-substituted series, the highest hrSIRT2 inhibiting activity was shown by the *meta* (**4b**) and the *para* (**4c**) analogues, **4b** being the most potent ($IC_{50} = 19.2 \mu M$) among all the tested derivatives. Similar potency against SIRT2 was also observed with the 2-(2-phenylpropyl)sulfonyl derivative **6a** ($IC_{50} = 24.2 \mu M$).

The structural variability of the compounds with *meta*, *orto*, and *para* substituents offers the possibility of different interaction in the binding site, that could reflect in some cases in a divergence in the activity on SIRT1 and SIRT2. In order to study the effect of the substitution of the (2-hydroxy-1-naphthylmethylene)amino-*N*-phenyl derivatives **2-6** on the binding in the NAD^+ pocket, **2-6** were docked to SIRT1 and SIRT2 homology models. The aim of the docking simulation was investigate about the hypothesis that the sirtinols derivatives were able to bind the SIRT1, 2 NAD^+ binding pockets (A, B, C) (Figure 2).

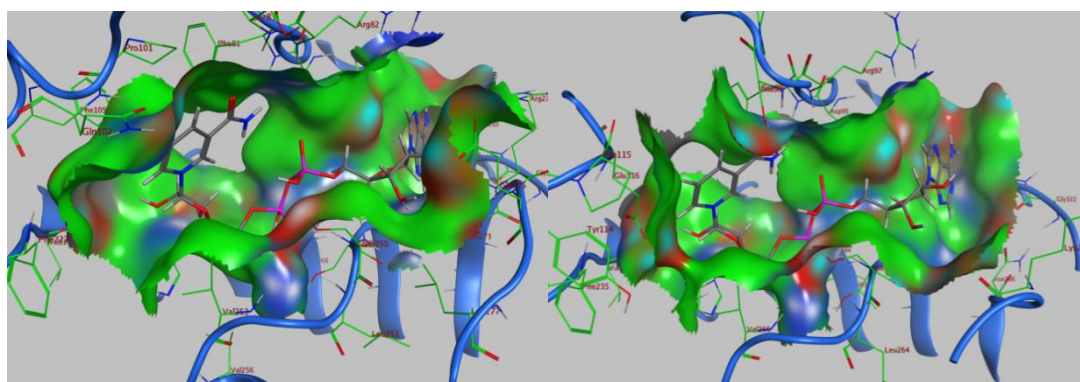


Figure 2. NAD^+ binding site overview. SIRT1 (left), SIRT2 (right) homology models.

Our docking simulations showed that in the most representative cases (**1a**, **1c**, **2b**, **4b**, **4c**, **6a**) in which there were a little but significant differences in the activity on SIRT1, 2 there is the same coherence in the binding mode (see pictures below).

In details compound **1a** in SIRT1 has H-bond between the carbonyl of the amide function with Arg274 and an CH- π interaction with Asp289, but is clearly evident that the β -naphthol ring is completely out of the binding site. While within SIRT2 compound **1a** has two H-bonds between -OH of the β -naphthol ring with Thr262 and Ser98 increasing the affinity of binding compared to SIRT1, moreover two favorable CH- π interaction with Asp95 and Ser263. The β -naphthol ring in this case is placed in the B-pocket (blue) and the phenyl ring was oriented towards the C-pocket (yellow).

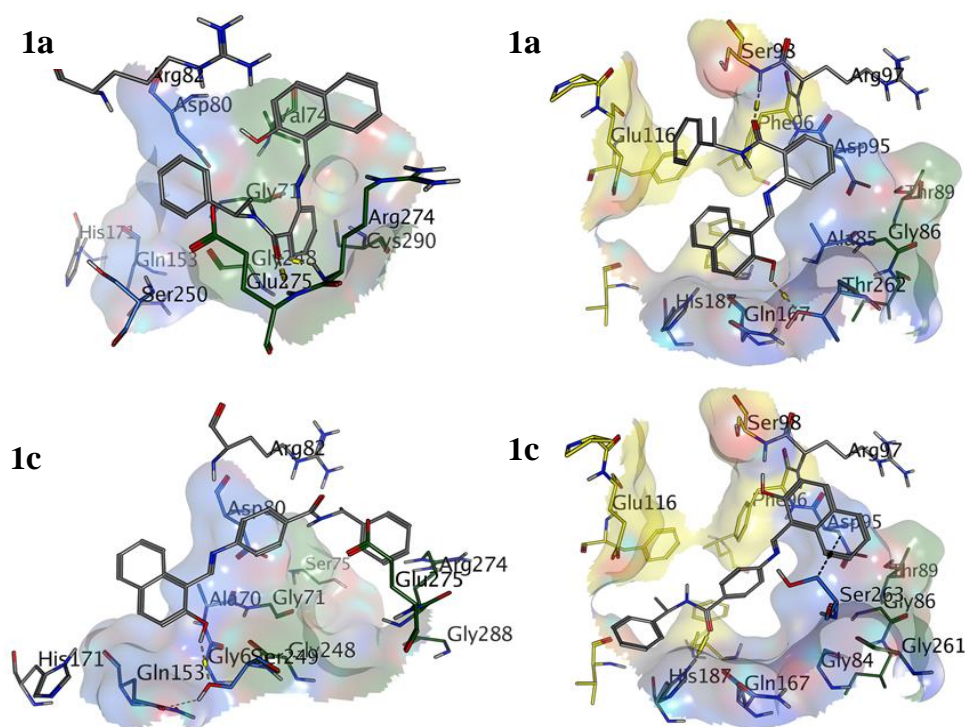


Figure 3. Docking poses for **1a** and **1c** in SIRT1 (left) and SIRT2 (right).

Compound **1c** in SIRT1 has H-bond between -OH of the β -naphthol ring with Ser249 and an CH- π interaction with Ala70. The molecule adopt an elongated conformation from B to A pocket with different solvent exposed areas. In SIRT2, **1c**

has H-bond between –OH of the β -naphthol ring with His187 and two favorable CH- π interaction with Asp95, Ser263. Also in this case an elongated conformation of the molecule can be seen but with a diverse orientation from A to C pocket in which the phenyl ring is placed near the Ac-Lys binding site with a potential improvement of binding affinity. Compound **2b** in SIRT1 has two H-bonds between -OH of the β -naphthol ring with Ser249 and Ser250, with the naphthol ring placed in the B pocket (Figure 4, blue). Nevertheless in SIRT2 **2b** is well positioned in the NAD⁺ binding site in which resulted stabilized by H-bond between the carbonyl of the amide function with His187; the phenyl ring is placed in the B pocket (blue) but should be noteworthy that in this case the β -naphthol ring is close to the Ac-Lys binding site (Figure 4).

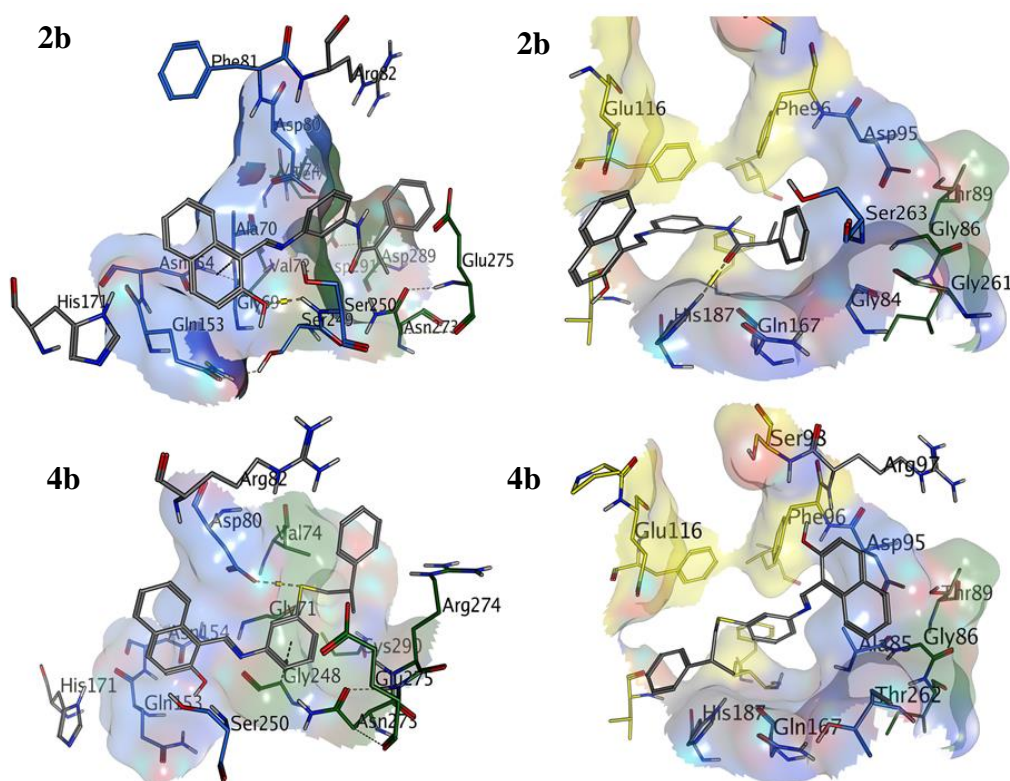


Figure 4. Docking poses for **2b** and **4b** in SIRT1 (left) and SIRT2 (right).

In SIRT1, **4b** does not have a perfect fit in the binding pose because there are different exposed area (Figure 4). In SIRT2, **4b** is binding from A to C pocket (Figure 4, right) and shows a correct fit in NAD⁺ binding site. This might be due to

openness of C-pocket in SIRT2 and to favorable interaction in the C-pocket between Phe96 and His187 established by **4b** in SIRT2 (Figure 4).

In SIRT1, compound **4c** does not show an optimal binding mode because of clashed areas with protein surface but **4c** has H-bonds between–OH of the β -naphthol ring with Ser249 and Ser250 and an additional H- π interaction with Ala70 that may help the binding stabilization (Figure 5). Nevertheless in SIRT2 **4c** has H-bond interaction with Asp95 in the B-pocket and H- π interaction, moreover H-bond between the sulfur of the thioether function and His187 could participate to stabilize the binding mode (Figure 5).

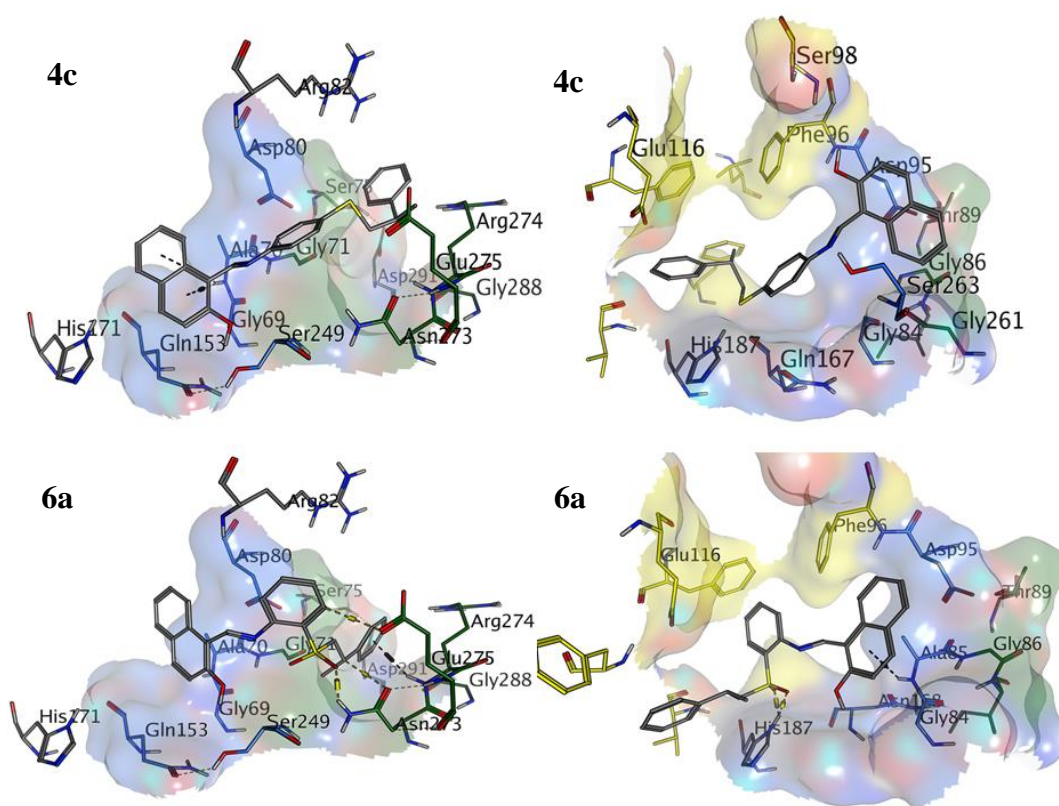


Figure 5. Docking poses for **4c** and **6a** in SIRT1 (left) and SIRT2 (right).

In SIRT1, compound **6a** binds from B to A pocket (Figure 5 blue-green) and shows H-bond between the sulphonyl and Asn273 and H- π interaction with Arg274. The naphthol ring is placed in the B-pocket (blue) and the phenyl ring completely out of the binding site. In SIRT2, the binding mode showed by **6a** seems well stabilized by H-bond between the sulphonyl and His 187 and an H- π interaction of the β -naphthol with Ala85. The β -naphthol is placed in the B-pocket and the rest of the molecular

moiety, fit inside of the C-pocket with the phenyl ring oriented towards the Ac-Lys binding site (Figure 5).

7.3 Conclusions

The conclusion from docking studies is that the most potent compounds show a common binding mode for SIRT2: the β -naphthol ring has enough space to fit in B-pocket and the rest of the scaffold can enter into the C-pocket. On the contrary, in the case of SIRT1, there is a less space in B-pocket, the scaffold has not optimal fit in it, and the C-pocket is practically empty, so that only suboptimal complementary binding is achieved in SIRT1.

7.4 Experimental Section

SIRT1/2 Inhibition Assay. The SIRT activity assay was performed using human recombinant SIRT1 and SIRT2 produced in *E. coli*. Compounds were tested using a modified Fluor de Lys fluorescence-based assay kit (AK-555, AK-556 BIOMOL). The assay procedure has two steps: in the first part the SIRT1/2 substrate, an acetylated Lys side chain comprising amino acids 379-382 (Arg-His-Lys-Lys(Ac)) (for SIRT1 assay) or 317-320 (Gln-Pro-Lys-Lys(Ac)) (for SIRT2 assay) of human p53 conjugated with aminomethylcoumarin is deacetylated during incubation at 37 °C for 1 h by SIRT1 or SIRT2 in the presence of NAD⁺ and the tested compounds. The second stage is initiated by the addition of the Developer II, including nicotinamide (NAM), a sirtuin inhibitor that stops the SIRT1/2 activity, and the fluorescent signal is produced. The fluorescence was measured on a fluorometric reader (Inphinite 200 TECAN) with excitation set at 360 nm and emission detection set at 460 nm. Experiments on the SIRT1 and 2 inhibition have been performed in triplicate. IC₅₀ data were analyzed using GraphPad Prism Software.

Molecular Modelling. No crystal structure is available for SIRT1, and for SIRT2 there is only apo structure available. Therefore, we were forced to build also homology model for SIRT2 in bioactive conformation. The template used for the homology model of SIRT1 and SIRT2 was the crystal structure of Sir2 homolog from *Archeaoglobus fulgidus* (Sir2-Af1) with NAD⁺ (PDB code: 1ici). The homology models of SIRT1 and SIRT2 were built using FUGUE and ORCHESTRA in SYBYL 1.3 (SYBYL-X 1.3, Tripos International, 1699 South Hanley Rd., St. Louis, Missouri, 63144, USA). The side chains were optimized by geometry optimization with Amber99 using MOE 2010.10 (Molecular Operating Environment (MOE) version 2010.10; Chemical Computing Group Inc.: Montreal, Canada). The ligand structures were built with MOE software and minimized using MMFF94 force field until a rmsd gradient of 0.05 kcal mol⁻¹Å⁻¹ was reached. The protein geometry was evaluated by Ramachandran plot and Verify 3D (Verify 3D Structure evaluation server: http://nihserver.mbi.ucla.edu/Verify_3D/). The docking simulations were performed in the NAD⁺ binding site of the homology models SIRT1 and -2 using MOE. Default values were used for all docking settings. The best ranked poses of

each docked ligand was included in the analysis. The docking results were visually inspected. The figures were prepared using MOE (version 2010.10).

SIRT1 homology model. SIRT1 *Homo Sapiens* sequence 555aa, was downloaded from NCBI (National Center for Biotechnology Information) AAH12499.1, saved as FASTA file and used as input for run FUGUE (SYBYL 1.3.11283). Sir2 homolog, from *Archeaoglobus fulgidus* (Sir2-Af1, PDB :1ICI) complexed with NAD⁺ ¹ (resolution : 2.10 Å), was used as template for align the sequences¹⁸⁷ (see below) and built the SIRT1 homology model in bioactive conformation. After the alignment with FUGUE, the SIRT1 homology was built using ORCHESTRA with a schematic workflow described below :

1. Building of the Conserved Regions (SCRs)
2. Search and Remodel Loops, in the model there are three missing loops:
 - Met1 : Pro40 ; Arg90 : Asp100 ; Tyr305 : Ser555 because the template area is missing.
3. Add and modeling Side-chains :
 - Clashes and Side-chains with abnormal conformation were modeled manually considering the template's Side-chains orientation.
4. Structure analysis :
 - Fixed Termini Treatment
 - Hydrogen and Charges were added
5. Geometry Optimization :
 - With Amber99 as Force Field, gradient 0.05 and Homo LP were adjusted.
6. Examination of the Model :
 - 266 Res, 289 Missing Res, 2 Gaps, 0 Missing Side-chains
 - Outlier (all are out of the NAD⁺ binding site) Ala89, Leu91, Pro96, Pro99, Pro121, Pro131, Cys134 see Ramachandran plot (Figure 6).

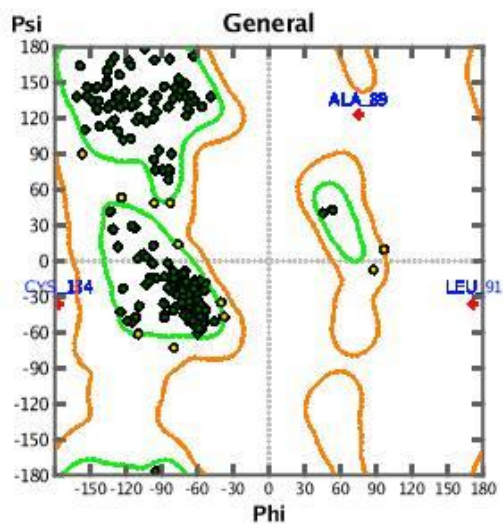


Figure 6. SIRT1 homology model Ramachandran plot.

Alignment SIRT1-Sir2Afl¹⁸⁷ template (ORCHESTRA, SYBYL)

```

query          1          11          21          31          41
model_s9_1    MIGTDPRTILKDLLPETIPPPELDDMTLWQIVINILSEPPKRKKRDKDINT
hslicia      -----PKRKKRDKDINT
              -----GSHHHHHHGHSHM
query          51          61          71          81          91
model_s9_1    IEDAVKLLQECKKIIVLTGAGVSVSCGIPDFRSRDGIYARLAVDFPDLPD
hslicia      IEDAVKLLQECKKIIVLTGAGVSVSCGIPDFRSRDGIYARLAVDFPDLPD
              DEKLLKTIAESKYLVALTGAGVSAESGIPTFRGKDGLWNR-----R

query          101         111         121         131         141
model_s9_1    PQAMFDIEYFRKDRPFKFAKEIYPGF--QPSLCHKFIALSDKEGKLL
hslicia      PQAMFDIEYFRKDRPFKFAKEIYPGF--QPSLCHKFIALSDKEGKLL
              PEELANPQAFKADPEKVVWKYAWRMEKVFNAQPNKAHQAFALERLGLVK

query          151         161         171         181         191
model_s9_1    RNYTQNIQTLEQVAGIQRIIQCHGSFATASCLICKYKVDCEAVRGALFSQ
hslicia      RNYTQNIQTLEQVAGIQRIIQCHGSFATASCLICKYKVDCEAVRGALFSQ
              CLITQNVDDLHERAGSRNVIIHLHGSLRVVRCSTSCNNSFEVESAPKI---P

query          201         211         221         231         241
model_s9_1    VVPRCPRCPADEPLAIMKPEIVFFGENLPEQFHRAMKYDKDEVLLIVIG
hslicia      VVPRCPRCPADEPLAIMKPEIVFFGENLPEQFHRAMKYDKDEVLLIVIG
              PLPKCDKCG-----SLLRPGVVWFGEMLPDVLDRAMREVERADVIVAG

query          251         261         271         281         291
model_s9_1    SSLKVRPVALIPSSIP-HEVPQILINREPLPHLH-FDVELLGDCDVIINE
hslicia      SSLKVRPVALIPSSIP-HEVPQILINREPLPHLH-FDVELLGDCDVIINE
              TSAVVQPAASLPLIVKQGGAIIEINPDETPLTPIADYSLRGKAGEVMDE

query          301         311         321         331         341
model_s9_1    LCHRLGGEYAKLCCNPVKLSEITEKPPRTQKELAYLSELPPPLHVSEDS
hslicia      LCHRLGGEY-----
              LVRHVRKALS-----

query          351         361         371         381         391
model_s9_1    SSPERTSPDSSVIVTLLDQAAKSNDDLVDSESKGCMEEKPQEVQTSRNV
hslicia      -----
              -----

query          401         411         421         431         441
model_s9_1    ESIAEQMENPDLKNGVSSSTGEKNERTSVAGTVRKCWPNRVAKEQISRRLD
hslicia      -----
              -----

query          451         461         471         481         491
model_s9_1    GNQYFLFPNRYIFHGAEVYSDEDDVLSSSSCGSNSDSGTCQSPSLEEP
hslicia      -----
              -----

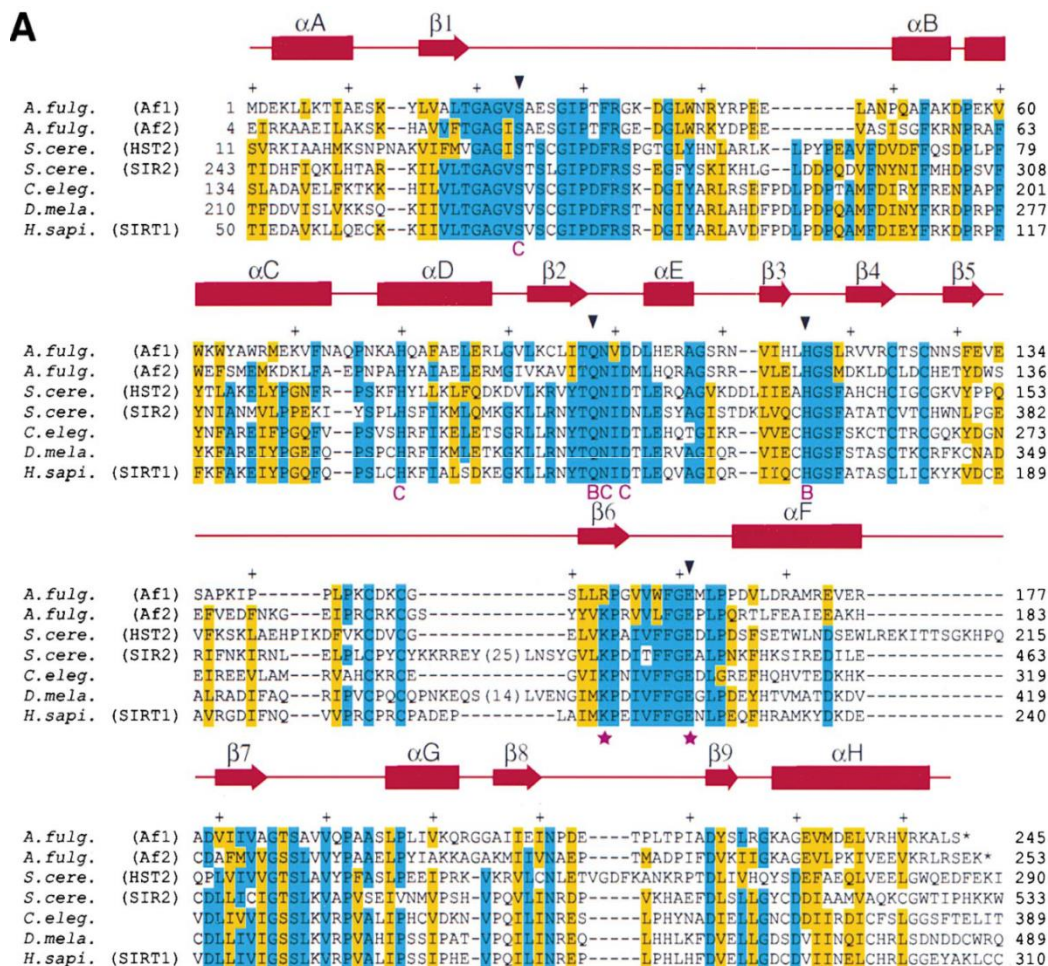
query          501         511         521         531         541
model_s9_1    MEDESEIEEFYNGLEDEPDVPERAGGAGFGTDGDDQEAINEAISVKQEV
hslicia      -----
              -----

query          551
model_s9_1    DMNYPSNKS
hslicia      -----

```

model_s9_1
hslicia

Joy Annotation:
alpha helix red x
beta strand blue x
3 - 10 helix maroon x



SIRT2 homology model. SIRT2 *Homo Sapiens* sequence 352aa, was downloaded from NCBI (National Center for Biotechnology Information) AAK51133.1, saved as FASTA file and used as input for run FUGUE (SYBYL 1.3.11283). Sir2 homolog, from *Archeaoglobus fulgidus* (Sir2-Af1, PDB : 1iCi , %ID 26.5) complexed with NAD^{+1} (resolution : 2.10 Å), was used as template for align the sequences and built the SIRT2 homology model in bioactive conformation. After the alignment¹⁸⁸ with FUGUE (see below), the SIRT2 homology was built using ORCHESTRA with a schematic workflow described below :

It is the same described for SIRT1.

Examination of the Model :

- 263 Res, 89 Missing Res, 3 Gaps, 0 Missing Side-chains
- Outlier (all are out of the NAD+ binding site) Thr64, Ala80, Ile81, Ile138, Thr243, Pro131, see Ramachandran plot (Figure 7).

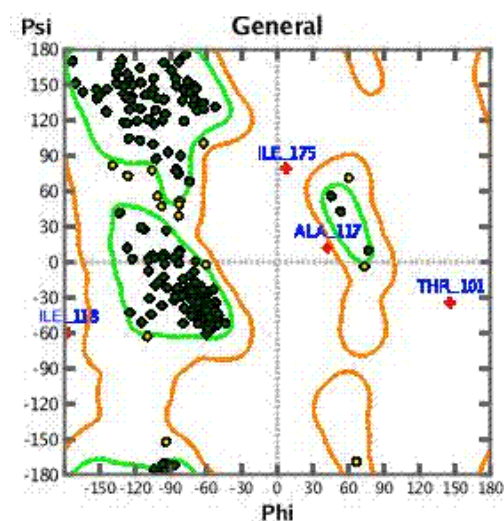


Figure 7. SIRT2 homology model Ramachandran plot.

Alignment SIRT2-model-Sir2Af1¹⁸⁸ template (ORCHESTRA, SYBYL)

```

query          1      11      21      31      41
model_s10_1   MDFLRNLF SQTLSLGSQKERLLDELTLEGVARYMQSERCRRVICLVGAGI
hslicia       -----S QKERLLDELTLEGVARYMQSERCRRVICLVGAGI
               -----GSHHHHHHGSHMDEKLLKTIA--ESKYLVALTGAGV

query          51      61      71      81      91
model_s10_1   STSAGIPDFRSPSTGLYDNLEKYHLPYPEAIFEISYFKKHPEPFFALAKE
hslicia       STSAGIPDFRSPSTGLYDNLEKYHLPYPEAIFEISYFKKHPEPFFALAKE
               SAESGIPTFRGK-DGLWNRYS-----PEELANPQAFKDPKVVWKWYAW

query          101     111     121     131     141
model_s10_1   LYPGQF--KPTICHYFMRLKDKGLLLRCYTQNIIDTLERIALGLEQEDLVE
hslicia       LYPGQF--KPTICHYFMRLKDKGLLLRCYTQNIIDTLERIALGLEQEDLVE
               RMEKVFNAQPNKAHQAFaelerLGVlKCLITQNVDDLHERAG--SRNVIH

query          151     161     171     181     191
model_s10_1   AHGTFYTSHCVSASCRHEYP LSWMKEKIFSEVTPKCEDCQSLVKPDI VFF
hslicia       AHGTFYTSHCVSASCRHEYP LSWMKEKIFSEVTPKCEDCQSLVKPDI VFF
               LHGSLRVVRC TSCNNSFEVE-----SAPKIPPLPKCDKCGSLLRPGVVWF

query          201     211     221     231     241
model_s10_1   GESLPARFFSCMQSDFLKV D LLLVMGTSLQVQPFASLISKAPLSTPRLLI
hslicia       GESLPARFFSCMQSDFLKV D LLLVMGTSLQVQPFASLISKAPLSTPRLLI
               GEMLPDVLDRAMREVERADV IIVAGTSAVVQPAASLPLIVKQRGGAIIE

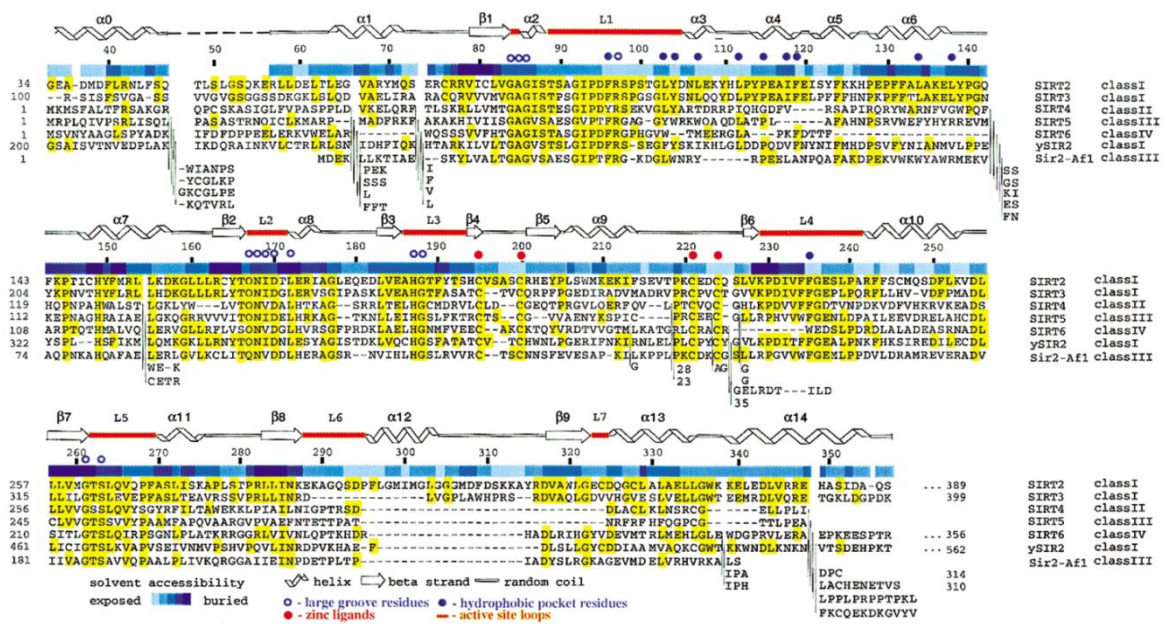
query          251     261     271     281     291
model_s10_1   -NKEKAGQSDPFLGMIMGLGGGMD FDSKKAYRDVAWLGECDQGCLALAE L
hslicia       -NKEKAGQSD-----AWLGECDQGCLALAE L
               INPDETPLTP IA-----DYSLRGKAGEVMDELVRH

query          301     311     321     331     341
model_s10_1   LGWKKELEDLVRREHASIDAQSGAGV PNPSTSASP KKSPPP AKDEARTTE
hslicia       LGWKK-----
               VRKALS-----

query          351
model_s10_1   REKPQ
hslicia       -----

```

Joy Annotation:
alpha helix **red x**
beta strand **blue x**
3 - 10 helix **maroon x**



8 SCREEN OF PSEUDOPEPTIDIC INHIBITORS OF HUMAN SIRTUINS 1-3: TWO LEAD COMPOUNDS WITH ANTIPROLIFERATIVE EFFECTS IN CANCER CELLS

QSAR MODELING IN THE DESIGN OF PSEUDOPEPTIDIC SIRT1 INHIBITORS

Abstract: In the past few years sirtuins have gained growing attention for their involvement in many biological processes such as cellular metabolism, apoptosis, aging and inflammation. In this paper, we report the synthesis of a library of thioacetylated pseudopeptides that were screened against human sirtuins 1-3 to reveal their in vitro inhibition activities. Molecular modeling studies were performed to acquire data about the binding modes of the inhibitors. Three sirtuin inhibitors were subjected to cellular studies and all of them showed an increase in acetylation of Lys382 of p53 after DNA damage. Furthermore, two of the compounds were able to inhibit both A549 lung carcinoma and MCF-7 breast carcinoma cell growth in micromolar concentration with the ability to arrest cancer cell cycle in the G₁ phase.

* Adapted with the permission from: [Mellini, P.](#); Kokkola, T.; Suuronen, T.; Salo, H.; Tolvanen, L.; Mai, A.; Lahtela-Kakkonen, M.; Jarho, E.M. *J Med Chem* 2013, 56: 6681-6695. Copyright 2012 American Chemical Society.

* Adapted with the permission from: Kokkonen, P.; [Mellini, P.](#); Nyrhilä, O.; Rahnasto-Rilla, M.; Poso, A.; Lahtela-Kakkonen, M.; and Jarho, E.M.. *Eur J Pharm Sci* ([manuscript in preparation](#)).

8.1 Introduction

The thioacetylated peptidic inhibitors have represented the first successful approach to develop potent competitive SIRT1/2 inhibitors.¹²⁵ The inhibition mechanism (Figure 1), elucidated by Smith and Denu, shows that after a fast nicotinamide cleavage, the thioacetyl inhibitor is readily converted to a stalled intermediate 1'-S-alkylamidate with a consequent retardation of the overall turnover rate.¹²⁷

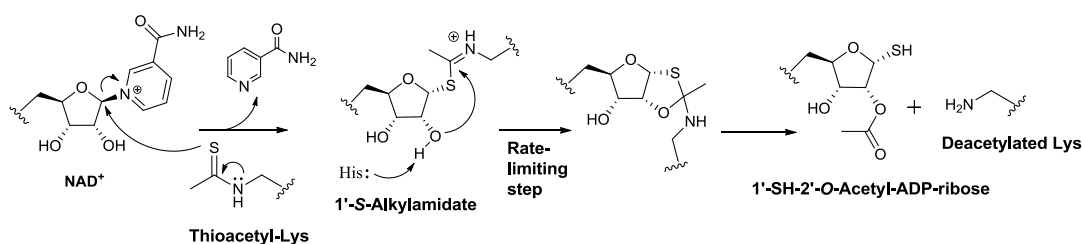


Figure 1. The mechanism of sirtuin inhibition of thioacetylated peptides.

In the scenario in which the peptidic scaffold gave compounds with potent inhibition activity^{129,133} but negligible drug-like properties, Suzuki et al.¹³² and few years after, Huhtiniemi and co-workers,¹³⁴ developed novel classes of pseudopeptides with an *N*^ε-thioacetyl lysine residue (Chart 1) in order to improve the cell permeability.

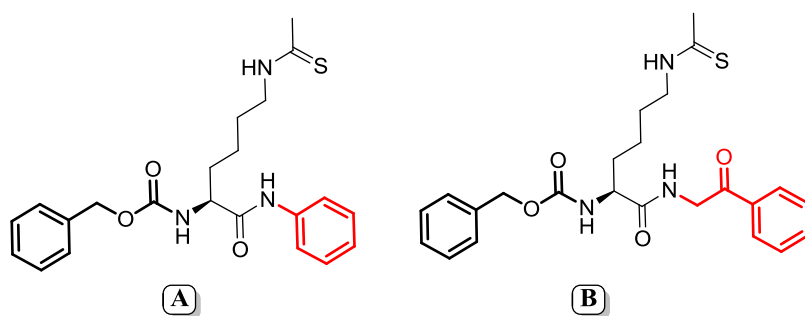


Chart 1. Reference compound A by Suzuki et al.¹³² and reference compound B by Huhtiniemi et al.¹³⁴

Pursuing the versatility of the pseudopeptidic scaffold, we focused our efforts on the preparation and biological evaluation of a novel fragment based library (Chart 2, Tables 1-3). The library was generated considering our previously reported binding hypothesis that was developed with SIRT3 as the target structure.¹³⁴ In this hypothesis, we suggested that a potential sirtuin inhibitor should create an H-bond network with Val292, Gly295, Glu296 and Glu325 (Figure 2). In addition, in the N-

terminal area of a pseudopeptidic compound the binding affinity could be improved by formation of a hydrogen bond to Leu298 and filling the cavity surrounded by residues Pro297, Leu298, Phe302 and Leu303. On the other hand, in the C-terminal a compound with aromatic interactions with Phe294 or a hydrogen bond with Glu325 might have good inhibition potency.

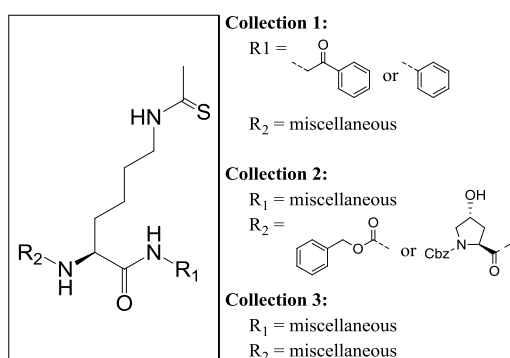


Chart 2. The general structure and the compound collections of the pseudopeptide library.

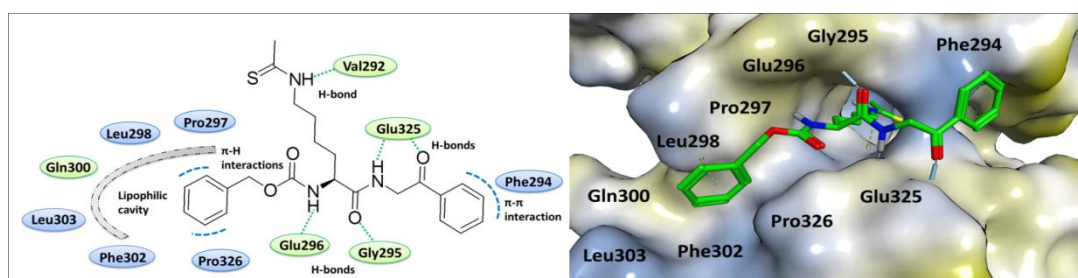


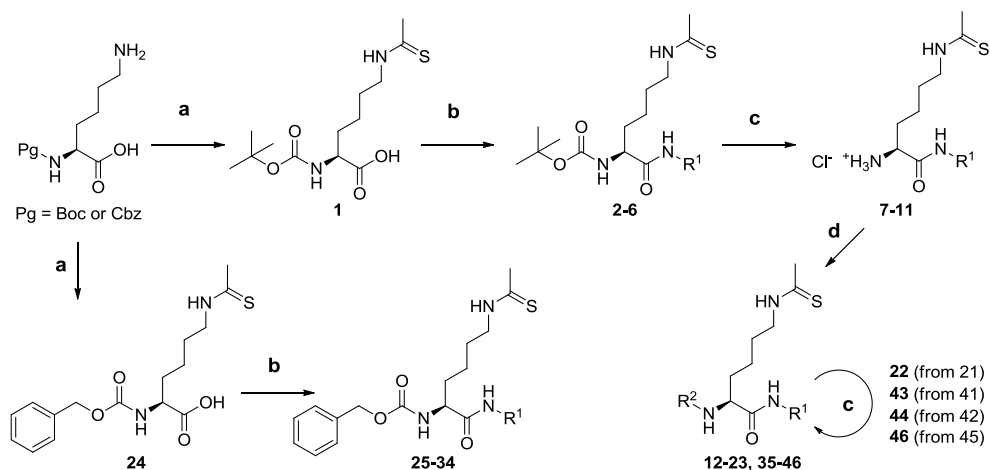
Figure 2. A scheme of the interaction pattern reported for a pseudopeptidic inhibitor in SIRT3 that fulfills the binding hypothesis. In cartoon, H-bonds and aromatic interactions are represented by dashed lines correspondingly in green and blue.

To improve the knowledge of pseudopeptidic interactions in various sirtuins and to get structure-activity relationship (SAR) data, a set of novel pseudopeptides was designed. A small library of pseudopeptides was synthesized (Chart 2, Tables 1-3) and screened *in vitro* against SIRT1-3 with the aim to understand how heterogeneous N- and C-terminal modifications might induce changes in the activity. Three compounds were selected for cellular studies. All three compounds were cell-

permeable and non-toxic. Furthermore, two of the compounds showed antiproliferative effects on two different cancer cell lines (A549 and MCF-7) causing cell cycle arrest at the G₁ phase.

8.2 Chemistry

The synthetic pathway to compounds **1-46** is depicted in Scheme 1. The *N*^ε-thioacetylated derivatives **1** and **24** were synthesized using ethyl dithioacetate and EtOH/10% (w/v) Na₂CO_{3(aq)} at rt for 12 h according to the literature.^{125,134} Compounds **2-6** and **25-34** were obtained with a coupling reaction between the activated acid **1** or **24** and an appropriate amine using the coupling agent TBTU (O-(benzotriazol-1-yl)-N,N,N',N'-tetramethyluronium tetrafluoroborate) in dimethylformamide (DMF)/pyridine under argon flow. The hydrochlorides **7-11**, **22**, **43**, **44**, **46** were gained via Boc (*tert*-butoxycarbonyl) deprotection¹⁸⁹ performed at 60 °C using 15 eq of HCl_(aq) 12 N, 2-propanol and 1,2-ethanedithiol as a scavenger for trapping the *tert*-butyl cation generated in situ. Initially, Boc deprotection was attempted in ethyl acetate under HCl-gas flow in the absence of a scavenger in order to precipitate the product as the HCl salt from the reaction mixture. However, the ¹H-spectrum revealed the disappearance of the thioacetyl methyl singlet (2.4 ppm in DMSO-*d*₆) but showed instead a methyl singlet at 1.8 ppm, a shift characteristic to an acetyl methyl (unpublished data). Thus, the required amount of HCl was optimized; 15 eq of HCl divided in three portions gave complete consumption of the starting material. This, together with the added scavenger, protected the thioacetyl group during the deprotection step. Compounds **12-23** and **35-46** were synthesized according to the above mentioned coupling procedure; in this case the appropriate acid was activated with TBTU to react with the corresponding unblocked amine. The hydrochloride release of the starting material **7** was a critical step that reduced the yields of the acetophenone (i.e. 2-oxo-2-phenyl ethyl) derivatives **12-18**, **42**. As a free amine, compound **7** underwent spontaneous side-reactions; most likely an intramolecular cyclization between the free amino group and the ketone function responsible for generating several byproducts during the coupling step.



R¹ in

2,7,12-18,42,44: 2-oxo-2-phenylethyl **28:** 2-hydroxy-2-phenylethyl
3,8,19-23: phenyl **29:** 2-(1*H*-indol-3-yl)ethyl
4,9,26,35-37,41,43,45,46: benzyl **30:** 2-(5-methoxy-1*H*-indol-3-yl)ethyl
5,10,38,39: 3-pyridyl **31:** 2-(5-(benzyloxy)-1*H*-indol-3-yl)ethyl
6,11,40: 1-(2-(3-pyridyl))ethyl **32:** 3-pyridyl
25: 1-(2-phenyl)ethyl **33:** 2-amino-2-oxoethyl
27: 2-(4-methoxyphenyl)-2-oxoethyl **34:** (S)-1-amino-1-oxopropan-2-yl

R² in

12,38: 3-phenylpropanoyl
13: 4-phenylbutanoyl
14,36: 6-phenylhexanoyl
15,19: 3-(3-pyridyl)propanoyl
16,23,35: *N*-Cbz-4-*trans*-hydroxy-L-prolyl
17,21,40,45: *N*-Boc-L-prolyl
18: 2-((2*S*,5*S*)-5-benzyl-3,6-dioxopiperazin-2-yl)acetyl
20: *N,N*-dimethylglycyl
22,46: L-prolyl HCl
37: 7-phenylheptanoyl
39: 3-(2-fluorophenyl)propanoyl
41,42: *N*-Boc-4-*trans*-hydroxy-L-prolyl
43,44: 4-*trans*-hydroxy-L-prolyl HCl

^aReagents and conditions: (a) Ethyl dithioacetate, EtOH/10% (w/v) Na₂CO_{3(aq)}, rt, 12 h; (b) appropriate amine or carboxylic acid, TBTU, DMF/Pyridine (1:1), argon flow, rt, 2-3 h; (c) 2-propanol, 1,2-ethanedithiol, HCl_(aq) 12 N, 15 eq, 60°C, 2-3 h.

8.3 Results and discussion

Structure-Activity Relationship. A compound library of 30 pseudopeptides was synthesized. One collection explored modifications in the N-terminus (Table 1), the other collection explored the modifications in the C-terminus (Table 2) and, in the third collection miscellaneous modifications at both termini were studied (Table 3, 4). All compounds were screened in vitro against SIRT1-3 at 50 μM concentration (Tables 1-4). However, the numbering of the target protein amino acids is adopted from SIRT3 in the structure-activity discussion unless otherwise noted. The main differences between SIRT1-3 substrate binding sites are labeled and the binding site overview can be seen in Figure 3, 4. The most representative docking poses for tested compounds can be found at the end of this paragraph (Structure-Activity Relationship).

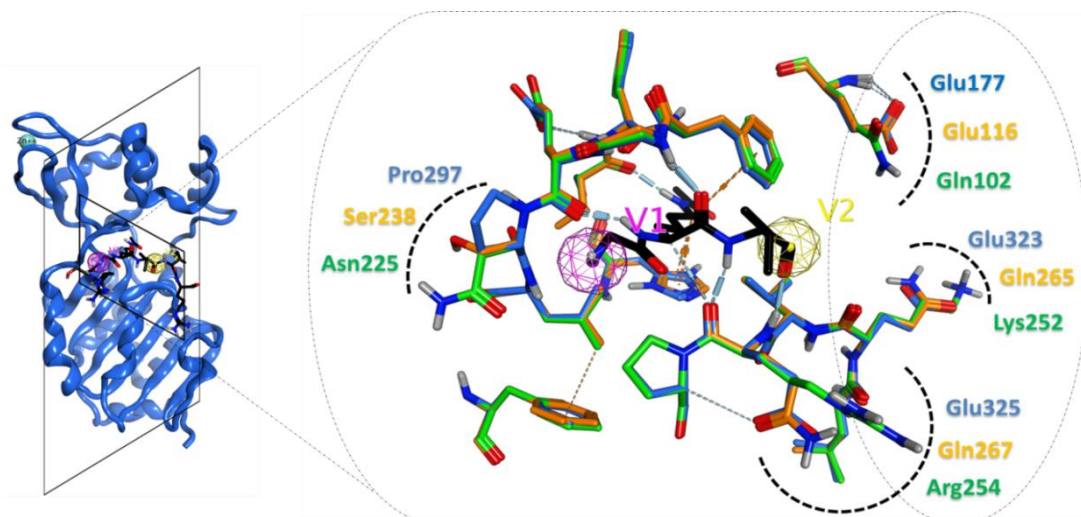


Figure 3. The overall structure of SIRT3 (PDB code: 3glr) is represented in blue ribbon (left). The superimposition of the substrate binding sites (right) of SIRT1 (green) and SIRT2 (orange) homology models and SIRT3 crystal structure (blue). The acetylated substrate is colored in black, the N- and C-terminal sides are represented by spheres V1 (pink) and V2 (yellow), respectively.

The first set of compounds with modifications in the N-terminus shared a 2-oxo-2-phenylethyl moiety in the C-terminus (**2**, **12-18** in Table 1). These compounds fulfill the hydrogen bonding network and the C-terminal π - π interaction requirements of the binding hypothesis (Figure 2). For SIRT1, the fulfillment of these requirements is enough to give highly potent compounds; despite the structural changes in the N-terminus compounds **12-18** gave $\geq 95\%$ inhibition. Compound **2** with the N-terminal Boc-group gave 91% SIRT1 inhibition, although weakest within this set it was still highly active. For SIRT2 and SIRT3, more variation was seen in the inhibitory activities suggesting that the optimization of the N-terminus is more critical for these enzymes. However, the C-terminal 2-oxo-2-phenylethyl moiety seems to be very good also for SIRT2 and SIRT3 because $\geq 90\%$ inhibition was achieved in several examples. Compounds **12-14** show the same trend for all the three enzymes; elongation of the chain improved inhibitory activity, the best compound being **14** with five methylene groups between the phenyl and carbonyl functions. Based on the modeling studies, compound **14** seems to be better complementary with the hydrophobic cavity compared to compounds **12** and **13**. Compound **2** with the N-

terminal Boc-group gave SIRT2 inhibition comparable to compound **14** but against SIRT1 and SIRT3 it showed decreased activity. Introduction of the pyridyl group did not improve the inhibition of any of the enzymes (**15** vs. **12**).

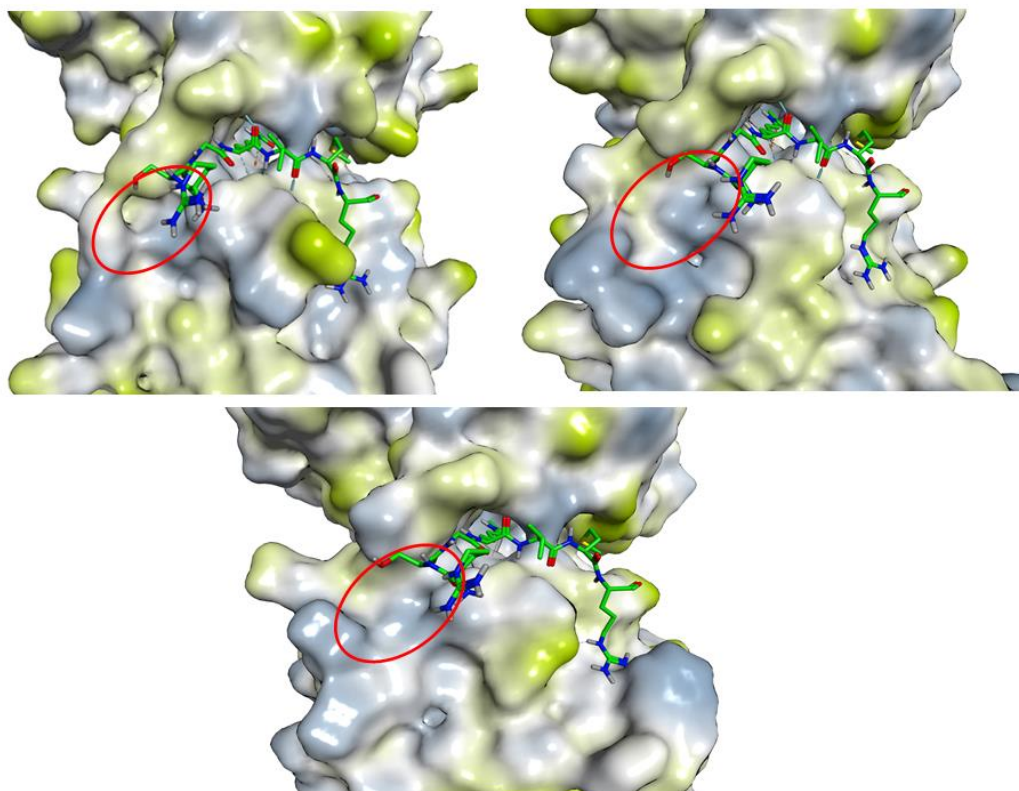


Figure 4. (A) SIRT1 homology model, (B) SIRT2 homology model and (C) SIRT3 crystal structure (PDB: 3GLR).

Compounds **16-18** were designed to improve the N-terminal interactions in the lipophilic cavity. Modeling studies also show that the hydroxyl moiety of the 4-hydroxy-L-prolyl group in compound **16** can form an additional H-bond with Gly295 (Figure 5d). Interestingly, compound **16** was the only compound within the whole compound library that achieved $\geq 90\%$ inhibition of all three studied sirtuins and thus, seems to possess a well-optimized structure. The second set of compounds with modifications in the N-terminus shared a phenyl moiety in the C-terminus (**19-23** in Table 1).

Table 1. Screening of the N-terminal modifications.

No.	R ₂	Inhibition-% @ 50 μM ^a		
		SIRT1	SIRT2	SIRT3
2		91 ± 0.6	87 ± 0.5	63 ± 1.2
12		96 ± 0.1	65 ± 1.5	68 ± 3.1
13		98 ± 0.1	76 ± 2.3	72 ± 0.2
14		98 ± 0.1	83 ± 0.4	82 ± 0.3
15		95 ± 0.3	58 ± 0.6	62 ± 1.3
16		99 ± 0.0	96 ± 0.3	90 ± 0.2
17		97 ± 0.4	95 ± 0.5	76 ± 1.2
18		96 ± 0.2	73 ± 1.2	61 ± 0.3
19		82 ± 0.2	39 ± 2.6	44 ± 0.3
20		62 ± 2.2	18 ± 1.1	16 ± 1.1
21		80 ± 0.5	44 ± 0.5	45 ± 2.2
22		86 ± 0.1	13 ± 3.1	19 ± 0.8
23		90 ± 0.5	54 ± 1.4	69 ± 1.3

^aFluor de Lys assay, values are means ± SD of at least three experiments.

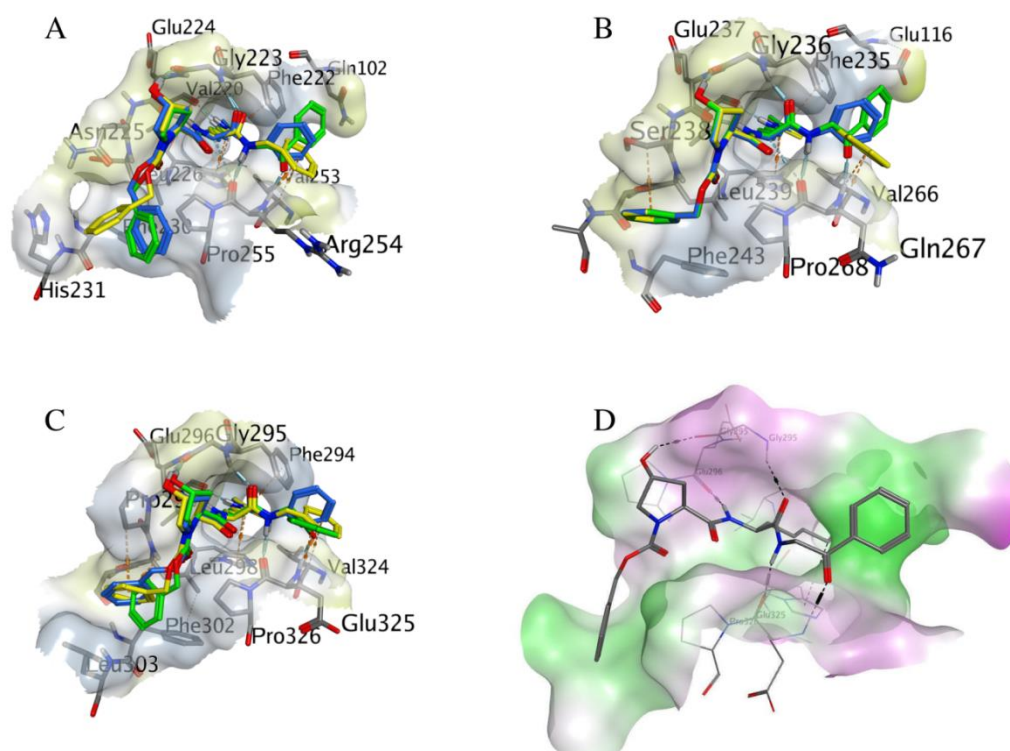


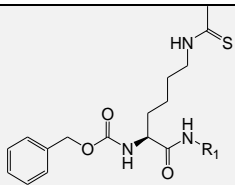
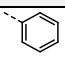
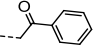
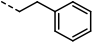
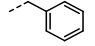
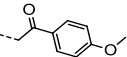
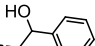
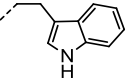
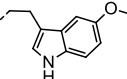
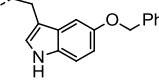
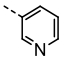
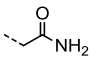
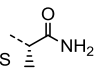
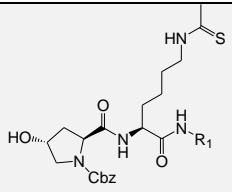
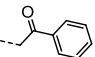
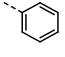
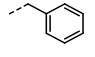
Figure 5. Docking poses for **16** (green), **23** (blue), **35** (yellow) in A) SIRT1, B) SIRT2, C) SIRT3. On the protein surface the light green represents the hydrophilic and the light blue the lipophilic areas. D) Compound **16** docked in SIRT3 highlighting the additional hydrogen bond between the hydroxyl group and Gly295.

These compounds are missing one H-bond of the hydrogen bonding network due to the lack of the C-terminal H-bond acceptor. Furthermore, the phenyl ring is not in the optimal position for the C-terminal π - π interaction. It is obvious that the C-terminal phenyl is not as good a structure as the above studied 2-oxo-2-phenylethyl moiety (**19**, **21**, **23** vs. **15**, **17**, **16**, respectively). Again, the N-terminal Cbz-4-hydroxy-L-prolyl moiety (**23**) gave the most potent compound (Figure 4). Boc-L-prolyl (**21**) instead, shows only comparable activity to the 3-(3-pyridyl)propanoyl fragment (**19**) in this series. Boc deprotection of **21** gave compound **22** with an L-prolyl moiety and further simplification gave compound **20** with an *N,N*-dimethyl-glycine. Against SIRT1, compound **22** was able to maintain inhibition (86%), possibly due to an H-bond from the NH-proton of the L-proline to Gly223 (SIRT1 numbering). Compound **20** lacks this proton and shows decreased activity (62%). However, against SIRT2 and SIRT3 both **20** and **22** show only weak inhibition. This is in line with our

previous finding with peptidic inhibitors that SIRT1 can be inhibited with smaller compounds. Small pseudopeptides provide an approach to gain SIRT1 selectivity; compound **22** shows highest SIRT1 selectivity among the pseudopeptide library.

The first set of compounds with modifications in the C-terminus shared a Cbz group in the N-terminus (**25-34** in Table 2). Although the C-terminal 2-oxo-2-phenylethyl moiety had proven to be a very good structure (Table 1), it was causing side-reactions during the synthesis reducing the yields. Thus, it was decided to explore whether a more stable group with similar activity could be found. The reduction (**28**) or deletion (**25**) of the carbonyl function (Figure 6) induced a uniform loss in potency, probably because of the lost H-bond to the carbonyl function. Compound **28** was tested as a mixture of diastereomers but modeling did not suggest favorable interactions for one over the other. Next, the phenyl function was positioned closer to the thioacetylated lysine giving the benzyl derivative **26**. For SIRT1 and SIRT3, this optimization of the C-terminal π - π interaction could compensate for the lost H-bond and high inhibition was observed. SIRT2 instead showed different behavior; the H-bond seems to be more crucial for the SIRT2 inhibition. These results were verified also by another set of compounds (Figure 5, Table 2); compared to compound **16**, compound **35** shows similar SIRT1 and SIRT3 inhibition but decreased SIRT2 inhibition. However, both of these compounds show higher inhibition compared to compound **23** with the C-terminal phenyl group. Larger C-terminal aromatic groups were studied by compounds **27** and **29-31**. The tryptamine moiety (**29**) does not show an optimal interaction with the Phe294. However, the tryptamine can have other hydrophobic interactions with surrounding hydrophobic residues. Also, in SIRT1 there is a possibility for the tryptamine nitrogen to form an additional hydrogen bond with Lys252 (SIRT1 numbering, compound **30** in Figure 6). Further bulkiness was gained by the methoxy (**30**) and benzyloxy (**31**) groups. These hydrophobic groups increase C-terminal hydrophobic interactions and improve potency. Also, the methoxy group in compound **27** can increase the hydrophobic interactions (Figure 6).

Table 2. Screening of the C-terminal modifications.

No.	R ₁	Inhibition-% @ 50 μM ^a		
		SIRT1	SIRT2	SIRT3
				
Ref.A		83 ± 0.5	81 ± 1.1	62 ± 1.5
Ref.B		97 ± 0.3	94 ± 0.3	74 ± 0.9
25		72 ± 3.5	52 ± 1.6	41 ± 1.9
26		91 ± 0.1	67 ± 0.6	71 ± 2.8
27		97 ± 0.1	97 ± 0.2	82 ± 1.3
28		77 ± 0.2	54 ± 3.1	45 ± 2.7
29		85 ± 0.7	61 ± 2.3	46 ± 3.8
30		88 ± 0.3	66 ± 1.1	63 ± 1.2
31		87 ± 0.4	79 ± 0.6	68 ± 2.8
32		84 ± 1.0	70 ± 1.3	59 ± 1.7
33		91 ± 0.3	72 ± 0.5	77 ± 0.1
34		96 ± 0.2	86 ± 0.2	85 ± 0.9
				
16		99 ± 0.0	96 ± 0.3	90 ± 0.2
23		90 ± 0.5	54 ± 1.4	69 ± 1.3
35		97 ± 0.2	87 ± 0.7	93 ± 0.1

^aFluor de Lys assay, values are means ± SD of at least three experiments.

Three smaller, more polar C-terminal fragments were also studied. The pyridyl group in compound **32** can have a π - π interaction to the protein but surrounding water provides competing interactions to the polar moiety. Compounds **33** and **34** lack an aromatic ring and cannot form π - π interactions. However, these compounds are able to retain a good inhibition potency which may be due to an additional H-bond to the terminal amide nitrogen. The stereochemistry of the chiral compound **34** apparently orientates the hydrogen bonding more properly.

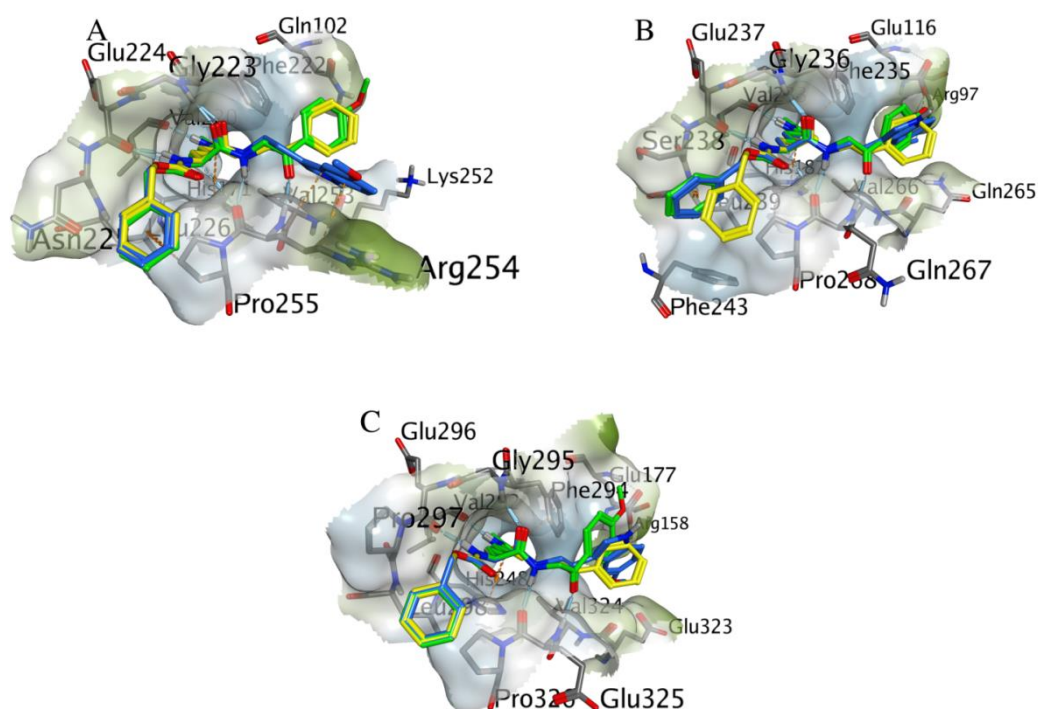


Figure 6. Docking poses for **25** (yellow), **27** (green), **30** (blue) in A) SIRT1, B) SIRT2, C) SIRT3. On the protein surface the light green represents the hydrophilic and the light blue the lipophilic areas.

A pyridyl group is often used to improve water solubility of compounds. Therefore, C-terminal pyridyl moieties were combined to miscellaneous N-terminal fragments (Table 3). Compounds **6** and **40** with the C-terminal 2-(3-pyridyl)ethyl fragment show weak to moderate sirtuin inhibition. Compounds **38** and **39** possess the C-terminal 3-pyridyl moiety. In compound **38**, the N-terminal Cbz group of compound **32** was replaced by a phenylethyl group giving decreased SIRT2 and SIRT3

inhibition. However, compound **39** with an ortho-fluoro substituent on the phenyl ring shows improved affinity towards all studied sirtuins compared to compounds **32** and **38**. The fluorine provides an H-bond acceptor that may form an additional H-bond to the enzyme backbone (Leu298 in SIRT3) but the GlideScore scoring function does not reward fluorine as a hydrogen bond acceptor. Finally, two compounds with C-terminal benzyl groups were studied (**36** and **37**). These compounds have an N-terminal phenyl moiety at the end of a long, flexible chain. The length of these N-terminal moieties is similar to Cbz-4-hydroxy-L-prolyl group. The flexibility of the chains of **36** and **37** allows the phenyl groups be buried deep in the lipophilic cavity. This gives excellent SIRT1 inhibition and good SIRT2 and SIRT3 inhibition.

Table 3. Screening of the miscellaneous modifications.

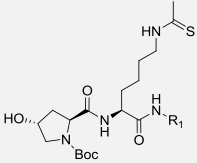
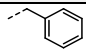
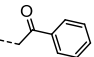
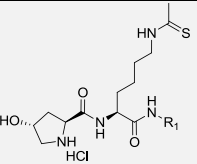
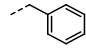
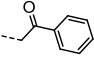
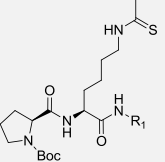
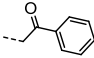
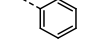
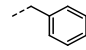
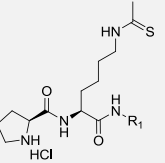
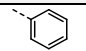
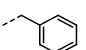
Structure	No.	R ₂	R ₁	Inhibition-% @ 50 μM ^a		
				SIRT1	SIRT2	SIRT3
	6			41 ± 1.9	28 ± 3.8	24. ± 0.3
	36			100 ± 0.1	71 ± 0.6	84 ± 0.2
	37			99 ± 0.2	74 ± 1.2	87 ± 0.3
	38			83 ± 1.0	21 ± 3.4	39 ± 1.2
	39			94 ± 0.4	74 ± 0.2	72 ± 0.6
	40			66 ± 0.5	49 ± 1.1	68 ± 3.0

^aFluor de Lys assay, values are means ± SD of at least three experiments.

In order to obtain preliminary SAR information a small series of proline derivatives **41-46** was designed starting from the results obtained by compounds **16**, **17**, **21-23** and **35**. The shift from N-Cbz-4-trans-hydroxy-L-prolil **16**, **35** (Table 2) to the corresponding N-Boc derivatives **41**, **42** (Table 4) alter only partially the inhibition activity. Boc deprotection of compound **41** gave compound **43** with an 4-trans-hydroxy-L-prolil moiety able to maintain the same SIRT1 inhibition but, slowly

reduced on SIRT2 and SIRT3. Interestingly Boc deprotection of **21** and **45** (Table 4) gave compounds **22** and **46** (Table 4) that retain a good SIRT1 inhibition but only weak against SIRT2 and SIRT3, confirming once again what proposed previously.

Table 4. Screening of proline derivatives.

No.	R ₁	Inhibition-% @ 50 μM ^a		
		SIRT1	SIRT2	SIRT3
				
41		83 ± 0.2	86 ± 0.3	92 ± 0.2
42		97 ± 0.1	96 ± 1.8	91 ± 0.1
				
43		89 ± 0.4	70 ± 0.9	78 ± 0.3
44		97 ± 0.1	Not available	Not available
				
17		97 ± 0.4	95 ± 0.5	76 ± 1.2
21		80 ± 0.5	44 ± 0.5	45 ± 2.2
45		94 ± 0.1	84 ± 0.2	83 ± 1.0
				
22		86 ± 0.1	13 ± 3.1	19 ± 0.8
46		95 ± 0.0	58 ± 0.4	58 ± 1.2

^aFluor de Lys assay, values are means ± SD of at least three experiments.

That SIRT1 can be inhibited by small C-terminal fragments, instead SIRT2 and SIRT3 require not only an improvement of H-bond interactions but, also the presence of bulky groups such as N-Cbz-4-trans-hydroxy-L-proline (**16**, **35**) able to fill the lipophilic cavity as we have discussed before in the binding hypothesis.

Three compounds with slightly different inhibition profiles, **16**, **27** and **30**, were chosen for IC₅₀ profile evaluation and cellular studies. Compound **16** was chosen because it is the only compound giving $\geq 90\%$ inhibition of all studied sirtuins. Compound **27** gives excellent SIRT1 and SIRT2 inhibition (97%) but slightly decreased SIRT3 inhibition (82%). Compound **30** has the highest selectivity towards SIRT1 among these three compounds; it shows 88% SIRT1 inhibition but 66% SIRT2 and 63% SIRT3 inhibition. Compounds **16** and **27** fulfill completely the binding hypothesis while compound **30** with its C-terminal tryptamine shows an alternative H-bond. The IC₅₀ values of the three chosen compounds (Table 5, Figure 7) follow nicely the preliminary screening results showing slightly different inhibition profiles. Also our previous experience with the thioacetylated compounds has indicated that the preliminary screening correlates well with the IC₅₀ values. This may be due to the reaction mechanism and formation of the stable 1'-S-alkylamidate intermediate.

Table 5. IC₅₀ values, cLogP, PSA and MW for compounds **16**, **27** and **30**.

No.	IC ₅₀ μ M (95% confidence interval) ^a			cLogP	PSA ^c	MW
	SIRT1	SIRT2	SIRT3			
16	0.24 (0.22-0.25)	1.80 (1.44-2.26)	3.89 (3.47-4.37)	2.61	287.85	568.69
27	0.89 (0.83-0.96)	2.53 (2.37-2.70)	8.35 (7.37-9.46)	3.66	262.74	485.60
30	5.98 (5.25-6.81)	25.8 (22.7-29.3)	29.4 (23.1-37.4)	4.50	257.70	510.65

^aFluor de Lys assay, values are calculated from three independent determinations giving altogether 27 data points. ^bCalculated logarithm of octanol/water partition coefficient, calculated with MOE 2011.10.³⁴ ^cTotal Polar Surface Area (\AA^2), calculated with MOE 2011.10 (Molecular Operating Environment (MOE), 2011.10; Chemical Computing Group Inc., 1010 Sherbooke St. West, Suite #910, Montreal, QC, Canada, H3A 2R7).

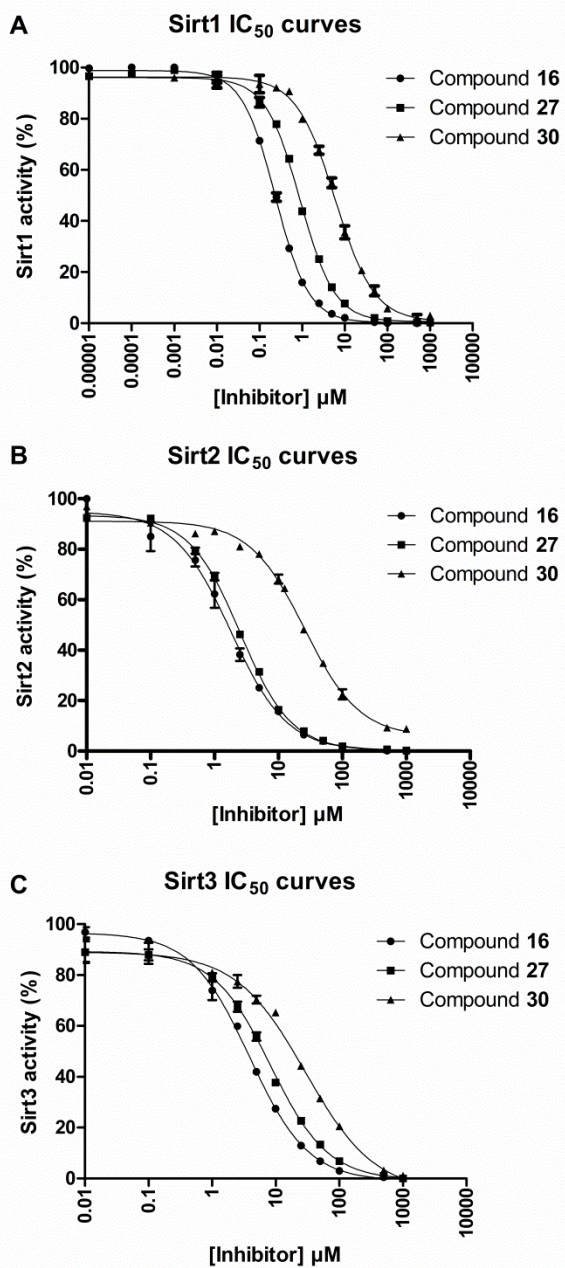
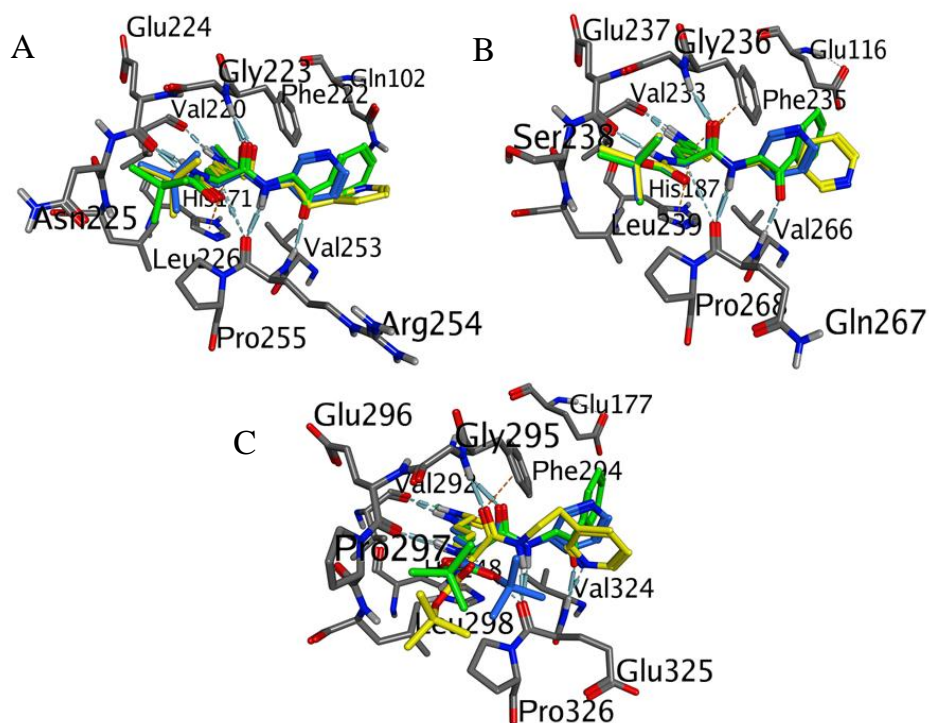


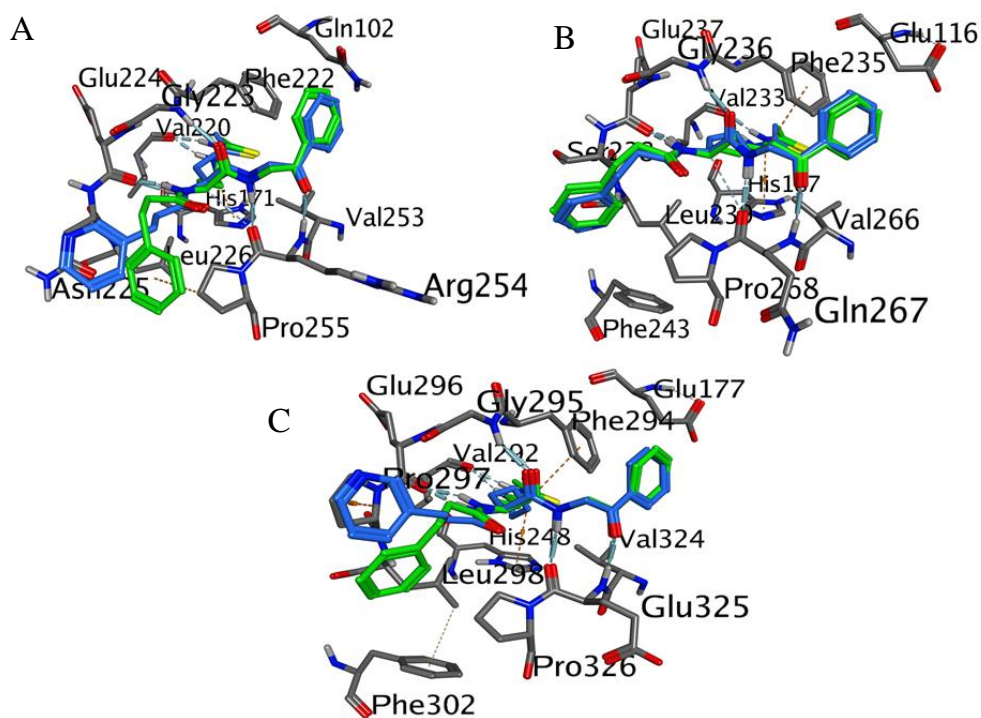
Figure 7. The IC₅₀ curves of compounds **16**, **27** and **30** for A) SIRT1, B) SIRT2 and C) SIRT3.

Docking poses.

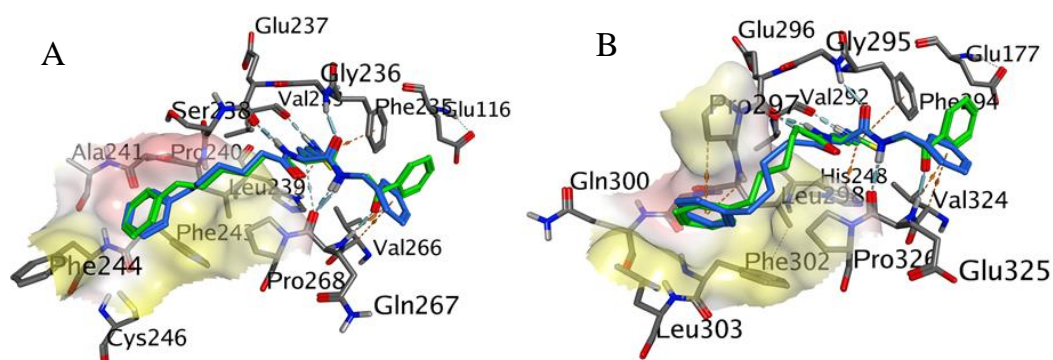
Compounds **2** (green), **5** (blue), **6** (yellow) in SIRT1 (A), SIRT2 (B), SIRT3 (C)



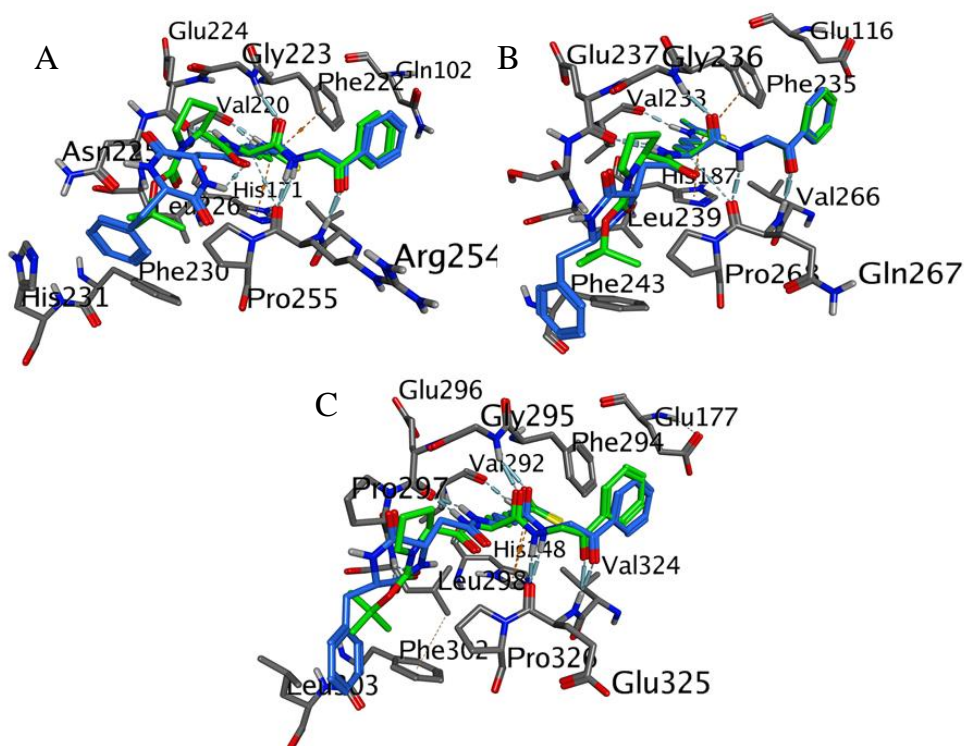
Compounds **12** (green), **15** (blue) in SIRT1 (A), SIRT2 (B), SIRT3 (C)



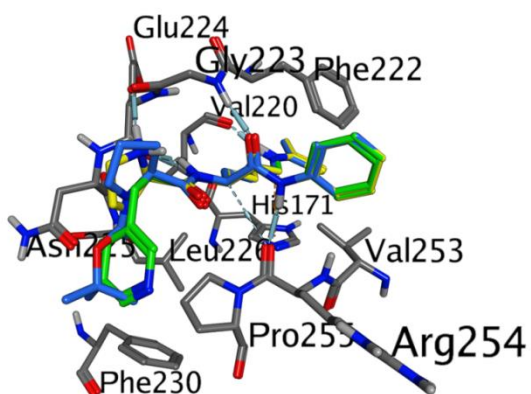
Compounds **14** (green), **36** (blue) in SIRT2 (A) and SIRT3 (B)



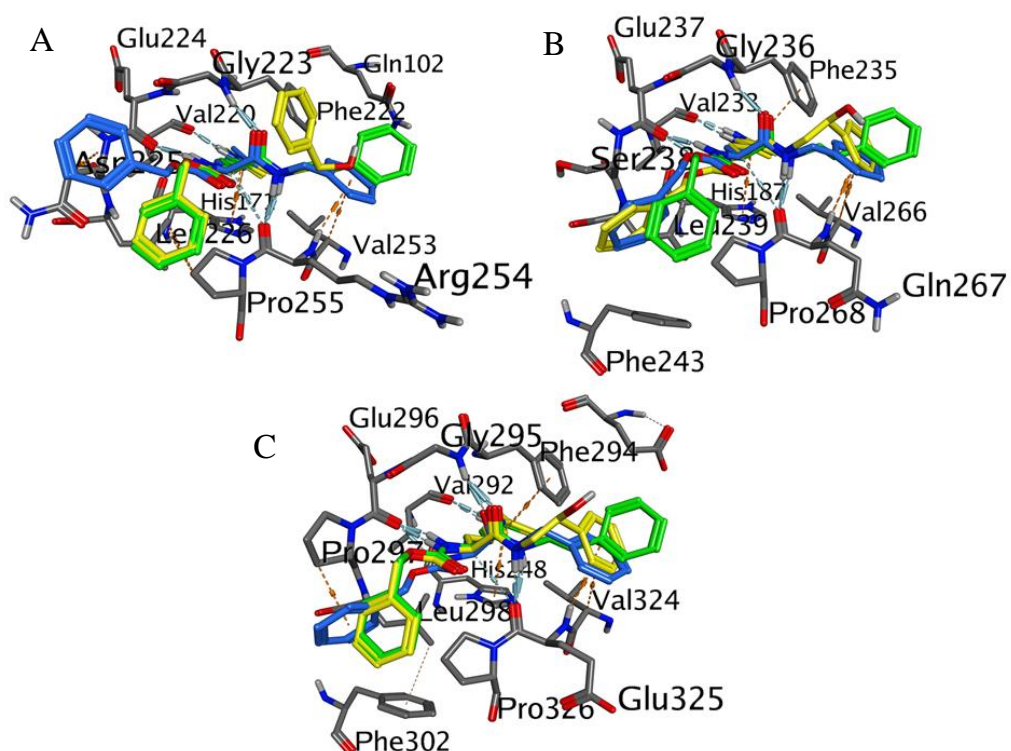
Compounds **17** (green), **18** (blue) in SIRT1 (A), SIRT2 (B) and SIRT3 (C)



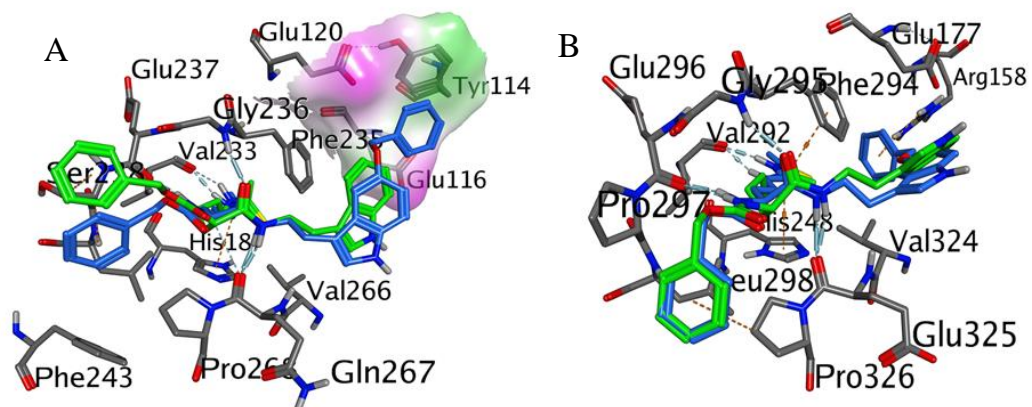
Compounds **19** (green), **21** (blue), **22** (yellow) in SIRT1



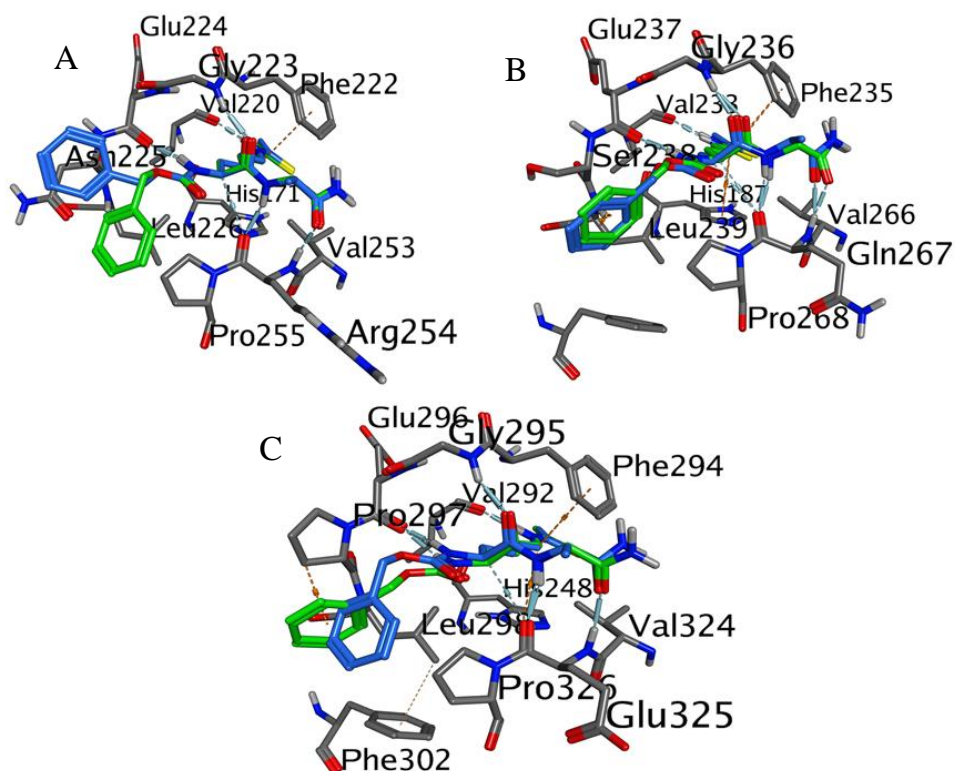
Compounds **25** (green), **26** (blue), **28** (yellow) in SIRT1 (A), SIRT2 (B) and SIRT3 (C)



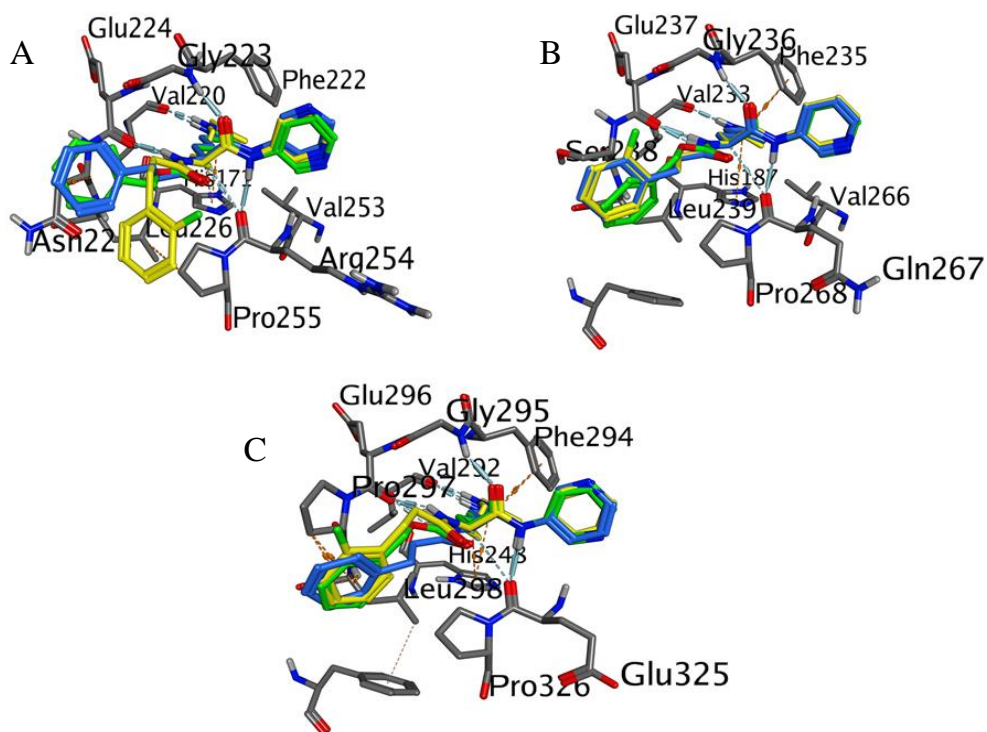
Compounds **29** (green), **31** (blue) in SIRT2 (A) and SIRT3 (B)



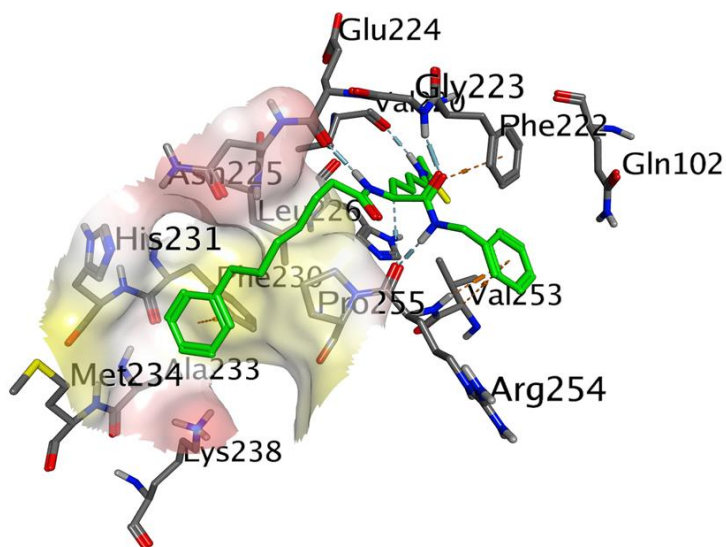
Compounds **33** (green), **34** (blue) in SIRT1 (A), SIRT2 (B) and SIRT3 (C)



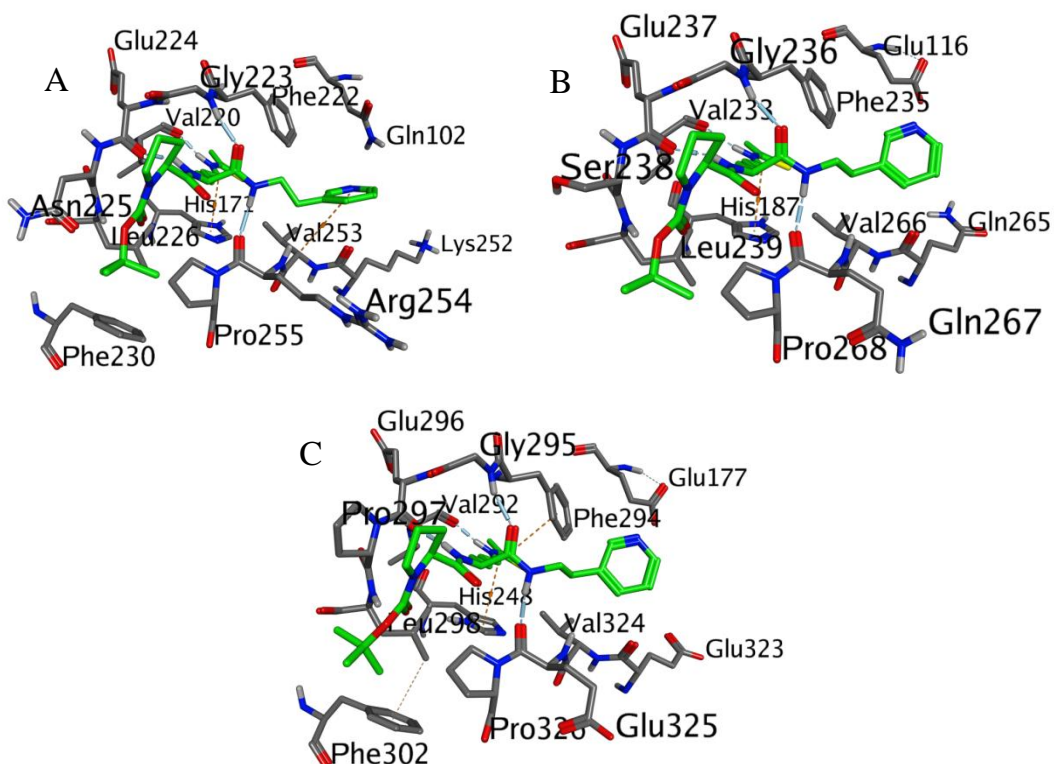
Compounds **32** (green), **38** (blue), **39** (yellow) in SIRT1 (A), SIRT2 (B) and SIRT3 (C)



Compound **37** in SIRT1



Compound **40** in SIRT1 (A), SIRT2 (B) and SIRT3 (C)



The effects of compounds 16, 27 and 30 in human cell lines. To get the first glimpse of the cell-penetration of the compounds, they were studied in two different cell-lines that we have previously used for this purpose; ARPE-19 retinal pigment epithelium cells and SH-SY5Y neuroblastoma cells.¹³⁴ In the literature, ARPE-19 cells have been used to investigate age-related macular degeneration, where SIRT1 is expected to have a therapeutic role¹⁹⁰ and in SH-SY5Y cells SIRT1 has been shown to have neuroprotective effects.¹⁹¹ Because SIRT1 is known to deacetylate Lys382 of p53,^{132,119} Western blot analysis was performed in order to detect changes in acetylation level of p53 after etoposide-induced DNA damage. Each of the compounds showed increased p53 acetylation in ARPE cells while the effect in SH-SY5Y cells was not as evident (Figure 8A). The low levels of lactate dehydrogenase (LDH) leakage from the treated cells indicate that the tested compounds were not toxic to the cells at the used concentration (Figure 8B).

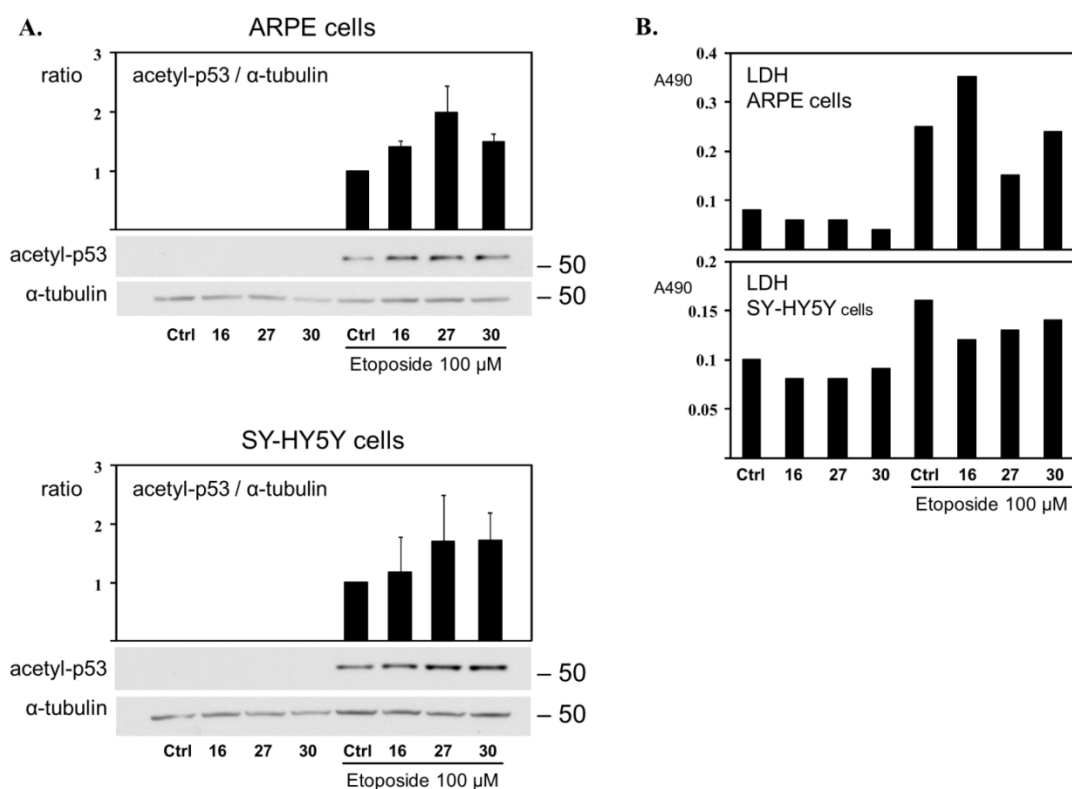


Figure 8. Inhibition of SIRT1 activity increases p53 acetylation after DNA damage. (A) Effect of 20 μ M compounds **16**, **27**, and **30** on p53 acetylation after 100 μ M etoposide (eto) treatment for 5 h in ARPE-19 and SH-SY5Y cell lines. The results are shown as mean \pm SEM of 2 independent experiments. The representative Western blots are shown below. (B) Effect of compounds **16**, **27** and **30** on LDH leakage from ARPE-19 and SH-SY5Y cells.

As sirtuin inhibition has been suggested as a potential therapy for breast and lung cancer,^{64,141,192} the effects of SIRT inhibitors **16**, **27**, and **30** on the proliferation of two tumor cell lines, A549 lung carcinoma and MCF-7 breast carcinoma, were measured with sulforhodamine B assay. Both A549 and MCF-7 cell growth was inhibited with $\geq 50 \mu$ M of **27** and **30** (Figure 9). The other tested SIRT inhibitor **16** did not show any substantial inhibitory effect on A549 or MCF-7 cell growth with concentrations up to 200 μ M (data not shown).

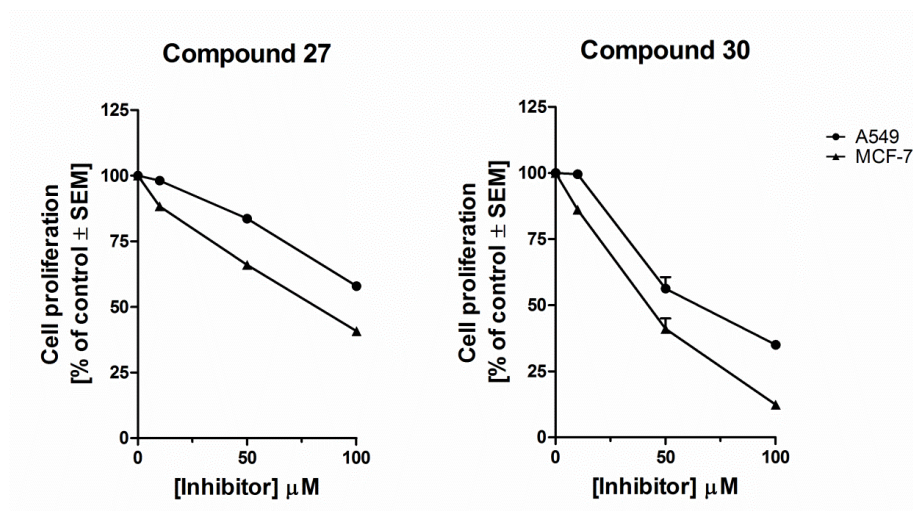


Figure 9. Effects of SIRT inhibitors on A549 and MCF-7 cell proliferation. The cells were treated with 0 to 100 μM of **27** (left) or **30** (right). Cell proliferation was determined by sulforhodamine B assay. The results are shown as mean \pm SEM of 2-3 independent experiments.

In order to understand the different inhibitory behavior of the three tested inhibitors on cell proliferation, the cellular p53 acetylation levels in the MCF-7 cells were examined (Figure 10A) and physicochemical parameters for the inhibitors were calculated (Table 5). The study showed that all the three compounds were able to increase the acetylation level of p53 but compound **16** was less effective than **27** and **30**. Despite being a potent SIRT1-3 inhibitor, compound **16** did not inhibit MCF-7 or A549 cell proliferation. This could be explained by cell type specific differences in membrane permeability, together with different physico-chemical properties of the compounds (Table 5). As these compounds are rather large, it can be speculated that compound **16** with the lowest cLogP and the highest polar surface area and molecular weight may have difficulties in cell-permeation. The compounds did not show any toxic effect when tested with LDH assay (Figure 10B).

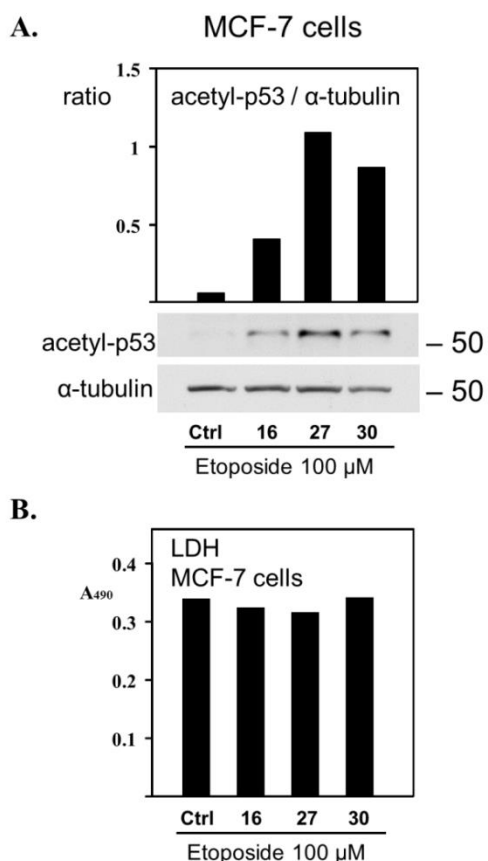


Figure 10. Inhibition of SIRT1 activity increases p53 acetylation after DNA damage in MCF-7 cells. (A) Effect of 50 μ M compounds **16**, **27**, and **30** on p53 acetylation in MCF-7 cells after 100 μ M etoposide (eto) treatment for 5 h. The test was performed once for each compound. (B) Effect of compounds **16**, **27**, and **30** on LDH leakage from MCF-7 cells.

Propidium iodide staining and flow cytometric DNA content analysis of MCF-7 and A549 cells treated with **27** and **30** was performed in order to detect the effect of these compounds on cell cycle progression. Cell cycle analysis revealed that both **27** and **30** arrested cancer cells in the G₁ phase, with > 50% reduction in DNA synthesis (S phase population), and no cell death was observed (Figure 11).

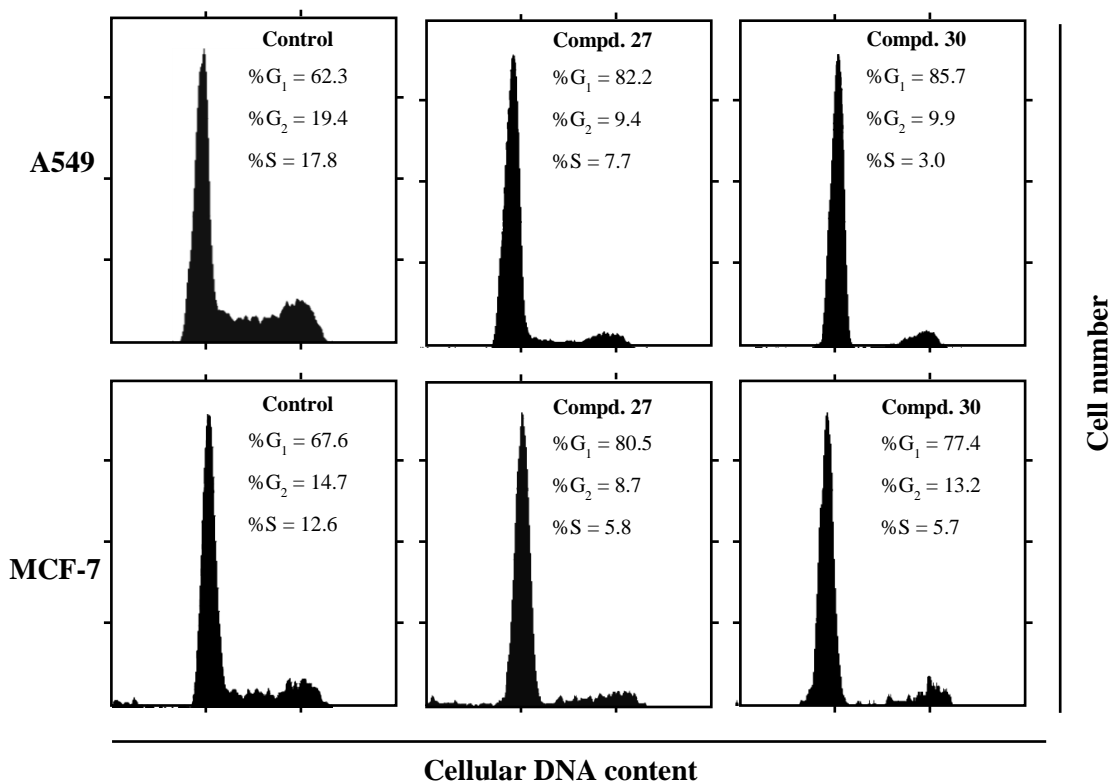


Figure 11. Effects of SIRT inhibitors on A549 and MCF-7 cell cycle. The cells were subjected to control treatment (0.5% DMSO) or treatment with 100 μ M of **27** or **30** for 18 h. Flow cytometric analysis of DNA content was done after propidium iodide staining. Percentage of cells in each phase of the cell cycle (G₁, G₂, and S) is indicated. Representative data from at least two independent experiments are shown.

8.4 Conclusions

A library of novel compounds around thioacetylated lysine scaffold was synthesized. The C-terminal 2-oxo-2-phenylethyl and benzyl moieties were found to be fragments that give excellent SIRT1 inhibitions (**2**, **12-18** and **26**, **35-37**). The N-terminal Cbz-, -Boc-4-hydroxy-L-prolyl or a long flexible chain attached to a phenyl group (**16**, **23**, **35** and **14**, **36**, **37**, **41**, **42**) also gave a positive contribution to the binding hypothesis hinting that the H-bond with Gly295 and groups that can be buried deep in the lipophilic cavity can improve inhibition potency. Three compounds, **16**, **27** and **30**, with slightly different inhibition profiles were chosen for more detailed studies. Their effect on tumor cell proliferation was studied in A549 lung carcinoma and MCF-7

breast carcinoma cell lines. Interestingly, the in vitro inhibition potency did not correlate with the cellular effect; the most potent compound **16** did not show any antiproliferative effect while the two other compounds inhibited cell growth at ≥ 50 μ M concentration. The difference may arise from different cell permeation of the compounds. Due to the observed induction of p53 acetylation in ARPE-19 and MCF-7 cells, SIRT1 is likely to be one of the cellular targets of compounds **27** and **30**. Compounds **27** and **30** were shown to be cell-permeable and non-toxic sirtuin inhibitors. They both inhibited cell growth by the arrest at the G₁ phase in two tumor cell-lines, although the effect of compound **30** was more pronounced. These two inhibitors are our new lead compounds that will be taken to further studies.

8.5 Experimental Section

Chemistry. Chemical reagents and solvents used in this study were commercial high purity quality. Organic solutions were dried over anhydrous sodium sulfate. Pyridine and dimethylformamide (DMF) were dried over molecular sieves. Compounds **1**, **24** were prepared using the same amounts and following the procedure reported by Huhtiniemi and coworkers.¹³⁴ Yields of all reactions refer to the purified products. NMR spectra were acquired on a Bruker Avance 500 AV (Bruker Biospin, Switzerland) spectrometer operating at 500.1 MHz for ¹H and 125.8 MHz for ¹³C. Chemical shift values are reported as δ (ppm) relatively to TMS (tetramethylsilane) as an internal reference; coupling constant are given in Hz. Positive ion mass spectra were recorded with a quadrupole ion trap mass spectrometer (Finnigan MAT, San Jose, CA) equipped with an electrospray ionization source (ESI-MS). The purity of the compounds was determined by Elemental analysis obtained by an Thermo Quest CE Instruments EA 1110 CHNS-O elemental analyzer and the Analytical results are within $\pm 0.40\%$ of the theoretical values (see Supporting Information). Purity of tested compounds was $\geq 95\%$. The purity of compounds **27** and **28** was also determined by HPLC (Agilent 1100 series) on a C-18 column (Zorbax Eclipse XDB-C18, 4.6*50 mm, 1.8 μ m) using 45% acetate buffer (20 mM, pH 5) and 55% MeOH as eluent, flow rate 1 mL/min, column temperature 50°C and detection at 265 nm.

(2S)-2-tert-Butyl 6-ethanethioamido-1-oxo-1-(2-oxo-2-phenylethylamino)hexan-2-ylcarbamate (2). To a solution of **1** (1.17 g, 3.84 mmol) in DMF (17.0 mL) under Argon flow were added TBTU (1.36 g, 4.2 mmol), pyridine (17.0 mL) and maintained under stirring for 10min at rt . After this time 2-Aminoacetophenone hydrochloride (0.66 g, 3.84 mmol) was added and the solution mixed 2h 30min at rt under Argon flow. Solvents were evaporated and the obtained oil was dissolved in EtOAc (180 mL), washed with HCl 0.5M, brine (two times), saturated NaHCO₃ and finally dried with Na₂SO₄ and evaporated under vacuo. The crude product obtained was purified by column chromatography using silica Kieselgel for flash and EtOAc : MeOH (9.5 : 0.5 v/v) as eluent phase to give the pure product as a sticky solid (1.34 g, 3.17 mmol, 83 %). ¹H-NMR (DMSO-*d*₆) : δ = 9.95 (s br, 1H), 8.13 (t, *J* = 5.36 Hz,

1H), 7.99 (d, $J = 7.57$ Hz, 2H), 7.67 (t, $J = 7.57$ Hz, 1H), 7.54 (t, $J = 7.57$ Hz, 2H), 6.90 (d, $J = 8.20$ Hz, 1H), 4.70-4.54 (m, 2H), 4.01-3.97 (m, 1H), 3.50-3.39 (m, 2H), 2.39 (s, 3H), 1.71-1.49 (m, 4H), 1.39-1.30 (m, 11H). $^{13}\text{C-NMR}$ (CDCl_3): $\delta = 201.06, 194.12, 172.33, 155.96, 134.43, 134.39, 129.13, 128.07, 54.11, 46.42, 46.12, 34.22, 32.67, 29.82, 28.46, 27.16, 22.88$. ESI-MS (m/z): 422.0 $[\text{M} + \text{H}]^+$, 444.20 $[\text{M} + \text{Na}]^+$. Anal. ($\text{C}_{21}\text{H}_{31}\text{N}_3\text{O}_4\text{S}$) C, H, N.

(2S)-2-tert-Butyl 6-ethanethioamido-1-oxo-1-(phenylamino)hexan-2-ylcarbamate (3). Compound **3** was prepared using **1** (1.2 g, 4.00 mmol), DMF (17.0 mL), TBTU (1.41 g, 4.4 mmol), pyridine (17.0 mL) and aniline (0.36 mL, 4.00 mmol) following the same procedure described for **2**. Purification by chromatography column using silica Kieselgel for flash and EtOAc : MeOH (9.5 : 0.5 v/v) to give the product as solid (1.11 g, 2.92 mmol, 73 %). $^1\text{H-NMR}$ ($\text{DMSO-}d_6$): $\delta = 9.94$ (s br, 1H), 9.91 (s, 1H), 7.59 (d, $J = 8.20$ Hz, 2H), 7.30 (t, $J = 8.20$ Hz, 2H), 7.04 (t, $J = 8.20$ Hz, 1H), 6.99 (d, $J = 7.57$ Hz, 1H), 4.07-4.01 (m, 1H), 3.49-3.42 (m, 2H), 2.36 (s, 3H), 1.68-1.49 (m, 4H), 1.38-1.30 (m, 11H).

(2S)-2-tert-Butyl 6-ethanethioamido-1-oxo-1-(benzylamino)hexan-2-ylcarbamate (4). Compound **4** was prepared using **1** (1.22 g, 4.0 mmol), DMF (17.0 mL), TBTU (1.41 g, 4.40 mmol), pyridine (17.0 mL) and benzylamine (0.43 mL, 4.0 mmol), following the same procedure described for **2**. The product obtained as light-yellow solid (1.42 g, 3.62 mmol, 90 %) was used without further purifications. $^1\text{H-NMR}$ ($\text{DMSO-}d_6$): $\delta = 9.93$ (s br, 1H), 8.29 (t, $J = 5.99$ Hz, 1H), 7.31-7.21 (-Ar, 5H), 6.86 (d, $J = 7.88$ Hz, 1H), 4.32-4.23 (m, 2H), 3.94-3.89 (m, 1H), 3.45-3.41 (m, 2H), 2.37 (s, 3H), 1.66-1.49 (m, 4H), 1.39-1.23 (m, 11H).

(2S)-2-tert-Butyl 6-ethanethioamido-1-oxo-1-(pyridin-3-ylamino)hexan-2-ylcarbamate (5). Compound **5** was prepared using **1** (1.02 g, 3.37 mmol), in DMF (15.0 mL), TBTU (1.19 g, 3.70 mmol), pyridine (15.0 mL) and 3-Aminopyridine (0.32 g, 3.37 mmol), following the same procedure described for **2**. The workup was made without HCl 0.5M and EtOAc was replaced by CH_2Cl_2 . Purification by chromatography column using silica Kieselgel for flash and EtOAc : CH_2Cl_2 : MeOH (3.5 : 5.5 : 1) as eluent phase to give the pure product as solid (0.49 g, 1.28 mmol, 38 %). $^1\text{H-NMR}$ ($\text{DMSO-}d_6$): $\delta = 10.17$ (s, 1H), 9.94 (s br, 1H), 8.73 (d, $J = 1.40$ Hz,

1H), 8.26 (dd, $J = 1.40, 4.73$ Hz, 1H), 8.03 (dt, $J = 1.40, 8.20$ Hz, 1H), 7.34 (dd, 4.73, 8.20 Hz, 1H), 7.08 (d, $J = 7.57$ Hz, 1H), 4.07-4.02 (m, 1H), 3.50-3.41 (m, 2H), 2.36 (s, 3H), 1.70-1.51 (m, 4H), 1.38-1.30 (m, 11H).

(2S)-2-tert-Butyl 6-ethanethioamido-1-oxo-1-[2-(pyridin-3-yl)ethylamino]hexan-2-ylcarbamate (6). Compound **6** was prepared using **1** (1.02 g, 3.37 mmol), DMF (15.0 mL), TBTU (1.19 g, 3.70 mmol), pyridine (15.0 mL) and 3-(2-Aminoethyl)pyridine dihydrobromide (0.96 g, 4.71 mmol), following the same procedure described for **2**. The workup was made using only NaHCO₃ 5% and EtOAc was replaced by CH₂Cl₂ (300 mL). Purification by chromatography column using silica Kieselgel for flash and EtOAc : CH₂Cl₂ : MeOH (3 : 5.5 : 1.5) as eluent phase to give the pure product as solid (0.86 g, 2.11 mmol, 63 %). ¹H-NMR (DMSO-*d*₆): $\delta = 9.93$ (s br, 1H), 8.42 (m, 2H), 7.87 (t, $J = 5.36$ Hz, 1H), 7.62 (dt, $J = 1.60, 7.57$ Hz, 1H), 7.30 (dd, $J = 4.73, 7.57$ Hz, 1H), 6.75 (d, $J = 8.20$ Hz, 1H), 3.84-3.79 (m, 1H), 3.44-3.24 (m, 4H), 2.74-2.71 (m, 2H), 2.37 (s, 3H), 1.52-1.34 (m, 13H), 1.25-1.16 (m, 2H). ¹³C-NMR (DMSO-*d*₆) : $\delta = 198.77, 172.10, 155.29, 149.59, 147.09, 136.66, 135.07, 123.47, 77.98, 54.25, 45.28, 32.81, 32.07, 31.74, 28.21, 26.93, 23.04$, (-NH-CH₂-CH₂-pyr under DMSO-*d*₆). ESI-MS (*m/z*): 409.15 [M + H]⁺. Anal. (C₂₀H₃₂N₄O₃S·0.03DMF·0.03hexane) C, H, N.

(2S)-2-Amino-6-ethanethioylamino-N-(2-oxo-2-phenylethyl)hexanamide hydrochloride (7). To a solution of **2** (1.34 g, 3.18 mmol) in 2-propanol (45.0 mL), 1,2-ethanedithiol (0.27 mL, 3.18 mmol) was added and after 1min under stirring at r.t HCl 12N (1.34 mL, 16.0 mmol) was added and the solution heated at 60°C; After 20min and 40min other HCl 12N (1.34 mL) was added; when the total mmol of HCl in the reaction flask were 48 mmol, the solution was maintained for 60 min at 60°C under stirring. After this time, 2-propanol was evaporated under reduced pressure and the yellow oil was washed with petroleum ether (2 x 20 mL), Et₂O (3 x 15 mL) and finally washed with CH₂Cl₂ (7x 5 mL) provides the product as light-yellow solid (0.99 g, 2.77 mmol, 87 %). ¹H-NMR (DMSO-*d*₆) : $\delta = 10.10$ (s br, 1H), 8.92 (t, $J = 5.36$ Hz, 1H), 8.30 (s, 3H), 8.02 (d, $J = 7.88$ Hz, 2H), 7.69 (t, $J = 7.88$ Hz, 1H), 7.56 (t, $J = 7.57$ Hz, 2H), 4.82-4.68 (m, 2H), 3.96-3.83 (m, 1H), 3.49-3.45 (m, 2H), 2.41 (s, 3H), 1.82-1.78 (m, 2H), 1.61-1.56 (m, 2H), 1.48-1.39 (m, 2H).

(2S)-2-Amino-6-ethanethioylamino-N-phenylhexanamide hydrochloride (8).

Compound **8** was prepared using **3** (1.10 g, 2.89 mmol), 2-propanol (37.0 mL), 1,2-ethanedithiol (0.24 mL, 2.89 mmol) and HCl 12N (1.10 mL, 13.1 mmol) added x three times, following the same procedure described for **7**, provides the product as light-yellow solid (0.75 g, 2.36 mmol, 82 %). ¹H-NMR (DMSO-*d*₆) : δ = 10.80 (s, 1H), 10.12 (s br, 1H), 8.37 (s, 3H), 7.65 (d, *J* = 7.57 Hz, 2H), 7.35 (t, *J* = 7.57 Hz, 2H), 7.11 (t, *J* = 7.57 Hz, 1H), 4.04-3.98 (m, 1H), 3.48-3.42 (m, 2H), 2.36 (s, 3H), 1.88-1.79 (m, 2H), 1.62-1.57 (m, 2H), 1.43-1.37 (m, 2H).

(2S)-2-Amino-6-ethanethioylamino-N-benzylhexanamide hydrochloride (9).

Compound **9** was prepared using **4** (1.42 g, 3.61 mmol) in 2-propanol (44.0 mL), 1,2-ethanedithiol (0.30 mL, 3.60 mmol) and HCl 12N (1.41 mL, 16.9 mmol) added x three times, following the same procedure described for **7**, to furnish a yellow oil that was washed with petroleum ether (2 x 20 mL), Et₂O (3 x 20 mL) and finally washed with CH₂Cl₂ (7x 5 mL) provides the product as white solid (1.12 g, 3.4 mmol, 94 %). ¹H-NMR (DMSO-*d*₆) : δ = 10.10 (s br, 1H), 9.03 (t, *J* = 5.80 Hz, 1H), 8.25 (s, 3H), 7.36-7.25 (-Ar, 5H), 4.38-4.31 (m, 2H), 3.81-3.77 (m, 1H), 3.45-3.42 (m, 2H), 2.38 (s, 3H), 1.81-1.71 (m, 2H), 1.59-1.53 (m, 2H), 1.39-1.25 (m, 2H).

(2S)-2-Amino-6-ethanethioylamino-N-(pyridin-3-yl)hexanamide

dihydrochloride (10). Compound **10** was prepared using **5** (1.04 g, 2.74 mmol), 2-propanol (35.0 mL), 1,2-ethanedithiol (0.23 mL, 2.74 mmol) and HCl 12N (1.44 mL, 17.28 mmol) added x three times, following the same procedure described for **7**, to furnish a yellow oil that was washed with petroleum ether (2 x 20 mL) and CH₂Cl₂: petroleum ether (1:1) (4 x 4 mL) provides the product as white powder (0.71 g, 2.0 mmol, 73 %). ¹H-NMR (DMSO-*d*₆) : δ = 12.17 (s, 1H), 10.14 (s br, 1H), 9.17 (d, *J* = 2.21 Hz, 1H), 8.60 (d, *J* = 5.36 Hz, 1H), 8.56-8.53 (m, 4H), 7.90 (dd, *J* = 5.36, 8.51 Hz, 1H), 4.18-4.14 (m, 1H), 3.50-3.40 (m, 2H), 2.36 (s, 3H), 1.97-1.86 (m, 2H), 1.64-1.54 (m, 2H), 1.46-1.40 (m, 2H).

(2S)-2-Amino-6-ethanethioylamino-N-[2-(pyridin-3-yl)ethyl]hexanamide

dihydrochloride (11). Compound **11** was prepared using **6** (0.57 g, 1.41 mmol), 2-propanol (19.5 mL), 1,2-ethanedithiol (0.12 mL, 1.42 mmol) and HCl 12N (0.74 mL, 8.89 mmol) added x three times, following the same procedure described for **7**, to

furnish a yellow oil that was washed with petroleum ether (10 mL), Et₂O (4 x 15 mL) and finally washed with CH₂Cl₂ (3 x 5 mL) provides the product as light yellow powder (0.52 g, 1.36 mmol, 97 %). ¹H-NMR (DMSO-*d*₆) : δ = 10.19 (s br, 1H), 8.89 (d, *J* = 1.26 Hz, 1H), 8.81-8.77 (m, 2H), 8.44 (d, *J* = 7.88 Hz, 1H), 8.27 (s, 3H), 7.95 (dd, *J* = 5.36, 7.88 Hz, 1H), 3.70-3.65 (m, 1H), 3.56-3.36 (m, 4H), 3.02-2.93 (m, 2H), 2.39 (s, 3H), 1.67-1.60 (m, 2H), 1.55-1.49 (m, 2H), 1.26-1.15 (m, 2H).

(2S)-2-(3-Phenylpropanoylamino)-6-ethanethioylamino-N-(2-oxo-2-

phenylethyl)hexanamide (12). To a solution of 3-phenylpropanoic acid (0.13 g, 0.87 mmol) in DMF (4.7 mL) under Argon flow were added TBTU (0.31 g, 0.97 mmol), pyridine (4.7 mL) and maintained under stirring for 10min at rt . After this time **7** (0.32 g, 0.89 mmol) was added and the solution mixed 3h at rt under Argon flow. Solvents were evaporated and the obtained oil was dissolved in CH₂Cl₂ (100 mL), washed with HCl 0.5M, brine (twice), NaHCO₃ 5%, finally dried with Na₂SO₄ and evaporated under vacuo. The crude product obtained was purified with two columns chromatography, using Aluminum oxide and silica Kieselgel for flash with EtOAc : Hexane : MeOH (7: 2: 1) as eluent phase to give the pure product as white solid (0.052 g, 0.11 mmol, 13 %). ¹H-NMR (DMSO-*d*₆) : δ = 9.95 (s br, 1H), 8.24 (t, *J* = 5.36 Hz, 1H), 8.03 (d, *J* = 8.20 Hz, 1H), 7.99 (d, *J* = 7.57 Hz, 2H), 7.67 (t, *J* = 7.57 Hz, 1H), 7.54 (t, *J* = 7.57 Hz, 2H), 7.28-7.15 (-Ar, 5H), 4.65-4.55 (m, 2H), 4.37-4.32 (m, 1H), 3.46-3.38 (m, 2H), 2.84-2.79 (m, 2H), 2.47-2.43 (m, 2H), 2.38 (s, 3H), 1.70-1.62 (m, 1H), 1.55- 1.47 (m, 3H), 1.29-1.22 (m, 2H). ¹³C-NMR (DMSO-*d*₆) : δ = 198.74, 195.13, 172.11, 171.35, 141.27, 134.95, 133.50, 128.77, 128.20, 128.17, 127.79, 125.80, 52.16, 45.83, 45.33, 36.72, 32.78, 31.83, 31.04, 26.90, 22.82. ESI-MS (*m/z*): 454.14 [M + H]⁺ . Anal. (C₂₅H₃₁N₃O₃S) C, H, N.

(2S)-2-(4-Phenylbutyrylamino)-6-ethanethioylamino-N-(2-oxo-2-

phenylethyl)hexanamide (13). Compound **13** was prepared using, 4-phenylbutanoic acid (0.18 g, 1.1 mmol), DMF (5.5 mL), TBTU (0.39 g, 1.21 mmol), pyridine (5.5 mL) and **7** (0.4 g, 1.1 mmol) following the same procedure and purification described for **12**; CH₂Cl₂ in the workup was replaced by EtOAc (200 mL). Compound **13** was obtained as white solid (0.11 g, 0.23 mmol, 21 %). ¹H-NMR (DMSO-*d*₆): δ = 9.93 (s br, 1H), 8.21 (t, *J* = 5.36 Hz, 1H), 7.98-7.96 (m, 3H),

7.65 (t, $J = 7.25$ Hz, 1H), 7.54 (t, $J = 7.25$ Hz, 2H), 7.29-7.16 (-Ar, 5H), 4.66-4.54 (m, 2H), 4.37-4.32 (m, 1H), 3.47-3.42 (m, 2H), 2.58-2.52 (m, 2H), 2.37 (s, 3H), 2.18-2.15 (m, 2H), 1.83-1.77 (m, 2H), 1.74-1.67 (m, 1H), 1.60-1.50 (m, 3H), 1.37-1.28 (m, 2H). ^{13}C -NMR (DMSO- d_6): 198.69, 195.10, 172.17, 171.86, 141.82, 134.95, 133.50, 128.76, 128.31, 128.23, 127.79, 125.69, 52.19, 45.85, 45.32, 34.66, 34.66, 32.78, 31.72, 27.08, 26.89, 22.97. ESI-MS (m/z): 468.20 [M + H] $^+$. Anal. (C₂₆H₃₃N₃O₃S) C, H, N.

(2S)-2-(6-Phenyhexanoylamino)-6-ethanethioylamino-N-(2-oxo-2-phenylethyl)hexanamide (14). Compound **14** was prepared using 6-phenyhexanoic acid (0.21 mL, 1.1 mmol), DMF (5.5 mL), TBTU (0.39 g, 1.21 mmol), pyridine (5.5 mL) and **7** (0.4 g, 1.1 mmol) following the same procedure and purification described for **12**; CH₂Cl₂ in the workup was replaced by EtOAc (200 mL). Compound **14** was obtained as white solid (0.12 g, 0.24 mmol, 22 %). ^1H -NMR (DMSO- d_6): $\delta = 9.93$ (s br, 1H), 8.20 (t, $J = 5.67$ Hz, 1H), 7.97 (d, $J = 7.25$ Hz, 2H), 7.92 (d, $J = 8.20$ Hz, 1H), 7.66 (t, $J = 7.25$ Hz, 1H), 7.54 (t, $J = 7.25$ Hz, 2H), 7.27-7.14 (-Ar, 5H), 4.65-4.54 (m, 2H), 4.36-4.31 (m, 1H), 3.46-3.42 (m, 2H), 2.57-2.54 (m, 2H), 2.38 (s, 3H), 2.18-2.10 (m, 2H), 1.73-1.66 (m, 1H), 1.59-1.49 (m, 7H), 1.36-1.24 (m, 4H). ^{13}C -NMR (DMSO- d_6): 198.75, 195.13, 172.21, 172.15, 142.25, 134.95, 133.51, 128.77, 128.22, 128.17, 127.79, 125.55, 52.10, 45.84, 45.33, 35.08, 35.05, 32.78, 31.77, 30.75, 28.27, 26.89, 25.07, 22.92. ESI-MS (m/z): 496.22 [M + H] $^+$. Anal. (C₂₈H₃₇N₃O₃S) C, H, N.

(2S)-2-[3-(Pyridine-3-yl)propanoylamino]-6-ethanethioylamino-N-(2-oxo-2-phenylethyl) hexanamide (15). Compound **15** was prepared using 3-(pyridin-3-yl)propanoic acid (0.085 g, 0.56 mmol), DMF (3.0 mL), TBTU (0.20 g, 0.61 mmol), pyridine (3.0 mL) and **7** (0.20 g, 0.56 mmol), following the same procedure described for **12** with 2h as reaction time. After the solvents evaporation the obtained oil was washed with EtOAc (3 x 7 mL), the residue solubilized with CH₃CN and selectively precipitated by EtOAc, dried under vacuo and purified by chromatography using silica Kieselgel for flash with CH₂Cl₂: EtOAc: MeOH (6: 2.5: 1.5) as eluent phase to give the pure product as white solid (0.050 g, 0.11 mmol, 20 %). ^1H -NMR (DMSO- d_6): $\delta = 9.97$ (s br, 1H), 8.43 (s, 1H), 8.38 (d, $J = 4.41$ Hz,

1H), 8.27 (t, $J = 5.36$ Hz, 1H), 8.06 (d, $J = 8.20$ Hz, 1H), 7.99 (d, $J = 7.57$ Hz, 2H), 7.67 (t, $J = 7.57$ Hz, 1H), 7.62 (d, $J = 7.47$ Hz, 1H), 7.54 (t, $J = 7.57$ Hz, 2H), 7.29 (dd, $J = 4.41, 7.47$ Hz, 1H), 4.65-4.55 (m, 2H), 4.36-4.32 (m, 1H), 3.44-3.38 (m, 2H), 2.85-2.82 (m, 2H), 2.55-2.42 (m, 2H), 2.38 (s, 3H), 1.69-1.62 (m, 1H), 1.55-1.44 (m, 3H), 1.27-1.18 (m, 2H). $^{13}\text{C-NMR}$ (DMSO- d_6): $\delta = 199.21, 195.61, 172.57, 171.48, 150.03, 147.67, 137.09, 136.28, 135.40, 134.03, 129.27, 128.30, 123.81, 52.61, 46.31, 45.81, 36.63, 33.27, 32.37, 28.58, 27.37, 23.29$. ESI-MS (m/z): 455.19 $[\text{M} + \text{H}]^+$. Anal. ($\text{C}_{24}\text{H}_{30}\text{N}_4\text{O}_3\text{S} \cdot 0.5 \text{H}_2\text{O}$) C, H, N.

(2S,4R)-N-[(2S)-6-Ethanethiolyamino-1-(2-oxo-2-phenylethylamino)-1-oxohexan-2-yl]-4-hydroxypyrrolidine-1-benzyloxycarbonyl-2-carboxamide (16). Compound **16** was prepared using N-Cbz-Hydroxy-L-proline (0.29 g, 1.10 mmol), DMF (5.8 mL), TBTU (0.39 g, 1.21 mmol), pyridine (5.8 mL) and **7** (0.39 g, 1.10 mmol) following the same procedure and purification described for **12**. Compound **16** was obtained as white solid (0.14 g, 0.25 mmol, 23 %). $^1\text{H-NMR}$ (DMSO- d_6): rotamers A+B $\delta = 9.91-9.88$ (m br, 1H), 8.19-8.13 (m, 2H), 7.99 (t, $J = 7.57$ Hz, 2H), 7.67 (t, $J = 7.57$ Hz, 1H), 7.54 (t, $J = 7.57$ Hz, 2H), 7.37-7.28 (-Ar, 5H), 5.10-4.97 (m, 3H), 4.57-4.53 (m, 2H), 4.43-4.41 (m, 0.5H), 4.35-4.26 (m, 2.5H), 3.52-3.44 (m, 2H), 3.39-3.35 (m, 2H), 2.38 (s, 1.5H), 2.37 (s, 1.5H) 2.14-2.05 (m, 1H), 1.90-1.86 (m, 1H), 1.78-1.72 (m, 0.5H), 1.65-1.52 (m, 1.5H), 1.48-1.34 (m, 2.5H), 1.29-1.19 (m, 1.5H). $^{13}\text{C-NMR}$ (DMSO- d_6): rotamers A+(B) $\delta = 198.72, 195.11, 172.01$ (171.90), 171.85 (171.71), 154.29 (154.01), 136.90, 134.92, 133.54, 128.78, 128.37 (128.17), 127.80, 127.46, 126.89, 68.48 (67.77), 65.93 (65.79), 58.80 (58.09), 55.34 (54.87), 52.39 (52.24), 45.85, 45.39 (45.29), 38.51, 32.77, 31.77 (31.57), 26.90 (26.82), 22.78. ESI-MS (m/z): 569.15 $[\text{M} + \text{H}]^+$. Anal. ($\text{C}_{29}\text{H}_{36}\text{N}_4\text{O}_6\text{S}$) C, H, N.

(2S)-N-[(2S)-6-Ethanethiolyamino-1-(2-oxo-2-phenylethylamino)-1-oxohexan-2-yl]-pyrrolidine-1-tert-butoxycarbonyl-2-carboxamide (17). Compound **17** was prepared using N-Boc-L-proline (0.18 g, 0.84 mmol), DMF (4.5 mL), TBTU (0.30 g, 0.93 mmol), pyridine (4.5 mL) and **7** (0.30 g, 0.84 mmol), following the same procedure described for **12**, the used amount of CH_2Cl_2 was 150 mL. Purification by two columns chromatography, using Aluminum oxide EtOAc : Hexane : MeOH (7:

1.5: 1.5) as eluent phase and silica Kieselgel for flash with EtOAc : Hexane : MeOH (7: 2: 1) to give the pure product as white solid (0.10 g, 0.19 mmol, 23 %). ¹H-NMR (DMSO-*d*₆) : rotamers A+B δ = 9.91 (s br, 1H), 8.27 (t, *J* = 5.36 Hz, 0.6H), 8.15 (t, *J* = 5.36 Hz, 0.4H), 7.98-7.92 (m, 3H), 7.66 (t, *J* = 7.25 Hz, 1H), 7.54 (t, *J* = 7.25 Hz, 2H), 4.69-4.55 (m, 2H), 4.39-4.32 (m, 1H), 4.17-4.15 (m, 1H), 3.47-3.37 (m, 3H), 3.28-3.25 (m, 1H), 2.38 (s, 3H), 2.14-2.00 (m, 1H), 1.86-1.67 (m, 4H), 1.62-1.52 (m, 3H), 1.41-1.30 (m, 11H). ¹³C-NMR (DMSO-*d*₆) : rotamers A+(B) δ = 198.77, 195.11 (195.03), 172.33, 171.97 (171.93), 153.76 (153.26), 134.92, 133.53, 128.78, 127.80, 78.64 (78.29), 59.28, 52.15, 46.74 (46.49), 45.85, 45.30, 32.77, 32.05 (31.80), 31.00 (29.58), 28.11 (28.00), 26.91, 23.98 (23.02), 22.85 (22.75). ESI-MS (*m/z*): 519.03 [M + H]⁺. Anal. (C₂₆H₃₈N₄O₅S) C, H, N.

(S)-2-(2-((2S,5S)-5-Benzyl-3,6-dioxopiperazin-2-yl)acetamido)-6-ethanethioamido-N-(2-oxo-2-phenylethyl)hexanamide (18). Compound **18** was prepared using [(2S,5S)-5-benzyl-3,6-dioxopiperazin-2-yl]acetic acid (0.20 g, 0.76 mmol), DMF (4.0 mL), TBTU (0.27 g, 0.87 mmol), pyridine (4.0 mL) and **7** (0.27 g, 0.75 mmol) following the same procedure described for **12** the used amount of CH₂Cl₂ was 160 mL. Purification by two columns chromatography, using silica Kieselgel for flash EtOAc : Hexane : MeOH (7: 1.5: 1.5) and CH₂Cl₂ : Hexane : MeOH (7: 1.5: 1.5) as eluent phase to give the pure product as white solid (0.050 g, 0.088 mmol, 12 %). ¹H-NMR (DMSO-*d*₆) : δ = 9.94 (s br, 1H), 8.28 (t, *J* = 5.67 Hz, 1H), 8.20 (s, 1H), 8.02 (d, *J* = 7.88 Hz, 1H), 7.97 (d, *J* = 7.57 Hz, 2H), 7.69-7.64 (m, 2H), 7.53 (t, *J* = 7.57 Hz, 2H), 7.29-7.19 (-Ar, 5H), 4.63-4.50 (m, 2H), 4.25-4.21 (m, 2H), 4.13-4.10 (m, 1H), 3.49-3.45 (m, 2H), 3.10 (m, 1H), 2.94 (m, 1H), 2.38-2.35 (m, 4H), 1.77-1.71 (m, 1H), 1.63-1.52 (m, 4H), 1.37-1.29 (m, 2H). ¹³C-NMR (DMSO-*d*₆) : δ = 198.91, 195.09, 172.02, 169.43, 167.19, 166.51, 136.47, 134.81, 133.39, 130.21, 128.71, 128.01, 127.63, 126.75, 54.87, 52.73, 51.50, 45.72, 45.52, 38.57, 37.67, 32.97, 31.41, 26.75, 22.81. ESI-MS (*m/z*): 566.14 [M + H]⁺, 588.23 [M + Na]⁺. Anal. (C₂₉H₃₅N₅O₅S) C, H, N.

(2S)-6-(Ethanethioylamino)-N-phenyl-2-[3-(pyridin-3-yl)propanoylamino]hexanamide (19). Compound **19** was prepared using 3-(pyridin-3-yl)propanoic acid (0.15 g, 1.0 mmol), DMF (4.7 mL), TBTU (0.35 g, 1.1 mmol), pyridine (4.7 mL) and **8** (0.32 g, 1.0 mmol) following the same procedure described for **12**, the used amount of CH₂Cl₂ was 170 mL and the workup was made without HCl 0.5M. Purification by two columns chromatography using Aluminum oxide and silica Kieselgel for flash, with EtOAc : Hexane : MeOH (7: 1: 2) as eluent phase to give the pure product as white solid (0.19 g, 0.46 mmol, 46 %). ¹H-NMR (DMSO-*d*₆): δ = 10.04 (s, 1H), 9.97 (s br, 1H), 8.44 (s, 1H), 8.38 (d, *J* = 4.88 Hz, 1H), 8.17 (d, *J* = 7.93 Hz, 1H), 7.63-7.58 (m, 3H), 7.32-7.27 (m, 3H), 7.05 (m, 1H), 4.40-4.36 (m, 1H), 3.44-3.41 (m, 2H), 2.85-2.82 (m, 2H), 2.54-2.46 (m, 2H), 2.36 (s, 3H), 1.69-1.62 (m, 1H), 1.57-1.48 (m, 3H), 1.32-1.18 (m, 2H). ¹³C-NMR (DMSO-*d*₆): δ = 198.80, 171.19, 170.76, 149.56, 147.18, 138.89, 136.57, 135.77, 128.68, 128.68, 123.29, 119.28, 53.22, 45.24, 36.07, 32.79, 31.81, 28.13, 26.92, 22.96. ESI-MS (*m/z*): 413.22 [M + H]⁺. Anal. (C₂₂H₂₈N₄O₂S) C, H, N.

(2S)-6-(Ethanethioylamino)-N-phenyl-2-[(dimethylamino)acetylamino]hexanamide (20). Compound **20** was prepared using a suspension of N,N-Dimethylglycine hydrochloride (0.13 g, 0.93 mmol), DMF (5.0 mL), TBTU (0.34 g, 1.05 mmol), pyridine (5.0 mL) and **8** (0.30 g, 0.96 mmol) following the same procedure described for **12**. Reaction time 2h, 30min, the used amount of CH₂Cl₂ was 130 mL and the workup was made without HCl 0.5M. Purification by column chromatography using silica Kieselgel for flash with CH₂Cl₂ : MeOH (6.5: 3.5) as eluent phase to give the pure product as white solid (0.074 g, 0.20 mmol, 21 %). ¹H-NMR (DMSO-*d*₆): δ = 10.08 (s, 1H), 9.94 (s br, 1H) 7.82 (d, *J* = 8.20 Hz, 1H), 7.58 (d, *J* = 7.88 Hz, 2H), 7.30 (t, *J* = 7.88 Hz, 2H), 7.05 (t, *J* = 7.88 Hz, 1H), 4.50-4.45 (m, 1H), 3.46-3.43 (m, 2H), 2.95 (d, *J* = 15.26 Hz, 1H) 2.92 (d, *J* = 15.26 Hz, 1H), 2.35 (s, 3H), 2.24 (s, 6H), 1.78-1.52 (m, 4H), 1.39-1.23 (m, 2H). ¹³C-NMR (DMSO-*d*₆): δ = 199.28, 170.93, 169.90, 139.22, 129.20, 123.91, 119.77, 62.94, 53.12, 45.89, 45.65, 33.24, 32.62, 27.38, 23.37. ESI-MS (*m/z*): 365.19 [M + H]⁺. Anal. (C₁₈H₂₈N₄O₂S) C, H, N.

(2S)-N-[(2S)-6-Ethanethioylamino-1-phenylamino-1-oxohexan-2-yl]-pyrrolidine-1-tert-butoxycarbonyl-2-carboxamide (21). Compound **21** was prepared using N-Boc-L-proline (0.28 g, 1.30 mmol), DMF (6.0 mL), TBTU (0.46 g, 1.43 mmol), pyridine (6.0 mL) and **8** (0.41 g, 1.29 mmol) following the same procedure described for **12**, the used amount of CH₂Cl₂ was 180 mL. Purification by column chromatography using silica Kieselgel for flash with EtOAc : MeOH (9.5: 0.5) as eluent phase to give the pure product as light yellow solid (0.30 g, 0.63 mmol, 49 %). ¹H-NMR (DMSO-*d*₆) : rotamers A+B δ = 10.06 (s, 0.6H), 9.93 (s br, 1H), 9.84 (s, 0.4H), 8.04 (d, *J* = 7.88 Hz, 1H), 7.59 (d, *J* = 7.57 Hz, 2H), 7.30 (t, *J* = 7.57 Hz, 2H), 7.04 (t, *J* = 7.57 Hz, 1H), 4.43-4.33 (m, 1H), 4.19-4.15 (m, 1H), 3.45-3.36 (m, 3H), 3.29-3.24 (m, 1H), 2.36 (s, 3H), 2.15-2.04 (m, 1H), 1.83-1.52 (m, 7H), 1.45-1.23 (m, 11H). ¹³C-NMR (DMSO-*d*₆) : rotamers A+(B) δ = 198.79, 172.55 (172.18), 170.58, 153.88 (153.29), 138.89 (138.81), 128.67, 123.27, 119.21 (119.14), 78.76 (78.34), 59.36 (59.31), 53.21, 46.72 (46.50), 45.22 (45.16), 32.75, 31.83 (31.49), 30.99 (29.77), 28.11 (27.98), 26.90, 23.91, 23.05 (23.02). ESI-MS (*m/z*): 477.03 [M + H]⁺, 499.19 [M + Na]⁺. Anal. (C₂₄H₃₆N₄O₄S) C, H, N.

(2S)-N-[(2S)-6-Ethanethioylamino-1-(phenylamino)-1-oxohexan-2-yl]-pyrrolidine-2-carboxamide hydrochloride (22). To a solution of **21** (0.10 g, 0.21 mmol) in 2-propanol (3.6 mL), 1,2-ethanedithiol (0.018 mL, 0.21 mmol) was added and after 1 min under stirring at r.t HCl 12N (0.11 mL, 1.32 mmol) was added and the solution heated at 60°C; After 20min and 40min other HCl 12N (0.11 mL) was added; when the total mmol of HCl in the reaction flask were 3.96 mmol, the solution was maintained for 60 min at 60°C under stirring. After this time, 2-propanol was evaporated under reduced pressure and the yellow oil was washed with petroleum ether (4 x 10 mL) and CH₂Cl₂: petroleum ether (1:1) (4 x 4 mL) provides the product as white solid (0.077 g, 0.18 mmol, 85 %). ¹H-NMR (DMSO-*d*₆) : δ = 10.23 (s, 1H), 10.11 (s br, 1H), 9.72 (s br, 1H), 8.85 (d, *J* = 7.57 Hz, 1H), 8.49 (s br, 1H), 7.61 (d, *J* = 7.25 Hz, 2H), 7.30 (t, *J* = 7.25 Hz, 2H), 7.05 (t, *J* = 7.25 Hz, 1H), 4.46-4.42 (m, 1H), 4.28-4.23 (m, 1H), 3.49-3.45 (m, 2H), 3.24-3.16 (m, 2H), 2.38-2.33 (m, 4H), 1.89-1.55 (m, 7H), 1.48-1.31 (m, 2H). ¹³C-NMR (DMSO-*d*₆) : δ = 198.77, 170.01, 168.22, 138.86, 128.69, 123.36, 119.21, 58.62, 53.95, 45.58, 45.03,

32.74, 31.58, 29.62, 26.81, 23.46, 23.07. ESI-MS (m/z): 377.20 $[M + H]^+$. Anal. ($C_{19}H_{29}ClN_4O_2S \cdot 0.3H_2O$) C, H, N.

(2S,4R)-N-[(2S)-6-Ethanethiolyamino-1-phenylamino-1-oxohexan-2-yl]-4-hydroxypyrrolidine-1-benzyloxycarbonyl-2-carboxamide (23). Compound **23** was prepared using N-Cbz-Hydroxy-L-proline (0.36 g, 1.35 mmol), DMF (6.3 mL), TBTU (0.47 g, 1.46 mmol), pyridine (6.3 mL) and **8** (0.42 g, 1.33 mmol) following the same procedure described for **12**, the used amount of CH_2Cl_2 was 200 mL. Purification by two columns chromatography using silica Kieselgel for flash with EtOAc : Hexane : MeOH (7: 1.5: 1.5) and EtOAc : Hexane : MeOH (7: 2: 1) as eluent phase to give the pure product as white solid (0.17 g, 0.32 mmol, 24 %). 1H -NMR (DMSO- d_6): rotamers A+B δ = 10.04 (s, 0.55H), 9.93-9.90 (m br, 1H), 9.82 (s, 0.45H), 8.26 (m, 1H), 7.63-7.59 (m, 2H), 7.37-7.30 (m, 7H), 7.08-7.03 (m, 1H), 5.13-4.97 (m, 3H), 4.44-4.41 (m, 0.5H), 4.38-4.34 (m, 1.5H), 4.28-4.23 (m, 1H), 3.53-3.47 (m, 2H), 3.39-3.35 (m, 2H), 2.36 (s, 1.45H), 2.35 (s, 1.55H) 2.14-2.07 (m, 1H), 1.90-1.84 (m, 1H), 1.79-1.73 (m, 0.5H), 1.67-1.20 (m, 5.5H). ^{13}C -NMR (DMSO- d_6): rotamers A+(B) δ = 198.77, 172.14 (171.83), 170.54, 154.43 (154.01), 138.88 (138.83), 136.86 (136.82), 128.68, 128.38 (128.16), 127.78 (127.49), 127.42 (126.94), 123.32 (123.28), 119.19 (119.11), 68.40 (67.60), 65.92 (65.87), 58.90 (57.90), 55.40 (54.80), 53.38 (53.30), 45.26 (45.20), 38.63, 32.75, 31.80 (31.38), 26.92 (26.72), 22.85 (22.80). ESI-MS (m/z): 527.11 $[M + H]^+$. Anal. ($C_{27}H_{34}N_4O_5S$) C, H, N.

(2S)- 2-Benzyl 6-ethanethioamido-1-oxo-1-(2-phenylethylamino)hexan-2-ylcarbamate (25). To a solution of **24** (0.23 g, 0.68 mmol) in DMF (3.5 mL) under Argon flow were added TBTU—(0.24 g, 0.75 mmol), pyridine (3.5 mL) and maintained under stirring for 10min at rt . After this time 2-phenylethanamine (0.087 mL, 0.69 mmol) was added and the solution mixed 2h, 30 min at rt under Argon flow. Solvents were evaporated and the obtained oil was dissolved in EtOAc (200 mL), washed with HCl 0.5M, brine, $NaHCO_3$ 5% (twice), finally dried with Na_2SO_4 and evaporated under vacuo. The crude product obtained was purified by column chromatography using silica Kieselgel for flash and EtOAc : CH_2Cl_2 : MeOH (4.5 : 4 : 1.5) as eluent phase to give the pure product as white solid (0.19 g, 0.44 mmol, 63

%). ¹H-NMR (CDCl₃) : δ = 7.77 (s br, 1H), 7.39-7.29 (m, 7H), 7.25-7.22 (m, 1H), 7.18 (m, 2H), 6.12 (s br, 1H), 5.45 (d, *J* = 7.57 Hz, 1H), 5.09 (s, 2H), 4.12-4.07 (m, 1H), 3.65-3.46 (m, 4H), 2.82-2.80 (m, 2H), 2.54 (s, 3H), 1.81-1.74 (m, 1H), 1.68-1.59 (m, 3H), 1.40-1.33 (m, 2H). ¹³C-NMR (DMSO-*d*₆) : δ = 198.75, 171.57, 155.81, 139.31, 136.98, 128.54, 128.21, 128.15, 127.64, 127.55, 125.94, 65.31, 54.63, 45.19, 40.02, 34.99, 32.74, 31.65, 26.83, 22.93. ESI-MS (*m/z*): 442.20 [M + H]⁺. Anal. (C₂₄H₃₁N₃O₃S) C, H, N.

(2S)- 2-Benzyl 6-ethanethioamido-1-oxo-1-(benzylamino)hexan-2-ylcarbamate (26). Compound **26** was prepared using **24** (0.23 g, 0.68 mmol), DMF (3.5 mL), TBTU (0.24 g, 0.75 mmol), pyridine (3.5 mL) and benzylamine (0.075 mL, 0.69 mmol), following the same procedure and purification described for **25**. Compound **26** was obtained as white solid (0.19 g, 0.45 mmol, 66 %). ¹H-NMR (CDCl₃) : δ = 7.69 (s br, 1H), 7.38-7.29 (m, 8H), 7.26-7.24 (m, 2H), 6.41 (s br, 1H), 5.45 (d, *J* = 7.57 Hz, 1H), 5.09 (s, 2H), 4.48-4.40 (m, 2H), 4.23-4.19 (m, 1H), 3.68-3.60 (m, 2H), 2.53 (s, 3H), 1.91-1.86 (m, 1H), 1.75-1.68 (m, 3H), 1.45-1.39 (m, 2H). ¹³C-NMR (DMSO-*d*₆) : δ = 198.74, 171.80, 155.90, 139.28, 136.97, 128.21, 128.11, 127.64, 127.55, 126.98, 126.58, 65.32, 54.67, 45.18, 41.97, 32.73, 31.56, 26.79, 23.01. ESI-MS (*m/z*): 428.18 [M + H]⁺, 450.19 [M + Na]⁺. Anal. (C₂₃H₂₉N₃O₃S) C, H, N.

(2S)- 2-Benzyl 6-ethanethioamido-1-oxo-1-[2-oxo-2-(4-methoxyphenyl)ethylamino]hexan-2-ylcarbamate (27). Compound **27** was prepared using **24** (0.33 g, 0.97 mmol), DMF (4.8 mL), TBTU (0.34 g, 1.06 mmol), pyridine (4.8 mL) and 2-amino-1-(4-methoxyphenyl)ethanone hydrochloride (0.19 g, 0.94 mmol) following the same procedure described for **25**. Purification by column chromatography using silica Kieselgel for flash and EtOAc : Hexane : MeOH (7 : 2 : 1) as eluent phase to give the pure product as white solid (0.27 g, 0.55 mmol, 57 %). ¹H-NMR (DMSO-*d*₆) : δ = 9.93 (s br, 1H), 8.17 (t, *J* = 5.36 Hz, 1H), 7.97 (d, *J* = 8.83 Hz, 2H), 7.45 (d, *J* = 8.20 Hz, 1H), 7.37-7.30 (m, 5H), 7.05 (d, *J* = 8.83 Hz, 2H), 5.06-5.01 (m, 2H), 4.64-4.49 (m, 2H), 4.09-4.05 (m, 1H), 3.84 (s, 3H), 3.48-3.40 (m, 2H), 2.37 (s, 3H), 1.74-1.67 (m, 1H), 1.60-1.50 (m, 3H), 1.41-1.30 (m, 2H). ¹³C-NMR (DMSO-*d*₆) : δ = 198.75, 193.35, 172.26, 163.34, 155.96, 137.03, 130.12, 128.31, 127.81, 127.78, 127.64, 113.98, 65.37, 55.54, 54.58, 45.47, 45.30, 32.80,

31.71, 26.88, 23.05. ESI-MS (m/z): 486.14 $[M + H]^+$. HPLC : Rt. 2.64 min, area percent 98.87 % 265nm. Anal. ($C_{25}H_{31}N_3O_5S \cdot 0.02\text{hexane}$) C, H, N.

(2S)- 2-Benzyl 6-ethanethioamido-1-oxo-1-(2-hydroxy-2-phenylethylamino)hexan-2-ylcarbamate (28). Compound **28** was prepared using **24** (0.33 g, 0.97 mmol), DMF (4.8 mL), TBTU (0.34 g, 1.06 mmol), pyridine (4.8 mL) and (*R,S*)-2-amino-1-phenylethanol (0.13 g, 0.95 mmol), following the same procedure described for **25**. Purification by column chromatography using silica Kieselgel for flash and EtOAc : Hexane : MeOH (7 : 2 : 1) as eluent phase to give the pure product as white solid (0.22 g, 0.48 mmol, 49 %). $^1\text{H-NMR}$ ($\text{DMSO-}d_6$) : diastereoisomer A+B $\delta = 9.93$ (s br, 1H), 7.87-7.83 (m, 1H), 7.40-7.23 (m, 11H), 5.46-5.44 (m, 1H), 5.06-5.00 (m, 2H), 4.63-4.58 (m, 1H), 3.99-3.93 (m, 1H), 3.47-3.39 (m, 2H), 3.36-3.31 (m, 0.4H), 3.26-3.24 (m, 1H), 3.16-3.11 (m, 0.6H), 2.38 (s, 3H), 1.58-1.43 (m, 4H), 1.32-1.18 (m, 2H). $^{13}\text{C-NMR}$ (CDCl_3) : diastereoisomer A+(B) $\delta = 200.89$ (200.86), 172.75, 156.49, 141.32, 135.92, 128.57, 128.57, 128.31, 128.00, 127.96, 125.75, 73.08 (72.99), 67.19, 54.63, 47.16, 45.79, 33.87, 32.22, 27.04 (27.00), 22.60. ESI-MS (m/z): 458.14 $[M + H]^+$ HPLC : Rt. 1.92 min, area percent 98.91 % 265nm. Anal. ($C_{24}H_{31}N_3O_4S \cdot 0.1\text{hexane} \cdot 0.01\text{EtOAc}$) C, H, N.

(2S)- 2-Benzyl 6-ethanethioamido-1-oxo-1-[2-(1H-indol-3yl)ethylamino]hexan-2-ylcarbamate (29). Compound **29** was prepared using **24** (0.33 g, 0.97 mmol), DMF (4.8 mL), TBTU (0.34 g, 1.06 mmol), pyridine (4.8 mL) and tryptamine (0.15 g, 0.94 mmol) following the same procedure described for **25**, the workup was made without HCl 0.5M. Purification by column chromatography using silica Kieselgel for flash and EtOAc : Hexane : MeOH (7 : 2 : 1) as eluent phase to give the pure product as white solid (0.32 g, 0.66 mmol, 68 %). $^1\text{H-NMR}$ ($\text{DMSO-}d_6$): $\delta = 10.79$ (s, 1H), 9.92 (s br, 1H), 7.97 (t, $J = 5.67$ Hz, 1H), 7.54 (d, $J = 7.88$ Hz, 1H), 7.37-7.32 (m, 7H), 7.13 (s, 1H), 7.05 (t, $J = 7.57$ Hz, 1H), 6.97 (t, $J = 7.57$ Hz, 1H), 5.06-4.99 (m, 2H), 3.95-3.91 (m, 1H), 3.45-3.40 (m, 2H), 3.38-3.26 (m, 2H), 2.82-2.79 (m, 2H), 2.36 (s, 3H), 1.64-1.46 (m, 4H), 1.35-1.22 (m, 2H). $^{13}\text{C-NMR}$ ($\text{DMSO-}d_6$): $\delta = 198.75$, 171.65, 155.93, 137.05, 136.21, 128.30, 127.75, 127.67, 127.16, 122.64, 120.87, 118.22, 118.18, 111.68, 111.32, 65.36, 54.69, 45.25, 39.47, 32.79, 31.70, 26.89,

25.13, 23.09. ESI-MS (*m/z*): 481.17 [M + H]⁺, 503.23 [M + Na]⁺. Anal. (C₂₆H₃₂N₄O₃S) C, H, N.

(2S)- 2-Benzyl 6-ethanethioamido-1-oxo-1-[2-(5-methoxy-1H-indol-3yl)ethylamino]hexan-2-ylcarbamate (30). Compound **30** was prepared using **24** (0.34 g, 1.00 mmol), DMF (4.5 mL), TBTU (0.36 g, 1.12 mmol), pyridine (4.5 mL) and 5-methoxytryptamine (0.19 g, 1.00 mmol) following the same procedure used for **25**, the workup was made without HCl 0.5M. Purification by column chromatography using silica Kieselgel for flash and EtOAc : Hexane : MeOH (7.5 : 2 : 0.5) as eluent phase to give the pure product as white solid (0.33 g, 0.65 mmol, 65 %). ¹H-NMR (DMSO-*d*₆): δ = 10.63 (s, 1H), 9.93 (s br, 1H), 7.97 (t, *J* = 5.36 Hz, 1H), 7.37-7.22 (m, 7H), 7.10 (s, 1H), 7.03 (s, 1H), 6.71 (d, *J* = 8.83 Hz, 1H), 5.07-5.00 (m, 2H), 3.97-3.90 (m, 1H), 3.76 (s, 3H), 3.46-3.29 (m, 4H), 2.79 (t, *J* = 7.25 Hz, 2H), 2.37 (s, 3H), 1.64-1.49 (m, 4H), 1.32-1.24 (m, 2H). ¹³C-NMR (DMSO-*d*₆): δ = 198.75, 171.67, 155.95, 152.96, 137.06, 131.36, 128.32, 127.76, 127.69, 127.47, 123.32, 111.97, 111.43, 111.02, 100.11, 65.37, 55.34, 54.72, 45.26, 39.34, 32.80, 31.72, 26.91, 25.18, 23.12. ESI-MS (*m/z*): 511.19 [M + H]⁺. Anal. (C₂₇H₃₄N₄O₄S) C, H, N.

(2S)- 2-Benzyl 6-ethanethioamido-1-oxo-1-[2-(5-benzyloxy-1H-indol-3yl)ethylamino]hexan-2-ylcarbamate (31). Compound **31** was prepared using **24** (0.34 g, 1.00 mmol), DMF (4.5 mL), TBTU (0.36 g, 1.12 mmol), pyridine (4.5 mL) and 5-benzyloxytryptamine hydrochloride (0.30 g, 1.00 mmol), following the same procedure used for **25**, the workup was made without HCl 0.5M. Purification by column chromatography using silica Kieselgel for flash and EtOAc : Hexane : MeOH (7.5 : 2 : 0.5) as eluent phase to give the pure product as white solid (0.22 g, 0.37 mmol, 37 %). ¹H-NMR (DMSO-*d*₆): δ = 10.66 (s, 1H), 9.93 (s br, 1H), 7.97 (t, *J* = 5.36 Hz, 1H), 7.50-7.23 (m, 12H), 7.16 (s, 1H), 7.11 (s, 1H), 6.81 (d, *J* = 10.40 Hz, 1H), 5.10-5.00 (m, 4H), 3.98-3.93 (m, 1H), 3.48-3.27 (m, 4H), 2.79 (t, *J* = 7.25 Hz, 2H), 2.37 (s, 3H), 1.61-1.46 (m, 4H), 1.36-1.23 (m, 2H). ¹³C-NMR (DMSO-*d*₆): δ = 198.76, 171.68, 155.96, 151.98, 137.81, 137.06, 131.56, 128.32, 128.32, 127.76, 127.69, 127.69, 127.59, 127.48, 123.44, 111.97, 111.59, 111.45, 101.83, 69.86,

65.37, 54.72, 45.26, 39.31, 32.80, 31.72, 26.91, 25.17, 23.12. ESI-MS (m/z): 587.22 $[M + H]^+$. Anal. ($C_{33}H_{38}N_4O_4S$) C, H, N.

(2S)-2-Benzyl 6-ethanethioamido-1-oxo-1-(pyridin-3-ylamino)hexan-2-ylcarbamate (32). Compound **32** was prepared using **24** (0.50 g, 1.47 mmol), DMF (7.0 mL), TBTU (0.52 g, 1.62 mmol), pyridine (7.0 mL) and 3-aminopyridine (0.14 g, 1.48 mmol), following the same procedure described for **25**, the workup was made without HCl 0.5M. Purification by two columns chromatography using Aluminum oxide and silica Kieselgel for flash, with CH_2Cl_2 : EtOAc: MeOH (5.5: 3: 1.5) as eluent phase to give the pure product as white solid (0.12 g, 0.29 mmol, 20 %). 1H -NMR ($DMSO-d_6$) : δ = 10.25 (s, 1H), 9.95 (s br, 1H), 8.76 (d, J = 2.21 Hz, 1H), 8.27 (dd, J = 1.58, 6.31 Hz, 1H), 8.05-8.03 (m, 1H), 7.63 (d, J = 7.57 Hz, 1H), 7.37-7.30 (m, 6H), 5.07-5.01 (m, 2H), 4.17-4.13 (m, 1H), 3.49-3.42 (m, 2H), 2.36 (s, 3H), 1.75-1.50 (m, 4H), 1.46-1.29 (m, 2H). ^{13}C -NMR ($DMSO-d_6$) : δ = 198.79, 171.67, 156.12, 144.23, 140.81, 136.95, 135.56, 128.33, 127.80, 127.72, 126.24, 123.63, 65.47, 55.54, 45.16, 32.80, 31.36, 26.91, 23.19. ESI-MS (m/z): 415.19 $[M + H]^+$. Anal. ($C_{21}H_{26}N_4O_3S$) C, H, N.

(2S)-2-Benzyl 6-ethanethioamido-1-oxo-1-(2-amino-2-oxoethylamino)hexan-2-ylcarbamate (33). Compound **33** was prepared using **24** (0.50 g, 1.47 mmol), DMF (7.0 mL), TBTU (0.52 g, 1.62 mmol), pyridine (7.0 mL) and glycineamide hydrochloride (0.16 g, 1.45 mmol), following the same procedure used for **25**, CH_2Cl_2 was replaced by CH_2Cl_2 : MeOH (9: 2) (250 mL). Purification by column chromatography using silica Kieselgel for flash, with CH_2Cl_2 : MeOH (8.5: 1.5) as eluent phase to give the pure product as white solid (0.21 g, 0.53 mmol, 37 %). 1H -NMR ($DMSO-d_6$) : δ = 9.92 (s br, 1H), 8.10 (t, J = 5.67 Hz, 1H), 7.49 (d, J = 7.57 Hz, 1H), 7.39-7.32 (m, 5H), 7.19 (s, 1H), 7.07 (s, 1H), 5.06-4.99 (m, 2H), 3.99-3.94 (m, 1H), 3.67-3.59 (m, 2H), 3.47-3.41 (m, 2H), 2.37 (s, 3H), 1.70-1.63 (m, 1H), 1.57-1.48 (m, 3H), 1.39-1.23 (m, 2H). ^{13}C -NMR ($DMSO-d_6$) : δ = 198.75, 172.04, 170.77, 156.12, 136.91, 128.32, 127.78, 127.69, 65.46, 54.72, 45.26, 41.86, 32.79, 31.27, 26.85, 23.01. ESI-MS (m/z): 395.19 $[M + H]^+$. Anal. ($C_{18}H_{26}N_4O_4S$) C, H, N.

(2S)-2-Benzyl 6-ethanethioamido-1-oxo-1-(((2S)-1-amino-1-oxopropan-2-yl)amino)hexan-2-ylcarbamate (34). Compound **34** was prepared using **24** (0.50

g, 1.47 mmol), DMF (7.0 mL), TBTU (0.52 g, 1.62 mmol), pyridine (7.0 mL) and L-alaninamide hydrochloride (0.18 g, 1.44 mmol), following the same procedure described for **25**, CH₂Cl₂ was replaced by CH₂Cl₂: MeOH (9: 2) (250 mL). Purification by column chromatography using silica Kieselgel for flash, with CH₂Cl₂: MeOH (8.5: 1.5) as eluent phase to give the pure product as white solid (0.34 g, 0.83 mmol, 58 %). ¹H-NMR (DMSO-*d*₆) : δ = 9.91 (s br, 1H), 7.87 (d, *J* = 7.25 Hz, 1H), 7.43 (d, *J* = 8.20 Hz, 1H), 7.38-7.29 (m, 6H), 6.99 (s, 1H), 5.04-4.99 (m, 2H), 4.22-4.16 (m(5), *J* = 7.25 Hz, 1H), 3.98-3.94 (m, 1H), 3.47-3.37 (m, 2H), 2.36 (s, 3H), 1.68-1.61 (m, 1H), 1.57-1.47 (m, 3H), 1.37-1.27 (m, 2H), 1.20 (d, *J* = 7.25 Hz, 3H). ¹³C-NMR (DMSO-*d*₆) : δ = 198.78, 174.12, 171.40, 156.01, 137.02, 128.34, 127.76, 127.62, 65.39, 54.61, 47.87, 45.30, 32.82, 31.52, 26.88, 23.04, 18.44. ESI-MS (*m/z*): 409.19 [M + H]⁺. Anal. (C₁₉H₂₈N₄O₄S) C, H, N.

(2S,4R)-N-[(2S)-6-Ethanethioylamino-1-benzylamino-1-oxohexan-2-yl]-4-hydroxypyrrolidine-1-benzyloxycarbonyl-2-carboxamide (35). Compound **35** was prepared using N-Cbz-Hydroxy-L-proline (0.30 g, 1.13 mmol), DMF (5.5 mL), TBTU (0.40 g, 1.24 mmol), pyridine (5.5 mL) and **9** (0.37 g, 1.12 mmol) following the same procedure described for **12**, CH₂Cl₂ was replaced by EtOAc (200 mL). Purification by two columns chromatography using silica Kieselgel for flash with EtOAc : Hexane : MeOH (7: 1.5: 1.5) and CH₂Cl₂ : MeOH (9.5 : 0.5) as eluent phase to give the pure product as white solid (0.53 g, 0.98 mmol, 87 %). ¹H-NMR (DMSO-*d*₆): rotamers A+B δ = 9.91-9.88 (m br, 1H), 8.37 (t, *J* = 5.99 Hz, 0.51H), 8.25 (t, *J* = 5.99 Hz, 0.49H), 8.15-8.13 (m, 1H), 7.38-7.20 (-Ar, 10H), 5.06-4.93 (m, 3H), 4.41-4.38 (m, 0.5H), 4.31-4.21 (m, 4.5H), 3.53-3.42 (m, 2H), 3.37-3.33 (m, 2H), 2.37 (s, 1.49H), 2.36 (s, 1.51H), 2.12-2.04 (m, 1H), 1.86-1.83 (m, 1H), 1.78-1.71 (m, 0.5H), 1.62-1.13 (m, 5.5H). ¹³C-NMR (DMSO-*d*₆): rotamers A + (B) δ = 198.74, 171.96 (171.71), 171.45, 154.44 (154.00), 139.29, 136.86 (136.81), 128.37, 128.20 (128.17), 127.78, 127.47 (127.44), 127.02 (126.98), 126.88 (126.69), 68.43 (67.76), 65.96 (65.79), 59.00 (58.09), 55.33 (54.88), 52.61 (52.49), 45.33 (45.24), 41.96 (41.92), 38.54, 32.77, 31.71 (31.27), 26.88 (26.80), 22.93 (22.88). ESI-MS (*m/z*): 541.21 [M + H]⁺. Anal. (C₂₈H₃₆N₄O₅S·0.03hexane) C, H, N.

(2S)-2-(6-Phenyhexanoylamino)-6-ethanethioylamino-N-benzylhexanamide (36).

Compound **36** was prepared using 6-phenyhexanoic acid (0.22 mL, 1.17 mmol), DMF (5.5 mL), TBTU (0.40 g, 1.24 mmol), pyridine (5.5 mL) and **9** (0.37 g, 1.12 mmol) following the same procedure described for **12**, CH₂Cl₂ was replaced by EtOAc (200 mL). Purification by two columns chromatography using silica Kieselgel for flash with EtOAc : Hexane : MeOH (7: 2: 1) as eluent phase to give the pure product as white solid (0.22 g, 0.47 mmol, 42 %). ¹H-NMR (DMSO-*d*₆) : 9.92 (s br, 1H), 8.37 (t, *J* = 5.99 Hz, 1H), 7.90 (d, *J* = 7.88 Hz, 1H), 7.32-7.14 (-Ar, 10H), 4.27-4.24 (m, 3H), 3.48-3.39 (m, 2H), 2.56-2.53 (m, 2H), 2.37 (s, 3H), 2.18-2.08 (m, 2H), 1.70-1.63 (m, 1H), 1.58-1.49 (m, 7H), 1.34-1.23 (m, 4H). ¹³C-NMR (DMSO-*d*₆) : δ = 198.75, 172.17, 171.83, 142.24, 139.40, 128.22, 128.18, 128.17, 127.00, 126.66, 125.55, 52.35, 45.28, 41.91, 35.08, 35.05, 32.78, 31.72, 30.74, 28.26, 26.87, 25.08, 23.02. ESI-MS (*m/z*): 468.25 [M + H]⁺. Anal. (C₂₇H₃₇N₃O₂S) C, H, N.

(2S)-2-(7-Phenyheptanoylamino)-6-ethanethioylamino-N-benzylhexanamide

(37). Compound **37** was prepared using 7-phenyheptanoic acid (0.24 mL, 1.12 mmol), DMF (5.5 mL), TBTU (0.40 g, 1.24 mmol), pyridine (5.5 mL) and **9** (0.37 g, 1.12 mmol) following the same procedure described for **12**, CH₂Cl₂ was replaced by EtOAc (200 mL). Purification by two columns chromatography using silica Kieselgel for flash with EtOAc : Hexane : MeOH (7: 2.5: 0.5) as eluent phase to give the pure product as white solid (0.10 g, 0.21 mmol, 18 %). ¹H-NMR (DMSO-*d*₆): 9.92 (s br, 1H), 8.37 (t, *J* = 6.30 Hz, 1H), 7.91 (d, *J* = 7.88 Hz, 1H), 7.31-7.14 (-Ar, 10H), 4.30-4.24 (m, 3H), 3.46-3.39 (m, 2H), 2.56-2.53 (m, 2H), 2.36 (s, 3H), 2.17-2.07 (m, 2H), 1.70-1.63 (m, 1H), 1.57-1.46 (m, 7H), 1.34-1.24 (m, 6H). ¹³C-NMR (DMSO-*d*₆): δ = 198.77, 172.24, 171.87, 142.28, 139.41, 128.22, 128.19, 128.19, 127.00, 126.67, 125.56, 52.37, 45.29, 41.92, 35.17, 35.11, 32.79, 31.69, 30.91, 28.45, 28.43, 26.87, 25.23, 23.03. ESI-MS (*m/z*): 482.24 [M + H]⁺. Anal. (C₂₈H₃₉N₃O₂S) C, H, N.

(2S)-2-(3-Phenylpropanoylamino)-6-ethanethioylamino-N-(pyridin-3-

ylamino)hexanamide (38). Compound **38** was prepared using 3-phenylpropionic acid (0.17 g, 1.13 mmol), DMF (2.8 mL), TBTU (0.40 g, 1.24 mmol), pyridine (2.8 mL) and **10** (0.40 g, 1.13 mmol) following the same procedure described for **12**, the

amount of CH₂Cl₂ was 140 mL and the workup was made without HCl 0.5M. Purification by column chromatography using silica Kieselgel for flash with EtOAc: CH₂Cl₂: Hexane: MeOH (5.5: 1.5: 1.5: 1.5) as eluent phase to give the pure product as white solid (0.18 g, 0.43 mmol, 38 %). ¹H-NMR (DMSO-*d*₆): δ = 10.26 (s, 1H), 9.94 (s br, 1H), 8.76 (d, *J* = 2.21 Hz, 1H), 8.27 (dd, *J* = 1.58, 4.73 Hz, 1H), 8.17 (d, *J* = 7.88 Hz, 1H), 8.03 (dt, *J* = 1.58, 8.20 Hz, 1H), 7.35 (dd, *J* = 4.73, 8.20 Hz, 1H), 7.27-7.15 (m, 5H), 4.42-4.38 (m, 1H), 3.47-3.40 (m, 2H), 2.84-2.81 (m, 2H), 2.53-2.42 (m, 2H), 2.36 (s, 3H), 1.73-1.66 (m, 1H), 1.63-1.49 (m, 3H), 1.37-1.20 (m, 2H). ¹³C-NMR (DMSO-*d*₆): δ = 198.77, 171.70, 171.37, 144.12, 141.11, 140.69, 135.50, 128.19, 128.19, 126.46, 125.94, 123.72, 53.13, 45.10, 36.45, 32.88, 31.67, 30.93, 27.05, 22.85.

ESI-MS (*m/z*): 413.18 [M + H]⁺ Anal. (C₂₂H₂₈N₄O₂S) C, H, N.

(2S)-2-[3-(2-Fluorophenyl)propanoylamino]-6-ethanethioylamino-N-(pyridin-3-ylamino)hexanamide (39). Compound **39** was prepared using 3-(2-fluorophenyl)propionic acid (0.15 g, 0.89 mmol), DMF (4.6 mL), TBTU (0.34 g, 1.06 mmol), pyridine (4.6 mL) and **10** (0.31 g, 0.87 mmol), following the same procedure described for **12**, the amount of CH₂Cl₂ was 140 mL and the workup was made without HCl 0.5M and brine. Purification by column chromatography using silica Kieselgel for flash with CH₂Cl₂: EtOAc: MeOH (5.5: 3.5: 1) as eluent phase to give the pure product as white solid (0.11 g, 0.25 mmol, 29 %). ¹H-NMR (DMSO-*d*₆): δ = 10.25 (s, 1H), 9.93 (s br, 1H), 8.75 (d, *J* = 2.21 Hz, 1H), 8.27 (dd, *J* = 1.58, 4.73 Hz, 1H), 8.20 (d, *J* = 7.88 Hz, 1H), 8.03 (dt, *J* = 1.58, 8.20 Hz, 1H), 7.34 (dd, 4.73, 8.20 Hz, 1H), 7.28 (m, 1H), 7.23 (m, 1H), 7.14-7.07 (m, 2H), 4.41-4.36 (m, 1H), 3.46-3.41 (m, 2H), 2.86-2.83 (m, 2H), 2.53-2.42 (m, 2H), 2.36 (s, 3H), 1.74-1.66 (m, 1H), 1.62-1.49 (m, 3H), 1.36-1.22 (m, 2H). ¹³C-NMR (DMSO-*d*₆): δ = 198.79, 171.40, 171.26, 160.53 (d, *J* = 242.29 Hz), 144.29, 140.90, 135.53, 130.60 (d, *J* = 4.62 Hz), 127.98 (d, *J* = 8.32 Hz), 127.71 (d, *J* = 15.72 Hz), 126.20, 124.23 (d, *J* = 3.70 Hz), 123.60, 114.92 (d, *J* = 21.27 Hz), 53.24, 45.19, 34.99, 32.77, 31.57, 26.91, 24.16, 22.98. ESI-MS (*m/z*): 431.21 [M + H]⁺. Anal. (C₂₂H₂₇FN₄O₂S) C, H, N.

(2S)-N-[(2S)-6-Ethanethioylamino-1-[2-(pyridin-3-yl)ethylamino]-1-oxohexan-2-yl]-pyrrolidine-1-tert-butoxycarbonyl-2-carboxamide (40). Compound **40** was prepared using N-Boc-L-proline (0.27 g, 1.26 mmol), DMF (7.2 mL), TBTU (0.49 g, 1.53 mmol), pyridine (7.2 mL) and **11** (0.48 g, 1.26 mmol), following the same procedure described for **12**, the amount of CH₂Cl₂ was 150 mL and the workup was made without HCl 0.5M and brine. Purification by column chromatography silica Kieselgel for flash with CH₂Cl₂: EtOAc: MeOH (5.5: 3: 1.5) as eluent phase to give the pure product as white solid (0.31 g, 0.61 mmol, 48 %). ¹H-NMR (DMSO-*d*₆) rotamers A+B: δ = 9.91 (s br, 1H), 8.41 (s, 2H), 8.02 (s br, 0.54H), 7.87-7.82 (m, 1.46H), 7.62 (m, 1H), 7.30-7.28 (m, 1H), 4.20-4.11 (m, 2H), 3.42-3.37 (m, 3H), 3.28-3.24 (m, 2H), 2.73 (t, *J* = 6.94 Hz, 2H), 2.36 (s, 3H), 2.10-2.02 (m, 1H), 1.77-1.70 (m, 3H), 1.61-1.13 (m, 16H). ¹³C-NMR (DMSO-*d*₆): rotamers A + (B) δ = 198.76, 172.18 (171.88), 171.36, 153.95 (153.29), 149.84, 147.37, 136.17, 134.75, 123.30, 78.79 (78.34), 59.50 (59.31), 52.25, 46.71 (46.47), 45.22, 32.75, 32.09 (31.97), 31.52, 30.99, 29.68, 28.10 (27.97), 26.88, 23.94, 23.04 (22.80). ESI-MS (*m/z*): 506.22 [M + H]⁺. Anal. (C₂₅H₃₉N₅O₄S) C, H, N.

(2S,4R)-N-[(2S)-6-Ethanethioylamino-1-(benzylamino)-1-oxohexan-2-yl]-4-hydroxypyrrolidine-1-tert-butoxycarbonyl-2-carboxamide (41). To a solution of N-Boc-Hydroxy-L-proline (0.72 g, 3.1 mmol) in DMF (30 mL) under Argon flow were added TBTU (1.10 g, 3.4 mmol), pyridine (30 mL) and maintained under stirring for 10min at rt . After this time **9** (1.02 g, 3.1 mmol) was added and the solution mixed 3h at rt under Argon flow. Solvents were evaporated and the obtained oil was dissolved in EtOAc (300 mL), washed with HCl 0.5M, brine (twice), NaHCO₃ 5%, finally dried with Na₂SO₄ and evaporated under vacuum. The crude product obtained was purified by columns chromatography, using silica Kieselgel for flash with EtOAc : Hexane : MeOH (7: 2: 1) as eluent phase to give the pure product as white solid (0.55 g, 1.10 mmol, 35 %). ¹H-NMR (DMSO-*d*₆) : rotamers A+B δ = 9.90 (s br, 1H), 8.43 (t, *J* = 5.67 Hz, 0.6H), 8.25 (t, *J* = 5.67 Hz, 0.4H), 8.02 (d, *J* = 7.88 Hz, 0.4H), 7.96 (d, *J* = 7.88 Hz, 0.6H), 7.30-7.23 (m, 5H), 4.99-4.96 (m, 1H), 4.28-4.20 (m, 5H), 3.44-3.37 (m, 3H), 3.26-3.24 (m, 1H), 2.37 (s, 3H), 2.06-1.99 (m, 1H), 1.87-1.51 (m, 5H), 1.36-1.25 (m, 11H). ¹³C-NMR (DMSO-*d*₆) : rotamers A+(B) δ = 198.79 (198.75), 172.35 (171.98), 171.54 (171.49), 154.18 (153.53), 139.28,

128.20, 127.03 (126.94), 126.71 (126.67), 78.87 (78.45), 68.38 (67.71), 58.69 (58.51), 55.02 (54.69), 52.50, 45.31 (45.23), 41.95, 38.41, 32.77, 31.88 (31.30), 28.10 (27.96), 26.90 (26.82), 22.96 (22.91). ESI-MS (m/z): 507.09 [M + H]⁺ Anal. (C₂₅H₃₈N₄O₅S) C, H, N.

(2S,4R)-N-[(2S)-6-Ethanethiolyamino-1-(2-oxo-2-phenylethylamino)-1-oxohexan-2-yl]-4-hydroxypyrrolidine-1-tert-butoxycarbonyl-2-carboxamide

(42). To a solution of N-Boc-Hydroxy-L-proline (0.69 g, 3.0 mmol) in DMF (30 mL) under Argon flow were added TBTU (1.06 g, 3.3 mmol), pyridine (30 mL) and maintained under stirring for 10min at rt. After this time **7** (1.07 g, 3.0 mmol) was added and the solution mixed 3h at rt under Argon flow. Solvents were evaporated and the obtained oil was dissolved in EtOAc (300 mL), washed with HCl 0.5M, brine (twice), NaHCO₃ 5%, finally dried with Na₂SO₄ and evaporated under vacuum. The crude product obtained was purified with two columns chromatography, using Aluminum oxide and silica Kieselgel for flash with EtOAc : Hexane : MeOH (7: 2: 1) as eluent phase to give the pure product as white solid (0.24 g, 0.45 mmol, 15 %). ¹H-NMR (DMSO-*d*₆) : rotamers A+B δ = 9.91 (s br, 1H), 8.24 (t, *J* = 5.26 Hz, 0.6H), 8.12 (t, *J* = 5.26 Hz, 0.4H), 8.04-7.97 (m, 3H), 7.66 (t, *J* = 7.25 Hz, 1H), 7.55 (t, *J* = 7.25Hz, 2H), 4.99-4.96 (m, 1H), 4.68-4.54 (m, 2H), 4.37-4.29 (m, 1H), 4.26-4.21 (m, 2H), 3.47-3.36 (m, 3H), 3.27-3.23 (m, 1H), 2.38 (s, 3H), 2.09-1.99 (m, 1H), 1.91-1.81 (m, 1H), 1.78-1.66 (m, 1H), 1.62-1.50 (m, 3H), 1.41-1.29 (m, 11H). ¹³C-NMR (DMSO-*d*₆) : rotamers A+(B) δ = 198.77 (198.72), 195.12 (195.02), 172.36, 171.91, 154.05 (153.52), 134.92, 133.54, 128.78, 127.80, 78.78 (78.45), 68.42, 67.73, 58.48 (58.42), 54.99 (54.70), 52.31 (52.19), 45.85 (45.30), 38.36, 32.78, 31.96 (31.58), 28.12 (27.99), 26.94 (26.82), 22.88 (22.71). ESI-MS (m/z): 535.06 [M + H]⁺ Anal. (C₂₆H₃₈N₄O₆S·0.01 H₂O) C, H, N.

(2S,4R)-N-[(2S)-6-Ethanethiolyamino-1-(benzylamino)-1-oxohexan-2-yl]-4-

hydroxypyrrolidine-2-carboxamide hydrochloride (43). Compound **43** was synthesized using **41** (0.28 g, 0.55 mmol) in 2-propanol (8.6 mL), 1,2-ethanedithiol (0.058 mL, 0.55 mmol) and HCl 12N (0.28 mL, 3.36 mmol) added x three times, following the same procedure described for **22**. The yellow oil as residue was washed with petroleum ether (4 x 10 mL) and CH₂Cl₂: petroleum ether (1:1) (4 x 4

mL) provides the product as white solid (0.22 g, 0.49 mmol, 90 %). ¹H-NMR (DMSO-*d*₆) : δ = 10.08 (s br, 1H), 9.87 (s br, 1H), 8.79 (d, *J* = 7.57 Hz, 1H), 8.68-8.57 (m, 2H), 7.33-7.22 (m, 5H), 5.51 (s, 1H), 4.42-4.37 (m, 2H), 4.33-4.23 (m, 3H), 3.46-3.42 (m, 2H), 3.07 (d, *J* = 11.98 Hz, 1H), 2.38 (s, 3H), 2.32-2.28 (m, 1H), 1.89-1.83 (m, 1H), 1.75-1.52 (m, 4H), 1.40-1.30 (m, 2H). ESI-MS (*m/z*):407.28 [M + H]⁺ Anal. (C₂₀H₃₁ClN₄O₃S) C, H, N.

(2S,4R)-N-((S)-6-ethanethioamido-1-oxo-1-((2-oxo-2-phenylethyl)amino)hexan-2-yl)-4-hydroxypyrrolidine-2-carboxamide hydrochloride (44). Compound **44** was synthesized using **42** (0.15 g, 0.33 mmol) in 2-propanol (4.7 ml), 1,2-ethanedithiol (0.030 mL, 0.33 mmol) and HCl 12N (0.15 ml, 1.8 mmol) added x three times following the same procedure described for **22**. The yellow oil residue was washed with petroleum ether (4 x 10 ml) and CH₂Cl₂: petroleum ether (1:1) (4 x 4 ml) providing the product as white solid (0.12 g, 0.25 mmol, 77%). ¹H-NMR (DMSO-*d*₆): δ = 10.07 (s br, 1H), 9.84 (s br 1H), 8.78 (d, *J* = 8.24 Hz, 1H), 8.66 (s br, 1H), 8.39 (t, *J* = 5.49 Hz, 1H), 7.98 (d, *J* = 7.32 Hz, 2H), 7.68 (t, *J* = 7.32 Hz, 1H), 7.55 (t, *J* = 7.32 Hz, 2H), 5.47 (s, 1H), 4.70-4.56 (m, 2H), 4.43-4.45 (m, 3H), 3.49-3.45 (m, 2H), 3.09-3.07 (m, 1H), 2.39 (s, 3H), 2.32-2.28 (m, 1H), 1.91-1.85 (m, 1H), 1.79-1.72 (m, 1H), 1.65-1.54 (m, 3H), 1.43-1.34 (m, 2H). ¹³C-NMR (DMSO-*d*₆) : δ = 198.78, 195.08, 171.29, 167.85, 134.89, 133.58, 128.80, 127.80, 68.98, 57.75, 53.42, 52.89, 45.85, 45.25, 32.78, 31.83, 30.67, 26.90, 22.86. ESI-MS (*m/z*): 435.22 [M + H]⁺. Anal. (C₂₁H₃₁ClN₄O₄S·0.04hexane·0.02 CH₂Cl₂) C, H, N.

2S)-N-[(2S)-6-Ethanethioylamino-1-(benzylamino)-1-oxohexan-2-yl]-pyrrolidine-1-tert-butoxycarbonyl-2-carboxamide (45). To a solution of Boc-L-proline (0.38 g, 1.75 mmol) in DMF (8.5 mL) under Argon flow were added TBTU (0.61 g, 1.9 mmol), pyridine (6.5 mL) and maintained under stirring for 10min at rt. After this time **9** (0.58 g, 1.75 mmol) was added and the solution mixed 3h at rt under Argon flow. Solvents were evaporated and the obtained oil was dissolved in EtOAc (200 mL), washed with HCl 0.5M, brine (twice), NaHCO₃ 5%, finally dried with Na₂SO₄ and evaporated under vacuum. The crude product obtained was purified by columns chromatography, using silica Kieselgel for flash with EtOAc : Hexane : MeOH (7: 2.5: 0.5) as eluent phase to give the pure product as white solid (0.58 g,

1.18 mmol, 67 %). ¹H-NMR (DMSO-*d*₆) : rotamers A+B δ = 9.92 (s br, 1H), 8.43 (t, *J* = 5.36 Hz, 0.6H), 8.28 (t, *J* = 5.36 Hz, 0.4H), 7.95-7.92 (m, 1H), 7.33-7.24 (m, 5H), 4.31-4.23 (m, 3H), 4.15-4.13 (m, 1H), 3.46-3.37 (m, 3H), 3.28-3.23 (m, 1H), 2.38 (s, 3H), 2.12-2.03 (m, 1H), 1.82-1.60 (m, 7H), 1.37-1.24 (m, 11H). ¹³C-NMR (DMSO-*d*₆): rotamers A+ (B) δ = 198.78, 172.34 (172.05), 171.53, 153.94 (153.32), 139.27, 128.19, 127.01, 126.96 (126.71), 78.79 (78.36), 59.51 (59.34), 52.40, 46.71 (46.49), 45.23, 41.94, 32.77, 31.92 (31.43), 30.99 (29.71), 28.10 (27.98), 26.85, 23.91 (23.01), 22.92. ESI-MS (*m/z*): 491.13 [M + H]⁺ Anal. (C₂₅H₃₈N₄O₄S) C, H, N.

(2S)-N-[(2S)-6-Ethanethiolyamino-1-(benzylamino)-1-oxohexan-2-yl]-pyrrolidine-2-carboxamide hydrochloride (46) Compound **46** was synthesized using **45** (0.53 g, 1.1 mmol) in 2-propanol (16 mL), 1,2-ethanedithiol (0.091 mL, 1.1 mmol) and HCl 12N (0.55 mL, 6.6 mmol) added x three times, following the same procedure described for **22** , to furnish the product as white solid (0.35 g, 0.81 mmol, 75 %). ¹H-NMR (DMSO-*d*₆) : δ = 10.09 (s br, 1H), 9.78 (s br, 1H), 8.74 (d, *J* = 7.88 Hz, 1H), 8.61-8.47 (m, 2H), 7.31-7.22 (m, 5H), 4.33-4.21 (m, 4H), 3.46-3.42 (m, 2H), 3.23-3.17 (m, 2H), 2.38 (s, 3H), 2.34-2.26 (m, 1H), 1.92-1.82 (m, 3H), 1.76-1.52 (m, 4H), 1.42-1.27 (m, 2H). ESI-MS (*m/z*): 391.28 [M + H]⁺ Anal. (C₂₀H₃₁ClN₄O₂S) C, H, N.

Elemental analysis data.

Compound	Formula	Calculated %			Found %		
		C	H	N	C	H	N
2	C ₂₁ H ₃₁ N ₃ O ₄ S	59.83	7.41	9.97	60.09	7.42	9.59
6	C ₂₀ H ₃₂ N ₄ O ₃ S·0.03DMF·0.03Hexane	58.12	7.80	13.55	58.25	7.67	13.17
12	C ₂₅ H ₃₁ N ₃ O ₃ S	66.20	6.89	9.26	66.53	6.58	9.24
13	C ₂₆ H ₃₃ N ₃ O ₃ S	66.78	7.11	8.99	66.90	6.96	8.74
14	C ₂₈ H ₃₇ N ₃ O ₃ S	67.85	7.52	8.48	68.07	7.45	8.23
15	C ₂₄ H ₃₀ N ₄ O ₃ S·0.5 H ₂ O	62.17	6.74	12.08	62.14	6.39	11.94
16	C ₂₉ H ₃₆ N ₄ O ₆ S	61.25	6.38	9.85	61.50	6.21	9.67
17	C ₂₆ H ₃₈ N ₄ O ₅ S	60.21	7.38	10.80	60.28	7.17	10.93
18	C ₂₉ H ₃₅ N ₅ O ₅ S	61.57	6.24	12.38	61.31	6.09	12.08
19	C ₂₂ H ₂₈ N ₄ O ₂ S	64.05	6.84	13.58	63.66	6.71	13.56
20	C ₁₈ H ₂₈ N ₄ O ₂ S	59.31	7.74	15.37	59.44	7.54	15.05
21	C ₂₄ H ₃₆ N ₄ O ₄ S	60.48	7.61	11.75	60.70	7.39	11.54
22	C ₁₉ H ₂₉ ClN ₄ O ₂ S·0.3H ₂ O	54.55	7.13	13.39	54.30	6.82	13.06
23	C ₂₇ H ₃₄ N ₄ O ₅ S	61.58	6.51	10.64	61.72	6.16	10.51
25	C ₂₄ H ₃₁ N ₃ O ₃ S	65.28	7.08	9.52	65.61	6.87	9.43
26	C ₂₃ H ₂₉ N ₃ O ₃ S	64.61	6.84	9.83	64.98	6.70	9.84
27	C ₂₅ H ₃₁ N ₃ O ₅ S·0.02hexane	61.91	6.47	8.62	62.28	6.26	8.64
28	C ₂₄ H ₃₁ N ₃ O ₄ S·0.1hexane·0.01 EtOAc	63.36	7.00	8.99	63.61	6.62	9.16
29	C ₂₆ H ₃₂ N ₄ O ₃ S	64.97	6.71	11.66	65.03	6.50	11.45
30	C ₂₇ H ₃₄ N ₄ O ₄ S	63.51	6.71	10.97	63.49	6.51	10.85
31	C ₃₃ H ₃₈ N ₄ O ₄ S	67.55	6.53	9.55	67.31	6.33	9.47
32	C ₂₁ H ₂₆ N ₄ O ₃ S	60.85	6.32	13.52	60.82	6.15	13.39
33	C ₁₈ H ₂₆ N ₄ O ₄ S	54.80	6.64	14.20	54.76	6.49	13.98
34	C ₁₉ H ₂₈ N ₄ O ₄ S	55.86	6.91	13.71	56.00	6.65	13.65
35	C ₂₈ H ₃₆ N ₄ O ₅ S·0.03hexane	62.30	6.76	10.31	62.68	6.91	10.21
36	C ₂₇ H ₃₇ N ₃ O ₂ S	69.34	7.97	8.99	69.67	7.85	8.63
37	C ₂₈ H ₃₉ N ₃ O ₂ S	69.82	8.16	8.72	69.78	8.02	8.50

38	C ₂₂ H ₂₈ N ₄ O ₂ S	64.05	6.84	13.58	63.81	6.64	13.32
39	C ₂₂ H ₂₇ FN ₄ O ₂ S	61.37	6.32	13.01	61.05	6.28	12.84
40	C ₂₅ H ₃₉ N ₅ O ₄ S	59.38	7.77	13.85	59.47	7.46	13.74
41	C ₂₅ H ₃₈ N ₄ O ₅ S	59.26	7.56	11.06	59.17	7.25	10.94
42	C ₂₆ H ₃₈ N ₄ O ₆ S·0.01 H ₂ O	58.38	7.16	10.47	57.99	6.86	10.29
43	C ₂₀ H ₃₁ ClN ₄ O ₃ S	54.22	7.05	12.65	54.11	6.74	12.53
44	C ₂₁ H ₃₁ ClN ₄ O ₄ S·0.04hexane·0.02 CH ₂ Cl ₂	53.62	6.68	11.76	53.97	6.64	11.44
45	C ₂₅ H ₃₈ N ₄ O ₄ S	61.20	7.81	11.42	60.81	7.44	11.32
46	C ₂₀ H ₃₁ ClN ₄ O ₂ S	56.26	7.32	13.12	55.93	7.00	13.01

SIRT1-3 in Vitro Assay. The Fluor de Lys fluorescence assays were based on the method described in the BIOMOL product sheet (Enzo Life Sciences) using the BIOMOL KI177 substrate for SIRT1 and the KI179 substrate for SIRT2 and SIRT3. The determined K_m value of SIRT1 for KI177 was 58 μ M and the K_m of SIRT2 for KI179 was 198 μ M.²⁹ The K_m of SIRT3 for KI179 was reported by BIOMOL to be 32 μ M. The K_m values of SIRT1, SIRT2 and SIRT3 for NAD⁺ were reported by BioMol to be 558 μ M, 547 μ M and 2 mM, respectively.

Briefly, assays were carried out using the Fluor de Lys acetylated peptide substrate at 0.7 K_m and NAD⁺ (Sigma N6522 or BIOMOL KI282) at 0.9 K_m , recombinant GST-SIRT1/2-enzyme or recombinant His-SIRT3 and SIRT assay buffer (KI286). GST-SIRT1 and GST-SIRT2 were produced as described previously.^{193,194} His-SIRT3 (BML-SE270) was purchased from Enzo Life Sciences. The buffer, Fluor de Lys acetylated peptide substrate, NAD⁺ and DMSO/compounds in DMSO (2.5 μ L in 50 μ L total reaction volume; DMSO from Sigma, D2650) were preincubated for 5 min at room temperature. The reaction was started by adding the enzyme. The reaction mixture was incubated for one hour at 37 °C. After that, Fluor de Lys developer (KI176) and 2 mM nicotinamide (KI283) in SIRT assay buffer (total volume 50 μ L) were added and the incubation was continued for 45 min at 37 °C. Fluorescence readings were obtained using EnVision 2104 Multilabel Reader (PerkinElmer) with excitation wavelength 370 nm and emission 460 nm.

The IC₅₀ values were determined as three independent determinations giving altogether 27 data-points. All the data-points were included in the calculation of the

best-fit value for non-linear curve fitting with GraphPad Prism5 (GraphPad Software, Inc.).

Cell Culture. Human retinal pigment epithelial cells (ARPE-19, obtained from ATCC, American Type Culture Collection) and SH-SY5Y neuroblastomas (DSMZ) were grown as described earlier in Huhtiniemi et al. 2011.¹³⁴ A549 lung carcinoma and MCF-7 breast carcinoma cells (both from ATCC) were maintained in Dulbecco's modified Eagle's medium (DMEM; Gibco) containing 10% fetal calf serum, 100 U/ml penicillin and 100 µg/ml streptomycin at +37°C in humidified atmosphere of 5% CO₂ / 95% air.

Western Blotting. Western blot analysis was done as described in Huhtiniemi et al. 2011.¹³⁴ The cells were plated to 12-well plates (Nunc) at a density of 10⁵ cells/well, and the experiments were initiated after 24 h. Test compounds and etoposide (Sigma) were added at the same time and incubated for 5 h before harvesting.

Lactate Dehydrogenase Assay. Lactate dehydrogenase (LDH) leakage from the cells to medium was used as a marker for cytotoxicity. LDH was measured from cell culture medium with CytoTox assay (Promega #G1780).

Cell proliferation and cell cycle analysis. For cell proliferation assays with sulforhodamine B, A549 and MCF-7 cells were plated to 96-well plates (Nunc) 24 h before the start of the treatments (3000 cells / well). The cells were treated with vehicle (0.5% DMSO) or test compounds for 48 h (A549 cells) or 72 h (MCF-7 cells). Sulforhodamine B staining was performed as previously described.¹⁹⁵ After treatments, 50 µl of 50% trichloroacetic acid (Sigma) was added to each well and incubated for 1 h at +4°C. The plates were then washed with water and air dried. The fixed cells were incubated with 100 µl of 0.4% sulforhodamine B solution (Sigma) at room temperature for 1 h. The plates were again washed with water and air dried, followed by solubilization of the bound dye with 200 µl of 10 mM Tris base solution. The results were measured with EnVision plate reader (PerkinElmer) at a wavelength of 565 nm. Cell cycle analysis of A549 and MCF-7 cells was done by propidium iodide staining as previously described.¹⁹⁶ The cells were plated to 6-well plates (Nunc) 6 h before the start of the treatments (0.6 × 10⁵ cells / well). The cells were

treated with vehicle (0.5% DMSO) or test compounds for 18 h. Both adherent and floating cells were harvested and fixed with ice-cold 70% ethanol. After overnight incubation at +4°C, the cells were collected by centrifugation and incubated with 150 µg/ml DNase free RNase (Thermo Scientific) for 1 h at +50°C. Propidium iodide (Sigma) was added to the final concentration of 8 µg/ml and incubation was continued for 2 h at +37°C. FACScanto II flow cytometer with FACSDiva software (Becton Dickinson) was used to analyze cellular DNA content and cell cycle.

Molecular Modeling. Homology models for SIRT1 and SIRT2 were built in bioactive conformation using the crystal structure of SIRT3 (PDB code 3glr)³⁰ in which is co-crystallized AceCS2-K^{Ac} peptide (⁶³⁹RSGK^{Ac}VMR) sequence, containing acetylated lysine 642 that has been identified to be deacetylated by SIRT3. The amino acid sequence of *Homo Sapiens* SIRT1 and SIRT2 was obtained from the NCBI (National Center for Biotechnology Information). The sequences of SIRT1 and SIRT2 were manually aligned with SIRT3 based on sequence similarity, (40% and 52.9% respectively, for alignments see below)³⁰ Homology models for the catalytic deacetylase core of SIRT1 (555 residues) and a full-length, homology modeled SIRT2 (352 residues) was constructed using ORCHESTRA in SYBYL 1.3 (following the same procedure described for Rotili et al 2012).¹⁴³ The geometry of the side chains was manually optimized to obtain a crude model. The models were polished with Protein Preparation Wizards available in the Schrödinger Suite 2009 (Schrödinger Suite 2009 Protein Preparation Wizard; Schrödinger, LLC: New York, NY, 2009). In that process, the bond orders were assigned and hydrogens were added. In addition, the exhaustive sampling method was used to optimize the hydrogen bonding, and determine the orientations of hydroxyl groups, amide groups of Asn and Gln amino acids, and the proper state and orientations of the histidine imidazole rings. To relax the structure of the initial SIRT1 and SIRT2 models, the models were subjected to a restrained minimization using OPLS2001 force field, with a 0.3 Å rmsd atom displacement limit. The protein geometry was evaluated by Ramachandran plot and Verify 3D (Verify3D Structure Evaluation Server: nihserver.mbi.ucla.edu/Verify_3D). SIRT1 outliers: Val293, Asp237; SIRT2 outliers: Ser63, Arg164, Asp213 and Gly224. The pseudopeptidic database was prepared using Ligprep (LigPrep, version 2.3; Schrödinger, LLC: New York, NY,

2009), the geometric optimization was carried out using OLPS2005 force field, and all possible ionization and tautomeric form were created at pH 8.0 ± 0.2 using EPIK (Epik, version 2.2, Schrödinger, LLC, New York, NY, 2011). The chiralities specified in the input structures were retained. Dockings were performed using Glide (Glide, version 5.5; Schrödinger, LLC: New York, NY, 2009). For the grid file and docking parameters were applied settings previously published by Huhtiniemi et al.¹³⁴ The figures were prepared using MOE (Molecular Operating Environment (MOE), 2011.10; Chemical Computing Group Inc., 1010 Sherbooke St. West, Suite #910, Montreal, QC, Canada, H3A 2R7).

Alignment SIRT1_SIRT3³⁰

SIRT1 *Homo Sapiens* sequence 555aa, was downloaded from NCBI (National Center for Biotechnology Information) AAH12499.1, and aligned with SIRT3 (PDB code: 3glr).

Alignment SIRT1 model using SIRT3 as template (ORCHESTRA, SYBYL)

```

          1          11          21          31          41
SIRT1 555aa  MIGTDPRTILKDLLLPETIPPELDDMTLWQIVINILSEPPKRRKRKDINT
Hom.model  -----NT
3GLR      -----GKLS

          51          61          71          81          91
SIRT1 555aa  IEDAVKLL--QECKKIIVLTGAGVSVSCGIPDFRSR-DGIYARLAVDFPD
Hom.model  IEDAVKLL--QECKKIIVLTGAGVSVSCGIPDFRSR-DGIYARLAVDFPD
3GLR      LQDVAELIRARACQRVVVMVGAGISTPSGIPDFRSPGSLYSNLQ--YD

          101         111         121         131         141
SIRT1 555aa  LPDPQAMFDIEYFRKDPRPFFKFAKEIYPGQFQPSLCHKFIALSCKEGKL
Hom.model  LPDPQAMFDIEYFRKDPRPFFKFAKEIYPGQFQPSLCHKFIALSCKEGKL
3GLR      LPYPEAIFELPFFFHNPKPFFTLAKELYPGNYKPNVTHYFLRLLHDKGLL

          151         161         171         181         191
SIRT1 555aa  LRNYTQNIDTLEQVAGIQ--RIIQCHGSFATASCLICKYKVDCEAVRGAL
Hom.model  LRNYTQNIDTLEQVAGIQ--RIIQCHGSFATASCLICKYKVDCEAVRGAL
3GLR      LRLYTQNIDGLERVSGIPASKLVEAHGTFASATCTVCQRPFPGEDIRADV

          201         211         221         231         241
SIRT1 555aa  FSQVVPRCPRCPADEPLAIMKPEIVFFGENLPEQFHRAMKYDKDEVDLLI
Hom.model  FSQVVPRCPRCPADEPLAIMKPEIVFFGENLPEQFHRAMKYDKDEVDLLI
3GLR      MADRVPRCPVCT-----GVVKPDI VFFGEPLPQRFL LHV-VDFPMADLLL

          251         261         271         281         291
SIRT1 555aa  VIGSSLKVRPVALIPSSIPHEVPQILINREPLPHL-----HFDVELLGDC

```

```

Hom.model      VIGSSLKVRPVALIPSSIPHEVPQILINREPLPHL-----HFDVELLGDC
3GLR          ILGTSLEVEPFASLTEAVRSSVPRLLINRDLVGPLAWHPRSRDVAQLGDV

SIRT1 555aa   301          311          321          331          341
Hom.model     DVIINELCHRLGGEYAKLCCNPVKLSEITEKPPRTQKELAYLSELPPPTPL
3GLR          DVIINELCHRLGGEYAK-----PRTQKELAY-----
              VHGVESLVELLGWTEEM-----RDLVQRETGKL-RSG-VMR

SIRT1 555aa   351          361          371          381          391
Hom.model     HVSESSSPERTSPPDSSVIVTLLDQAAKSNDDLVDVSESKGCMEEKPQEV
3GLR          -----

SIRT1 555aa   401          411          421          431          441
Hom.model     QTSRNVESIAEQMENPDLKNVGSSTGEKNERTSVAGTVRKWCWPNRVAKEQ
3GLR          -----

SIRT1 555aa   451          461          471          481          491
Hom.model     ISRRLDGNQYLFLPPNRYIFHGAEVYSDSEDDVLSSSSCGSNSDSGTCQS
3GLR          -----

SIRT1 555aa   501          511          521          531          541
Hom.model     PSLEEPMEDESEIEEFYNGLEDEPDVPERAGGAGFGTDGDDQEAINAIS
3GLR          -----

SIRT1 55aa    551          561
Hom.model     VKQEVTD MNYP SNKS
3GLR          -----

```

Key

Joy Annotation:

alpha helix	red	x
beta strand	blue	x
3 - 10 helix	maroon	x

Alignment SIRT2_SIRT3³⁰

SIRT2 *Homo Sapiens* sequence 352aa, was downloaded from NCBI (National Center for Biotechnology Information) AAK51133.1, and aligned with SIRT3 (PDB code: 3glr).

Alignment SIRT2 model using SIRT3 as template (ORCHESTRA, SYBYL)

```

SIRT2 352aa      1          11          21          31          41
MDFLRNLFSTLSLGSQKERLLDELTLLEGVARYMQSERCRRVICLVGAGI
Hom.model -----LTLEGVARYMQSERCRRVICLVGAGI
3GLR -----GKLSLQDVAELIRARACQRVVVMVGAGI

SIRT2 352aa      51          61          71          81          91
STSAGIPDFRSPSTGLYDNLEKYHLPYPEAIFEISYFKKHPEPFFALAKE
Hom.model STSAGIPDFRSPSTGLYDNLEKYHLPYPEAIFEISYFKKHPEPFFALAKE
3GLR STPSGIPDFRSPSGGLYSNLQDYDLPYPEAIFELPFFFFHNPKPFFTLAKE

SIRT2 352aa     101         111         121         131         141
LYPGQFKPTICHYFMRLKDKGLLLRCTQNIDTLERIAGLEQEDLVEAH
Hom.model LYPGQFKPTICHYFMRLKDKGLLLRCTQNIDTLERIAGLEQEDLVEAH
3GLR LYPGNYKPNVTHYFLRLLHDKGLLRLRYTQNIDGLERVSGIPASKLVEAH

SIRT2 352aa     151         161         171         181         191
GTFYTSHCVSASCRHEYPLSWMKEKIFSEVTPKCEDCQSLVKPDI VFFGE
Hom.model GTFYTSHCVSASCRHEYPLSWMKEKIFSEVTPKCEDCQSLVKPDI VFFGE
3GLR GTFASATCTV--CQRPFPGEDIRADVMADRVPRCPVCTGVVVKPDI VFFGE

SIRT2 352aa     201         211         221         231         241
SLPARFFSCMQSDFLKVDLLVMGTSLQVQPFASLISKAPLSTPRLINK
Hom.model SLPARFFSCMQSDFLKVDLLVMGTSLQVQPFASLISKAPLSTPRLINK
3GLR PLPQRFLLVH-VDFPMADLLILGTSLEVEPFASL TEAVRSSVPRLINR

SIRT2 352aa     251         261         271         281         291
EKAGQSDPFLGMIMGLGGGMDFDSKKAYRDVAWLGECDQGCLALAE LLGW
Hom.model EKAGQSDPFLGMIMGLGGGMDFDSKKAYRDVAWLGECDQGCLALAE LLGW
3GLR DLVGPLAW-----HPRS RDVAQLGDVVHGVESLVELL GW

SIRT2 352aa     301         311         321         331         341
KKELEDLVRREHASIDAQSGAGVNPSTSPKPKSPPPAKDEARTTEREK
Hom.model KKELEDLVRREHASI-----
3GLR TEEMRDLVQRETGKL--RSG-VMR-----

SIRT2 352aa     351
PQ
Hom.model --
3GLR --

```

Key

Joy Annotation:

alpha helix	red	x
beta strand	blue	x
3 - 10 helix	maroon	x

9 DESIGN AND SYNTHESIS OF PSEUDOPEPTIDIC AND PEPTIDIC ACTIVITY-BASED PROBES AS SIRT1-3 INHIBITORS. USEFUL TOOLS IN UNDERSTANDING THEIR SUBCELLULAR LOCALIZATION AND SPECIFICITY.

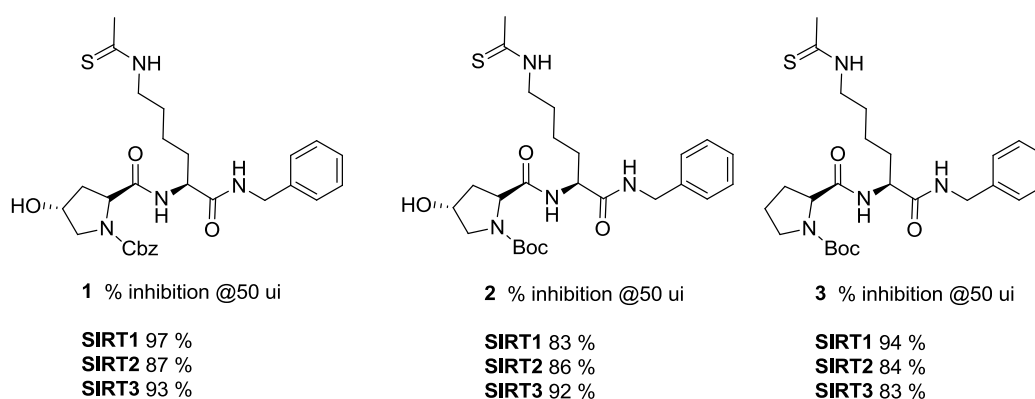
Abstract: The seven sirtuin isoforms SIRT1-7 show different cellular localization. SIRT1, SIRT6, and SIRT7 being nuclear, SIRT2 cytoplasmic and SIRT3-5 mitochondrial. Due to this, the development of specific inhibitors with enzymatic efficacy must face the difficulty to reach the cellular target. Here we propose the design and synthesis of potential pseudo-peptidic and peptidic inhibitors of human SIRT1-3 labeled with Thiazole orange for live cellular imaging. Furthermore, we aim to develop the first SIRT3 peptidic inhibitor based on AceCS2 sequence containing a peptidic shuttle for mitochondrial delivery.

* Adapted with the permission from: Mellini, P.; Kokkola, T.; Suuronen, T.; Nyrhilä, O.; Leppänen, J.; Mai, A.; Lahtela-Kakkonen, M.; and Jarho, E.M.

9.1 Introduction

The seven sirtuin isoforms SIRT1-7 show different cellular localization, SIRT1, SIRT6, and SIRT7 being nuclear, SIRT2 cytoplasmic and SIRT3-5 mitochondrial. Due to this, develop specific inhibitors with enzymatic efficacy must face the difficulty to reach the cellular target. Recently we have developed pan SIRT1-3 pseudopeptidic inhibitors in which N-terminal Cbz- or Boc-L-prolyl moiety gave the most potent compounds of the series (Chart 1).¹⁹⁷ Activity-based probes for SIRTs enable to allow subcellular localization/specificity of inhibitor might be valuable tools in understanding the sirtuin biology. Pursuing the results from our previous fragment based library, we designed and synthesized two selected pseudopeptidic inhibitors with 4-trans-hydroxy- and L-prolil moiety. The inhibitors were conjugated with an appropriate fluorophore (Thiazole orange) for confocal microscopy, in order to detect their subcellular localization. Furthermore in this study following a rational selection of side chains, based on sequence of AceCS2 a known SIRT3 substrate¹²⁸ and our previous reported prolyl scaffold, we designed also potential SIRT3 inhibitors linked with a molecular shuttle for mitochondrial delivery, and Thiazole orange for cellular imaging.

Chart 1. L-proline derivatives

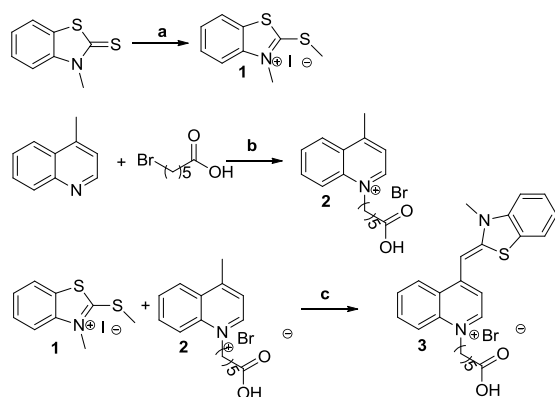


9.2 Chemistry

The Thiazole orange (to) was obtained following the procedure according to the literature¹⁹⁸ (Scheme 1). The N^ε-thioacetylated compound **4** was synthesized using ethyl dithioacetate and EtOH/10% (w/v) Na₂CO_{3(aq)} at rt for 12h according to the literature.^{125,134} Compound **5** (Scheme 2) was obtained with a coupling reaction

between the activated acid **4** and benzylamine using the coupling agent TBTU (O-(benzotriazol-1-yl)-N,N,N',N'-tetramethyluronium tetrafluoroborate) in dimethylformamide (DMF)/pyridine under argon flow following the procedure reported previously.¹⁹⁷

Scheme 1^a Synthesis of Thiazole orange (to)

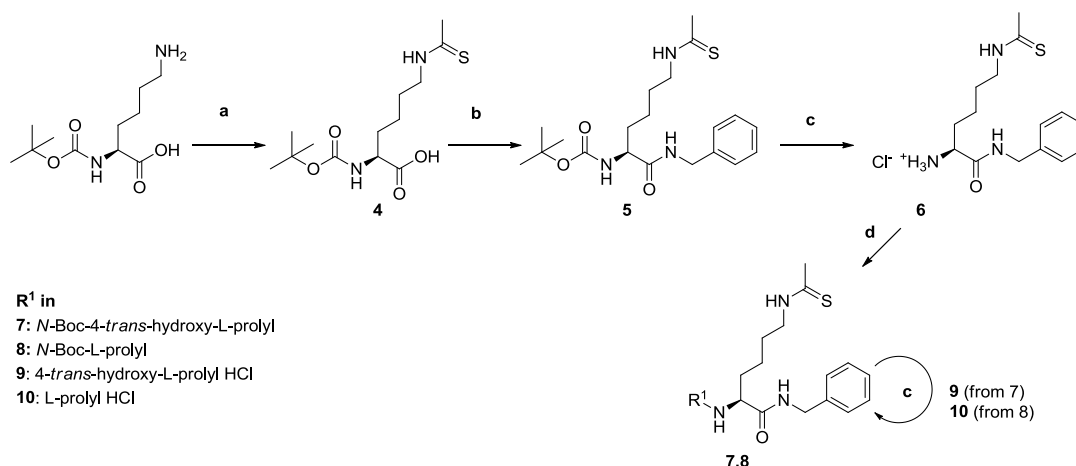


^aReagents and conditions: (a) CH_3I , 45°C , 4h; (b) neat 125°C , 4h; (c) Et_3N , CH_2Cl_2 , rt, 24h.

The hydrochloride **6**, **9**, **10** (Scheme 2) were gained via Boc (tert-butoxycarbonyl) deprotection performed at 60°C using 15 equiv of $\text{HCl}_{(\text{aq})}$ 12N, 2-propanol and 1,2-ethanedithiol as a scavenger for trapping the tert-butyl cation generated in situ.¹⁹⁷ Compounds **7**, **8** (Scheme 2) were synthesized according to the above mentioned coupling reaction, in this case N-Boc-L-proline and N-Boc-4-trans-hydroxy-L-proline were activated with TBTU to react with the corresponding unblocked amine **6**. Compounds **11** and **12** were synthesized (Scheme 3) simply by a coupling reaction between the pseudopeptidic inhibitors **9**, **10** and compound **3** (to) using the coupling agent COMU ((1-Cyano-2-ethoxy-2-oxoethylideneaminoxy)dimethylamino-morpholino-carbenium hexafluoro-phosphate) in dimethylformamide (DMF) and N,N-diisopropylethylamine (DIPEA). To obtain compounds **13-15** (Figure 4), H-Arg(Pbf) N-terminal protected with a 9-fluorenylmethoxycarbonyl (Fmoc) preloaded in 2-ClTrt resin was used and a solid phase peptide synthesis (SPPS) protocol was utilized. Compounds **13-15** were synthesized using the appropriate aminoacids

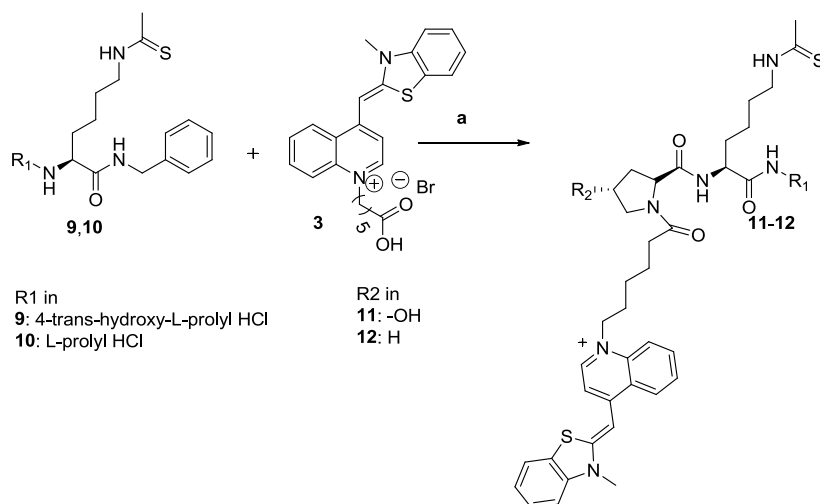
following the Fmoc strategy in which COMU, DIPEA and DMF were used for coupling reaction and piperidine 20% for the deprotection.

Scheme 2^a Synthesis of pseudopeptidic inhibitors



^aReagents and conditions: (a) Ethyl dithioacetate, EtOH/10% (w/v) Na₂CO_{3(aq)}, rt, 12h; (b) appropriate amine or carboxylic acid, TBTU, DMF/Pyridine (1:1), argon flow, rt, 2-3h; (c) 2-propanol, 1,2-ethanedithiol, HCl_(aq) 12N, 15 eq, 60°C, 2-3 h.

Scheme 3^a Preparation of Probes 11, 12



^aReagents and conditions: (a) COMU, DIPEA (10eq), DMF, argon flow, rt, 2-3h.

Cleavage from the resin with TFA 92.5: TIS 2.5: H₂O 2.5 (v/v/v) gave a free carboxylic acid. Initially the purification of **11-15** by RP-HPLC (reverse phase) was carried out using 0.1 % of TFA that allowed the best separation of peaks. However

$^1\text{H-NMR}$ and LC-MS analysis revealed the presence of an impurity generated during the purification and corresponding to the N^ϵ -acetyl methyl (compound **12** Figure 1A $^1\text{H-NMR}$, Figure 2 LC-MS) analogue. Using AcOH 0.05 % this side effect that reduced the final purity of compounds could be reduced but not completely eliminated (compound **12**, Figure 1B $^1\text{H-NMR}$, Figure 3 LC-MS).

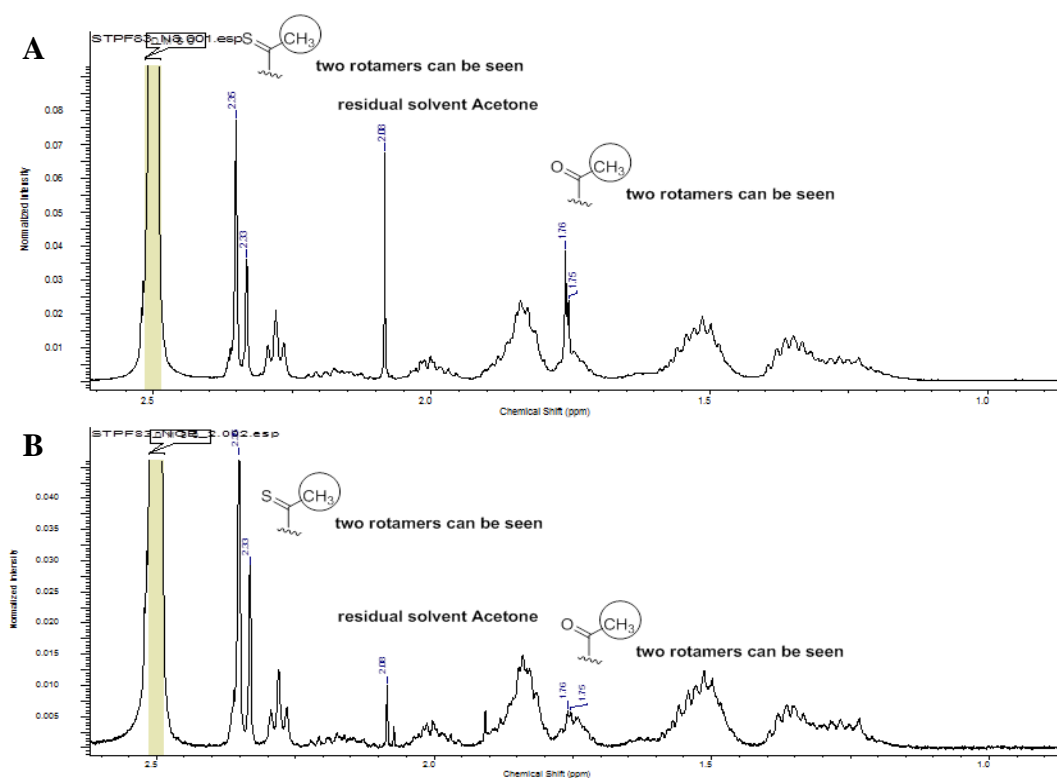


Figure 1. $^1\text{H-NMR}$ window of compound **12** (2.5-1.0 ppm). (A) After purification using 0.1 % TFA; (B) after purification using 0.05 % AcOH (HPLC purity 96 %).

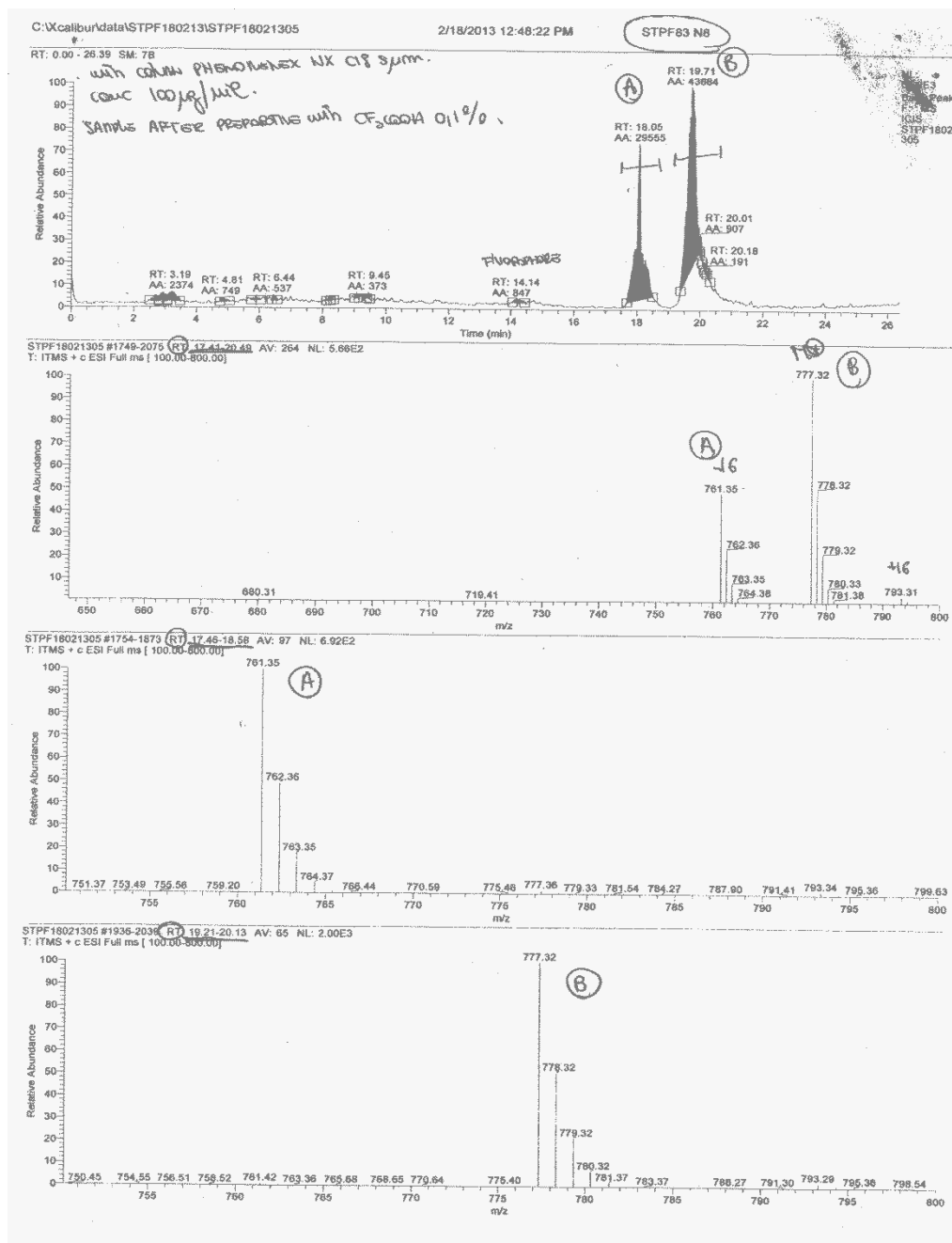


Figure 2. LC-MS of compound **12** after purification with 0.1 % of TFA. (A) Signal corresponding to Acetylated byproduct, Rt: 18 min, M^+ 761.35. (B) Signal corresponding to Thioacetylated product, Rt 19.71 min, M^+ 777.32.

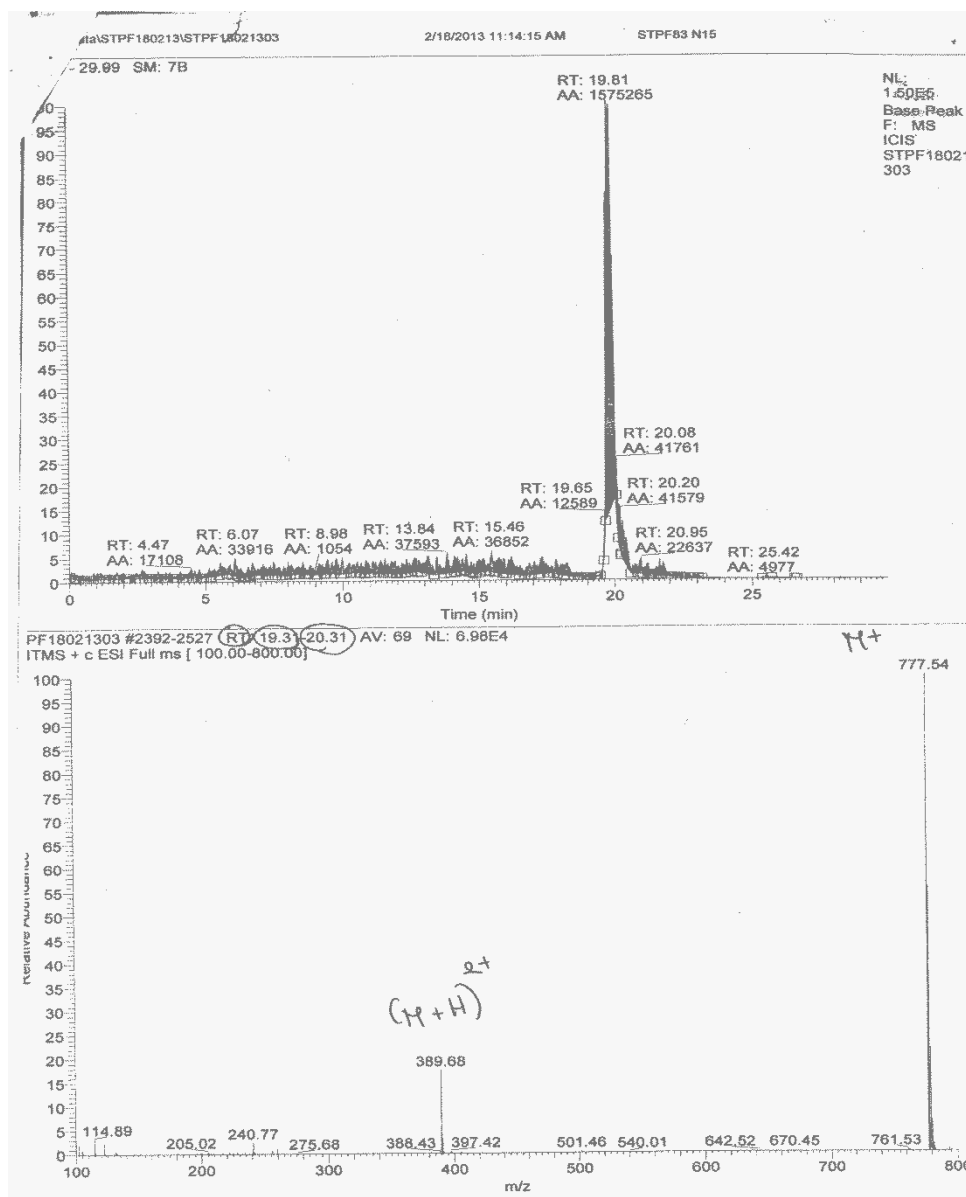
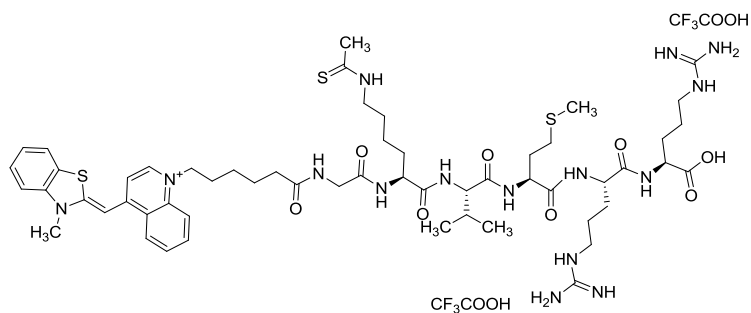
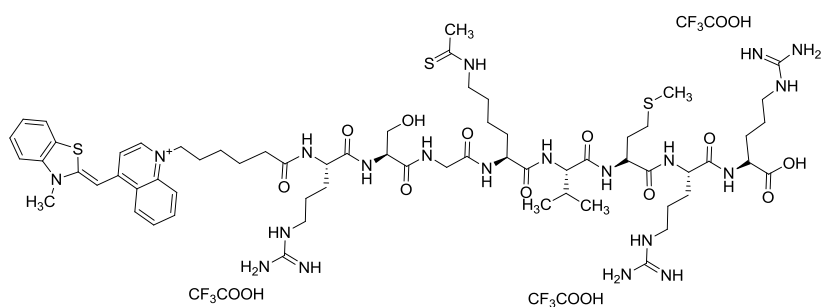


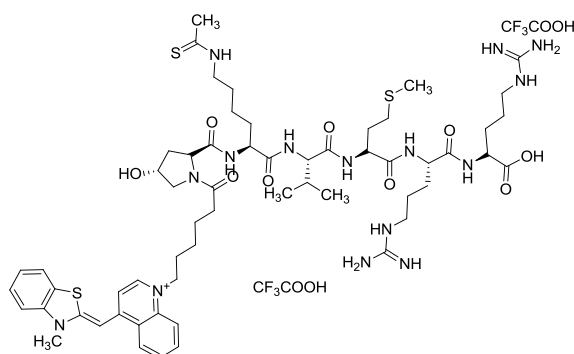
Figure 3. LC-MS of compound **12** after purification with 0.05 % of AcOH. Signal corresponding to Thioacetylated product, Rt: 19.81 min, M^+ 777.54.



Compound 13.



Compound 14.



Compound 15.

Figure 4. Structure of compounds 13-15.

9.3 Results and discussion

Compounds 11 and 12 were designed simply by the idea to detect the subcellular localization of the potential SIRT1-3 inhibitor. The fluorophore Thiazole orange (to) was chosen considering that in the past few years has gained growing attention not only for its high molar extinction coefficient that allows to use it at low concentrations but, mainly for its cell permeability that make it an ideal cellular

fluorophore. As lipophilic cation Thiazole orange rapidly enters in living cells in which can be excited at 511 nm (λ_{max} Abs) and directly observed with an emission at 525 nm (λ_{max} E_m).¹⁹⁸⁻²⁰³ N^ε-Thioacetylated Lys peptide are known substrate competitive inhibitors¹²⁶ of sirtuins, and differently to the smaller pseudopeptidic derivatives the potential binding mode cannot be predicted easily because of too rotatable bonds. In designing **11** and **12**, we had to consider not only the binding mode of pseudopeptidic fragment but also the correct place in which Thiazole orange could be bound to the inhibitor and more importantly, its geometric isomerism. In contrast with the above cited literature¹⁹⁸⁻²⁰³ (Figure 5 left) more specific information regarding the geometric isomerism of Thiazole orange (Figure 5 right) were proposed by Seits²⁰⁴, O'Leary²⁰⁵, Armitage²⁰⁶ and co-workers.

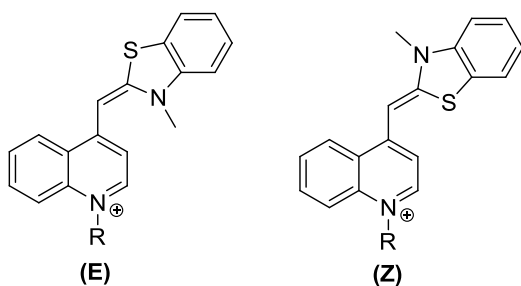


Figure 5. Two potential geometric isomers of Thiazole orange.

From computational to NMR studies they proved that the only isomer detected of Thiazole orange was the (Z). As showed in Figure 6 also in our hands through a simple NOESY spectrum was evident that geometric isomer of Thiazole orange was (Z). Once confirmed the structural isomer, we started to consider in which portion of the pseudopeptidic inhibitor this bulky fluorophore could be bound. The analysis of protein surface close to the substrate binding region of SIRT1-3, together to our previous results¹⁹⁷ suggested that in the N-terminal position of pseudopeptidic inhibitors bulky group might be well tolerated. Again, in Figure 7 the structures of SIRT1-3 reveal a small lipophilic cavity close to the N-terminal site of bound substrate that might accommodate the bulky Thiazole orange. Indeed 4-trans-hydroxy-L-prolyl and L-prolyl moieties that well fit in the substrate binding region were chosen and linked to Thiazole orange using a flexible spacer 6-bromohexanoic acid.

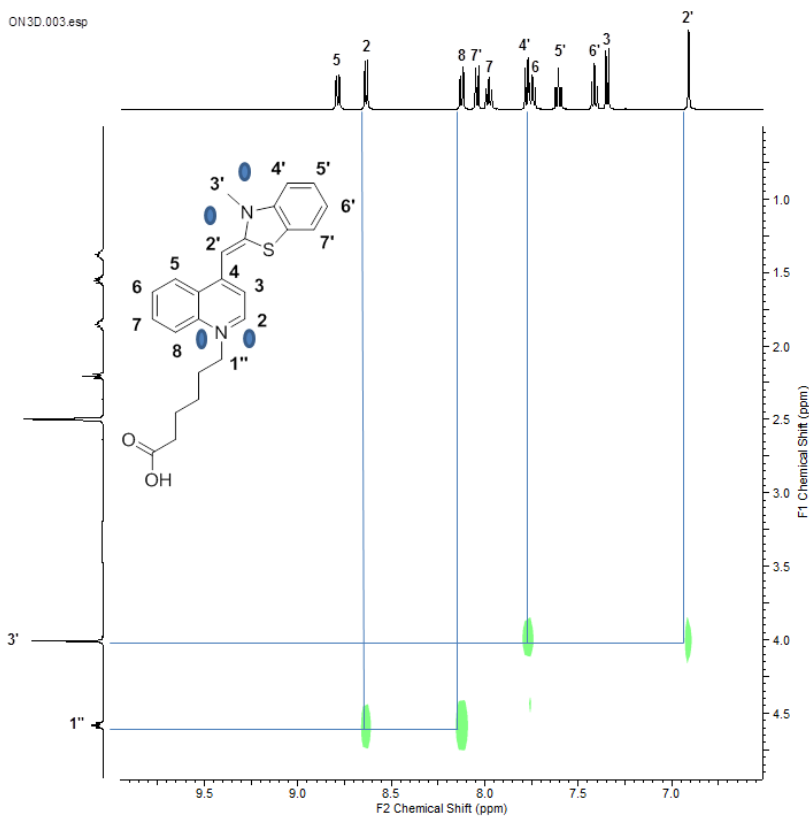


Figure 6. A window of NOESY spectrum of Thiazole orange (**3**). Spectrum processed with ACD/NMR Processor Academic Edition.

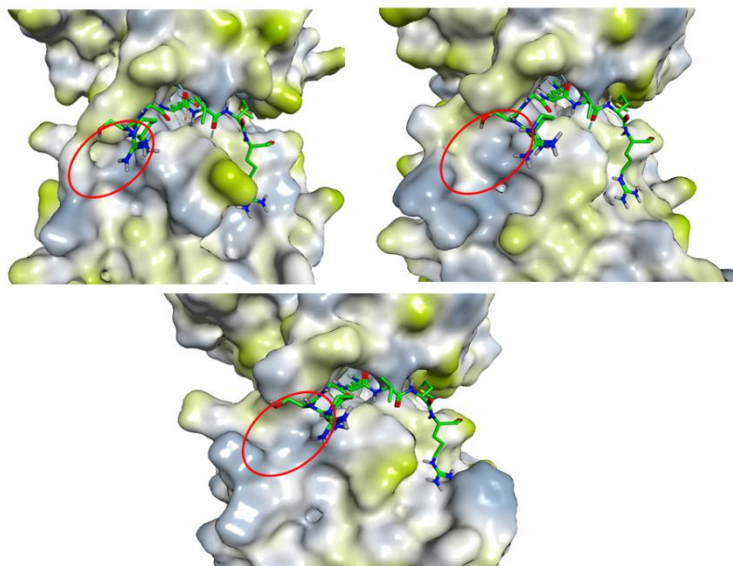


Figure 7. (A) SIRT1 homology model, (B) SIRT2 homology model and (C) SIRT3 crystal structure (PDB: 3GLR). The N-terminal lipophilic cavity is evidenced in red.

After this first approach in which we aimed to develop light-up pseudopeptidic inhibitors to detect their cellular localization, we considered the difficulty to reach the desired target. As introduced previously the seven isoforms SIRT1-7 are differently located within the cellular compartments and it depends upon cell type, stress conditions and interaction with other proteins.³¹ SIRT1 being nuclear but can be also found in cytoplasm in which SIRT2 is predominantly located³². SIRT3 is localized to the mitochondria³³ and that make it a difficult target to reach. As reviewed by Murphy and co-workers²⁰⁷ various strategies have been used to target small molecules to mitochondria, particularly conjugation to lipophilic cations and peptides that let them pass easily through phospholipid bilayers, enabling their accumulation into the mitochondrial matrix in response to the membrane potential. Close to these well-established features, in particular for mitochondrial penetrating peptides (MPP) in which peptides have to incorporate positive charges and lipophilic sidechains, in our case also the potential binding mode of inhibitor must be considered. Compounds **13-15** were designed based on sequence of AceCS2 a known SIRT3 substrate and N-terminal coupled with Thiazole orange. The C-terminal residues from lys642 to 646 of AceCS2 sequence have two positive charges from arginine and lipophilic aminoacids that should respect not only the binding requirements for enzymatic inhibition activity but also the feature for the correct mitochondrial delivery. Compound **13** was designed considering the amino acids beyond positions -1 and +4 (calculating from the N-acetyl-lysine K642), compound **14** considered the amino acids -3 and +4 and finally compound **15** was designed with an N-terminal pseudopeptidic fragment and C-terminal +4 residues of AceCS2 sequence. Biological assays for the above mentioned probes **11-15** are ongoing.

9.4 Conclusion

A new approach in designing sirtuin inhibitors has been carried out. Enzymatic and cellular assays will be performed in order to check the inhibitor subcellular localization and the possibility of a specific mitochondrial delivery. The design of more specific and “intelligent” sirtuin inhibitors could be a new valuable tool for better understands the sirtuin inhibitors.

9.5 Experimental Section

Chemistry. Chemical reagents and solvents used in this study were commercial high purity quality. Organic solutions were dried over anhydrous sodium sulfate. Pyridine and dimethylformamide (DMF) were dried over molecular sieves. The Thiazole orange (to) **3** was obtained following the procedure according to the literature¹⁹⁸. Compounds **4-6** were synthesized following the same procedure previously reported by us.¹⁹⁷ Yields of all reactions refer to the purified products. NMR spectra were acquired on a Bruker Avance 500 AV (Bruker Biospin, Switzerland) spectrometer operating at 500.1 MHz for ¹H and 125.8 MHz for ¹³C. Chemical shift values are reported as δ (ppm) relatively to TMS (tetramethylsilane) as an internal reference; coupling constant are given in Hz. Positive ion mass spectra were recorded with a quadrupole ion trap mass spectrometer (Finnigan MAT, San Jose, CA) equipped with an electrospray ionization source (ESI-MS). The purity of the compounds **7-10** was determined by Elemental analysis obtained by a Thermo Quest CE Instruments EA 1110 CHNS-O elemental analyzer and the Analytical results are within $\pm 0.40\%$ of the theoretical values. The purity of compound **11-15** was determined using Shimadzu LC-10Avp (Shimadzu, Kyoto, Japan) with a reverse phase column (Phenomenex Gemini NX C18, 150 x 4.60mm, 5 μ m) detection at 215nm and 512nm using as solvent A H₂O x 0.05% AcOH and B (CH₃CN/MeOH) x 0.05% AcOH; Flow rate : 1.0 mL/min.

(2S,4R)-N-[(2S)-6-Ethanethioylamino-1-(benzylamino)-1-oxohexan-2-yl]-4

hydroxypyrrolidine-1-tert-butoxycarbonyl-2-carboxamide (7). To a solution of N-Boc-Hydroxy-L-proline (0.72 g, 3.1 mmol) in DMF (30 mL) under Argon flow were added TBTU (1.10 g, 3.4 mmol), pyridine (30 mL) and maintained under stirring for 10min at rt. After this time **6** (1.02 g, 3.1 mmol) was added and the solution mixed 3h at rt under Argon flow. Solvents were evaporated and the obtained oil was dissolved in EtOAc (300 mL), washed with HCl 0.5M, brine (twice), NaHCO₃ 5%, finally dried with Na₂SO₄ and evaporated under vacuo. The crude product obtained was purified by columns chromatography, using silica Kieselgel for

flash with EtOAc : Hexane : MeOH (7: 2: 1) as eluent phase to give the pure product as white solid (0.55 g, 1.10 mmol, 35 %). $^1\text{H-NMR}$ ($\text{DMSO-}d_6$) : rotamers A+B δ = 9.90 (s br, 1H), 8.43 (t, J = 5.67 Hz, 0.6H), 8.25 (t, J = 5.67 Hz, 0.4H), 8.02 (d, J = 7.88 Hz, 0.4H), 7.96 (d, J = 7.88 Hz, 0.6H), 7.30-7.23 (m, 5H), 4.99-4.96 (m, 1H), 4.28-4.20 (m, 5H), 3.44-3.37 (m, 3H), 3.26-3.24 (m, 1H), 2.37 (s, 3H), 2.06-1.99 (m, 1H), 1.87-1.51 (m, 5H), 1.36-1.25 (m, 11H). $^{13}\text{C-NMR}$ ($\text{DMSO-}d_6$) : rotamers A+(B) δ = 198.79 (198.75), 172.35 (171.98), 171.54 (171.49), 154.18 (153.53), 139.28, 128.20, 127.03 (126.94), 126.71 (126.67), 78.87 (78.45), 68.38 (67.71), 58.69 (58.51), 55.02 (54.69), 52.50, 45.31 (45.23), 41.95, 38.41, 32.77, 31.88 (31.30), 28.10 (27.96), 26.90 (26.82), 22.96 (22.91). ESI-MS (m/z): 507.09 [$\text{M} + \text{H}$] $^+$. Anal. ($\text{C}_{25}\text{H}_{38}\text{N}_4\text{O}_5\text{S}$) C, H, N. Calculated: C 59.26, H 7.56, N 11.06; Found: C 59.17, H 7.25, N 10.94.

2S)-N-[(2S)-6-Ethanethiylamino-1-(benzylamino)-1-oxohexan-2-yl]-

pyrrolidine-1-tert-butoxycarbonyl-2-carboxamide (8). To a solution of Boc-L-proline (0.38 g, 1.75 mmol) in DMF (8.5 mL) under Argon flow were added TBTU (0.61 g, 1.9 mmol), pyridine (6.5 mL) and maintained under stirring for 10min at rt. After this time **6** (0.58 g, 1.75 mmol) was added and the solution mixed 3h at rt under Argon flow. Solvents were evaporated and the obtained oil was dissolved in EtOAc (200 mL), washed with HCl 0.5M, brine (twice), NaHCO_3 5%, finally dried with Na_2SO_4 and evaporated under vacuo. The crude product obtained was purified by columns chromatography, using silica Kieselgel for flash with EtOAc : Hexane : MeOH (7: 2.5: 0.5) as eluent phase to give the pure product as white solid (0.58 g, 1.18 mmol, 67 %). $^1\text{H-NMR}$ ($\text{DMSO-}d_6$) : rotamers A+B δ = 9.92 (s br, 1H), 8.43 (t, J = 5.36 Hz, 0.6H), 8.28 (t, J = 5.36 Hz, 0.4H), 7.95-7.92 (m, 1H), 7.33-7.24 (m, 5H), 4.31-4.23 (m, 3H), 4.15-4.13 (m, 1H), 3.46-3.37 (m, 3H), 3.28-3.23 (m, 1H), 2.38 (s, 3H), 2.12-2.03 (m, 1H), 1.82-1.60 (m, 7H), 1.37-1.24 (m, 11H). $^{13}\text{C-NMR}$ ($\text{DMSO-}d_6$) : rotamers A+ (B) δ = 198.78, 172.34 (172.05), 171.53, 153.94 (153.32), 139.27, 128.19, 127.01, 126.96 (126.71), 78.79 (78.36), 59.51 (59.34), 52.40, 46.71 (46.49), 45.23, 41.94, 32.77, 31.92 (31.43), 30.99 (29.71), 28.10 (27.98), 26.85, 23.91 (23.01), 22.92. ESI-MS (m/z): 491.13 [$\text{M} + \text{H}$] $^+$. Anal. ($\text{C}_{25}\text{H}_{38}\text{N}_4\text{O}_4\text{S}$) C, H, N. Calculated: C 61.20, H 7.81, N 11.42; Found: C 60.81, H 7.44, N 11.32.

(2S,4R)-N-[(2S)-6-Ethanethiolyamino-1-(benzylamino)-1-oxohexan-2-yl]-4-hydroxypyrrolidine-2-carboxamide hydrochloride (9). To a solution of **7** (0.28 g, 0.55 mmol) in 2-propanol (8.6 mL), 1,2-ethanedithiol (0.058 mL, 0.55 mmol) was added and after 1 min under stirring at r.t HCl 12N (0.28 mL, 3.36 mmol) was added and the solution heated at 60°C; After 20min and 40min other HCl 12N (0.28 mL) was added; when the total mmol of HCl in the reaction flask were 10.1 mmol, the solution was maintained for 60 min at 60°C under stirring. After this time, 2-propanol was evaporated under reduced pressure and the yellow oil was washed with petroleum ether (4 x 10 mL) and CH₂Cl₂: petroleum ether (1:1) (4 x 4 mL) provides the product as white solid (0.22 g, 0.49 mmol, 90 %). ¹H-NMR (DMSO-*d*₆) : δ = 10.08 (s br, 1H), 9.87 (s br, 1H), 8.79 (d, *J* = 7.57 Hz, 1H), 8.68-8.57 (m, 2H), 7.33-7.22 (m, 5H), 5.51 (s, 1H), 4.42-4.37 (m, 2H), 4.33-4.23 (m, 3H), 3.46-3.42 (m, 2H), 3.07 (d, *J* = 11.98 Hz, 1H), 2.38 (s, 3H), 2.32-2.28 (m, 1H), 1.89-1.83 (m, 1H), 1.75-1.52 (m, 4H), 1.40-1.30 (m, 2H). ESI-MS (*m/z*): 407.28 [M + H]⁺. Anal. (C₂₀H₃₁ClN₄O₃S) C, H, N. Calculated: C 54.22, H 7.05, N 12.65; Found: C 54.11, H 6.74, N 12.52.

(2S)-N-[(2S)-6-Ethanethiolyamino-1-(benzylamino)-1-oxohexan-2-yl]-pyrrolidine-2-carboxamide hydrochloride (10). Compound **10** was synthesized using **8** (0.53 g, 1.1 mmol) in 2-propanol (16 mL), 1,2-ethanedithiol (0.091 mL, 1.1 mmol) and HCl 12N (0.55 mL, 6.6 mmol) added x three times, following the same procedure described for **9**, to furnish the product as white solid (0.35 g, 0.81 mmol, 75 %). ¹H-NMR (DMSO-*d*₆) : δ = 10.09 (s br, 1H), 9.78 (s br, 1H), 8.74 (d, *J* = 7.88 Hz, 1H), 8.61-8.47 (m, 2H), 7.31-7.22 (m, 5H), 4.33-4.21 (m, 4H), 3.46-3.42 (m, 2H), 3.23-3.17 (m, 2H), 2.38 (s, 3H), 2.34-2.26 (m, 1H), 1.92-1.82 (m, 3H), 1.76-1.52 (m, 4H), 1.42-1.27 (m, 2H). ESI-MS (*m/z*): 391.28 [M + H]⁺ Anal. (C₂₀H₃₁ClN₄O₂S) C, H, N. Calculated: C 56.26, H 7.32, N 13.12; Found C 55.93, H 7.00, N 13.01.

to-(2S,4R)-N-[(2S)-6-Ethanethiolyamino-1-(benzylamino)-1-oxohexan-2-yl]-4-hydroxypyrrolidine-2-carboxamide (11).

To a solution of **3** (0.18 g, 0.36 mmol) in DMF (10 mL) under Argon flow were added COMU (0.17 g, 0.40 mmol), DIPEA (0.74 mL) and maintained under stirring for 2 min at rt. After this time **9** (0.16 g, 0.36 mmol) was added and the solution mixed 2h at rt under Argon flow. Solvents were evaporated and the obtained oil was dissolved in CH₂Cl₂ (300 mL), washed with HCl 0.5M, brine (twice), dried with Na₂SO₄, evaporated under vacuo and finally washed with Et₂O (2 x 15 mL). Of the crude product obtained (0.25g) only 0.05 g were purified by preparative RP-HPLC on a C18 column using two steps with preparative column: Phenomenex Gemini NX 5µm C18 150 x 21,2mm to furnish 0.02 g (0.025 mmol) of **11**.

Conditions used for purification:

1. 50mg dissolved in 3.3mL of 45% B (B= (CH₃CN/MeOH)x 0,1% TFA)), Flow : 18mL/min; Gradient : B 45%, 5.00min 52%, 20.00min 100%, 25.00min 100%.
2. 26mg (from the preliminary prep.) dissolved in 2.5mL 40%B, (B= (CH₃CN/MeOH)x 0,05% AcOH), Flow : 16mL/min; Gradient : B 30%, 7.00min 35%, 14.00min 45%, 32.00min 100% STOP.

¹H-NMR (DMSO-*d*₆): rotamers A+B δ = 9.92 (s br, 1H), 8.81-8.78 (m, 1H), 8.61 (d, *J* = 7.25 Hz, 1H), 8.45 (t, *J* = 5.99 Hz, 0.3H), 8.32 (d, *J* = 8.20 Hz, 0.3 H), 8.20 (t, *J* = 5.99 Hz, 0.7H), 8.13-8.10 (m, 1H), 8.06-8.04 (m, 1H), 8.01-7.95 (m, 1.7H), 7.81-7.75 (m, 2H), 7.62 (dt, *J* = 8.51, 1 Hz, 1H), 7.42 (dt, *J* = 8.51, 1 Hz, 1H), 7.38-7.36 (m, 1H), 7.29-7.15 (m, 5H), 6.94 (pseudo d, 1H), 4.58-4.55 (m, 2H), 4.50-4.47 (m, 0.3H), 4.34-4.17 (m, 4.7H), 4.03 (pseudo d, 3H), 3.64-3.61 (m, 1H), 3.46-3.33 (m, 3H), 2.35 (pseudo d, 3H), 2.26-2.14 (m, 2H), 2.03-1.99 (m, 1H), 1.97-1.72 (m, 5H), 1.66-1.44 (m, 5H), 1.41-1.23 (m, 4H). ESI-MS (*m/z*): 793.34 [M]⁺, 794.31 [M + H]⁺, 397.40 [M + H]²⁺. RP-HPLC: Rt. 19.15 min, area percent 92.81% 215 nm.

Quality control:

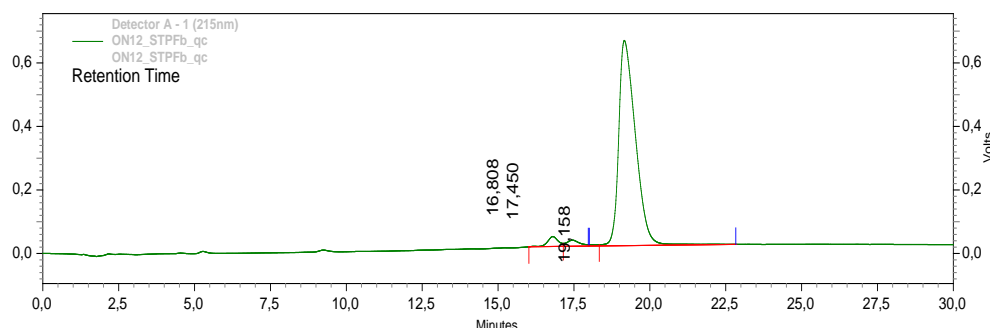
Sample conc. 400µg/mL dissolved in 30% B B = (CH₃CN/MeOH) x 0.05% AcOH

Column: Phenomenex Gemini NX 5µm C18 150x 4.60 mm

Flow: 1mL/min

Gradient: B 30%, 7.00 min 35%, 14.00 min 45%, 30.00 min 100% STOP

Detection: 215/512 nm (reported here 215nm).



Detector A - 1 (215nm)

Pk #	Retention Time	Area	Area %	Height	Height %
1	16,808	1331928	4,991	31228	4,485
2	17,450	584972	2,192	19254	2,765
3	19,158	24770657	92,817	645774	92,750
Totals		26687557	100,000	696256	100,000

to-(2S)-N-[(2S)-6-Ethanethiolyamino-1-(benzylamino)-1-oxohexan-2-yl]-pyrrolidine-2-carboxamide (12). To a solution of **3** (0.30 g, 0.62 mmol) in DMF (12 mL) under Argon flow were added COMU (0.30 g, 0.7 mmol), DIPEA (1.1 mL) and maintained under stirring for 2 min at rt. After this time **10** (0.27 g, 0.63 mmol) was added and the solution mixed 2h at rt under Argon flow. Solvents were evaporated and the obtained oil was dissolved in CH₂Cl₂ (300 mL), washed with HCl 0.5M, brine (twice), dried with Na₂SO₄, evaporated under vacuo. The red gum obtained was solubilized in CH₂Cl₂ and precipitated with cold ether to furnish a red solid (0.40 g). Of the crude product obtained 0.045 g were purified by preparative RP-HPLC using preparative column: Phenomenex Gemini NX 5µm C18 150 x 21,2mm to yield 0.021 g (0.027 mmol) of pure product **12**.

Conditions used for purification:

Solvent A H₂O x 0.05% AcOH and B (CH₃CN/MeOH) x 0.05% AcOH; Flow rate : 18 mL/min Gradient 30% B, 7 min 35%, 14 min 45%, 32 min 100%, Rt: 18.50 min, Area percent 96.0 % 215 nm / 512 nm.

¹H-NMR (DMSO-*d*₆) : rotamers A+B δ = 9.92 (s br, 1H), 8.82-8.78 (m, 1H), 8.61 (d, *J* = 7.19 Hz, 1H), 8.44 (t, *J* = 6.19 Hz, 0.3H), 8.22-8.18 (m, 1H), 8.14 (t, *J* = 8.70 Hz, 1H), 8.06-8.04 (m, 1H), 7.99-7.95 (m, 1H), 7.89 (d, *J* = 8.20 Hz, 0.7H), 7.81-7.74 (m, 2H), 7.62 (td, *J* = 7.53, 1.0 Hz, 1H), 7.43 (td, *J* = 7.53, 1.0 Hz, 1H), 7.37 (m, 1H), 7.29-7.16 (m, 5H), 6.94 (pseudo d, 1H), 4.57 (t, *J* = 7.36 Hz, 2H), 4.41-4.39 (m, 0.4H), 4.32-4.19 (m, 3.6H), 4.03 (pseudo d, 3H), 3.58-3.46 (m, 0.8 H), 3.46-3.35 (m, 3.2H), 2.35 (pseudo d, 3H), 2.29 (m, 1.3H), 2.20-2.14 (m, 0.7H), 2.04-1.98 (m, 1H), 1.92-1.72 (m, 5.8H), 1.68-1.46 (m, 5.2H), 1.40-1.24 (m, 4H). ESI-MS (*m/z*): 777.51 [M]⁺, 778.22 [M + H]⁺, 389.65 [M + H]²⁺. RP-HPLC: Rt. 18.50 min, area percent 96.01% 215 nm.

Quality control:

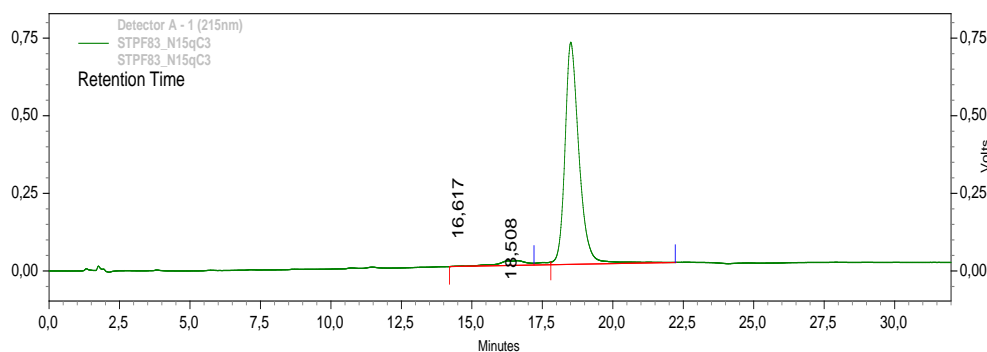
Sample conc: 350µg/mL dissolved in 40% B B = (CH₃CN/MeOH) x 0.05% AcOH

Column: Phenomenex Gemini NX 5µm C18 150x 4.60 mm

Flow: 1mL/min

Gradient: B 30%, 7.00 min 35%, 14.00 min 45%, 32.00 min 100% STOP

Detection: 215/512 nm (reported here 215nm).



Detector A - 1 (215nm)

Pk #	Retention Time	Area	Area %	Height	Height %
1	16,617	1029197	3,989	15051	2,062
2	18,508	24774417	96,011	714984	97,938
Totals		25803614	100,000	730035	100,000

General procedure for the synthesis of 13-15.

H-Arg(Pbf)-2-ClTrt resin (Loading 0.6 mmol/g) was used as solid support for the synthesis of compounds **13-15**. The synthesis was performed in a 10 mL syringe equipped with a frit. H-Arg(Pbf)-2-ClTrt resin was swelled for 2h with 4 mL of DMF. In the coupling phase the selected N^α-Fmoc amino acid (5 equiv) was preactivated (4 min) with the coupling agent COMU (5 equiv) and DIPEA (10 equiv) in 3.5 mL of DMF under argon flow. The obtained solution was added on the resin and shaken for 60 min (the coupling reaction of Arginine and ThioAc-lysine to the resin was repeated two times). After this time, the resin was washed 5 times with DMF (5 x 6 mL). In the deprotection phase, N^α-Fmoc protection was removed with 4 mL of 20% (V/V) piperidine in DMF for 17 min. Then the resin was washed 5 times with DMF (5 x 6 mL). The cycle coupling followed by Fmoc deprotection was repeated until the desired resin-bound peptide was completed. In the last step before to remove the probe from the resin, after the deprotection phase, Thiazole orange (5 equiv) was activated with COMU and coupled using the same condition as well as Fmoc aminoacids (reaction time 1h 30 min). After this step, the resin was washed 5 times with DMF (5 x 6 mL), DCM (5 x 6 mL) and MeOH (5 x 6 mL) and dried overnight under vacuum. The dried resin was shaken in a cleavage cocktail 9.7 mL of TFA: TIS: H₂O V/V/V (92.5: 2.5: 2.5) for 2h the filtered off and washed with other 9.7 mL of cocktail. The light yellow solution obtained contained in a flask is evaporated of 1/4 under vacuum, then placed in ice bed in which Et₂O was added until complete precipitation of product as orange-red solid.

to-Gly-Lys-(ThioAc)-Val-Met-Arg-Arg-COOH (**13**)

Crude product 0.154 g (using 0.096 mmol, 0.150 g of resin).

Purification:

0.035 g of crude product were dissolved in 3,5 mL 10% B (B = (CH₃CN/MeOH)x 0,05% AcOH); Flow : 8mL/min; Gradient : B 10%, 20.00min 45%, 26.00min 60%, 35.00min 60% STOP. Preparative column used: Supelcogel ODP-50 5μm C18 250 x 21,2mm. 0.015 g (0.012 mmol) of pure compound **13** were obtained. ESI-MS (*m/z*): 1190.51 [M]⁺, 596.04 [M + H]²⁺, 397.95 [M + 2H]³⁺. RP-HPLC Rt. 15.57 min, area percent 96.74% 215 nm.

Quality control:

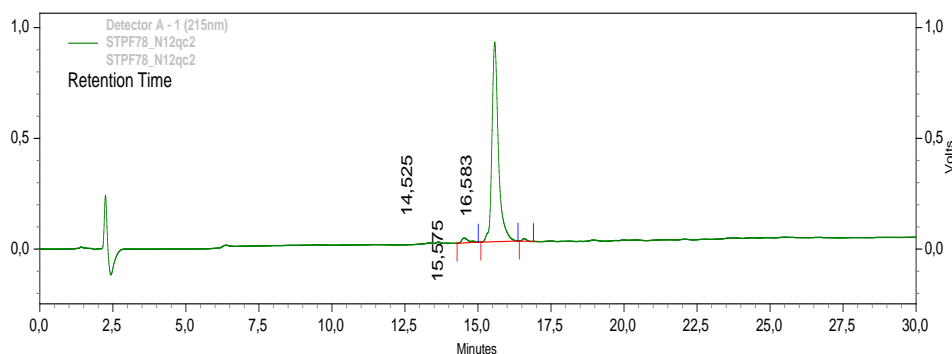
Sample conc: 600µg/mL dissolved in 20% CH₃CN

Column: Phenomenex Gemini NX 5µm C18 150x 4.60 mm

Flow: 1mL/min

Gradient: B 10%, 20.00 min 45%, 30.00 min 60% STOP (B= CH₃CN/MeOH) x 0.05% AcOH

Detection: 215/512 nm (reported here 215nm).



Detector A - 1 (215nm)

Pk #	Retention Time	Area	Area %	Height	Height %
1	14,525	358566	2,493	21768	2,329
2	15,575	13917091	96,746	900973	96,396
3	16,583	109592	0,762	11916	1,275
Totals		14385249	100,000	934657	100,000

to-Arg-Ser-Gly-Lys-(ThioAc)-Val-Met-Arg-Arg-COOH (14)

Crude product 0.136 g (using 0.096 mmol, 0.150 g of resin).

Purification:

0.025 g of crude product were dissolved in 3,0 mL 10% B, (B = (CH₃CN/MeOH)x 0,05% AcOH), Flow : 8mL/min; Gradient : B 10%, 20.00 min 45%, 26.00 min 60%, 30.00 min 60% STOP. Preparative column used: Supelcogel ODP-50 5µm C18 250 x 21,2mm. 0.018 g (0.012 mmol) of **14** as red solid were obtained. ESI-MS (*m/z*): 717.62 [M + H]²⁺, 478.99 [M + 2H]³⁺, 359.52 [M + 3H]⁴⁺. RP-HPLC Rt: 11.33 min, area percent 86.64% 215 nm.

Quality control:

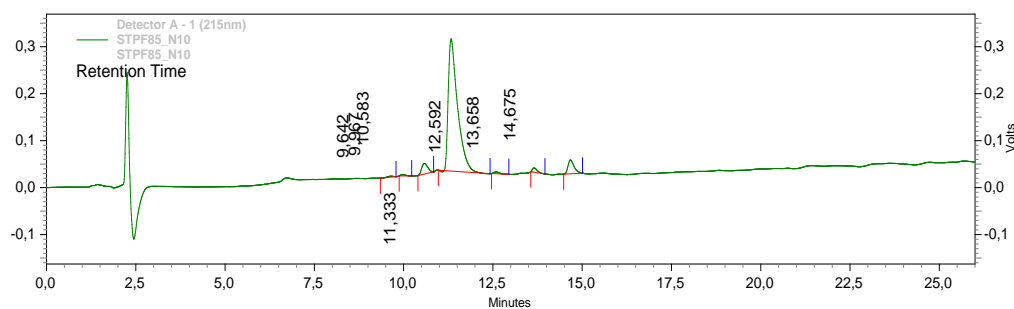
Sample conc: 600µg/mL dissolved in 20% CH₃CN

Column: Phenomenex Gemini NX 5µm C18 150x 4.60 mm

Flow: 1mL/min

Gradient: B 10%, 20.00 min 45%, 26.00 min 60% STOP (B = CH₃CN/MeOH) x 0.05% AcOH)

Detection: 215/512 nm (reported here 215nm).



Detector A - 1 (215nm)

Pk #	Retention Time	Area	Area %	Height	Height %
1	9,642	20011	0,340	1849	0,528
2	9,967	26563	0,452	2704	0,772
3	10,583	268182	4,559	22513	6,429
4	11,333	5096476	86,640	281078	80,273
5	12,592	37804	0,643	3705	1,058
6	13,658	81887	1,392	9014	2,574
7	14,675	351415	5,974	29289	8,365
Totals		5882338	100,000	350152	100,000

to-Pro(OH)-Lys-(ThioAc)-Val-Met-Arg-Arg-COOH (15)

Crude product: 0.128 g (using 0.096 mmol, 0.150 g of resin).

Purification:

0.041 g of crude product were dissolved in 4,0 mL 10% B, (B = (CH₃CN/MeOH)x 0,05% AcOH), Flow : 8mL/min; Gradient : B 10%, 20.00 min 45%, 26.00 min 60%, 40.00 min 60% STOP. Preparative column used: Supelcogel ODP-50 5µm C18 250 x 21,2mm. 0.019 g (0.015 mmol) of **15** as red solid were obtained. ESI-MS (*m/z*): 1246.42 [M]⁺, 624.05 [M + H]²⁺, 416.60 [M + 2H]³⁺. RP-HPLC Rt. 16.10 min, area percent 96.77% 215 nm (this is a preliminary result that has to be confirmed the final data is not available yet).

10 DESIGN AND SYNTHESIS OF PYRIDINIUM SALTS AS INHIBITORS OF HUMAN SIRTUINS

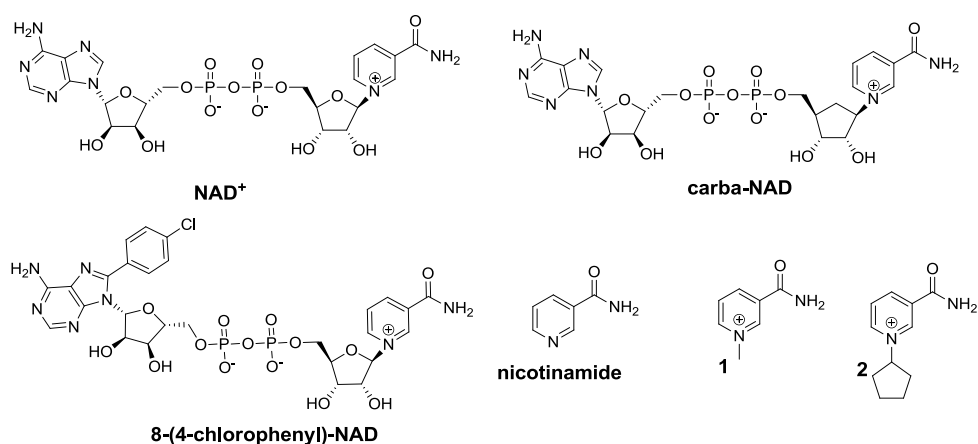
Abstract: Starting from the chemical structure of nicotinamide and NAD^+ a small array of pyridinium salts was synthesized and screened against SIRT1. Compound **6** that that showed the best SIRT1 inhibition was assayed also against SIRT2. Compound **6** slightly increased acetyl p53 and acetyl-a-tubulin levels, without affect cell viability of U937 cells.

*Adapted with the permission from Mellini, P.; Carafa, V.; Altucci, L.; Mai A.

10.1 Introduction

From yeast to human sirtuins the NAD^+ binding site has been found highly conserved. NAD^+ binds in a cleft adjacent to the acetyl lysine side chain that is formed by three pockets: A, B, C. The adenine-ribose binding site (pocket A) is an exposed surface area in which adenine has H bonds with backbone amides Leu215, Val232 and side chains Asp231 and Thr26 (Sirt2Tm numbering PDB code: 2H4F). The ribose moiety has H bond with Gly216²⁶, the phosphate groups binds between A and B pockets and show several H bonds with Ala22, Phe33, Arg34, Ser189, Ser190 and with a conserved water molecule.²⁶ Conserved residues His116 and Phe33 located in the B pocket makes H bonds and van der Waals interactions with the nicotinamide ribose ring. Finally the nicotinamide moiety is positioned in hydrophobic cavity the so called C pocket and forms H bonds interactions with Ile100, Asp101 and a conserved water molecule.²⁶ The design of NAD^+ mimetic compounds represents one of the first approaches used to develop sirtuin inhibitors (Chart 1).¹²¹⁻¹²⁴ Unfortunately due to their poor cellular permeability, stability and negligible drug-like properties NAD^+ mimetics are considered only useful molecular probes. In 2006 Suzuki et al.¹¹⁰ reported the screening of a homemade library of compounds comprised also by pyridinium salts of nicotinamide (**1**, **2** Chart 1) that at 300 μM showed only a weak or null inhibition against SIRT1. In this work, we aim to start the first step in order to move from NAD^+ structure to drug-like molecules inhibitors of human sirtuins. Considering both the structural features of nicotinamide and NAD^+ (Chart 1), we designed a small array of simple pyridinium salts (**3-6**) as potential nicotinamide/ NAD^+ mimetic compounds (Scheme 1).

Chart 1. Structure of NAD^+ , nicotinamide and their derivatives.

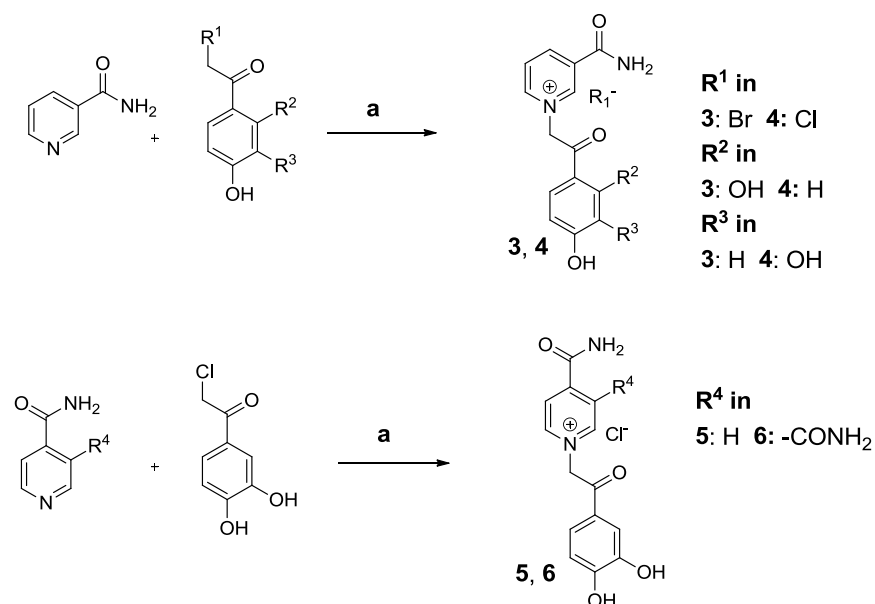


The compounds were screened at 50 μM in vitro against SIRT1. One compound was selected for be tested also on SIRT2 and for cellular studies.

10.2 Chemistry

The synthetic pathway followed for the preparation of **3-6** is depicted in Scheme 1. Compounds **3-6** were synthesized simply by reacting of substituted pyridine with the appropriate alkylating agent in CH_3CN or DMA at reflux for 4-24h.

Scheme 1^a



^aReagents and conditions: **3-5** CH_3CN reflux 4-24h; **6** N,N-Dimethylacetamide (DMA) reflux 14h.

10.3 Results and discussion

Compounds **3-6** were designed considering how described above, or else the fact that NAD^+ binding site offers the possibility of several H-bonds interactions. The pyridine ring has been functionalized with an acetophenon moiety and hydroxyl

groups that allow not only an appreciable flexibility (Figure 1) of the scaffold but also the possibility of H-bond interactions.

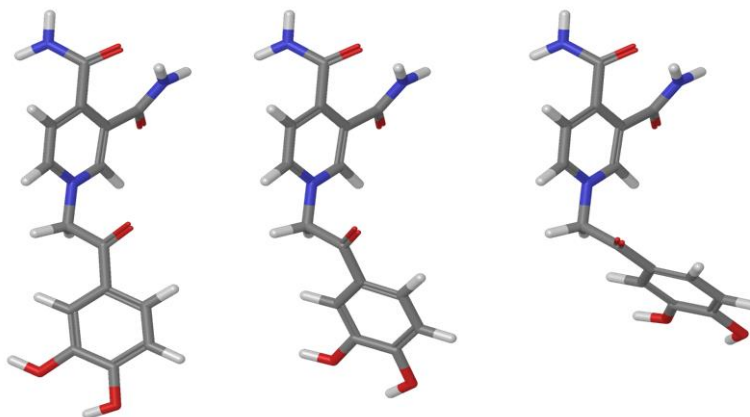


Figure 1. Two rotamers of the minimized structure (left) of compound **6** generated by rotation around the C α carbon of acetophenone moiety. Maestro 9.2 Schrödinger, LLC, New York, NY, 2011.

Compounds **3-6** screened at 50 μ M against SIRT1 show an appreciable inhibition activity that range from 20-42 % of inhibition (Figure 2). Little differences can be seen and let us speculate that the best inhibition showed by compound **6** is due to the additional carbamoyl function, but this has to be confirmed with an exhaustive SAR investigation. Compound **6** that can be considered our new starting point for develop more potent compounds, has been also tested against SIRT2 (Figure 2) for which shows the same trend of inhibition seen for SIRT1.

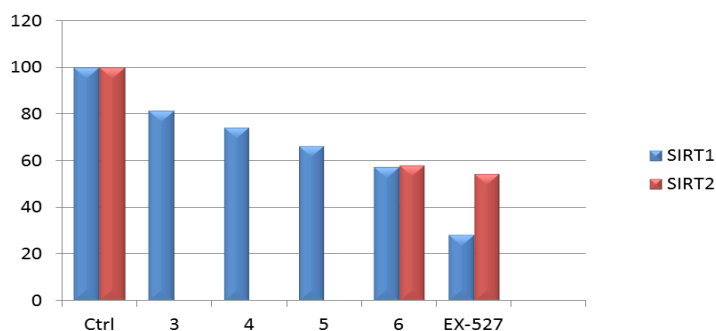


Figure 2. Inhibitory activity of compounds **3-6** at 50 μ M against SIRT1 (blue) and SIRT2 (red). The data represent the mean of two experiment (standard deviation is not reported).

SIRT1/2 inhibition by compound **6** was confirmed by Western blot analyses (Figure 3). The acetylation levels of α -tubulin and p53 (MCF-7 cells) were determined after the treatment with 50 μ M of **6**. EX-527, etoposide (10 μ M) and SAHA (5 μ M) were used as reference compounds.

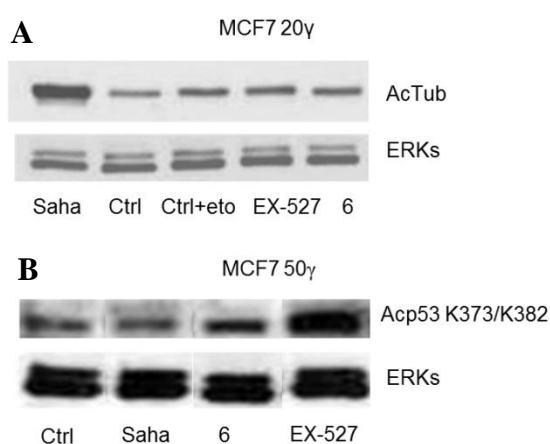


Figure 3. Western blot analyses of compound **6** (50 μ M). A) α -tubulin acetylation; B) p53 acetylation in MCF-7 cells. EX-527, etoposide (10 μ M) and SAHA (5 μ M) were used as reference compounds.

Compound **6** showed a little but significant increase of α -tubulin and p53 acetylation these evidences let us speculate that at the condition used compound **6** is cell permeable. The effect of **6** on cell cycle progression was evaluated and at 50 μ M for 30 h in the human U937 leukemia cell line. As shown in Figure 4 differently to SAHA and MS275 compound **6** does not cause any detectable effect under the tested conditions.

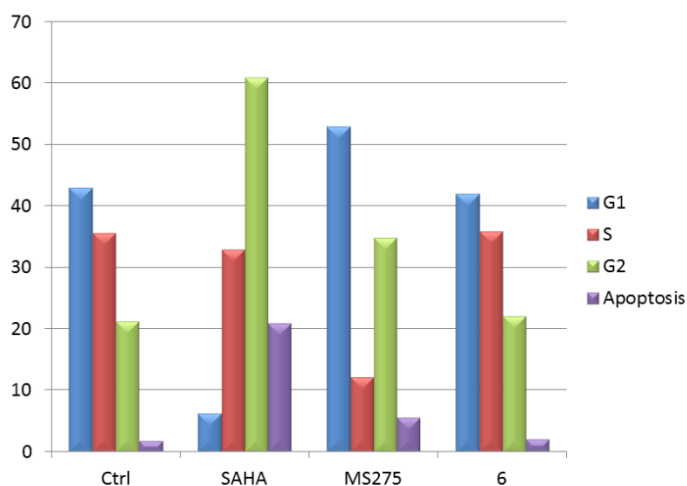


Figure 4. Cell cycle effect in a given phase of cell cycle and apoptosis induction of compound **6** in U937 cells (50 μ M, 30h). SAHA and MS275 (5 μ M) were used as reference compounds.

10.4 Conclusions

A small array of pyridinium salts has been synthesized and screened against SIRT1. One of them, compound **6** was found the first pyridinium salt reported to date with SIRT1/2 inhibition properties. Compound **6** might be a new starting point for a SAR investigation in order to find more potent derivatives.

10.5 Experimental Section

Chemistry. Chemical reagents including carprofen and solvent used in this study were purchased from Sigma-Aldrich Chemical Co. (Milano, Italy) and were of analytical grade. Melting points were determined on a Tottoli apparatus (Buchi) and are uncorrected. Infrared spectra were recorded on neat compounds on a Perkin-Elmer Spectrum-One spectrophotometer equipped with an ATR detector; band frequencies are reported in wave number (cm^{-1}). ^1H NMR spectra were acquired on a Bruker Avance 400 spectrometer operating at 400 MHz. Chemical shift values, unless otherwise stated, are reported as δ (ppm) relatively to TMS (tetramethylsilane) as internal reference; coupling constants are given in Hz. Yields of all reactions refer to the purified products. Mass spectra were recorded on: API-TOF Mariner by Perspective Biosystem (Stratford, Texas, USA), samples were injected by an Harvard pump using a flow rate of 5-10 $\mu\text{l}/\text{min}$, infused in the Electrospray system. Elemental analyses were obtained by a PE 2400 (Perkin-Elmer) analyser and have been used to determine purity of the described compounds, that is $>95\%$. Analytical results are within $\pm 0.40\%$ of the theoretical values.

3-carbamoyl-1-(2-(2,4-dihydroxyphenyl)-2-oxoethyl)pyridin-1-ium bromide (3).

To a warm solution of 2-bromo-1-(2,4-dihydroxyphenyl)ethanone (0.286 g, 1.2 mmol) in CH_3CN (4 mL) a solution of nicotinamide (0.151 g, 1.2 mmol) in CH_3CN (4 mL) in was added and refluxed for 4h. After this time the obtained precipitate was filtered off and washed with CH_3CN (3 x 10 mL), Et_2O (3 x 10 mL) and dried under reduced pressure to furnish **3** (0.28 g, 0.78 mmol, 65.47 %). ^1H -NMR ($\text{DMSO}-d_6$): δ = 11.23 (s br, 1H), 10.65 (s br, 1H), 9.45 (s, 1H), 9.10 (d, J = 6.11 Hz, 1H), 9.03 (d, J = 6.11 Hz, 1H), 8.57 (s, 1H), 8.35-8.32 (m, 1H), 8.17 (s, 1H), 7.73 (d, J = 8.80 Hz, 1H), 6.46-6.43 (m, 2H), 6.23 (s, 2H). ESI-MS (m/z): 273.10 $[\text{M}]^+$. Anal. ($\text{C}_{14}\text{H}_{13}\text{BrN}_2\text{O}_4$) Calculated: C 47.61, H 3.71, N 7.93; Found: C 47.41, H 3.53, N 7.77.

3-carbamoyl-1-(2-(3,4-dihydroxyphenyl)-2-oxoethyl)pyridin-1-ium chloride (4).

To a warm solution of 2-chloro-1-(3,4-dihydroxyphenyl)ethanone (1.23 g, 6.6 mmol) in CH_3CN (20 mL) a solution of nicotinamide (0.40 g, 3.3 mmol) in CH_3CN (7 mL)

in was added and refluxed for 24h. After this time the obtained precipitate was filtered off and washed with EtOAc (3 x 10 mL), Et₂O (3 x 10 mL) and dried under reduced pressure to furnish **4** (0.62 g, 2.0 mmol, 60.85 %). ¹H-NMR (DMSO-*d*₆): δ = 9.52 (s, 1H), 9.13-9.11 (m, 2H), 8.74 (s br, 1H), 8.37-8.34 (m, 1H), 8.17 (s br, 1H), 7.48-7.44 (m, 2H), 6.99 (d, *J* = 8.31 Hz, 1H), 6.42 (s, 2H). ESI-MS (*m/z*): 273.14 [M]⁺. Anal. (C₁₄H₁₃ClN₂O₄) Calculated: C 54.47, H 4.24, N 9.07; Found: C 54.80, H 4.35, N 9.15.

4-carbamoyl-1-(2-(3,4-dihydroxyphenyl)-2-oxoethyl)pyridin-1-ium chloride (5).

To a warm solution of 2-chloro-1-(3,4-dihydroxyphenyl)ethanone (1.21 g, 6.5 mmol) in CH₃CN (10 mL) a solution of nicotinamide (0.40 g, 3.3 mmol) CH₃CN (15 mL) in was added and refluxed for 12h. After this time the obtained precipitate was filtered off and washed with CH₃CN (3 x 10 mL), EtOAc (3 x 10 mL) and dried under reduced pressure to furnish **5** (0.48 g, 1.55 mmol, 47.11 %). ¹H-NMR (DMSO-*d*₆): δ = 10.01 (s br, 2H), 9.14 (d, *J* = 6.36 Hz, 2H), 8.82 (s br, 1H), 8.54 (d, *J* = 6.36 Hz, 2H), 8.29 (s br, 1H), 7.49-7.45 (m, 2H), 6.99 (d, *J* = 8.31 Hz, 1H), 6.42 (s, 2H). ESI-MS (*m/z*): 273.11 [M]⁺. Anal. (C₁₄H₁₃ClN₂O₄) Calculated: C 54.47, H 4.24, N 9.07; Found: C 54.52, H 4.50, N 9.21.

3,4-dicarbamoyl-1-(2-(3,4-dihydroxyphenyl)-2-oxoethyl)pyridin-1-ium chloride (6).

To a warm solution of 2-chloro-1-(3,4-dihydroxyphenyl)ethanone (1.13 g, 6.0 mmol) in DMA (3 mL) a solution of pyridine-3,4-dicarboxamide (0.50 g, 3.0 mmol) was added and refluxed for 14h. After this time EtOAc was added until the precipitation of compound was completed, then the precipitate was filtered off and washed with EtOAc (3 x 15 mL) and MeOH (3 x 15 mL). The solid obtained was dissolved under reflux in a mixture MeOH/CH₃CN 1:1 (V/V) and after cooling was slowly precipitated with cold Et₂O dried under reduced pressure to furnish **6** (0.25 g, 0.71 mmol, 23.6 %). ¹H-NMR (DMSO-*d*₆): δ = 10.05 (s br, 2H), 9.28 (s, 1H), 9.10 (d, *J* = 6.36 Hz, 1H), 8.50 (s, 1H), 8.31-8.27 (m, 2H), 8.16 (s, 1H), 8.04 (s, 1H), 7.48-7.43 (m, 2H), 6.98 (d, *J* = 8.07 Hz, 1H), 6.36 (s, 2H). ESI-MS (*m/z*): 316.13 [M]⁺.

Anal. (C₁₅H₁₄ClN₃O₅) Calculated: C 51.22, H 4.01, N 11.95; Found: C 51.60, H 4.13, N 11.72.

SIRT1/2 Inhibition Assay. The SIRT activity assay was performed using human recombinant SIRT1 and SIRT2 produced in *E. coli*. Compounds were tested using a modified Fluor de Lys fluorescence-based assay kit (AK-555, AK-556 BIOMOL). The assay procedure has two steps: in the first part the SIRT1/2 substrate, an acetylated Lys side chain comprising amino acids 379-382 (Arg-His-Lys-Lys (Ac)) (for SIRT1 assay) or 317-320 (Gln-Pro-Lys-Lys(Ac)) (for SIRT2 assay) of human p53 conjugated with aminomethylcoumarin is deacetylated during incubation at 37 °C for 1 h by SIRT1 or SIRT2 in the presence of NAD⁺ and the tested compounds. The second stage is initiated by the addition of the Developer II, including nicotinamide (NAM), a sirtuin inhibitor that stops the SIRT1/2 activity, and the fluorescent signal is produced. The fluorescence was measured on a fluorometric reader (Inphinite 200 TECAN) with excitation set at 360 nm and emission detection set at 460 nm. Experiments on the SIRT1 and 2 inhibitions have been performed in triplicate. IC₅₀ data were analyzed using GraphPad Prism Software.

Cell lines. Human leukemia cell lines (U937) was grown in RPMI 1640 medium (EuroClone) supplemented with 10% heat-inactivated FBS (Sigma Aldrich), 1% glutamine (EuroClone), 1% penicillin/streptomycin (EuroClone) and 0.1% gentamycin (EuroClone), and kept at 37°C in air and 5% CO₂. Conversely, adherent MCF7 (human breast cancer) cells were grown in D-MEM medium (EuroClone) supplemented with the same components described above and in the same incubation settings.

Western Blot analyses of p53 and α -tubulin acetylation. To detect acetylation of p53 (K373/382) and α -tubulin, 50 μ g and 20 μ g of total protein extracts (MCF7 cells), respectively, were separated on a 10% polyacrylamide gels and blotted for 2 h at 70V. Western blots were shown for acetylated p53 (K373/382) (Upstate, dilution

1:500) and α -tubulin (Sigma, dilution 1:1000). Total ERKs (Santa Cruz, dilution 1:1000) represent equal loading.

Cell Cycle and Cell death Analysis on U937 cells. Cells were collected and resuspended in 500 μ L of hypotonic buffer (0.1% Triton X-100, 0.1% sodium citrate, 50 μ g/mL propidium iodide (PI)). Then the cells were incubated in the dark for 30 min. Samples were acquired on a FACS-Calibur flow cytometer using the Cell Quest software (Becton Dickinson). Analyses were performed with standard procedures using ModFit LT version3 software (Verity). All experiment were performed in triplicate.

11 REFERENCES

- (1) Rodriguez, A.; Bjerling, P. The Links between Chromatin Spatial Organization and Biological Function. *Biochem. Soc. Trans.* **2013**, *41*, 1634–1639.
- (2) Tachiwana, H.; Kagawa, W.; Osakabe, A.; Kawaguchi, K.; Shiga, T.; Hayashi-Takanaka, Y.; Kimura, H.; Kurumizaka, H. Structural Basis of Instability of the Nucleosome Containing a Testis-Specific Histone Variant, Human H3T. *Proc. Natl. Acad. Sci. U. S. A.* **2010**, *107*, 10454–10459.
- (3) Bártoová, E.; Krejčí, J.; Harnicarová, A.; Galiová, G.; Kozubek, S. Histone Modifications and Nuclear Architecture: A Review. *J. Histochem. Cytochem. Off. J. Histochem. Soc.* **2008**, *56*, 711–721.
- (4) Helin, K.; Dhanak, D. Chromatin Proteins and Modifications as Drug Targets. *Nature* **2013**, *502*, 480–488.
- (5) Jenuwein, T.; Allis, C. D. Translating the Histone Code. *Science* **2001**, *293*, 1074–1080.
- (6) Grunstein, M. Histone Acetylation in Chromatin Structure and Transcription. *Nature* **1997**, *389*, 349–352.
- (7) Wolffe, A. P.; Guschin, D. Review: Chromatin Structural Features and Targets That Regulate Transcription. *J. Struct. Biol.* **2000**, *129*, 102–122.
- (8) Strahl, B. D.; Allis, C. D. The Language of Covalent Histone Modifications. *Nature* **2000**, *403*, 41–45.
- (9) Yang, X.-J.; Seto, E. The Rpd3/Hda1 Family of Lysine Deacetylases: From Bacteria and Yeast to Mice and Men. *Nat. Rev. Mol. Cell Biol.* **2008**, *9*, 206–218.
- (10) Klar, A. J.; Fogel, S.; Macleod, K. MAR1-a Regulator of the HMa and HMalpha Loci in SACCHAROMYCES CEREVISIAE. *Genetics* **1979**, *93*, 37–50.
- (11) Gottlieb, S.; Esposito, R. E. A New Role for a Yeast Transcriptional Silencer Gene, SIR2, in Regulation of Recombination in Ribosomal DNA. *Cell* **1989**, *56*, 771–776.

- (12) Aparicio, O. M.; Billington, B. L.; Gottschling, D. E. Modifiers of Position Effect Are Shared between Telomeric and Silent Mating-Type Loci in *S. Cerevisiae*. *Cell* **1991**, *66*, 1279–1287.
- (13) Braunstein, M.; Rose, A. B.; Holmes, S. G.; Allis, C. D.; Broach, J. R. Transcriptional Silencing in Yeast Is Associated with Reduced Nucleosome Acetylation. *Genes Dev.* **1993**, *7*, 592–604.
- (14) Brachmann, C. B.; Sherman, J. M.; Devine, S. E.; Cameron, E. E.; Pillus, L.; Boeke, J. D. The SIR2 Gene Family, Conserved from Bacteria to Humans, Functions in Silencing, Cell Cycle Progression, and Chromosome Stability. *Genes Dev.* **1995**, *9*, 2888–2902.
- (15) Derbyshire, M. K.; Weinstock, K. G.; Strathern, J. N. HST1, a New Member of the SIR2 Family of Genes. *Yeast Chichester Engl.* **1996**, *12*, 631–640.
- (16) Frye, R. A. Characterization of Five Human cDNAs with Homology to the Yeast SIR2 Gene: Sir2-like Proteins (sirtuins) Metabolize NAD and May Have Protein ADP-Ribosyltransferase Activity. *Biochem. Biophys. Res. Commun.* **1999**, *260*, 273–279.
- (17) Frye, R. A. Phylogenetic Classification of Prokaryotic and Eukaryotic Sir2-like Proteins. *Biochem. Biophys. Res. Commun.* **2000**, *273*, 793–798.
- (18) Landry, J.; Slama, J. T.; Sternglanz, R. Role of NAD(+) in the Deacetylase Activity of the SIR2-like Proteins. *Biochem. Biophys. Res. Commun.* **2000**, *278*, 685–690.
- (19) Smith, J. S.; Brachmann, C. B.; Celic, I.; Kenna, M. A.; Muhammad, S.; Starai, V. J.; Avalos, J. L.; Escalante-Semerena, J. C.; Grubmeyer, C.; Wolberger, C.; Boeke, J. D. A Phylogenetically Conserved NAD⁺-Dependent Protein Deacetylase Activity in the Sir2 Protein Family. *Proc. Natl. Acad. Sci. U. S. A.* **2000**, *97*, 6658–6663.
- (20) Smith, B. C.; Denu, J. M. Sir2 Protein Deacetylases: Evidence for Chemical Intermediates and Functions of a Conserved Histidine. *Biochemistry (Mosc.)* **2006**, *45*, 272–282.
- (21) Barber, M. F.; Michishita-Kioi, E.; Xi, Y.; Tasselli, L.; Kioi, M.; Moqtaderi, Z.; Tennen, R. I.; Paredes, S.; Young, N. L.; Chen, K.; Struhl, K.; Garcia, B. A.;

- Gozani, O.; Li, W.; Chua, K. F. SIRT7 Links H3K18 Deacetylation to Maintenance of Oncogenic Transformation. *Nature* **2012**, *487*, 114–118.
- (22) Dölle, C.; Rack, J. G. M.; Ziegler, M. NAD and ADP-Ribose Metabolism in Mitochondria. *FEBS J.* **2013**, *280*, 3530–3541.
- (23) Du, J.; Zhou, Y.; Su, X.; Yu, J. J.; Khan, S.; Jiang, H.; Kim, J.; Woo, J.; Kim, J. H.; Choi, B. H.; He, B.; Chen, W.; Zhang, S.; Cerione, R. A.; Auwerx, J.; Hao, Q.; Lin, H. Sirt5 Is a NAD-Dependent Protein Lysine Demalonylase and Desuccinylase. *Science* **2011**, *334*, 806–809.
- (24) Gil, R.; Barth, S.; Kanfi, Y.; Cohen, H. Y. SIRT6 Exhibits Nucleosome-Dependent Deacetylase Activity. *Nucleic Acids Res.* **2013**, *41*, 8537–8545.
- (25) Jiang, H.; Khan, S.; Wang, Y.; Charron, G.; He, B.; Sebastian, C.; Du, J.; Kim, R.; Ge, E.; Mostoslavsky, R.; Hang, H. C.; Hao, Q.; Lin, H. SIRT6 Regulates TNF- α Secretion through Hydrolysis of Long-Chain Fatty Acyl Lysine. *Nature* **2013**, *496*, 110–113.
- (26) Hoff, K. G.; Avalos, J. L.; Sens, K.; Wolberger, C. Insights into the Sirtuin Mechanism from Ternary Complexes Containing NAD⁺ and Acetylated Peptide. *Struct. Lond. Engl. 1993* **2006**, *14*, 1231–1240.
- (27) Hawse, W. F.; Hoff, K. G.; Fatkins, D. G.; Daines, A.; Zubkova, O. V.; Schramm, V. L.; Zheng, W.; Wolberger, C. Structural Insights into Intermediate Steps in the Sir2 Deacetylation Reaction. *Struct. Lond. Engl. 1993* **2008**, *16*, 1368–1377.
- (28) Davenport, A. M.; Huber, F. M.; Hoelz, A. Structural and Functional Analysis of Human SIRT1. *J. Mol. Biol.* **2013**.
- (29) Moniot, S.; Schutkowski, M.; Steegborn, C. Crystal Structure Analysis of Human Sirt2 and Its ADP-Ribose Complex. *J. Struct. Biol.* **2013**, *182*, 136–143.
- (30) Jin, L.; Wei, W.; Jiang, Y.; Peng, H.; Cai, J.; Mao, C.; Dai, H.; Choy, W.; Bemis, J. E.; Jirousek, M. R.; Milne, J. C.; Westphal, C. H.; Perni, R. B. Crystal Structures of Human SIRT3 Displaying Substrate-Induced Conformational Changes. *J. Biol. Chem.* **2009**, *284*, 24394–24405.
- (31) Michishita, E.; Park, J. Y.; Burneskis, J. M.; Barrett, J. C.; Horikawa, I. Evolutionarily Conserved and Nonconserved Cellular Localizations and Functions of Human SIRT Proteins. *Mol. Biol. Cell* **2005**, *16*, 4623–4635.

- (32) North, B. J.; Marshall, B. L.; Borra, M. T.; Denu, J. M.; Verdin, E. The Human Sir2 Ortholog, SIRT2, Is an NAD⁺-Dependent Tubulin Deacetylase. *Mol. Cell* **2003**, *11*, 437–444.
- (33) Shi, T.; Wang, F.; Stieren, E.; Tong, Q. SIRT3, a Mitochondrial Sirtuin Deacetylase, Regulates Mitochondrial Function and Thermogenesis in Brown Adipocytes. *J. Biol. Chem.* **2005**, *280*, 13560–13567.
- (34) Yuan, H.; Su, L.; Chen, W. Y. The Emerging and Diverse Roles of Sirtuins in Cancer: A Clinical Perspective. *Oncotargets Ther.* **2013**, *6*, 1399–1416.
- (35) Xu, F.; Gao, Z.; Zhang, J.; Rivera, C. A.; Yin, J.; Weng, J.; Ye, J. Lack of SIRT1 (Mammalian Sirtuin 1) Activity Leads to Liver Steatosis in the SIRT1^{+/-} Mice: A Role of Lipid Mobilization and Inflammation. *Endocrinology* **2010**, *151*, 2504–2514.
- (36) Sugden, M. C.; Caton, P. W.; Holness, M. J. PPAR Control: It's SIRTainly as Easy as PGC. *J. Endocrinol.* **2010**, *204*, 93–104.
- (37) Guarente, L. Sirtuins as Potential Targets for Metabolic Syndrome. *Nature* **2006**, *444*, 868–874.
- (38) Li, X.; Zhang, S.; Blander, G.; Tse, J. G.; Krieger, M.; Guarente, L. SIRT1 Deacetylates and Positively Regulates the Nuclear Receptor LXR. *Mol. Cell* **2007**, *28*, 91–106.
- (39) Hallows, W. C.; Lee, S.; Denu, J. M. Sirtuins Deacetylate and Activate Mammalian Acetyl-CoA Synthetases. *Proc. Natl. Acad. Sci. U. S. A.* **2006**, *103*, 10230–10235.
- (40) Iwahara, T.; Bonasio, R.; Narendra, V.; Reinberg, D. SIRT3 Functions in the Nucleus in the Control of Stress-Related Gene Expression. *Mol. Cell. Biol.* **2012**, *32*, 5022–5034.
- (41) Kincaid, B.; Bossy-Wetzel, E. Forever Young: SIRT3 a Shield against Mitochondrial Meltdown, Aging, and Neurodegeneration. *Front. Aging Neurosci.* **2013**, *5*, 48.
- (42) Osborne, B.; Cooney, G. J.; Turner, N. Are Sirtuin Deacylase Enzymes Important Modulators of Mitochondrial Energy Metabolism? *Biochim. Biophys. Acta* **2013**.

- (43) Huang, J.-Y.; Hirschey, M. D.; Shimazu, T.; Ho, L.; Verdin, E. Mitochondrial Sirtuins. *Biochim. Biophys. Acta* **2010**, *1804*, 1645–1651.
- (44) Bharathi, S. S.; Zhang, Y.; Mohsen, A.-W.; Uppala, R.; Balasubramani, M.; Schreiber, E.; Uechi, G.; Beck, M. E.; Rardin, M. J.; Vockley, J.; Verdin, E.; Gibson, B. W.; Hirschey, M. D.; Goetzman, E. S. SIRT3 Regulates Long-Chain Acyl-CoA Dehydrogenase by Deacetylating Conserved Lysines Near the Active Site. *J. Biol. Chem.* **2013**.
- (45) Laurent, G.; German, N. J.; Saha, A. K.; de Boer, V. C. J.; Davies, M.; Koves, T. R.; Dephoure, N.; Fischer, F.; Boanca, G.; Vaitheesvaran, B.; Lovitch, S. B.; Sharpe, A. H.; Kurland, I. J.; Steegborn, C.; Gygi, S. P.; Muoio, D. M.; Ruderman, N. B.; Haigis, M. C. SIRT4 Coordinates the Balance between Lipid Synthesis and Catabolism by Repressing Malonyl CoA Decarboxylase. *Mol. Cell* **2013**, *50*, 686–698.
- (46) Lerrer, B.; Cohen, H. Y. The Guardian: Metabolic and Tumour-Suppressive Effects of SIRT6. *EMBO J.* **2013**, *32*, 7–8.
- (47) Sebastián, C.; Zwaans, B. M. M.; Silberman, D. M.; Gymrek, M.; Goren, A.; Zhong, L.; Ram, O.; Truelove, J.; Guimaraes, A. R.; Toiber, D.; Cosentino, C.; Greenson, J. K.; MacDonald, A. I.; McGlynn, L.; Maxwell, F.; Edwards, J.; Giacosa, S.; Guccione, E.; Weissleder, R.; Bernstein, B. E.; Regev, A.; Shiels, P. G.; Lombard, D. B.; Mostoslavsky, R. The Histone Deacetylase SIRT6 Is a Tumor Suppressor That Controls Cancer Metabolism. *Cell* **2012**, *151*, 1185–1199.
- (48) Song, N.-Y.; Surh, Y.-J. Janus-Faced Role of SIRT1 in Tumorigenesis. *Ann. N. Y. Acad. Sci.* **2012**, *1271*, 10–19.
- (49) Liu, T.; Liu, P. Y.; Marshall, G. M. The Critical Role of the Class III Histone Deacetylase SIRT1 in Cancer. *Cancer Res.* **2009**, *69*, 1702–1705.
- (50) Hiratsuka, M.; Inoue, T.; Toda, T.; Kimura, N.; Shirayoshi, Y.; Kamitani, H.; Watanabe, T.; Ohama, E.; Tahimic, C. G. T.; Kurimasa, A.; Oshimura, M. Proteomics-Based Identification of Differentially Expressed Genes in Human Gliomas: Down-Regulation of SIRT2 Gene. *Biochem. Biophys. Res. Commun.* **2003**, *309*, 558–566.

- (51) Kim, H.-S.; Vassilopoulos, A.; Wang, R.-H.; Lahusen, T.; Xiao, Z.; Xu, X.; Li, C.; Veenstra, T. D.; Li, B.; Yu, H.; Ji, J.; Wang, X. W.; Park, S.-H.; Cha, Y. I.; Gius, D.; Deng, C.-X. SIRT2 Maintains Genome Integrity and Suppresses Tumorigenesis through Regulating APC/C Activity. *Cancer Cell* **2011**, *20*, 487–499.
- (52) Lai, C.-C.; Lin, P.-M.; Lin, S.-F.; Hsu, C.-H.; Lin, H.-C.; Hu, M.-L.; Hsu, C.-M.; Yang, M.-Y. Altered Expression of SIRT Gene Family in Head and Neck Squamous Cell Carcinoma. *Tumour Biol. J. Int. Soc. Oncodevelopmental Biol. Med.* **2013**, *34*, 1847–1854.
- (53) Ong, C.-A. J.; Shapiro, J.; Nason, K. S.; Davison, J. M.; Liu, X.; Ross-Innes, C.; O'Donovan, M.; Dinjens, W. N. M.; Biermann, K.; Shannon, N.; Worster, S.; Schulz, L. K. E.; Luketich, J. D.; Wijnhoven, B. P. L.; Hardwick, R. H.; Fitzgerald, R. C. Three-Gene Immunohistochemical Panel Adds to Clinical Staging Algorithms to Predict Prognosis for Patients with Esophageal Adenocarcinoma. *J. Clin. Oncol. Off. J. Am. Soc. Clin. Oncol.* **2013**, *31*, 1576–1582.
- (54) Liu, P. Y.; Xu, N.; Malyukova, A.; Scarlett, C. J.; Sun, Y. T.; Zhang, X. D.; Ling, D.; Su, S.-P.; Nelson, C.; Chang, D. K.; Koach, J.; Tee, A. E.; Haber, M.; Norris, M. D.; Toon, C.; Rooman, I.; Xue, C.; Cheung, B. B.; Kumar, S.; Marshall, G. M.; Biankin, A. V.; Liu, T. The Histone Deacetylase SIRT2 Stabilizes Myc Oncoproteins. *Cell Death Differ.* **2013**, *20*, 503–514.
- (55) Sunami, Y.; Araki, M.; Hironaka, Y.; Morishita, S.; Kobayashi, M.; Liew, E. L.; Edahiro, Y.; Tsutsui, M.; Ohsaka, A.; Komatsu, N. Inhibition of the NAD-Dependent Protein Deacetylase SIRT2 Induces Granulocytic Differentiation in Human Leukemia Cells. *PLoS One* **2013**, *8*, e57633.
- (56) Alhazzazi, T. Y.; Kamarajan, P.; Verdin, E.; Kapila, Y. L. Sirtuin-3 (SIRT3) and the Hallmarks of Cancer. *Genes Cancer* **2013**, *4*, 164–171.
- (57) Zhao, Y.; Yang, H.; Wang, X.; Zhang, R.; Wang, C.; Guo, Z. Sirtuin-3 (SIRT3) Expression Is Associated with Overall Survival in Esophageal Cancer. *Ann. Diagn. Pathol.* **2013**.
- (58) Lyssiotis, C. A.; Cantley, L. C. SIRT6 Puts Cancer Metabolism in the Driver's Seat. *Cell* **2012**, *151*, 1155–1156.

- (59) Marquardt, J. U.; Fischer, K.; Baus, K.; Kashyap, A.; Ma, S.; Krupp, M.; Linke, M.; Teufel, A.; Zechner, U.; Strand, D.; Thorgeirsson, S. S.; Galle, P. R.; Strand, S. Sirtuin-6-Dependent Genetic and Epigenetic Alterations Are Associated with Poor Clinical Outcome in Hepatocellular Carcinoma Patients. *Hepatol. Baltim. Md* **2013**, *58*, 1054–1064.
- (60) Kiran, S.; Chatterjee, N.; Singh, S.; Kaul, S. C.; Wadhwa, R.; Ramakrishna, G. Intracellular Distribution of Human SIRT7 and Mapping of the Nuclear/nucleolar Localization Signal. *FEBS J.* **2013**, *280*, 3451–3466.
- (61) Martínez-Redondo, P.; Santos-Barriopedro, I.; Vaquero, A. A Big Step for SIRT7, One Giant Leap for Sirtuins... in Cancer. *Cancer Cell* **2012**, *21*, 719–721.
- (62) Li, L.; Bhatia, R. The Controversial Role of Sirtuins in Tumorigenesis - SIRT7 Joins the Debate. *Cell Res.* **2013**, *23*, 10–12.
- (63) Kim, J. K.; Noh, J. H.; Jung, K. H.; Eun, J. W.; Bae, H. J.; Kim, M. G.; Chang, Y. G.; Shen, Q.; Park, W. S.; Lee, J. Y.; Borlak, J.; Nam, S. W. Sirtuin7 Oncogenic Potential in Human Hepatocellular Carcinoma and Its Regulation by the Tumor Suppressors MiR-125a-5p and MiR-125b. *Hepatol. Baltim. Md* **2013**, *57*, 1055–1067.
- (64) Elangovan, S.; Ramachandran, S.; Venkatesan, N.; Ananth, S.; Gnana-Prakasam, J. P.; Martin, P. M.; Browning, D. D.; Schoenlein, P. V.; Prasad, P. D.; Ganapathy, V.; Thangaraju, M. SIRT1 Is Essential for Oncogenic Signaling by Estrogen/estrogen Receptor A in Breast Cancer. *Cancer Res.* **2011**, *71*, 6654–6664.
- (65) Kim, J.-E.; Lou, Z.; Chen, J. Interactions between DBC1 and SIRT 1 Are Deregulated in Breast Cancer Cells. *Cell Cycle Georget. Tex* **2009**, *8*, 3784–3785.
- (66) Yu, E. J.; Kim, S.-H.; Heo, K.; Ou, C.-Y.; Stallcup, M. R.; Kim, J. H. Reciprocal Roles of DBC1 and SIRT1 in Regulating Estrogen Receptor A Activity and Co-Activator Synergy. *Nucleic Acids Res.* **2011**, *39*, 6932–6943.
- (67) Jung-Hynes, B.; Nihal, M.; Zhong, W.; Ahmad, N. Role of Sirtuin Histone Deacetylase SIRT1 in Prostate Cancer. A Target for Prostate Cancer Management via Its Inhibition? *J. Biol. Chem.* **2009**, *284*, 3823–3832.

- (68) Nakane, K.; Fujita, Y.; Terazawa, R.; Atsumi, Y.; Kato, T.; Nozawa, Y.; Deguchi, T.; Ito, M. Inhibition of Cortactin and SIRT1 Expression Attenuates Migration and Invasion of Prostate Cancer DU145 Cells. *Int. J. Urol. Off. J. Jpn. Urol. Assoc.* **2012**, *19*, 71–79.
- (69) Noh, S. J.; Baek, H. A.; Park, H. S.; Jang, K. Y.; Moon, W. S.; Kang, M. J.; Lee, D. G.; Kim, M. H.; Lee, J. H.; Chung, M. J. Expression of SIRT1 and Cortactin Is Associated with Progression of Non-Small Cell Lung Cancer. *Pathol. Res. Pract.* **2013**, *209*, 365–370.
- (70) Tseng, R.-C.; Lee, C.-C.; Hsu, H.-S.; Tzao, C.; Wang, Y.-C. Distinct HIC1-SIRT1-p53 Loop Deregulation in Lung Squamous Carcinoma and Adenocarcinoma Patients. *Neoplasia N. Y. N* **2009**, *11*, 763–770.
- (71) Xie, M.; Liu, M.; He, C.-S. SIRT1 Regulates Endothelial Notch Signaling in Lung Cancer. *PloS One* **2012**, *7*, e45331.
- (72) Portmann, S.; Fahrner, R.; Lechleiter, A.; Keogh, A.; Overney, S.; Laemmle, A.; Mikami, K.; Montani, M.; Tschan, M. P.; Candinas, D.; Stroka, D. Antitumor Effect of SIRT1 Inhibition in Human HCC Tumor Models in Vitro and in Vivo. *Mol. Cancer Ther.* **2013**, *12*, 499–508.
- (73) Chen, J.; Zhang, B.; Wong, N.; Lo, A. W. I.; To, K.-F.; Chan, A. W. H.; Ng, M. H. L.; Ho, C. Y. S.; Cheng, S.-H.; Lai, P. B. S.; Yu, J.; Ng, H.-K.; Ling, M.-T.; Huang, A.-L.; Cai, X.-F.; Ko, B. C. B. Sirtuin 1 Is Upregulated in a Subset of Hepatocellular Carcinomas Where It Is Essential for Telomere Maintenance and Tumor Cell Growth. *Cancer Res.* **2011**, *71*, 4138–4149.
- (74) Jang, K. Y.; Hwang, S. H.; Kwon, K. S.; Kim, K. R.; Choi, H. N.; Lee, N.-R.; Kwak, J.-Y.; Park, B.-H.; Park, H. S.; Chung, M. J.; Kang, M. J.; Lee, D. G.; Kim, H. S.; Shim, H.; Moon, W. S. SIRT1 Expression Is Associated with Poor Prognosis of Diffuse Large B-Cell Lymphoma. *Am. J. Surg. Pathol.* **2008**, *32*, 1523–1531.
- (75) Park, H. S.; Bae, J. S.; Noh, S. J.; Kim, K. M.; Lee, H.; Moon, W. S.; Chung, M. J.; Kang, M. J.; Lee, D. G.; Jang, K. Y. Expression of DBC1 and Androgen Receptor Predict Poor Prognosis in Diffuse Large B Cell Lymphoma. *Transl. Oncol.* **2013**, *6*, 370–381.

- (76) Li, L.; Wang, L.; Li, L.; Wang, Z.; Ho, Y.; McDonald, T.; Holyoake, T. L.; Chen, W.; Bhatia, R. Activation of p53 by SIRT1 Inhibition Enhances Elimination of CML Leukemia Stem Cells in Combination with Imatinib. *Cancer Cell* **2012**, *21*, 266–281.
- (77) Chen, W.; Bhatia, R. Roles of SIRT1 in Leukemogenesis. *Curr. Opin. Hematol.* **2013**, *20*, 308–313.
- (78) Kozako, T.; Aikawa, A.; Shoji, T.; Fujimoto, T.; Yoshimitsu, M.; Shirasawa, S.; Tanaka, H.; Honda, S.; Shimeno, H.; Arima, N.; Soeda, S. High Expression of the Longevity Gene Product SIRT1 and Apoptosis Induction by Sirtinol in Adult T-Cell Leukemia Cells. *Int. J. Cancer J. Int. Cancer* **2012**, *131*, 2044–2055.
- (79) Brodeur, G. M. Neuroblastoma: Biological Insights into a Clinical Enigma. *Nat. Rev. Cancer* **2003**, *3*, 203–216.
- (80) Cheung, N.-K. V.; Dyer, M. A. Neuroblastoma: Developmental Biology, Cancer Genomics and Immunotherapy. *Nat. Rev. Cancer* **2013**, *13*, 397–411.
- (81) Marshall, G. M.; Liu, P. Y.; Gherardi, S.; Scarlett, C. J.; Bedalov, A.; Xu, N.; Iraci, N.; Valli, E.; Ling, D.; Thomas, W.; van Bekkum, M.; Sekyere, E.; Jankowski, K.; Trahair, T.; Mackenzie, K. L.; Haber, M.; Norris, M. D.; Biankin, A. V.; Perini, G.; Liu, T. SIRT1 Promotes N-Myc Oncogenesis through a Positive Feedback Loop Involving the Effects of MKP3 and ERK on N-Myc Protein Stability. *PLoS Genet.* **2011**, *7*, e1002135.
- (82) Stenzinger, A.; Endris, V.; Klauschen, F.; Sinn, B.; Lorenz, K.; Warth, A.; Goepfert, B.; Ehemann, V.; Muckenhuber, A.; Kamphues, C.; Bahra, M.; Neuhaus, P.; Weichert, W. High SIRT1 Expression Is a Negative Prognosticator in Pancreatic Ductal Adenocarcinoma. *BMC Cancer* **2013**, *13*, 450.
- (83) Gong, D.-J.; Zhang, J.-M.; Yu, M.; Zhuang, B.; Guo, Q.-Q. Inhibition of SIRT1 Combined with Gemcitabine Therapy for Pancreatic Carcinoma. *Clin. Interv. Aging* **2013**, *8*, 889–897.
- (84) Wauters, E.; Sanchez-Arévalo Lobo, V. J.; Pinho, A. V.; Mawson, A.; Herranz, D.; Wu, J.; Cowley, M. J.; Colvin, E. K.; Njicop, E. N.; Sutherland, R. L.; Liu, T.; Serrano, M.; Bouwens, L.; Real, F. X.; Biankin, A. V.; Rooman, I. Sirtuin-1

- Regulates Acinar-to-Ductal Metaplasia and Supports Cancer Cell Viability in Pancreatic Cancer. *Cancer Res.* **2013**, *73*, 2357–2367.
- (85) Meza, R.; Jeon, J.; Renehan, A. G.; Luebeck, E. G. Colorectal Cancer Incidence Trends in the United States and United Kingdom: Evidence of Right- to Left-Sided Biological Gradients with Implications for Screening. *Cancer Res.* **2010**, *70*, 5419–5429.
- (86) Kriegl, L.; Vieth, M.; Kirchner, T.; Menssen, A. Up-Regulation of c-MYC and SIRT1 Expression Correlates with Malignant Transformation in the Serrated Route to Colorectal Cancer. *Oncotarget* **2012**, *3*, 1182–1193.
- (87) Kikuchi, K.; Noguchi, A.; Takahashi, H.; Zheng, H.; Kameda, Y.; Sekiguchi, H.; Akaike, M.; Miyagi, Y.; Takano, Y. High SIRT1 Expression and Low DBC1 Expression Are Associated with Poor Prognosis in Colorectal Cancer. *J. Cancer Ther. Res.* **2013**, *2*, 1.
- (88) Yamakuchi, M.; Lowenstein, C. J. MiR-34, SIRT1 and p53: The Feedback Loop. *Cell Cycle Georget. Tex* **2009**, *8*, 712–715.
- (89) Takahashi, T.; Saikawa, Y.; Kitagawa, Y. Gastric Cancer: Current Status of Diagnosis and Treatment. *Cancers* **2013**, *5*, 48–63.
- (90) Cha, E. J.; Noh, S. J.; Kwon, K. S.; Kim, C. Y.; Park, B.-H.; Park, H. S.; Lee, H.; Chung, M. J.; Kang, M. J.; Lee, D. G.; Moon, W. S.; Jang, K. Y. Expression of DBC1 and SIRT1 Is Associated with Poor Prognosis of Gastric Carcinoma. *Clin. Cancer Res. Off. J. Am. Assoc. Cancer Res.* **2009**, *15*, 4453–4459.
- (91) Zhou, X.; Fan, L. X.; Sweeney, W. E., Jr; Denu, J. M.; Avner, E. D.; Li, X. Sirtuin 1 Inhibition Delays Cyst Formation in Autosomal-Dominant Polycystic Kidney Disease. *J. Clin. Invest.* **2013**, *123*, 3084–3098.
- (92) Zhou, X.; Fan, L. X.; Sweeney, W. E., Jr; Denu, J. M.; Avner, E. D.; Li, X. Sirtuin 1 Inhibition Delays Cyst Formation in Autosomal-Dominant Polycystic Kidney Disease. *J. Clin. Invest.* **2013**, *123*, 3084–3098.
- (93) Chen, J.; Zhou, Y.; Mueller-Steiner, S.; Chen, L.-F.; Kwon, H.; Yi, S.; Mucke, L.; Gan, L. SIRT1 Protects against Microglia-Dependent Amyloid-Beta Toxicity through Inhibiting NF-kappaB Signaling. *J. Biol. Chem.* **2005**, *280*, 40364–40374.

- (94) Donmez, G.; Wang, D.; Cohen, D. E.; Guarente, L. SIRT1 Suppresses Beta-Amyloid Production by Activating the Alpha-Secretase Gene ADAM10. *Cell* **2010**, *142*, 320–332.
- (95) Qin, W.; Yang, T.; Ho, L.; Zhao, Z.; Wang, J.; Chen, L.; Zhao, W.; Thiagarajan, M.; MacGrogan, D.; Rodgers, J. T.; Puigserver, P.; Sadoshima, J.; Deng, H.; Pedrini, S.; Gandy, S.; Sauve, A. A.; Pasinetti, G. M. Neuronal SIRT1 Activation as a Novel Mechanism Underlying the Prevention of Alzheimer Disease Amyloid Neuropathology by Calorie Restriction. *J. Biol. Chem.* **2006**, *281*, 21745–21754.
- (96) Valor, L. M.; Guiretti, D. What's Wrong with Epigenetics in Huntington's Disease? *Neuropharmacology* **2013**.
- (97) Cattaneo, E.; Rigamonti, D.; Goffredo, D.; Zuccato, C.; Squitieri, F.; Sipione, S. Loss of Normal Huntingtin Function: New Developments in Huntington's Disease Research. *Trends Neurosci.* **2001**, *24*, 182–188.
- (98) Parker, J. A.; Arango, M.; Abderrahmane, S.; Lambert, E.; Tourette, C.; Catoire, H.; Néri, C. Resveratrol Rescues Mutant Polyglutamine Cytotoxicity in Nematode and Mammalian Neurons. *Nat. Genet.* **2005**, *37*, 349–350.
- (99) Jeong, H.; Cohen, D. E.; Cui, L.; Supinski, A.; Savas, J. N.; Mazzulli, J. R.; Yates, J. R., 3rd; Bordone, L.; Guarente, L.; Krainc, D. Sirt1 Mediates Neuroprotection from Mutant Huntingtin by Activation of the TORC1 and CREB Transcriptional Pathway. *Nat. Med.* **2012**, *18*, 159–165.
- (100) Pallos, J.; Bodai, L.; Lukacsovich, T.; Purcell, J. M.; Steffan, J. S.; Thompson, L. M.; Marsh, J. L. Inhibition of Specific HDACs and Sirtuins Suppresses Pathogenesis in a Drosophila Model of Huntington's Disease. *Hum. Mol. Genet.* **2008**, *17*, 3767–3775.
- (101) Luthi-Carter, R.; Taylor, D. M.; Pallos, J.; Lambert, E.; Amore, A.; Parker, A.; Moffitt, H.; Smith, D. L.; Runne, H.; Gokce, O.; Kuhn, A.; Xiang, Z.; Maxwell, M. M.; Reeves, S. A.; Bates, G. P.; Neri, C.; Thompson, L. M.; Marsh, J. L.; Kazantsev, A. G. SIRT2 Inhibition Achieves Neuroprotection by Decreasing Sterol Biosynthesis. *Proc. Natl. Acad. Sci. U. S. A.* **2010**, *107*, 7927–7932.
- (102) Obeso, J. A.; Rodriguez-Oroz, M. C.; Goetz, C. G.; Marin, C.; Kordower, J. H.; Rodriguez, M.; Hirsch, E. C.; Farrer, M.; Schapira, A. H. V.; Halliday, G.

- Missing Pieces in the Parkinson's Disease Puzzle. *Nat. Med.* **2010**, *16*, 653–661.
- (103) Outeiro, T. F.; Kontopoulos, E.; Altmann, S. M.; Kufareva, I.; Strathearn, K. E.; Amore, A. M.; Volk, C. B.; Maxwell, M. M.; Rochet, J.-C.; McLean, P. J.; Young, A. B.; Abagyan, R.; Feany, M. B.; Hyman, B. T.; Kazantsev, A. G. Sirtuin 2 Inhibitors Rescue Alpha-Synuclein-Mediated Toxicity in Models of Parkinson's Disease. *Science* **2007**, *317*, 516–519.
- (104) Liu, L.; Arun, A.; Ellis, L.; Peritore, C.; Donmez, G. Sirtuin 2 (SIRT2) Enhances 1-Methyl-4-Phenyl-1,2,3,6-Tetrahydropyridine (MPTP)-Induced Nigrostriatal Damage via Deacetylating Forkhead Box O3a (Foxo3a) and Activating Bim Protein. *J. Biol. Chem.* **2012**, *287*, 32307–32311.
- (105) Suzuki, K.; Koike, T. Mammalian Sir2-Related Protein (SIRT) 2-Mediated Modulation of Resistance to Axonal Degeneration in Slow Wallerian Degeneration Mice: A Crucial Role of Tubulin Deacetylation. *Neuroscience* **2007**, *147*, 599–612.
- (106) Trapp, J.; Jochum, A.; Meier, R.; Saunders, L.; Marshall, B.; Kunick, C.; Verdin, E.; Goekjian, P.; Sippl, W.; Jung, M. Adenosine Mimetics as Inhibitors of NAD⁺-Dependent Histone Deacetylases, from Kinase to Sirtuin Inhibition. *J. Med. Chem.* **2006**, *49*, 7307–7316.
- (107) Heltweg, B.; Trapp, J.; Jung, M. In Vitro Assays for the Determination of Histone Deacetylase Activity. *Methods San Diego Calif* **2005**, *36*, 332–337.
- (108) North, B. J.; Schwer, B.; Ahuja, N.; Marshall, B.; Verdin, E. Preparation of Enzymatically Active Recombinant Class III Protein Deacetylases. *Methods San Diego Calif* **2005**, *36*, 338–345.
- (109) Nie, H.; Chen, H.; Han, J.; Hong, Y.; Ma, Y.; Xia, W.; Ying, W. Silencing of SIRT2 Induces Cell Death and a Decrease in the Intracellular ATP Level of PC12 Cells. *Int. J. Physiol. Pathophysiol. Pharmacol.* **2011**, *3*, 65–70.
- (110) Suzuki, T.; Imai, K.; Nakagawa, H.; Miyata, N. 2-Anilinobenzamides as SIRT Inhibitors. *ChemMedChem* **2006**, *1*, 1059–1062.
- (111) Suzuki, T.; Khan, M. N. A.; Sawada, H.; Imai, E.; Itoh, Y.; Yamatsuta, K.; Tokuda, N.; Takeuchi, J.; Seko, T.; Nakagawa, H.; Miyata, N. Design,

- Synthesis, and Biological Activity of a Novel Series of Human Sirtuin-2-Selective Inhibitors. *J. Med. Chem.* **2012**, *55*, 5760–5773.
- (112) Heltweg, B.; Gathbonton, T.; Schuler, A. D.; Posakony, J.; Li, H.; Goehle, S.; Kollipara, R.; Depinho, R. A.; Gu, Y.; Simon, J. A.; Bedalov, A. Antitumor Activity of a Small-Molecule Inhibitor of Human Silent Information Regulator 2 Enzymes. *Cancer Res.* **2006**, *66*, 4368–4377.
- (113) Medda, F.; Russell, R. J. M.; Higgins, M.; McCarthy, A. R.; Campbell, J.; Slawin, A. M. Z.; Lane, D. P.; Lain, S.; Westwood, N. J. Novel Cambinol Analogs as Sirtuin Inhibitors: Synthesis, Biological Evaluation, and Rationalization of Activity. *J. Med. Chem.* **2009**, *52*, 2673–2682.
- (114) Lugin, J.; Ciarlo, E.; Santos, A.; Grandmaison, G.; dos Santos, I.; Le Roy, D.; Roger, T. The Sirtuin Inhibitor Cambinol Impairs MAPK Signaling, Inhibits Inflammatory and Innate Immune Responses and Protects from Septic Shock. *Biochim. Biophys. Acta* **2013**, *1833*, 1498–1510.
- (115) Fridén-Saxin, M.; Seifert, T.; Landergren, M. R.; Suuronen, T.; Lahtela-Kakkonen, M.; Jarho, E. M.; Luthman, K. Synthesis and Evaluation of Substituted Chroman-4-One and Chromone Derivatives as Sirtuin 2-Selective Inhibitors. *J. Med. Chem.* **2012**, *55*, 7104–7113.
- (116) Napper, A. D.; Hixon, J.; McDonagh, T.; Keavey, K.; Pons, J.-F.; Barker, J.; Yau, W. T.; Amouzegh, P.; Flegg, A.; Hamelin, E.; Thomas, R. J.; Kates, M.; Jones, S.; Navia, M. A.; Saunders, J. O.; DiStefano, P. S.; Curtis, R. Discovery of Indoles as Potent and Selective Inhibitors of the Deacetylase SIRT1. *J. Med. Chem.* **2005**, *48*, 8045–8054.
- (117) Gertz, M.; Fischer, F.; Nguyen, G. T. T.; Lakshminarasimhan, M.; Schutkowski, M.; Weyand, M.; Steegborn, C. Ex-527 Inhibits Sirtuins by Exploiting Their Unique NAD⁺-Dependent Deacetylation Mechanism. *Proc. Natl. Acad. Sci. U. S. A.* **2013**, *110*, E2772–2781.
- (118) Zhao, X.; Allison, D.; Condon, B.; Zhang, F.; Gheyi, T.; Zhang, A.; Ashok, S.; Russell, M.; MacEwan, I.; Qian, Y.; Jamison, J. A.; Luz, J. G. The 2.5 Å Crystal Structure of the SIRT1 Catalytic Domain Bound to Nicotinamide Adenine Dinucleotide (NAD⁺) and an Indole (EX527 Analogue) Reveals a

- Novel Mechanism of Histone Deacetylase Inhibition. *J. Med. Chem.* **2013**, *56*, 963–969.
- (119) Solomon, J. M.; Pasupuleti, R.; Xu, L.; McDonagh, T.; Curtis, R.; DiStefano, P. S.; Huber, L. J. Inhibition of SIRT1 Catalytic Activity Increases p53 Acetylation but Does Not Alter Cell Survival Following DNA Damage. *Mol. Cell. Biol.* **2006**, *26*, 28–38.
- (120) Hubbard, B. P.; Loh, C.; Gomes, A. P.; Li, J.; Lu, Q.; Doyle, T. L.; Disch, J. S.; Armour, S. M.; Ellis, J. L.; Vlasuk, G. P.; Sinclair, D. A. Carboxamide SIRT1 Inhibitors Block DBC1 Binding via an Acetylation-Independent Mechanism. *Cell Cycle Georget. Tex* **2013**, *12*, 2233–2240.
- (121) Zhao, K.; Harshaw, R.; Chai, X.; Marmorstein, R. Structural Basis for Nicotinamide Cleavage and ADP-Ribose Transfer by NAD(+)-Dependent Sir2 Histone/protein Deacetylases. *Proc. Natl. Acad. Sci. U. S. A.* **2004**, *101*, 8563–8568.
- (122) Szczepankiewicz, B. G.; Dai, H.; Koppetsch, K. J.; Qian, D.; Jiang, F.; Mao, C.; Perni, R. B. Synthesis of Carba-NAD and the Structures of Its Ternary Complexes with SIRT3 and SIRT5. *J. Org. Chem.* **2012**, *77*, 7319–7329.
- (123) Sanders, B. D.; Zhao, K.; Slama, J. T.; Marmorstein, R. Structural Basis for Nicotinamide Inhibition and Base Exchange in Sir2 Enzymes. *Mol. Cell* **2007**, *25*, 463–472.
- (124) Pesnot, T.; Kempter, J.; Schemies, J.; Pergolizzi, G.; Uciechowska, U.; Rumpf, T.; Sippl, W.; Jung, M.; Wagner, G. K. Two-Step Synthesis of Novel, Bioactive Derivatives of the Ubiquitous Cofactor Nicotinamide Adenine Dinucleotide (NAD). *J. Med. Chem.* **2011**, *54*, 3492–3499.
- (125) Fatkins, D. G.; Monnot, A. D.; Zheng, W. Nepsilon-Thioacetyl-Lysine: A Multi-Facet Functional Probe for Enzymatic Protein Lysine Nepsilon-Deacetylation. *Bioorg. Med. Chem. Lett.* **2006**, *16*, 3651–3656.
- (126) Smith, B. C.; Denu, J. M. Acetyl-Lysine Analog Peptides as Mechanistic Probes of Protein Deacetylases. *J. Biol. Chem.* **2007**, *282*, 37256–37265.
- (127) Smith, B. C.; Denu, J. M. Mechanism-Based Inhibition of Sir2 Deacetylases by Thioacetyl-Lysine Peptide. *Biochemistry (Mosc.)* **2007**, *46*, 14478–14486.

- (128) Fatkins, D. G.; Zheng, W. Substituting N(epsilon)-Thioacetyl-Lysine for N(epsilon)-Acetyl-Lysine in Peptide Substrates as a General Approach to Inhibiting Human NAD(+)-Dependent Protein Deacetylases. *Int. J. Mol. Sci.* **2008**, *9*, 1–11.
- (129) Kiviranta, P. H.; Suuronen, T.; Wallén, E. A. A.; Leppänen, J.; Tervonen, J.; Kyrylenko, S.; Salminen, A.; Poso, A.; Jarho, E. M. N(epsilon)-Thioacetyl-Lysine-Containing Tri-, Tetra-, and Pentapeptides as SIRT1 and SIRT2 Inhibitors. *J. Med. Chem.* **2009**, *52*, 2153–2156.
- (130) Kokkonen, P.; Rahnasto-Rilla, M.; Kiviranta, P. H.; Huhtiniemi, T.; Laitinen, T.; Poso, A.; Jarho, E.; Lahtela-Kakkonen, M. Peptides and Pseudopeptides as SIRT6 Deacetylation Inhibitors. *ACS Med. Chem. Lett.* **2012**, *3*, 969–974.
- (131) Asaba, T.; Suzuki, T.; Ueda, R.; Tsumoto, H.; Nakagawa, H.; Miyata, N. Inhibition of Human Sirtuins by in Situ Generation of an Acetylated Lysine-ADP-Ribose Conjugate. *J. Am. Chem. Soc.* **2009**, *131*, 6989–6996.
- (132) Suzuki, T.; Asaba, T.; Imai, E.; Tsumoto, H.; Nakagawa, H.; Miyata, N. Identification of a Cell-Active Non-Peptide Sirtuin Inhibitor Containing N-Thioacetyl Lysine. *Bioorg. Med. Chem. Lett.* **2009**, *19*, 5670–5672.
- (133) Huhtiniemi, T.; Suuronen, T.; Lahtela-Kakkonen, M.; Bruijn, T.; Jääskeläinen, S.; Poso, A.; Salminen, A.; Leppänen, J.; Jarho, E. N(epsilon)-Modified Lysine Containing Inhibitors for SIRT1 and SIRT2. *Bioorg. Med. Chem.* **2010**, *18*, 5616–5625.
- (134) Huhtiniemi, T.; Salo, H. S.; Suuronen, T.; Poso, A.; Salminen, A.; Leppänen, J.; Jarho, E.; Lahtela-Kakkonen, M. Structure-Based Design of Pseudopeptidic Inhibitors for SIRT1 and SIRT2. *J. Med. Chem.* **2011**, *54*, 6456–6468.
- (135) Jamonnak, N.; Hirsch, B. M.; Pang, Y.; Zheng, W. Substrate Specificity of SIRT1-Catalyzed Lysine Nepsilon-Deacetylation Reaction Probed with the Side Chain Modified Nepsilon-Acetyl-Lysine Analogs. *Bioorganic Chem.* **2010**, *38*, 17–25.
- (136) He, B.; Du, J.; Lin, H. Thiosuccinyl Peptides as Sirt5-Specific Inhibitors. *J. Am. Chem. Soc.* **2012**, *134*, 1922–1925.
- (137) Grozinger, C. M.; Chao, E. D.; Blackwell, H. E.; Moazed, D.; Schreiber, S. L. Identification of a Class of Small Molecule Inhibitors of the Sirtuin Family of

- NAD-Dependent Deacetylases by Phenotypic Screening. *J. Biol. Chem.* **2001**, 276, 38837–38843.
- (138) Mai, A.; Massa, S.; Lavu, S.; Pezzi, R.; Simeoni, S.; Ragno, R.; Mariotti, F. R.; Chiani, F.; Camilloni, G.; Sinclair, D. A. Design, Synthesis, and Biological Evaluation of Sirtinol Analogues as Class III Histone/protein Deacetylase (Sirtuin) Inhibitors. *J. Med. Chem.* **2005**, 48, 7789–7795.
- (139) Orecchia, A.; Scarponi, C.; Di Felice, F.; Cesarini, E.; Avitabile, S.; Mai, A.; Mauro, M. L.; Sirri, V.; Zambruno, G.; Albanesi, C.; Camilloni, G.; Failla, C. M. Sirtinol Treatment Reduces Inflammation in Human Dermal Microvascular Endothelial Cells. *PLoS One* **2011**, 6, e24307.
- (140) Wang, J.; Kim, T. H.; Ahn, M. Y.; Lee, J.; Jung, J. H.; Choi, W. S.; Lee, B. M.; Yoon, K. S.; Yoon, S.; Kim, H. S. Sirtinol, a Class III HDAC Inhibitor, Induces Apoptotic and Autophagic Cell Death in MCF-7 Human Breast Cancer Cells. *Int. J. Oncol.* **2012**, 41, 1101–1109.
- (141) Peck, B.; Chen, C.-Y.; Ho, K.-K.; Di Fruscia, P.; Myatt, S. S.; Coombes, R. C.; Fuchter, M. J.; Hsiao, C.-D.; Lam, E. W.-F. SIRT Inhibitors Induce Cell Death and p53 Acetylation through Targeting Both SIRT1 and SIRT2. *Mol. Cancer Ther.* **2010**, 9, 844–855.
- (142) Lara, E.; Mai, A.; Calvanese, V.; Altucci, L.; Lopez-Nieva, P.; Martinez-Chantar, M. L.; Varela-Rey, M.; Rotili, D.; Nebbioso, A.; Roperio, S.; Montoya, G.; Oyarzabal, J.; Velasco, S.; Serrano, M.; Witt, M.; Villar-Garea, A.; Imhof, A.; Inhof, A.; Mato, J. M.; Esteller, M.; Fraga, M. F. Salermide, a Sirtuin Inhibitor with a Strong Cancer-Specific Proapoptotic Effect. *Oncogene* **2009**, 28, 781–791.
- (143) Rotili, D.; Tarantino, D.; Nebbioso, A.; Paolini, C.; Huidobro, C.; Lara, E.; Mellini, P.; Lenoci, A.; Pezzi, R.; Botta, G.; Lahtela-Kakkonen, M.; Poso, A.; Steinkühler, C.; Gallinari, P.; De Maria, R.; Fraga, M.; Esteller, M.; Altucci, L.; Mai, A. Discovery of Salermide-Related Sirtuin Inhibitors: Binding Mode Studies and Antiproliferative Effects in Cancer Cells Including Cancer Stem Cells. *J. Med. Chem.* **2012**, 55, 10937–10947.

- (144) Kalle, A. M.; Mallika, A.; Badiger, J.; Alinakhi; Talukdar, P.; Sachchidanand. Inhibition of SIRT1 by a Small Molecule Induces Apoptosis in Breast Cancer Cells. *Biochem. Biophys. Res. Commun.* **2010**, *401*, 13–19.
- (145) Rotili, D.; Tarantino, D.; Carafa, V.; Lara, E.; Meade, S.; Botta, G.; Nebbioso, A.; Schemies, J.; Jung, M.; Kazantsev, A. G.; Esteller, M.; Fraga, M. F.; Altucci, L.; Mai, A. Identification of Tri- and Tetracyclic Pyrimidinediones as Sirtuin Inhibitors. *ChemMedChem* **2010**, *5*, 674–677.
- (146) Rotili, D.; Carafa, V.; Tarantino, D.; Botta, G.; Nebbioso, A.; Altucci, L.; Mai, A. Simplification of the Tetracyclic SIRT1-Selective Inhibitor MC2141: Coumarin- and Pyrimidine-Based SIRT1/2 Inhibitors with Different Selectivity Profile. *Bioorg. Med. Chem.* **2011**, *19*, 3659–3668.
- (147) Rotili, D.; Tarantino, D.; Carafa, V.; Paolini, C.; Schemies, J.; Jung, M.; Botta, G.; Di Maro, S.; Novellino, E.; Steinkühler, C.; De Maria, R.; Gallinari, P.; Altucci, L.; Mai, A. Benzodeazaflavins as Sirtuin Inhibitors with Antiproliferative Properties in Cancer Stem Cells. *J. Med. Chem.* **2012**, *55*, 8193–8197.
- (148) Bedalov, A.; Gatbonton, T.; Irvine, W. P.; Gottschling, D. E.; Simon, J. A. Identification of a Small Molecule Inhibitor of Sir2p. *Proc. Natl. Acad. Sci. U. S. A.* **2001**, *98*, 15113–15118.
- (149) Hirao, M.; Posakony, J.; Nelson, M.; Hruby, H.; Jung, M.; Simon, J. A.; Bedalov, A. Identification of Selective Inhibitors of NAD⁺-Dependent Deacetylases Using Phenotypic Screens in Yeast. *J. Biol. Chem.* **2003**, *278*, 52773–52782.
- (150) Posakony, J.; Hirao, M.; Stevens, S.; Simon, J. A.; Bedalov, A. Inhibitors of Sir2: Evaluation of Splitomicin Analogues. *J. Med. Chem.* **2004**, *47*, 2635–2644.
- (151) Pagans, S.; Pedal, A.; North, B. J.; Kaehlcke, K.; Marshall, B. L.; Dorr, A.; Hetzer-Egger, C.; Henklein, P.; Frye, R.; McBurney, M. W.; Hruby, H.; Jung, M.; Verdin, E.; Ott, M. SIRT1 Regulates HIV Transcription via Tat Deacetylation. *PLoS Biol.* **2005**, *3*, e41.
- (152) Neugebauer, R. C.; Uchiechowska, U.; Meier, R.; Hruby, H.; Valkov, V.; Verdin, E.; Sippl, W.; Jung, M. Structure-Activity Studies on Splitomicin

- Derivatives as Sirtuin Inhibitors and Computational Prediction of Binding Mode. *J. Med. Chem.* **2008**, *51*, 1203–1213.
- (153) Freitag, M.; Schemies, J.; Larsen, T.; El Gaghlab, K.; Schulz, F.; Rumpf, T.; Jung, M.; Link, A. Synthesis and Biological Activity of Splitomicin Analogs Targeted at Human NAD(+)-Dependent Histone Deacetylases (sirtuins). *Bioorg. Med. Chem.* **2011**, *19*, 3669–3677.
- (154) Howitz, K. T.; Bitterman, K. J.; Cohen, H. Y.; Lamming, D. W.; Lavu, S.; Wood, J. G.; Zipkin, R. E.; Chung, P.; Kisielewski, A.; Zhang, L.-L.; Scherer, B.; Sinclair, D. A. Small Molecule Activators of Sirtuins Extend *Saccharomyces Cerevisiae* Lifespan. *Nature* **2003**, *425*, 191–196.
- (155) Trapp, J.; Meier, R.; Hongwiset, D.; Kassack, M. U.; Sippl, W.; Jung, M. Structure-Activity Studies on Suramin Analogues as Inhibitors of NAD⁺-Dependent Histone Deacetylases (sirtuins). *ChemMedChem* **2007**, *2*, 1419–1431.
- (156) Lain, S.; Hollick, J. J.; Campbell, J.; Staples, O. D.; Higgins, M.; Aoubala, M.; McCarthy, A.; Appleyard, V.; Murray, K. E.; Baker, L.; Thompson, A.; Mathers, J.; Holland, S. J.; Stark, M. J. R.; Pass, G.; Woods, J.; Lane, D. P.; Westwood, N. J. Discovery, in Vivo Activity, and Mechanism of Action of a Small-Molecule p53 Activator. *Cancer Cell* **2008**, *13*, 454–463.
- (157) McCarthy, A. R.; Pirrie, L.; Hollick, J. J.; Ronseaux, S.; Campbell, J.; Higgins, M.; Staples, O. D.; Tran, F.; Slawin, A. M. Z.; Lain, S.; Westwood, N. J. Synthesis and Biological Characterisation of Sirtuin Inhibitors Based on the Tenovins. *Bioorg. Med. Chem.* **2012**, *20*, 1779–1793.
- (158) Pirrie, L.; McCarthy, A. R.; Major, L. L.; Morkūnaitė, V.; Zubrienė, A.; Matulis, D.; Lain, S.; Lebl, T.; Westwood, N. J. Discovery and Validation of SIRT2 Inhibitors Based on Tenovin-6: Use of a ¹H-NMR Method to Assess Deacetylase Activity. *Mol. Basel Switz.* **2012**, *17*, 12206–12224.
- (159) Disch, J. S.; Evindar, G.; Chiu, C. H.; Blum, C. A.; Dai, H.; Jin, L.; Schuman, E.; Lind, K. E.; Belyanskaya, S. L.; Deng, J.; Coppo, F.; Aquilani, L.; Graybill, T. L.; Cuozzo, J. W.; Lavu, S.; Mao, C.; Vlasuk, G. P.; Perni, R. B. Discovery of thieno[3,2-D]pyrimidine-6-Carboxamides as Potent Inhibitors of SIRT1, SIRT2, and SIRT3. *J. Med. Chem.* **2013**, *56*, 3666–3679.

- (160) Uciechowska, U.; Schemies, J.; Neugebauer, R. C.; Huda, E.-M.; Schmitt, M. L.; Meier, R.; Verdin, E.; Jung, M.; Sippl, W. Thiobarbiturates as Sirtuin Inhibitors: Virtual Screening, Free-Energy Calculations, and Biological Testing. *ChemMedChem* **2008**, *3*, 1965–1976.
- (161) Maurer, B.; Rumpf, T.; Scharfe, M.; Stolfa, D. A.; Schmitt, M. L.; He, W.; Verdin, E.; Sippl, W.; Jung, M. Inhibitors of the NAD⁺-Dependent Protein Desuccinylase and Demalonylase Sirt5. *ACS Med. Chem. Lett.* **2012**, *3*, 1050–1053.
- (162) Zhang, Y.; Au, Q.; Zhang, M.; Barber, J. R.; Ng, S. C.; Zhang, B. Identification of a Small Molecule SIRT2 Inhibitor with Selective Tumor Cytotoxicity. *Biochem. Biophys. Res. Commun.* **2009**, *386*, 729–733.
- (163) Wu, J.; Li, Y.; Chen, K.; Jiang, H.; Xu, M.-H.; Liu, D. Identification of Benzofuran-3-yl(phenyl)methanones as Novel SIRT1 Inhibitors: Binding Mode, Inhibitory Mechanism and Biological Action. *Eur. J. Med. Chem.* **2013**, *60*, 441–450.
- (164) Feng, Y.; Wu, J.; Chen, L.; Luo, C.; Shen, X.; Chen, K.; Jiang, H.; Liu, D. A Fluorometric Assay of SIRT1 Deacetylation Activity through Quantification of Nicotinamide Adenine Dinucleotide. *Anal. Biochem.* **2009**, *395*, 205–210.
- (165) Salo, H. S.; Laitinen, T.; Poso, A.; Jarho, E.; Lahtela-Kakkonen, M. Identification of Novel SIRT3 Inhibitor Scaffolds by Virtual Screening. *Bioorg. Med. Chem. Lett.* **2013**, *23*, 2990–2995.
- (166) Galli, U.; Mesenzani, O.; Coppo, C.; Sorba, G.; Canonico, P. L.; Tron, G. C.; Genazzani, A. A. Identification of a Sirtuin 3 Inhibitor That Displays Selectivity over Sirtuin 1 and 2. *Eur. J. Med. Chem.* **2012**, *55*, 58–66.
- (167) Zhang, Q.; Zeng, S. X.; Zhang, Y.; Zhang, Y.; Ding, D.; Ye, Q.; Meroueh, S. O.; Lu, H. A Small Molecule Inauhizin Inhibits SIRT1 Activity and Suppresses Tumour Growth through Activation of p53. *EMBO Mol. Med.* **2012**, *4*, 298–312.
- (168) Kahyo, T.; Ichikawa, S.; Hatanaka, T.; Yamada, M. K.; Setou, M. A Novel Chalcone Polyphenol Inhibits the Deacetylase Activity of SIRT1 and Cell Growth in HEK293T Cells. *J. Pharmacol. Sci.* **2008**, *108*, 364–371.

- (169) Taylor, D. M.; Balabadra, U.; Xiang, Z.; Woodman, B.; Meade, S.; Amore, A.; Maxwell, M. M.; Reeves, S.; Bates, G. P.; Luthi-Carter, R.; Lowden, P. A. S.; Kazantsev, A. G. A Brain-Permeable Small Molecule Reduces Neuronal Cholesterol by Inhibiting Activity of Sirtuin 2 Deacetylase. *ACS Chem. Biol.* **2011**, *6*, 540–546.
- (170) Choi, S. H.; Quinti, L.; Kazantsev, A. G.; Silverman, R. B. 3-(N-Arylsulfamoyl)benzamides, Inhibitors of Human Sirtuin Type 2 (SIRT2). *Bioorg. Med. Chem. Lett.* **2012**, *22*, 2789–2793.
- (171) Chopra, V.; Quinti, L.; Kim, J.; Vollar, L.; Narayanan, K. L.; Edgerly, C.; Cipicchio, P. M.; Lauver, M. A.; Choi, S. H.; Silverman, R. B.; Ferrante, R. J.; Hersch, S.; Kazantsev, A. G. The Sirtuin 2 Inhibitor AK-7 Is Neuroprotective in Huntington's Disease Mouse Models. *Cell Rep.* **2012**, *2*, 1492–1497.
- (172) Borra, M. T.; Smith, B. C.; Denu, J. M. Mechanism of Human SIRT1 Activation by Resveratrol. *J. Biol. Chem.* **2005**, *280*, 17187–17195.
- (173) Nayagam, V. M.; Wang, X.; Tan, Y. C.; Poulsen, A.; Goh, K. C.; Ng, T.; Wang, H.; Song, H. Y.; Ni, B.; Entzeroth, M.; Stünkel, W. SIRT1 Modulating Compounds from High-Throughput Screening as Anti-Inflammatory and Insulin-Sensitizing Agents. *J. Biomol. Screen.* **2006**, *11*, 959–967.
- (174) Milne, J. C.; Lambert, P. D.; Schenk, S.; Carney, D. P.; Smith, J. J.; Gagne, D. J.; Jin, L.; Boss, O.; Perni, R. B.; Vu, C. B.; Bemis, J. E.; Xie, R.; Disch, J. S.; Ng, P. Y.; Nunes, J. J.; Lynch, A. V.; Yang, H.; Galonek, H.; Israelian, K.; Choy, W.; Iffland, A.; Lavu, S.; Medvedik, O.; Sinclair, D. A.; Olefsky, J. M.; Jirousek, M. R.; Elliott, P. J.; Westphal, C. H. Small Molecule Activators of SIRT1 as Therapeutics for the Treatment of Type 2 Diabetes. *Nature* **2007**, *450*, 712–716.
- (175) Vu, C. B.; Bemis, J. E.; Disch, J. S.; Ng, P. Y.; Nunes, J. J.; Milne, J. C.; Carney, D. P.; Lynch, A. V.; Smith, J. J.; Lavu, S.; Lambert, P. D.; Gagne, D. J.; Jirousek, M. R.; Schenk, S.; Olefsky, J. M.; Perni, R. B. Discovery of imidazo[1,2-B]thiazole Derivatives as Novel SIRT1 Activators. *J. Med. Chem.* **2009**, *52*, 1275–1283.
- (176) Matsuya, Y.; Kobayashi, Y.; Uchida, S.; Itoh, Y.; Sawada, H.; Suzuki, T.; Miyata, N.; Sugimoto, K.; Toyooka, N. Search for a Novel SIRT1 Activator:

- Structural Modification of SRT1720 and Biological Evaluation. *Bioorg. Med. Chem. Lett.* **2013**, *23*, 4907–4910.
- (177) Bemis, J. E.; Vu, C. B.; Xie, R.; Nunes, J. J.; Ng, P. Y.; Disch, J. S.; Milne, J. C.; Carney, D. P.; Lynch, A. V.; Jin, L.; Smith, J. J.; Lavu, S.; Iffland, A.; Jirousek, M. R.; Perni, R. B. Discovery of oxazolo[4,5-B]pyridines and Related Heterocyclic Analogs as Novel SIRT1 Activators. *Bioorg. Med. Chem. Lett.* **2009**, *19*, 2350–2353.
- (178) Mai, A.; Valente, S.; Meade, S.; Carafa, V.; Tardugno, M.; Nebbioso, A.; Galmozzi, A.; Mitro, N.; De Fabiani, E.; Altucci, L.; Kazantsev, A. Study of 1,4-Dihydropyridine Structural Scaffold: Discovery of Novel Sirtuin Activators and Inhibitors. *J. Med. Chem.* **2009**, *52*, 5496–5504.
- (179) Pacholec, M.; Bleasdale, J. E.; Chrnyk, B.; Cunningham, D.; Flynn, D.; Garofalo, R. S.; Griffith, D.; Griffor, M.; Loulakis, P.; Pabst, B.; Qiu, X.; Stockman, B.; Thanabal, V.; Varghese, A.; Ward, J.; Withka, J.; Ahn, K. SRT1720, SRT2183, SRT1460, and Resveratrol Are Not Direct Activators of SIRT1. *J. Biol. Chem.* **2010**, *285*, 8340–8351.
- (180) Huber, J. L.; McBurney, M. W.; Distefano, P. S.; McDonagh, T. SIRT1-Independent Mechanisms of the Putative Sirtuin Enzyme Activators SRT1720 and SRT2183. *Future Med. Chem.* **2010**, *2*, 1751–1759.
- (181) Dai, H.; Kustigian, L.; Carney, D.; Case, A.; Considine, T.; Hubbard, B. P.; Perni, R. B.; Riera, T. V.; Szczepankiewicz, B.; Vlasuk, G. P.; Stein, R. L. SIRT1 Activation by Small Molecules: Kinetic and Biophysical Evidence for Direct Interaction of Enzyme and Activator. *J. Biol. Chem.* **2010**, *285*, 32695–32703.
- (182) Gertz, M.; Nguyen, G. T. T.; Fischer, F.; Suenkel, B.; Schlicker, C.; Fränzel, B.; Tomaschewski, J.; Aladini, F.; Becker, C.; Wolters, D.; Steegborn, C. A Molecular Mechanism for Direct Sirtuin Activation by Resveratrol. *PLoS One* **2012**, *7*, e49761.
- (183) Wu, J.; Zhang, D.; Chen, L.; Li, J.; Wang, J.; Ning, C.; Yu, N.; Zhao, F.; Chen, D.; Chen, X.; Chen, K.; Jiang, H.; Liu, H.; Liu, D. Discovery and Mechanism Study of SIRT1 Activators That Promote the Deacetylation of Fluorophore-Labeled Substrate. *J. Med. Chem.* **2013**, *56*, 761–780.

- (184) Hubbard, B. P.; Gomes, A. P.; Dai, H.; Li, J.; Case, A. W.; Considine, T.; Riera, T. V.; Lee, J. E.; E, S. Y.; Lamming, D. W.; Pentelute, B. L.; Schuman, E. R.; Stevens, L. A.; Ling, A. J. Y.; Armour, S. M.; Michan, S.; Zhao, H.; Jiang, Y.; Sweitzer, S. M.; Blum, C. A.; Disch, J. S.; Ng, P. Y.; Howitz, K. T.; Rolo, A. P.; Hamuro, Y.; Moss, J.; Perni, R. B.; Ellis, J. L.; Vlasuk, G. P.; Sinclair, D. A. Evidence for a Common Mechanism of SIRT1 Regulation by Allosteric Activators. *Science* **2013**, *339*, 1216–1219.
- (185) Baur, J. A.; Ungvari, Z.; Minor, R. K.; Le Couteur, D. G.; de Cabo, R. Are Sirtuins Viable Targets for Improving Healthspan and Lifespan? *Nat. Rev. Drug Discov.* **2012**, *11*, 443–461.
- (186) Khwaja, F. S.; Quann, E. J.; Pattabiraman, N.; Wynne, S.; Djakiew, D. Carprofen Induction of p75NTR-Dependent Apoptosis via the p38 Mitogen-Activated Protein Kinase Pathway in Prostate Cancer Cells. *Mol. Cancer Ther.* **2008**, *7*, 3539–3545.
- (187) Min, J.; Landry, J.; Sternglanz, R.; Xu, R. M. Crystal Structure of a SIR2 Homolog-NAD Complex. *Cell* **2001**, *105*, 269–279.
- (188) Finnin, M. S.; Donigian, J. R.; Pavletich, N. P. Structure of the Histone Deacetylase SIRT2. *Nat. Struct. Biol.* **2001**, *8*, 621–625.
- (189) Ashworth, I. W.; Cox, B. G.; Meyrick, B. Kinetics and Mechanism of N-Boc Cleavage: Evidence of a Second-Order Dependence upon Acid Concentration. *J. Org. Chem.* **2010**, *75*, 8117–8125.
- (190) Bhattacharya, S.; Chaum, E.; Johnson, D. A.; Johnson, L. R. Age-Related Susceptibility to Apoptosis in Human Retinal Pigment Epithelial Cells Is Triggered by Disruption of p53-Mdm2 Association. *Invest. Ophthalmol. Vis. Sci.* **2012**, *53*, 8350–8366.
- (191) Wu, Y.; Li, X.; Zhu, J. X.; Xie, W.; Le, W.; Fan, Z.; Jankovic, J.; Pan, T. Resveratrol-Activated AMPK/SIRT1/autophagy in Cellular Models of Parkinson's Disease. *Neurosignals* **2011**, *19*, 163–174.
- (192) Sun, Y.; Sun, D.; Li, F.; Tian, L.; Li, C.; Li, L.; Lin, R.; Wang, S. Downregulation of Sirt1 by Antisense Oligonucleotides Induces Apoptosis and Enhances Radiation Sensitization in A549 Lung Cancer Cells. *Lung Cancer Amst. Neth.* **2007**, *58*, 21–29.

- (193) Kiviranta, P. H.; Leppänen, J.; Rinne, V. M.; Suuronen, T.; Kyrlylenko, O.; Kyrlylenko, S.; Kuusisto, E.; Tervo, A. J.; Järvinen, T.; Salminen, A.; Poso, A.; Wallén, E. A. A. N-(3-(4-Hydroxyphenyl)-Propenoyl)-Amino Acid Tryptamides as SIRT2 Inhibitors. *Bioorg. Med. Chem. Lett.* **2007**, *17*, 2448–2451.
- (194) Tervo, A. J.; Kyrlylenko, S.; Niskanen, P.; Salminen, A.; Leppänen, J.; Nyrönen, T. H.; Järvinen, T.; Poso, A. An in Silico Approach to Discovering Novel Inhibitors of Human Sirtuin Type 2. *J. Med. Chem.* **2004**, *47*, 6292–6298.
- (195) Shoemaker, R. H. The NCI60 Human Tumour Cell Line Anticancer Drug Screen. *Nat. Rev. Cancer* **2006**, *6*, 813–823.
- (196) Nuutinen, U.; Ropponen, A.; Eeva, J.; Eray, M.; Pellinen, R.; Wahlfors, J.; Pelkonen, J. The Effect of Microenvironmental CD40 Signals on TRAIL- and Drug-Induced Apoptosis in Follicular Lymphoma Cells. *Scand. J. Immunol.* **2009**, *70*, 565–573.
- (197) Mellini, P.; Kokkola, T.; Suuronen, T.; Salo, H. S.; Tolvanen, L.; Mai, A.; Lahtela-Kakkonen, M.; Jarho, E. M. Screen of Pseudopeptidic Inhibitors of Human Sirtuins 1-3: Two Lead Compounds with Antiproliferative Effects in Cancer Cells. *J. Med. Chem.* **2013**, *56*, 6681–6695.
- (198) Carreon, J. R.; Stewart, K. M.; Mahon, K. P., Jr; Shin, S.; Kelley, S. O. Cyanine Dye Conjugates as Probes for Live Cell Imaging. *Bioorg. Med. Chem. Lett.* **2007**, *17*, 5182–5185.
- (199) Fonseca, S. B.; Pereira, M. P.; Mourta, R.; Gronda, M.; Horton, K. L.; Hurren, R.; Minden, M. D.; Schimmer, A. D.; Kelley, S. O. Rerouting Chlorambucil to Mitochondria Combats Drug Deactivation and Resistance in Cancer Cells. *Chem. Biol.* **2011**, *18*, 445–453.
- (200) Svanvik, N.; Westman, G.; Wang, D.; Kubista, M. Light-up Probes: Thiazole Orange-Conjugated Peptide Nucleic Acid for Detection of Target Nucleic Acid in Homogeneous Solution. *Anal. Biochem.* **2000**, *281*, 26–35.
- (201) Carreon, J. R.; Mahon, K. P., Jr; Kelley, S. O. Thiazole Orange-Peptide Conjugates: Sensitivity of DNA Binding to Chemical Structure. *Org. Lett.* **2004**, *6*, 517–519.

- (202) Wittenhagen, L. M.; Carreon, J. R.; Prestwich, E. G.; Kelley, S. O. Phototoxicity of Peptidoconjugates Modulated by a Single Amino Acid. *Angew. Chem. Int. Ed Engl.* **2005**, *44*, 2542–2546.
- (203) Yousif, L. F.; Stewart, K. M.; Horton, K. L.; Kelley, S. O. Mitochondria-Penetrating Peptides: Sequence Effects and Model Cargo Transport. *Chembiochem Eur. J. Chem. Biol.* **2009**, *10*, 2081–2088.
- (204) Karunakaran, V.; Pérez Lustres, J. L.; Zhao, L.; Ernsting, N. P.; Seitz, O. Large Dynamic Stokes Shift of DNA Intercalation Dye Thiazole Orange Has Contribution from a High-Frequency Mode. *J. Am. Chem. Soc.* **2006**, *128*, 2954–2962.
- (205) Evenson, W. E.; Boden, L. M.; Muzikar, K. A.; O’Leary, D. J. ¹H and ¹³C NMR Assignments for the Cyanine Dyes SYBR Safe and Thiazole Orange. *J. Org. Chem.* **2012**, *77*, 10967–10971.
- (206) Silva, G. L.; Ediz, V.; Yaron, D.; Armitage, B. A. Experimental and Computational Investigation of Unsymmetrical Cyanine Dyes: Understanding Torsionally Responsive Fluorogenic Dyes. *J. Am. Chem. Soc.* **2007**, *129*, 5710–5718.
- (207) Smith, R. A. J.; Hartley, R. C.; Murphy, M. P. Mitochondria-Targeted Small Molecule Therapeutics and Probes. *Antioxid. Redox Signal.* **2011**, *15*, 3021–3038.